Designing Functionality into Step-Growth Polymers from Liquid Crystallinity to Additive Manufacturing

Katherine Valentine Heifferon

Dissertation submitted to the faculty of the Virginia Polytechnic Institute and State University in partial fulfillment of the requirements for the degree of

Doctor of Philosophy
In
Chemistry

Timothy E. Long, Chair
Sam R. Turner
Robert B. Moore
Christopher B. Williams

May 13th, 2019
Blacksburg, VA

Keywords: polyesters, polysulfones, liquid crystalline, additive manufacturing, step-growth polymerization

Designing Functionality into Step-Growth Polymers from Liquid Crystallinity to Additive Manufacturing

Katherine Valentine Heifferon

ABSTRACT

Step-growth polymerization facilitates the synthesis of a wide range of industrially applicable polymers, such as polyesters and polysulfones. The choice of backbone and end group structure within these polymers drastically impacts the final material properties and processability emphasizing the necessity for thorough understanding of structure-property relationships. Seemingly simple changes, such as exchanging a monomer for its regioisomer, affects the polymers fundamental packing structure triggering a domino effect ultimately influencing the morphological, thermal, mechanical and barrier properties. In conjunction, end groups provide a means by which tunable mechanical properties and application into unique processing methods can be achieved.

Synthesizing polyesters with bibenzoate based monomers generates a large range of morphologies. Linear, 4,4' bibenzoate (4,4'BB), is widely considered a mesogenic monomer due to its ability to impart a liquid crystalline (LC) morphology on semi-aromatic polyesters with linear aliphatic spacers. In this body of work, semi-aromatic polyesters using one of 4,4'BB's regioisomers, either 3,4'BB or 3,3'BB, largely resulted in amorphous or semi-crystalline polymers depending on the selection of aliphatic diol. Incorporation of the *meta* isomer (3,4'BB) into traditionally LC polymers, such as poly(diethylene glycol 4,4'-bibenzoate) and poly(butylene 4,4'-bibenzoate), through copolymerization afforded two polymer series with tunable LC properties. The 3,4'BB

exhibited selective disruption of crystalline domains over the LC phase generating a number of polymers with LC glass morphologies.

The application of 3,4'BB to a fully-aromatic polyester enabled the synthesis of a novel melt-processable homopolyester with high thermal stability, poly(p-phenylene 3,4' bibenzoate). This structure afforded a nematic LC morphology which revealed beneficial shear-thinning properties similar to industrial standards. The unique LC morphology of this homopolyester inspired further characterization of the range of achievable properties using the basic structure, poly(phenylene bibenzoate), with all the possible regioisomers. This study afforded six polymers systematically varied in chain linearity from a completely *meta* to a completely *para* backbone configuration. A range of morphologies were achieved from high Tg amorphous polymers for the *meta* configurations to semi-crystalline or LC in the polymers with greater linearity.

End group functionalization generates influence on polymer properties while limiting the impact on beneficial properties achieved through the backbone structure and packing. Post-polymerization reactions or the addition of a monofunctional endcapper to the polymerization both achieve end group control. In this dissertation, the addition of a monofunctional diester with a sulfonate moiety to a semi-aromatic LC polyester synthesis resulted in a telechelic ionomer. The non-covalent interaction of the ionic groups will hopefully improve the compression and transverse mechanical properties of the LCP. In contrast, post-polymerization functionalization incorporated acrylate groups onto the ends of a basic polysulfones. These reactive groups provided a handle for photo-curing which enabled the 3D printing of the polysulfones using vat photopolymerization.

Designing Functionality into Step-Growth Polymers from Liquid Crystallinity to Additive Manufacturing

Katherine Valentine Heifferon

GENERAL AUDIENCE ABSTRACT

The research within this dissertation encompasses the design of new plastics for consumer and high-performance applications. Since the emergence of synthetic plastics in the 1920's, these materials have become a necessity in our everyday life with a range of applications in food packaging, microelectronics, architecture, medical devices, automotive, and aerospace. Benefits over metals and glass primarily result from their light weight and wide range of mechanical properties which allow a range of material properties from soft and flexible plastic grocery bags to tough car parts.

Different classes of plastics (polymers) are based primarily on the chemicals used to produce the materials, for example polyesters and polysulfones. The chemical structure of these core materials drastically impacts the final properties of the polymers, which in turn influences their application space. This work focused on how subtle changes to these starting chemical structures allows us to tune the final polymer properties.

Within the class of polyesters, a focus was placed on materials known as liquid crystalline (LC) polyesters. A liquid crystalline polymer can achieve a physical state between a solid and a liquid which imparts many beneficial properties on the material processing. Liquid-crystal television displays utilized these properties to provide drastically thinner TV's with higher resolution. Alternatively, LC polyesters find applications traditionally as high-performance fibers, insulators in microelectronics, and

stainless-steel replacements in medical applications. Studying the role of chemical structure on the properties of LC polyester enabled the design of materials which improve upon the current technological standards. These changes enabled the design of LC polyesters with lower processing temperatures and the use of fewer starting materials which will inevitably save energy and money during their production.

In the case of polysulfones, changing the chemical structure at the end of the polymer chain facilitated the application of novel processing methods, such as 3D printing. The ability to process using this method reduces the amount of material waste during production and provides an opportunity to design novel parts with intricate structures, inaccessible through traditional means.

Acknowledgments

First and foremost, I would like to thank my advisor Dr. Timothy Long. He guided me through years of research topics and provided a generous lab space with extensive instrumentation. He constantly strove to keep our group well-funded taking that responsibility off the students shoulders so that I could continue to focus on the day to day aspect of my research. His high expectations of my work, writing, and presentation style pushed me to be a far stronger polymer chemist than I would have been otherwise. My committee, Dr. Robert Moore, Dr. Richard Turner, and Dr. Chris Williams supported and guided me through this dissertation journey, often acting as a bouncing board for ideas and questions. Dr. Turner and Dr. Williams proved to be wonderful collaborators on the company projects we worked on together. I could not have asked for better mentorship throughout my time at Virginia Tech. Outside of my committee, I had the pleasure to work with so many wonderful faculty members and staff within the Department of Chemistry and Macromolecules Innovation Institute (MII). I would like to extend a special thanks to the amazing Joli Huynh who constantly went above and beyond in her job as an academic advisor. She always made sure everything was in order with my degree program and always made me feel welcome in her office whether I had a question, just wanted to chat and catch up, or just really wanted a starburst.

Over my five years of research, I had the immense pleasure of working with some of the nicest and brightest students at Virginia Tech. The Long group has been the best support system I could have asked for over my graduate career. They provided non-judgmental guidance and constantly pushed each other to achieve bigger and better with our research. Dr. Ashley Nelson, my first mentor, showed me my first true taste of

graduate research and made a bigger impact on my career in the short time we had together during her final year than she could have ever imagined. She became a role model whose path I followed throughout my graduate career. Dr. Ryan Mondschein became my second unofficial mentor whose tough love support drove me to achieve more in my research than I would have dreamed of. Thank you for dealing with all of my questions and for all the wonderful conversations about polyesters we had. To Emily Wilts and Dr. Jana Herzberger, who provided endless conversations about work and life. I will cherish our friendship for years to come and please know that I would have gone insane long ago from the pressure without you both around to vent to. The Long group has included many amazing people over my time here, Johanna Vandebrand, Josh Wolfgang, Jack Bryant, Keyton Feller, James Brown, Chris Kasprazak, Clay Arrington, Boer Liu, Mark Cashman, Cam Chatham, Philip Scott, Tyler White, Xi Chen, Kevin Drummey, Dr. Mingtao Chen, Dr. Allison Pekkanen, Dr. Justin Sirrine, Dr. Joseph Dennis, Dr. Evan Margaretta, Dr. Keren Zhang, Dr. Alison Schultz and Dr. Chainika Jangu. I thank you sincerely for all of our conversations about research, help in the lab, fun nights downtown, softball games, and friendship throughout my time at Virginia Tech. I would like to extend a special thank you to my current charge, Cody Weyhrich, whose help on my projects over this past year was instrumental in completing a number of important chapters. I wish you the best of luck as you continue your graduate school journey.

I have had the extreme fortune of working with some amazing post docs and wonderful researchers. Their mentorship and assistance, even when their own schedules were crammed full of experiments and work to get done, meant the world to me. Dr.

Nicholas Moon, Dr. Maruti Hegde, Dr. Chixia Tian, Dr. Akanksha Kanitkar, Dr. Donald Aduba, Dr. Gayan Appuhamillage, Dr. Bruce Orler, and Dr. Charles Carfagna, I thank you all whole heartedly for your guidance and support. My research and skill as a scientist are so much better for knowing you all.

I have had the amazing opportunity to collaborate on a number of occasions with graduate students throughout different departments around VT. Their support pushed my research to new understandings and provided the foundation for many of the studies I have included in this body of work. These people include to Viswanath Meenakshisundaram, Nick Chartrain, Glenn Spiering, Dr. Elliot Edling, Dr. Samantha Talley, Lin Ju, and Lindsey Anderson.

Throughout this process my friends have been a constant source of support and distraction from the stresses of day to day life. To Lindsey Anderson and Samantha Talley, I valued our time together as roommates more than you can imagine. Thank you for putting up with my craziness and your friendship/support meant a lot. I will miss our discussion about pets immensely but good luck on your own next career steps. To Jennifer McCord, you have become one of my very best friends and I cannot thank you enough for all of the runs, wine and baking nights, wedding planning support, and doggy play dates we have had together. I am going to miss you so much, but I will always keep in touch. To Drew Korovich, thank you for letting me steal your girlfriend away on a regular basis, for the many game nights, and for entertaining Zach with endless video games while I am working late. To Stephanie Molony, our frequent skype dates have kept me sane throughout the graduate school process. Thank you for all the times you let me vent about work and all the fun we had ignoring school while we planned our weddings

together. To the Lynchburg crew (EJ, Sara, Jordie and Michael), thank you for welcoming Zach and I into your family. You can never begin to imagine how much our time together meant to me and I will miss you all tons.

Most importantly I want to thank my family, the craziest and most wonderful group of people in the world. I love you all more than you could possibly know. To my parents, Maureen and Scott Valentine, you have supported and loved me through every winding turn on this journey. You always make me want to be a stronger woman and scientist. My dreams became a reality because of your love and guidance throughout my entire life. To my sister, Anna Valentine, whose amazing spirit always makes me want to get out into the world and experience everything life has to offer. Thank you for bringing me out of my shell and making me see that sometimes I have to put the work away and enjoy life. To my grandparents, Stephanie Albanese, Gary Welpley, Gordon Valentine, and Lois Valentine, your love and support means the world to me. Thank you for always being proud of my accomplishments and giving me a place to call home when home was 10 hours away. A special thank you to those I love who are no longer here, Pat Smith, Thomas Smith, and Sister Margaret Agnes, who I hope are looking down from heaven proud of the life I have created for myself. Thank you to all my cousins, aunts, uncles, and godparents/godsiblings (who are family in all ways but blood). You always make me smile and have provided me love and support as I took this step in my career. I have miss being near you and I hope you all know that you are a such a big part of my success.

Finally, to my wonderful husband, Zachary Heifferon, who followed me to Virginia on this crazy path five years ago without any idea of where it would lead us. You have absorbed all my stresses and worries, provided a safe harbor to come home to

every night, and never let me feel like I couldn't finish this. Without you here, I would have quit long ago and with your support I excelled beyond all my hopes and dreams. Thank you for loving and supporting me through all the ups and the downs. I look forward to growing with you throughout our life, especially as we begin this next step of our journey together in Delaware.

My time at Virginia Tech is coming to a close and it will always remain a huge part of my life. This school and the people I have met here have seen me grow immeasurably over these past five years. I will always be grateful to each and every person who has supported me along this journey. Thank you.

Attributions

Prof. Timothy E. Long is the director of the Macromolecules Innovation Institute (MII) as well as a professor in the Department of Chemistry. He is the author's research advisor and mentor.

Prof. S. Richard Turner is a professor in the Department of Chemistry and a member of the author's PhD committee. He was a collaborator on Chapter 4, 6, 7, and 8.

Prof. Robert B. Moore is the director of the MACR degree program and a professor in the Department of Chemistry. He is a member of the author's PhD committee and was a collaborator on Chapter 4, 6, and 7.

Prof. Christopher B. Williams is the associate director of MII and an associate professor in the Department of Mechanical Engineering. He is a member of the author's PhD committee and a collaborator on chapter 9.

Dr. Ryan J. Mondschein was a PhD graduate student in Prof. Long's research group and contributed to Chapter 4 and 8.

Dr. Samantha J. Talley was a PhD graduate student in Prof. Moore's research group and a collaborator on Chapter 4, 6, and 7.

Dr. Maruti Hegde was a postdoctoral associate for Prof. Long and a contributor to Chapter 6.

Glenn A. Spiering is a PhD graduate student in Prof. Moore's research group and a contributor on Chapter 6 and 7.

Cody W. Weyhrich is a PhD graduate student in Prof. Long's research group and currently mentored by the author. He was a collaborator on Chapter 8 and 9.

Clay B. Arrington is a PhD graduate student in Prof. Long's research group and a contributor to Chapter 9.

Dr. Justin M. Sirrine was a PhD graduate student in Prof. Long's research group and a collaborator on Chapter 9.

Viswanath Meenakshisundaram is a PhD graduate student in Prof. William's research group and a collaborator on Chapter 9.

Nicholas A. Chartrain is a PhD graduate student in Prof. William's research group and a contributor on Chapter 9.

Table of Contents

List of Figures

List of Tables

List of Schemes

Chapter 1: Introduction

1.1 Dissertation Overview

This dissertation encompasses the structure-property relationships of high-performance step-growth polymers with an emphasis placed on polyesters and polysulfones. The expanse of applications utilizing step-growth polymers has grown exponentially since their discovery in the 1920's.[1] This varied and complex polymerization family affords a wide range of polymer properties from soft or rigid thermosets to melt processable thermoplastics. Semi-aromatic polyesters, such as poly(ethylene terephthalate), encompass a 70 % of the current industrial fiber production.[2] Polysulfones (PSU), first introduced by Union Carbide in the 1960's, possess high thermal and chemical stability. Their exceptional toughness properties made them optimal for many water purification membrane applications.[3,4] Industry exhibit great interest into these two types of polymers enabling research into their structure-property relationship to have a large impact.

Polymer research demonstrates that within a polymer structure seemingly simple changes to the backbone and end groups drastically impact the properties of these materials. Changing something as small as the regioisomer of a monomer within a polyester exhibits a domino effect on the fundamental polymer persistence length and chain coiling inevitably impacting the thermal, mechanical, and barrier properties.[5,6] These small changes result in a range of polyester morphologies from amorphous to semi-crystalline to liquid crystalline. End groups within step-growth polymers act as a functional handle with which to impart influence over polymer properties. Attaching reactive groups or pendant non-covalent interaction sites through acrylates or ionic salts

influence morphological properties even expanding the manufacturing processes available to these materials.

Chapter 2 provides a literature review covering the influence of polymer structure-property-processing relationships within two advanced architecture applications, nanoporous foams and phase change materials. Both applications are used in the construction sector and work to improve energy efficiency within homes in order to reduce greenhouse gas emissions. Polymer focused research in this field continually develops improved materials for this application space. This work primarily focuses on thoughtfully designed polymers with improved efficiency for solid-solid phase change materials as well as polymers with greater CO_2 solubility.

Chapter 3 reviews the area of segmented liquid crystalline copolyesters, providing a history of the field and recent advances in synthetic techniques. This chapter expands understanding of how choice of polymerization technique influences final polymer morphology and chain packing. These choices ultimately impact orientation and phase separation properties of the polymer matrix.

Chapter 4 describes the synthesis and characterization of two series of novel semi-aromatic (co)polyesters with tunable liquid crystalline (LC) properties. This study investigated the exchange of the diester monomer, 4,4'-bibenzoate (4,4'BB) with its kinked (*meta*) regioisomer, 3,4'-bibenzoate (3,4'BB), in two common LC polyesters. While, the *meta* isomer disrupted crystallization at low incorporation, a less drastic impact on LC properties occurred resulting in a range of polymers with LC glass morphologies and tunable thermomechanical properties.

Chapter 5 evaluates the structure-property-morphology relationship of a α,ω-functionalized LC polyester with the matching backbone structure poly(hexamethylene 4,4'-bibenzoate). The polymerization included a monofunctional end group with a sulfonate moiety to afford a series of telechelic ionomers. This ionic group imparted non-covalent interactions at the end of the polymer chains influencing the polymer thermal, melt rheological, and morphological properties.

Chapter 6 describes a synthetic strategy to achieving a novel fully-aromatic LC homopolyester, poly(*p*-phenylene 3,4'-bibenzoate). The use of the *meta* bibenzoate monomer instead of the common mesogenic monomer, 4,4'BB, afforded a melt processable fully-aromatic homopolyester. Depending on processing methods, this unique polymer afforded either a LC glass or semi-crystalline morphology at room temperature. Comparisons to Vectra® demonstrated similar shear-thinning behavior in the power law region and tunable zero-shear viscosities.

Chapter 7 details the range of polymer properties generated through the exchange of regioisomeric monomers within the same basic repeat unit structure, poly(phenylene bibenzoate). Three diacid monomers (4,4'BB, 3,4'BB, and 3,3'BB) and two dipivilate monomers (hydroquinone dipivilate or resorcinol dipivilate) afforded six polymers with different variation of backbone configurations from entirely linear to fully kinked. This polymer series facilitated control over the morphology of a fully-aromatic polyester with high thermally stability ranging from semi-crystalline to LC glass to high T_g amorphous.

Chapter 8 chronicles the application of the dimethyl 3,3'-bibenzoate monomer to the synthesis of a series of novel semi-aromatic polyesters with different linear and cycloaliphatic diols. The rigidity of the aliphatic diol exhibited an influence over the

polymer's crystallizability, T_g, and thermomechanical properties. Comparison of these polymers against previously synthesized 4,4'BB or 3,4'BB based polymers further elucidated the structure-property relationships for these materials.

Chapter 9 describes the post-polymerization functionalization of polysulfones with acrylate moieties. The introduction of this reactive end group fostered a pathway to converting the thermoplastic to a thermoset upon UV-irradiation. This generated a means to process the polysulfones using the additive manufacturing technique, vat photopolymerization.

Chapter 10 summarizes the overall conclusions of the work discussed while Chapter 11 suggests future work to continue the research described in this dissertation.

References

(1) Odian, G. G., *Principles of polymerization*; Wiley: New York, 1991.

(2) Geyer, R.; Jambeck, J. R.; Law, K. L., Production, use, and fate of all plastics ever made, *Science Advances* **2017**, *3*.

(3) Johnson, R. N.; Farnham, A. G.; Clendinning, R. A.; Hale, W. F.; Merriam, C. N., Poly(aryl ethers) by nucleophilic aromatic substitution. I. Synthesis and properties, *Journal of Polymer Science Part A: Polymer Chemistry* **1967**, *5*, 2375.

(4) Hale, W. F.; Farnham, A. G.; Johnson, R. N.; Clendinning, R. A., Poly(Aryl ethers) by nucleophilic aromatic substitution. II. Thermal stability, *Journal of Polymer Science Part A: Polymer Chemistry* **1967**, *5*, 2399.

(5) Heifferon, K. V.; Mondschein, R. J.; Talley, S. J.; Moore, R. B.; Turner, S. R.; Long, T. E., Tailoring the glassy mesophase range of thermotropic polyesters through copolymerization of 4,4'-bibenzoate and kinked isomer, *Polymer* **2019**, *163*, 125.

(6) Mondschein, R. J.; Dennis, J. M.; Liu, H.; Ramakrishnan, R. K.; Nazarenko, S.; Turner, S. R.; Long, T. E., Synthesis and Characterization of Amorphous Bibenzoate (Co)polyesters: Permeability and Rheological Performance, *Macromolecules* **2017**, *50*, 7603.

Chapter 2: Advanced Polymers for Reduced Energy Consumption in Architecture

(Published in *Macromolecular Rapid Communication* **2019**, *40* (3), 1800597)

Katherine V. Heifferon and Timothy E. Long

Macromolecules Innovation Institute, Department of Chemistry, Virginia Tech, Blacksburg, VA 24061

Keywords: nanoporous foams; microencapsulation; structure-property relations; insulation; phase-change materials

2.1 Abstract

In an effort to slow the progress of climate change, the current scientific community has focused on the reduction of greenhouse gases in order to limit the global average temperature inflation to less than 2 °C. The improvement of thermal controlling construction materials could potentially result in lower energy homes/ reduced emissions and lowering the thermal conductivity of insulation materials improves home energy efficiency. Nanoporous insulation foams impart a drastic decrease in the thermal conductivity but many polymer properties must be assessed to produce these materials. Passive phase change materials also represent another key energy saving device to control heat flux within a living space. Research into unique polymeric systems provides novel means of encapsulation or creating polymeric crosslinked matrices to prevent leakage and improve mechanical robustness. These two areas of polymer research in architecture represent key advancements for construction materials aimed towards energy savings and energy related emissions control.

2.2 Introduction

In the past fifty years, climate change has emerged as one of the most controversial and important problems facing our society. Scientists revealed that the current CO_2 levels on earth exceed the levels estimated for the past 400,000 years.[1] This drastic increase in CO_2 levels and subsequent global climate change led to the 2009 UN Copenhagen Summit in which the participating countries agreed to make efforts toward limiting further global average temperature increase to less than 2 °C.[2] As a result, scientists have placed significant research focus on reducing greenhouse gases to meet this goal. Global initiatives to lower emissions of CO_2 target new legislation and funding of scientific research to innovate those areas exhibiting the largest disruptive impact.[1] The EIA report in 2009 identified that 80 % of U.S. greenhouse emissions evolved from energy-related sources, therefore it can be well understood that the biggest impact will come from the development of technologies to improve efficiency of energy use.[1]

The long lifetime of housing results in the architecture and construction sector receiving significant scrutiny. This includes CO_2 emissions from the development of building materials to the energy and fossil fuels involved in heating and cooling a home. In 2003, the US Climate Change Science Program estimated that the building sector produced 37% of the total CO_2 emissions in North America and 10% of the total global CO_2 emissions.[3] The European Union also determined that 40% of their energy related emissions arose from the building sector, making this area highly important.[4] These residential emissions originate significantly from electricity use in heating and cooling living spaces, therefore focus has been placed on creating more efficient heat/cooling solutions to reduce energy expenditures. A few case studies in Europe implemented passive houses and zero-energy housing concepts in an effort to significantly improve

energy efficiency to combat this issue.[1] These houses possess a very low heating load and low total energy demand. The addition of thicker insulation, triple glazing of windows, and energy production components, such as solar panels, resulted in a net zero energy utilization. Thiers et al. analyzed two examples of net zero energy housing (NZE) built in France using thick layers (15-20 cm) of traditional foamed materials, triple glazed windows, insulated external doors, a thermal bridge, and a variety of low energy heating systems.[5] The net energy determined from a life cycle assessment of these two houses exhibited values of -5 to 10 $kWh_{pe}m^{-2}yr^{-1}$, outperforming previous energy loss of -130 $kWh_{pe}m^{-2}yr^{-1}$ for non-NZE homes in the same area.[5] Another example of a passive home that invokes the principle of responsive design includes Lumenhaus, developed at Virginia Tech. Lumenhaus automatically adjusts its temperature in order to optimize energy use through a weather station on the roof of the house. This weather station decreases the possibility of human error and overheating within the home through an automatic adjustment.[6] In 2009, Nowalski et al. estimated that 10,000 NZE homes already exist in Europe. Despite this important step in energy efficiency, these systems are limited to newly developed homes and will not impact the millions of homes that already exist. Instead, innovations to be utilized in the renovation of pre-existing structures must be emphasized, such as improved efficiency in insulation and heating/cooling systems.[7]

Improvements to current insulation techniques and efficiency of energy use comprise the largest factors to reduce energy related CO_2 emissions. One common method of enhancing insulation properties in homes results from applying a thicker layer of traditional insulation materials. Unfortunately, restricted urban areas and

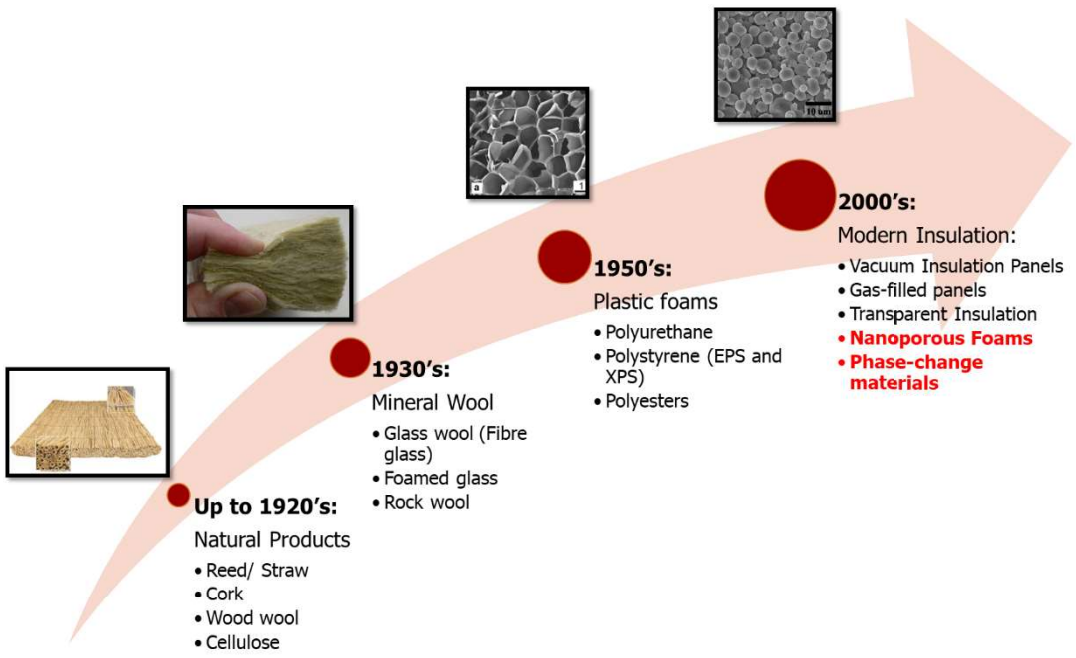

Figure 2.1. Basic history of insulation development throughout the ages exhibiting the transition from natural materials to man-made plastics. Modern research focuses on improving upon the current plastic foams through the use of novel passive and dynamic insulation materials. Adapted with permission.[10-13] 2014, Renewable and Sustainable Energy Reviews; 2015, Sustainable Materials and Technologies; 2012, Polymer; 2011, Chemical Engineering Journal.

refurbishment of historic homes limits use of thicker layered insulation.[8] Instead, the reduction of overall thermal conductivity directly correlates with improved insulation efficiency enabling the use of thinner insulation while maintaining energy savings.[9]

Figure 2.1 illustrates the improvement of insulation materials throughout history emphasizing the shift in scientific focus to modern dynamic and passive insulation systems that improve insulation efficiency.[10-13] This research promises to revolutionize energy efficient homes through the use of nanoporous insulation foams. This area, focused currently in polymeric materials research, could significantly improve insulation efficiency in homes drastically reducing energy loss.

Human intervention in heating/cooling systems also poses an enormous threat to energy efficiency in homes accounting for significant of energy loss. Implementation of automated temperature control systems eliminate human intervention by maintaining a consistent comfortable living temperature. Incorporation of active or passive energy storage systems, such as Latent heat storage systems (LHSS), into the building envelope or in conjunction with heating systems implements control over these thermal fluctuations. Previous studies demonstrated that incorporation of LHSSs into a building design drastically lowers thermal mass loss or thermal discomfort whereby reducing energy loss.[14] Passive LHSSs, such as phase change materials (PCM), enable incorporation into building envelopes without the need for extra energy use related to controlling the storage system. Polymers have been utilized primarily as encapsulation materials to contain the PCM, but recent advances into solid-solid PCM illustrate new and creative methods to apply polymers to these systems in order improve mechanical stability.

Recent materials advances in both phase change materials and nanoporous foams indicate key areas of intersection between polymeric materials and architecture research leading to significant energy saving potential for homes and drastic CO_2 emission improvement. This review covers the role of polymeric properties on both the formation of nanoporous foams as well as the application into PCM.

2.3 Structure-Property-Relationships of Nanoporous foams

2.3.1 Fundamentals of insulation materials

Fundamentally understanding the origin of physical properties for insulation materials will facilitate scientific improvement of the thermal management in homes, reducing CO_2 emissions. Fouriers Law describes heat transfer through a material as the energy flux, Ø ($\frac{mW}{m^2}$), equivalent to the product of the thermal conductivity $\left(k, \frac{mW}{mK}\right)$ and temperature gradient $\left(\nabla T, \frac{K}{m}\right)$ as seen in **Equation (2.1)**. Energy flux depends on the

$$\emptyset = -k\nabla T \quad \textbf{(2.1)}$$

summation of the four main mechanisms of heat transfer that occur in insulative materials. The more measurable material property, thermal conductivity, directly compares to this summation of energy flux.[15] Thermal conductivity describes the ability of a material to move heat across its bulk within a certain time period. The sum of the thermal conductivity as a result of conduction in the gas phase (λ_g), conduction within the solid phase (λ_s), convection of the gas (λ_c), and thermal radiation (λ_r) controls this term, as seen in **Equation (2.2)**.

$$\lambda_T = \lambda_g + \lambda_s + \lambda_c + \lambda_r \quad \textbf{(2.2)}$$

In order to achieve the lowest thermal conductivity possible, the mechanisms of heat transfer must be understood. The initial choice of material used influences the thermal conductivity from conduction in the solid phase (λ_s). The lattice vibrations of atoms comprise the primary form of energy/heat transport in solid phase conduction. Atoms connected with springs in a linear structure illustrates this motion in **Figure 2.2**.[16] Solely lattice vibrations comprise non-conductive materials, while conductive materials also transfer energy through translational motions of free electrons.[17] The benefit of

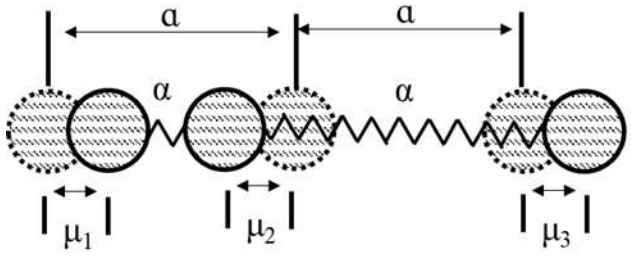

Figure 2.2. Energy transfer through a solid through lattice vibrations as demonstrated by linear spring ball model. Symbol a represents the distance between the atoms, α is the force constant, and μ the displacement of the atoms. Adapted from Ziman, J.[16]

translational motion of free electrons in metals results in high thermal conductivities, such as aluminum (237,000 mW/mK) and iron (80,300 mW/mK), which result in poor insulating materials. Choosing non-conductive solid materials restrict these motions and enables good insulation properties.[18] Unfortunately, the overall limits on material properties force scientists to increase the porosity of the material to decrease the overall bulk volume whereby reducing the impact of this term.

Porous structures aid as well in the reduction of λ_c. Heat transfer from convection occurs through two distinct mechanisms, random molecular motion (e.g. conduction) and bulk/macroscopic motion. For insulating materials, this type of convection occurs in the case of a gas in motion across a bounding surface, where the gas and solid maintain different temperatures. Low fluid velocity close to the heated surface results in a diffusion mechanism where random molecular motion dominates. Further away from the boundary layer, the velocity increases, pushing the flow of the heat away from the solid surface and into the bulk gas. A high density of small pores in an insulating material, restricts the heat transfer mechanism to random molecular motion due to a smaller bulk

volume. The reduction in macroscopic motion significantly reduces the overall heat transfer resulting from convection. [17]

Traditional insulation focuses on the reduction of these two λ factors and usually comprise porous materials developed through either foaming or drawing fibers, which exhibit low bulk thermal conductivity values, 20-50 mW/mK.[19] Fibrous insulation includes inorganic wools, such as glass wool and stone wool, as well as organic fibers like sheep-wool, cotton-wool, cellulose, and coconut fibers. Glass-wool and stone-wool comprised 60 % of the insulation market in Europe in 2005 and still continue to be prevalent options.[20] Heating borosilicate or other glass at 1400 °C and pulling the molten mass through rotating nozzles creates the fibrous glass wool. A similar technique produces stone wool, and spinning melted dolerite or diabase wheel creates fibers. Thermal conductivity varies from 30-40 mW/mK based on temperature and moisture content.[9] Benefits of these materials arise from the ability to cut at the building site and introduce holes into the material without affecting the overall conductivity, but extreme processing temperatures and relatively high thermal conductivity outweigh these benefits.[9] Most fibrous insulation possesses a similar thermal conductivity to the glass wool and stone wool, but varies in weight and potential applications.

Foamed insulation includes natural materials (such as cork) and more commonly foamed synthetic polymers, for example polystyrene (PS) and polyurethane (PU). The expansion of the reacting polymer with gases (CO_2, C_6H_{12}, or HFC), or through expansion foaming on site produce PU foams. Expanded and extruded polystyrene (EPS

and XPS respectively) both use polystyrene to create an insulative material through different processing techniques.[13,21]

Figure 2.3 illustrates the microstructure observed for extruded polystyrene foam using CO_2 as the blowing agent.[13] Heating small spheres of polystyrene containing expanding agents with water vapor results in a partly open pore foam structure, typical of EPS, that can be cast into boards. In contrast, XPS uses an expansion gas to foam melted polystyrene as it extrudes through a nozzle. PU foams result in a lower thermal conductivity (20-30 mW/(mK)) in comparison to the XPS and EPS systems (30-40 mW/mK). Unfortunately, higher health concerns arise with PU foams synthesized from isocyanates and multifunctional alcohols, due to the release of isocyanates and hydrogen cyanide when burned.[9] Each of these systems maintains the ability to be cut on site and perforated without harming the overall thermal conductivity of the material.

Thermal conductivity, as a result of heat transfer from radiation (λ_r), is a unique area that does not impact the λ_T as drastically as the λ_s and λ_c, but remains an important factor to consider when developing an insulation material. This form of heat transfer

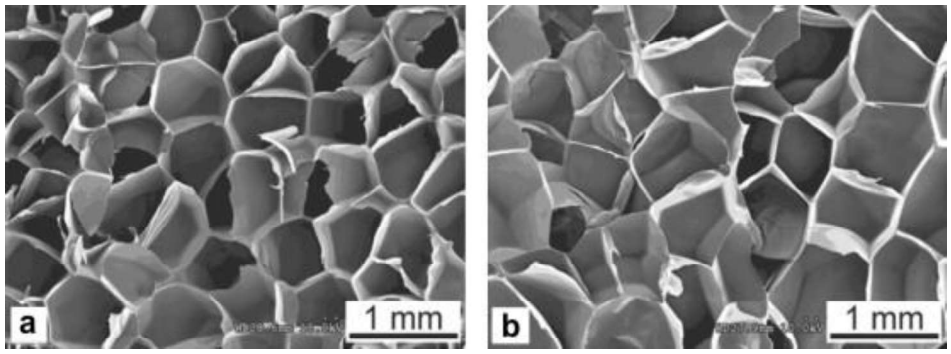

Figure 2.3. Extruded polystyrene foam utilizing CO_2 (a) with and (b) without the co-blowing agent water. Reprinted with permission.[13] 2012, Polymer.

performs better in a vacuum rather than relying on a material, such as atoms, to transfer heat. Electromagnetic waves transport the energy from the surface of a solid, liquid, or gas and results from changes in the electron configurations of molecules. The net radiative heat exchange combines the amount of energy that can be absorbed by the surface and the emissivity, which measures the energy emitting efficiency of the surface. The lowest thermal conductivity values arise from a low adsorption coefficient and high emissivity ($0 < \varepsilon < 1$). [17] The combination of emissivity and pore size in porous insulation materials regulates the thermal conductivity due to radiation. Materials with an emissivity $\varepsilon < 0.8$ and pore diameter $\delta < 1$ mm result in a decrease in the λ_r to below 4 $\frac{mW}{mK}$.[22] Other studies show examples of λ_r increasing when the pore size decreases below the wavelength of infrared radiations (10 μm). Overall though, there are insignificant effects observed on the λ_T due to the decreased overall value of λ_r. [22,23]

After choosing the bulk material, other mechanisms of heat transfer control thermal conductivity of the insulation. The most plausible next step to consider consists of the heat transfer as a result of conduction in the gas phase. The mechanism for heat transfer in the gas phase results from the collision of gas molecules and the resulting transfer of energy between atoms, illustrated in **Figure 2.4**.[17] In the construction industry, air comprises the most common gas used in insulation with a thermal conductivity of 26 $\frac{mW}{mK}$ at room temperature. Placing the insulation under vacuum and removing the air constitutes the most common method of reducing this term. Examples of a system that utilize this method of thermal conductivity reduction consist of vacuum insulation panels (VIPs). Several drawbacks to the use of VIPs, such as the fragility of the packaging,

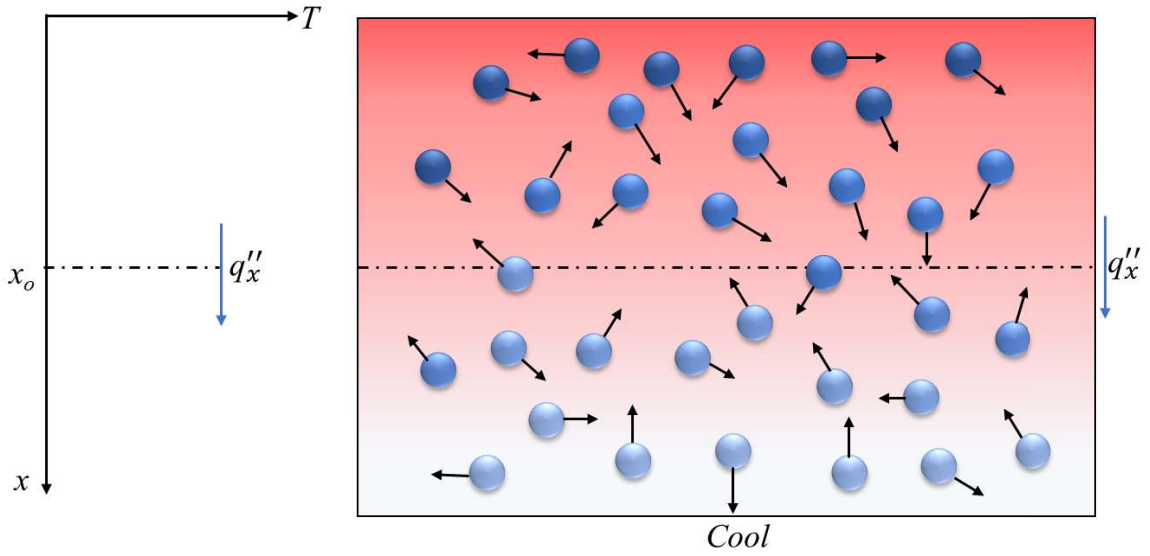

Figure 2.4. Conduction of heat through gas due to the molecular motion of the atoms. The symbol q_x" represents heat flux while x represents the distance over which the temperature gradient is measured. Adapted from Incorpera et al.[17]

make them unfavorable for commercial construction. If punctured, air floods the VIP resulting in a drastic thermal conductivity change. This restricts the adaptability of these materials due to restrictions in cutting at a building sight with a potential loss of vacuum.[9] As a result of these restrictions, scientists are moving towards another method of lowering λ_g that relies on the manipulation of the physical understanding of this mechanism of heat transfer. A pore size in an insulating foam equivalent to or smaller than the mean free path of the gas particle moving through the insulation results in a gas particle energy dissipating mechanism occurring through transference with the walls of the cell rather than colliding with another gas molecule.

Quantification of the Knudsen effect occurs through calculation of the Knudsen number (Kn), which equates to the mean free path of a gas molecule (l_g =70 nm for air at room temperature) divided by the average pore size of the foam (φ). This number

inversely relates to the thermal conductivity resulting from gas conduction (λ_g'), observed in **Equation (2.3).**

$$\lambda_g{}' = \frac{\lambda_{go}{}'}{(1 + \beta Kn)} \quad (2.3)$$

λ_{go}' equates to the thermal conductivity of the gas and β, which refers to the energy transfer parameter between the gas and the solid structure. This concludes that decreasing the pore size of a foam below a micrometer results in a significant decrease in the thermal conductivity through the shift in the energy dissipation mechanism of the gas molecule. Due to their small pore size and relatively homogenous pore density, aerogels constitute the first material to prove this concept. Notario et al. identified that nanoporous polymeric foams could produce a similar effect. The thermal conductivity of PMMA foamed blends with nanometer- and micrometer-scale pore size demonstrated a sharp drop below 100 nm (**Figure 2.5**). The relative density of the foam (dividing foam density with solid density) also increases linearly with the increase in thermal conductivity. Further studies demonstrated that foams imparting the Knudsen effect exhibit minimized impact of pore structure (open or closed) on the overall conductivity. A pore size of less than 100 nm with a relative density of 0.05 (ρ_{foam}/ρ_{solid}) facilitates a thermal conductivity of 20 mW/(mK). The lowest thermal conductivity achieved by this group was 7 mW/(mK) with a cell size of 10 nm, equivalent to aerogel values.[24]

2.3.2 Foaming Techniques

Nanoporous foams encompass any foamed polymer with a pore diameter of less than 100 nm. Novel blowing techniques achieve these small pores homogenously throughout

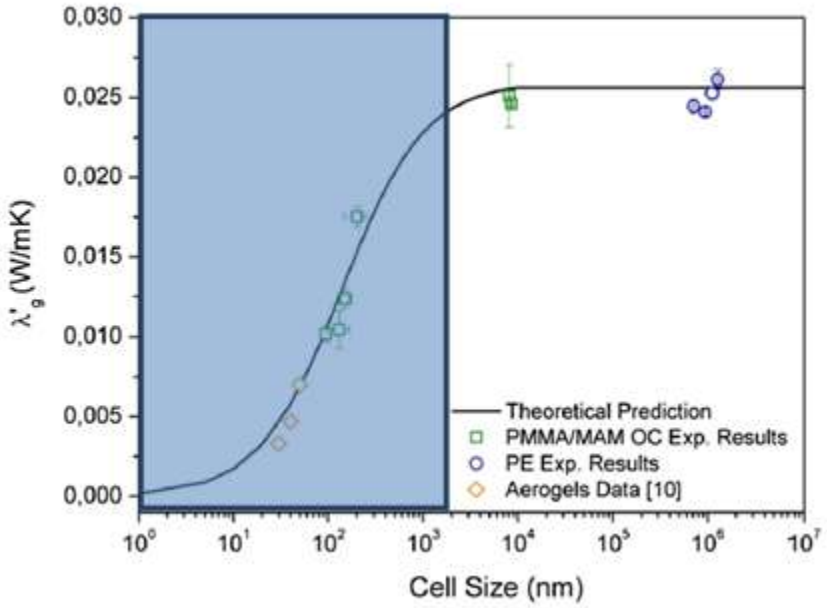

Figure 2.5. Thermal conductivity analysis for a variety of cell sizes foams and aerogels in comparison to predicted Knudsen equation. Knudsen regime highlighted in blue. Adapted with permission.[24] 2015, Polymer.

the polymer film. Before the revelation of chlorofluorocarbons (CFC) negative environmental impact, microporous foams utilized CFC based blowing agents. The environmental inertness and accessibility of CO_2 stimulated its later focus.[25] CO_2 based foaming occurs during the supercritical phase of the gas (SCO_2) by exceeding the critical point of pressure and temperature. SCO_2 foaming occurs in one of three methods: one-step batch, two-step batch, or continuous foaming. During batch foaming, CO_2 saturates thin films in an autoclave than through either a temperature or pressure drop the polymer film becomes supersaturated with SCO_2 causing pore formation.[26] One-step batch foaming results from saturation of a polymer film in an autoclave with supercritical CO_2 through application of high pressure (~300 bar) and an empirically derived temperature and time. Due to plasticization of the material and an increase in free volume in the film due to CO_2 incorporation, the polymer transitions into the rubbery state. In this state,

SCO_2 expansion and pore formation occurs during sample depressurization when the CO_2 returns to the gaseous state. In this style of foaming, saturation temperature and the rate of depressurization control the microstructure of the foam. For PMMA, larger pore sizes and lower pore density (number of cells per cm^3) in the foams result from higher saturation temperatures and attributed to decreased CO_2 solubility at higher temperatures. Using lower temperatures effectively increases the solubility, resulting in a larger number of nucleation sites for pore formation affording smaller pore size and higher pore density. Additionally, faster depressurization generates smaller pore size and higher pore density.[27] Recent advancement in the one-step batch foaming techniques stemmed from the development of a new autoclave with the capability to achieve very fast depressurization rates. Notario et al. utilized this new system to achieve a depressurization rate of 30 MPa/min, enabling a nanoporous structure not previously achieved.[24] Alternatively, TOP industry in France developed an autoclave with a capacity of 300 cm^3, which is able to achieve saturation pressures of 20-30 MPa. Pinto et al. indicated that this foaming technique enabled films as thick as 50 mm x 15 mm x 3 mm with nanoporous structure.[28]

Two-step batch foaming varies significantly from the one-step procedure. Initially, the saturation of the polymer occurs at a high pressure and a low temperature similar to the one-step procedure. Reducing the pressure to atmospheric levels quenches the polymer and induces a supersaturated, glassy polymer. Heating the saturated polymer above the T_g then results in nucleation and growth of the porous structure. Foaming temperature and time control this method. Unlike the one-step foaming, which requires the use of a plasticizable polymer that forms a rubbery state upon saturation, a larger

variety of polymers utilize the two-step foaming procedure to form microporous structures. The downfall of this procedure occurs with the added cost of the second processing step.[27] A fewer number of groups have demonstrated successful formation of nanoporous materials using the two-step method. These groups focused on PMMA, polysulfones, polyetherimides, and other high-performance polymers.[29-35] The current autoclaves used in batch foaming limit the production of large-scale films. Recent work using a high-pressure vessel with a capacity of 300 cm^3 demonstrates the scalability of this technique even with this limit.[24]

In contrast, continuous processing facilitates a faster production, enabling commercialization in this technique in comparison to batch methods.[36] This method utilizes SCO_2 assisted extrusion where polymers saturated with CO_2 are fed into the extruder at reduced temperatures due to vitrification. The subsequent pore nucleation that occurs after extrusion through the die results in a pressure drop.[36,37] While commonly used to form microporous structures, few studies exist in the literature that analyze a continuous processing method to produce nanoporous foams, and BASF holds patents in this area.[37]

2.3.3 Effect of CO_2 solubility

Polymer's structural characteristics play a large role on the size, density, and processing of nanoporous foams. Microporous foams utilize large varieties of homopolymers, ranging from polystyrene to fluorinated polymers. Nanofoams comprise only a select few of these homopolymers, for example PMMA as illustrated in **Figure 2.6**.[24] The determining factors for the formation of nanofoams falls on the T_g and the

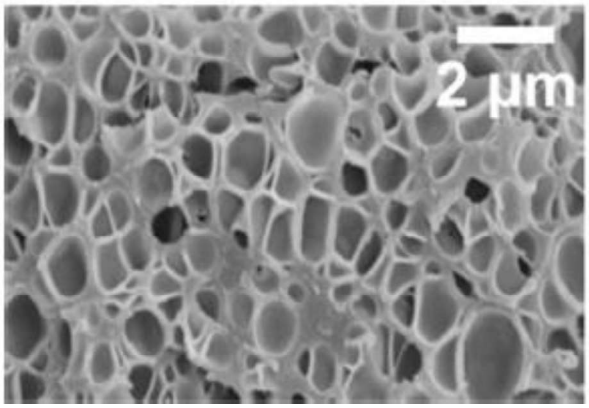

Figure 2.6. Nanocellular foam from a PMMA/MAM blend. Reprinted with permission.[24] 2015, Polymer.

CO_2 solubility of the polymer. During the initial saturation of CO_2 into the polymer film, the cloud point is reached at the maximum absorption of CO_2 into the polymer. The CO_2-philic nature of the polymers dictates this maximum value. Recent studies indicate that solubility improves pore size and pore density, providing decreased thermal conductivity.[26] The work performed on PMMA, polystyrene, and poly(ether imide) (PEI) demonstrate the hallmark for homopolymer formation of nanoporous foams.[32,34] Their combined thermal properties and CO_2-philic nature make them ideal candidates for foaming, resulting in pores with diameters of 100 nm. As a result of the unique Lewis accepting characteristics of CO_2, the addition of electron donating groups into the polymer enhance solubility. PMMAs and poly(ether imide)s CO_2-philic nature arise from the carbonyl groups in the back-bone and side-chain of the polymers (**Figure 2.7**).

The interaction with these functional groups likely arises from a Lewis donor acceptor pair interaction, in which CO_2 acts as an electron acceptor and the carbonyl, an electron donor. The carbon in CO_2 coordinates either once or twice with the two electron pairs of the carbonyl, resulting in an interaction between the polymer and the SCO_2.

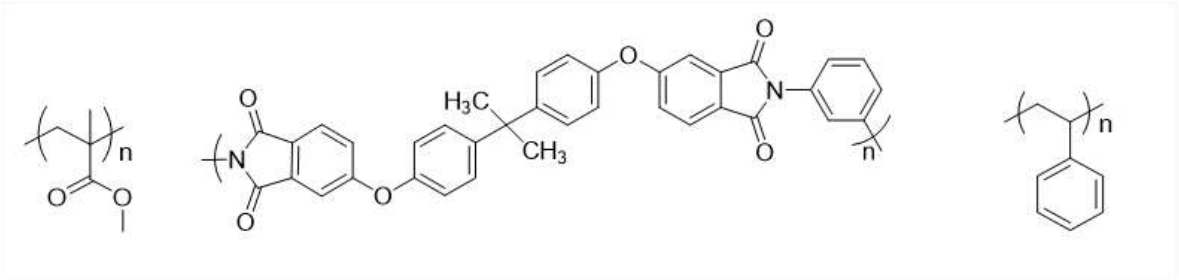

Figure 2.7. Chemical structure of poly(methyl methacrylate), poly(ether imide), and polystyrene (left to right)

Kazarian et al. identified the interactions between CO_2 and polymers using Fourier transform infrared spectroscopy (FTIR).[38] Other groups, such as Ewing et al., demonstrated that for polyketones, increased carbonyl concentration enhanced the CO_2 solubility. This enhancement continues until the system achieves a maximum concentration where the system enters a regime controlled by intermolecular interactions resulting in a lowered CO_2 capacity.[39] The lack of a strong Lewis donor results in a lower impact of this factor for PS in comparison to the other polymers. Kazarian et al. observed FTIR bending modes consistent with weaker electrostatic interactions between CO_2 and the phenyl rings of PS, typically referred to as pi-pi stacking.[38,40] Thus, PMMA and PEI exhibit higher CO_2 solubility than PS. Lower solubility results in larger pore size and lower pore density for the PS homopolymer at the same processing temperatures and depressurization rates. Instead, induction of smaller pore sizes occurs through the manipulation of these processing parameters.[40]

Guo et al. determined that the amount of CO_2 absorbed into PMMA foams, as a result of increasing pressure, greatly influences whether or not a nanofoam occurs. Studies show the persistence of a nanopore morphology occurs when the polymer absorbs 30 wt % of CO_2.[41] Polymers with a higher maximum CO_2 solubility theoretically induce smaller pore morphologies at easier processing conditions (lower pressure). Other

methods, such as the addition of polar fluorine atoms, also enhance solubility in microporous foams, but currently do not make an appearance in their nanoporous counterparts with the exception of their addition into block-copolymers.[42,43]

In situations, such as PET, where both phenyl rings and carbonyls are present, the susceptibility to assume that an increase in solubility would occur comes easily. Unfortunately, the crystallizability of PET significantly reduces the overall solubility and negates the benefits of both interactions, which negates this assumption.[38] Wen et al. recently studied the formation of a nanoporous structures through a two-step batch method using poly(phthalazinone ether sulfone ketone). This amorphous high performance engineering thermoplastic combines both the pi-pi stacking of PS with the carbonyl groups of PMMA while eliminating the restriction of crystallinity.[35] In this study, the formation of a nanoporous structure occurred when the saturation pressure in the first step achieved 5 to 6 MPa at foaming temperatures of 140-170 °C. The authors observed the transition from a closed pore to a bicontinuous nanoporous structure upon use of higher saturation pressures, which increased the CO_2 concentration prior to foaming. From this evaluation, a critical concentration of 2.8 CO_2/100 g of polymer was determined necessary to achieve a nanoporous structure. Krause et al. studied two other high-performance polymers, PEI and polysulfones, which exhibit similar bicontinuous nanoporous structures. In this study, a critical CO_2 saturation level of 47 cm^3 (STP)/cm^3 (polymer) or higher was required to achieve pore diameters of less than 100 nm.[32]

2.3.4 Effect of T_g on pore size

Glass transition temperatures of the homopolymers largely affects the processing of the polymer films. For amorphous materials, adding CO_2 to the polymer results in an increase in free volume within the film. Higher free volume results in a decrease of T_g through plasticization. Depression of the T_g occurs linearly with the pressure applied during the saturation stage and the resulting increase in CO_2. Ruiz et al. discovered that the T_g of PS and PMMA both observed a 50 °C decrease during a one-step foaming process. This study utilized a saturation temperature ranging from 20-80 °C, saturation pressure of 30 MPa for 16 h, and depressurization rates ranging from 15-1.2 MPa/min.[27] Krause et al. discovered that nanopore growth occurs at a temperature between the original T_g of the homopolymer and the T_g caused by plasticization. In the case of one-step batch methods, higher pore density and smaller pore size occur when utilizing a foaming temperature closer to the T_g after plasticization. Cracking occurs during the depressurization stage when using a temperature well below the T_g of the polymer post-

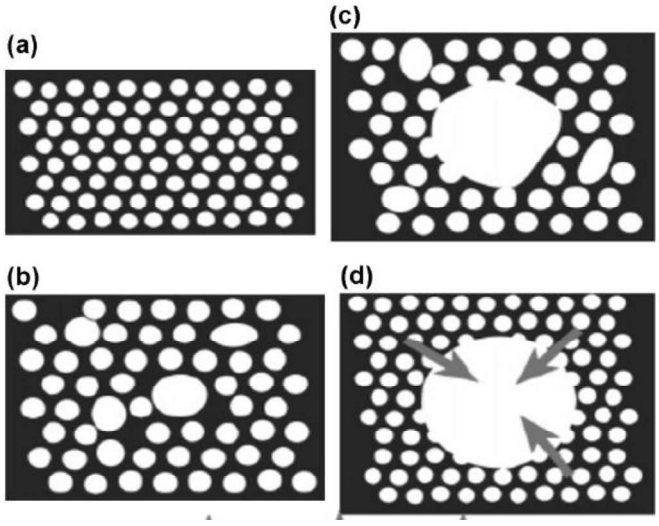

Figure 2.8. Effect of foaming temperature (T_f) on pore formation (a) $T_f << T_g$ (b) $T_f < T_g$ (c) $T_f = T_g$ (d) $T_f > T_g$. Reproduced with permission.[26] 2015, Progress in Polymer Science.

plasticization due to the glassy nature of the polymer. Using higher temperatures closer to the pure polymer T_g, results in microporous foams due to the decrease in the solubility of CO_2 in the polymer and lower viscosity resulting in gas release (**Figure 2.8**).[26]

This was further corroborated by Costeaux et al. at Dow Chemical Company whose studies also demonstrated higher porosity and larger pore size when utilizing the same processing temperatures resulting from a lower T_g after plasticization. This occurs as a result of the larger difference between the foaming temperature and the T_g, giving the pores a longer time to expand before the polymer reaches the glassy state.[44] The restrictions in the processing conditions induced by T_g results in careful consideration of polymers used in foaming. Polymers with higher T_g's (PEI, around 217 °C) require higher temperatures and higher pressures in order to achieve the same pore size scale as lower T_g samples. Zhou et al. utilized PEI to produce nanoscale foams through a high pressure and high temperature method.[45] Lower T_g near 110 °C of PMMA and PS, enable the use of lower processing temperatures.

In the case of a two-step batch method, the T_g imparts temperature bounds considered the "foaming window" for the polymer during the second stage. The temperature minimum or T_{lower} is equated to the glass transition temperature of the plasticized polymer after CO_2 saturation. The T_{upper} or maximum temperature is associated with the T_g of the pure polymer. Beyond the $T_{upper,}$ pore structures become destabilized as a result of diffusion of the gas out of the film and viscosity decrease, while temperatures lower than T_{lower} result in a glassy state prohibiting gas release.[32,35] Wen et al. studied the effect of the foaming window on the porous structure of poly(phthalazinone ether sulfone

ketone). The authors noted that as the saturation pressure of the first step was increased, resulting in a higher CO_2 concentration, the T_{lower} was reduced due to further plasticization, broadening the foaming window.

2.3.5 Morphology-driven nanopores

The phase-separated morphologies resulting from block copolymers foster intrigue in the nanopore community due to their ability to nucleate pore growth.[46] Initial research into this area with microporous materials focused around the use of random, non-phase-separated copolymers, to impart better CO_2 solubility properties into non-polar polymers. The work of Costeux et al. demonstrated a similar technique utilizing blends of polymers. Incorporating acrylic polymers into PS improved the solubility of PS resulting in smaller pore sizes and high pore density.[47] Similar to blends, the design of random copolymers tailors the pore size of the nanostructure. More recent focus on block copolymers results from their use in directing pore nucleation. Work in this area began in the early 2000's on block copolymers of PS and fluorinated polymers, such as poly(perfluorooctylethyl methacrylate) (PFMA). The choice of these two polymers resulted from their exceedingly different χ parameters, which induced controlled phase-separated morphologies. Yokoyama et al. studied PS-PFMA block copolymers with a variety of molecular weights to achieve spherical morphologies when cast into thin films. This spherical morphology created a template for tunable pore sizes (10-30 nm) using a one-step, batch foaming method.[48] This template works through the selective absorption of SCO_2 in the CO_2-philic regions (PFMA) located in the interior of the spherical morphology. When the pressure of the CO_2 pushed against the sphere during expansion,

the elastic force of the surrounding matrix block resisted and limited the size of the pores. Yokoyama et al. expanded this work further to include poly [styrene-(*b)*-4-(perfluorooctylpropyloxy)styrene]. This system exhibited the same morphology and expansion mechanism to produce pores around 40 nm.[49] Forest et al., in more recent work, examined the use of ABS terpolymers to generate nanoporous foams. This unique method used a gaseous foaming process instead of supercritical CO_2, and the size of each block determined the formation of a biphasic system or spherical morphology. When the polymer achieved a spherical morphology, nucleation of the pores in the butadiene block enabled a pore size of 100 nm.[50] Block copolymers provide opportunities toward the direct nucleation of pores, but their complexity and relatively high cost of production make them less likely to be commercialized than a blend or readily available homopolymers.

In order to address the cost associated with block copolymer structures, Wang et al. studied the formation of nanoporous films nucleated instead from PMMA/TPU blends exhibiting spherical morphologies. This study utilized both a one-step and two-step foaming process and achieved an average pore size of 205 nm, further exhibiting a superinsulative thermal conductivity value of 24.8 mW/mK. The introduction of TPU also imparted toughness and ductile fracture behavior onto the final foamed polymer in comparison to neat PMMA microporous films.[34,51] This improvement of mechanical properties in nanoporous structures relative to their microporous counterparts has been demonstrated in a variety of cases, although the literature primarily focuses on the analysis of PMMA.[33,34,51] These characteristics have been attributed to the confinement effect of the polymer chains within the walls of the nanoporous films.[33]

Blending nanoparticles into PMMA revealed another method for templating polymers for the formation of nanoporous foams. Pinto et al. formed nanocomposites of ZnO and PMMA in an effort to induce heterogenous nucleation of pores during CO_2 foaming using a two-step foaming method. This method consistently achieved a pore size of less than 1 μm and a minimum of about 200 nm.[52]

2.3.6 Commercialization

The difficulty in the large-scale preparation of thicker foams needed for thermal applications limits translation of nanoporous foams to industry. Few studies analyze the ability to produce nano-foams in thicker films necessary for this translation. Krausser et al. and Aher et al. both used a two-step, solid-state foaming technique and the high T_g effect described previously to create flat thick films of PEI.[53,54] Thick films of nanoporous PMMA, while currently unachievable, provoke curiosity in scientists through a wide number of studies. BASF patented a one-step, batch foaming process that achieves pore sizes between 40 and 150 nm, resulting in significant thermal conductivity improvement.[26,37] Ideally, an optimal industrial system would utilizes a continuous method of foaming, resulting in homogenous nanoporous foams of scales less than 100 nm and high porosity using inexpensive materials. Currently, PMMA is the most likely candidate for commercialization due to its low cost and high CO_2 solubility. The main competition that nano-foams currently face on the market are vacuum insulation panels and aerogels. Vacuum insulation panels (VIPs) achieve thermal conductivity of 3 to 4 mW/mK, currently lower than applicable nanofoams, but these systems lack the ease of installation afforded to nanofoams. Aerogels achieve thermal conductivity levels of 13

mW/mK, similar to that achieved by thin film nanofoams. The production of nanofoams on a large scale could offer a solution to the high production cost that currently plague the aerogel field.

2.4 Polymers in Phase Change Materials

2.4.1 Fundamentals of phase change materials

Latent heat storage systems (LHSSs) comprise a unique use of advanced materials with significant energy waste reduction potential. Research on LHSSs occurred as early as the 1960's, but are now becoming more common in home insulation systems.[55] Common heat storage systems include phase change materials (PCM). These systems use the endothermic energy transitions that occur when melting crystals to absorb and store energy effectively in the form of heat. Recrystallization upon cooling releases the thermal energy into the surrounding environment.[56] A variety of different areas of home insulation incorporate PCMs, e.g., active building systems, passive systems, and thermal comfort control. The greatest interest lies in passive systems due to the lower cost of implementation while maintaining energy savings and decreasing reliance on human monitoring/control.[57] Passive PCM systems use only the physical properties of the material to absorb energy rather than employ a secondary cooling system. Incorporating these systems into the walls, floors, and ceilings of buildings result in the most effective energy management.[58]

Both organic and inorganic chemicals comprise PCMs and selection for each application is based on their transition temperature and stability. Hundreds of different PCM materials make up this field with melting temperatures ranging from -100 to 800

°C. Materials with melting points near room temperature represent the focus of research in building applications.[58] Paraffins (n-alkane chains) and fatty acids comprise the most common organic materials due to their low cost and large range of working temperatures. Inorganic PCMs consist of salt hydrates, such as $K_2HPO_4 \cdot 6H_2O$, which exhibits better thermal conductivity in comparison to their organic counterparts and benefit from improved flame resistance and higher heat storage capacity. Unfortunately, significant disadvantages for their use result from large supercooling and phase segregation.[56] The one pitfall of developing PCMs for industrial applications comes from transition of the material into a liquid. This transition imparts the necessity to develop leak-proof packaging. Current technology involves specially designed pouches and envelopes that trap the PCMs with a macroencapsulation technique demonstrated in **Figure 2.9**.[56] Incorporation of these systems into passive building applications showed positive results in the decreased temperature variation within the test homes resulting in lower energy loss, demonstrating their effectiveness.[59] Unfortunately, like VIPs, macroencapsulated envelopes require protection from punctures, which result in leaking during the phase change.

Another method of storing PCMs, known as microencapsulation, coats small spheres

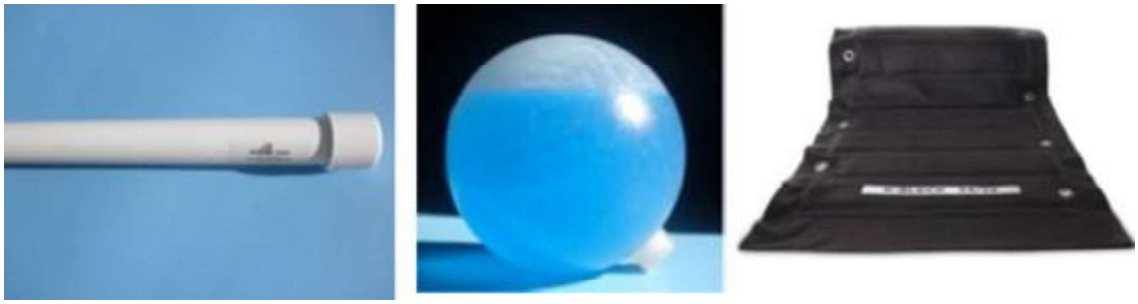

Figure 2.9. Commercial macroencapsulation systems for PCMs. Reprinted with permission.[56] 2015, Energy and Buildings.

of the PCM in a hard layer of polymer. These microcapsules increase the surface area to absorb heat and withstand volume changes. BASF produces these commercially and promotes the ability to incorporate them into a variety of construction materials, such as Gypsum board, which facilitates implementation.[60,61] While macroencapsulated PCMs require puncture protection, microencapsulated systems do not. The formation of solid-solid phase change materials represents a unique area of PCM that only recently gained attention. This field utilizes microphase separated block copolymers that exhibit phase transitions associated with heat storage without flow of the material. This area is currently limited by low heat storage capabilities relative to industry standards.

2.4.2 Microencapsulation of Phase Change Materials

Passive microencapsulated phase change materials demonstrate a major development in thermal energy storage and are becoming more popular in the construction sector. Current methods of implementation into homes rely on macro- and microencapsulation of a small molecule PCMs. The benefits of microencapsulated systems far outweigh the current macroencapsulated PCMs. There are five major methods of developing microencapsulated systems: interfacial polymerization, emulsion polymerization, *in-situ* polymerization, spray drying, and coacervation. Each method requires the use of certain polymer structures as well as specific physical properties to achieve the core-shell architecture.

2.4.2.1 Interfacial Polymerization

Interfacial polymerization creates an oil-water emulsion of the monomers/prepolymers and separates the two types of monomers into the separate phases

to prevent uncontrolled polymerization. [62,63] Typically, the oil layer contains the phase change material, a non-polar monomer, and a surfactant used to stabilize the emulsion of the two phases. In contrast, the aqueous layer contains the secondary polar monomer. This emulsion creates oil droplets that polymerize at the interface between the two phases resulting in the formation of a shell around the PCM. PU comprise the primary shells used in interfacial polymerization. [64] Jun-Feng et al. developed PU microencapsulated n-octadecane through interfacial polymerization. Diethylentriamine's high polarity and hydrogen bonding enabled use as the water-soluble monomer, and toluene 2,4-diisocyanates are the hydrophobic candidate for the oil-soluble monomer. This achieved microencapsulated PCM with an average diameter range of 5-10 μm.[62] More recently, Castro et. al used mini-emulsion interfacial polymerization to create a PU shell around n-docosane. The system utilized a poly(vinyl alcohol) stabilizer with a homogenizer to achieve very small droplets of oil inside the shell.[65] Aside from the synthetic restrictions of this polymerization technique, the high elastic properties, strength, and ability to achieve a smooth shell surface make PUs good shell candidates. Also tailoring the mechanical properties with various hard and soft segments allows for unique tunability of the final product.[66]

2.4.2.2 In-situ polymerization

In-situ polymerization varies from the interfacial polymerization since the monomers remain within the aqueous phase, while the phase change materials are in the oil phase. Formation of the microcapsules occurs through the stabilization of the PCM droplet in the presence of a negatively charged surfactant. Adding positively charged pre-polymer

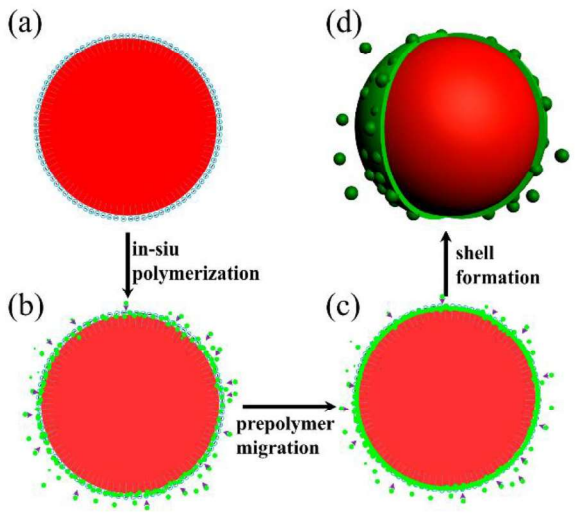

Figure 2.10. Illustration of microencapsulation through in-situ polymerization. A) formation of stable PCM oil droplets with surfactant B) pre-polymer association around droplet C) crosslinking/polymerization of the polymer D) final microcapsule. Adapted with permission.[68] 2018, Polymers.

results in association around the stabilized droplets. Finally, heating initiates polymerization to form the shell.[67] This process is illustrated in a general schematic in **Figure 2.10**.[68] Common reactions for this technique include urea-formaldehyde (U-F) or maleimine-formaldehyde (M-F) polycondensation.[69,70] The availability of nitrogen atoms allows the conversion of the monomer to a positive charge through the adjustment of the solution pH, enabling the association to the surfactant. These combinations of monomers form network structures, creating a chemically crosslinked shell around the PCM. Jin et al. used *in-situ* polymerization to form <10 μm microcapsules of paraffin employing a U-F shell.[70] Unfortunately, industry limits the use of these resins due to concerns over the toxic properties of formaldehyde and its potential release during the aging of U-F networks. The lower health risks associated with PUs and M-F polymer networks encouraged their use as safer options. A wide range of PU-based monomers can be considered as alternatives since they contain the necessary basic atoms for easy charge placement. Recent work revealed that stabilization of *in-situ* polymerization can occur

through the use of SiO_2 particles to create a pickering emulsion.[69] Other studies in this area focused on the enhancement of thermal stability and permeability resistance of these microcapsules utilizing comb-like polymers inside the core of the microcapsule rather than small molecule oils. Unfortunately, the use of the comb-like polymers resulted in too significant of a decrease in the enthalpy of fusion relative to the small molecule analogs, even though the thermal stability improved greatly.[68]

2.4.2.3 Emulsion polymerization

Emulsion/suspension polymerization, while very similar to an interfacial polymerization, differs through the employment of chain-growth monomers. In this method, the oil phase includes both non-polar vinyl monomers and PCM, and the emulsification of the oil phase in the aqueous phase creates the small droplets. The phase location of the initiator varies depending on the requirements of the system. During polymerization, the polymer begins to precipitate from the oil phase and deposit at the interface of the droplet, creating the shell.[71] Different derivatives of acrylates traditionally comprise the polymers for this application. A large variety of paraffin waxes utilize PMMA as a shell material making it currently the most commonly used polymer. In order to enhance the mechanical properties, reduce leaks, and smooth the surface of the spherical shells, researchers utilize a variety of crosslinking agents.[72] Initiation occurs using heat or UV-irradiation to create a radical and propagate through the vinyl groups of the monomers. The work done by Refat et al. with a benzoyl peroxide initiator, demonstrate the utility of thermal initiation, but other factors, such as high cost, long times, and polymer degradation limit use. Both Wang et al. and Ma et al. studied instead UV-active initiators in the microencapsulation of paraffin with PMMA and discovered

this technique achieves a smooth shell with a diameter of 0.2 μm.[61,73] Capsules by Ma et al. showed good thermal stability when incorporated into gypsum boards. This technique demonstrates utility in the creation of PS shells with crosslinking agents, such as divinyl benzene, and a large variety of PCMs. The unique hydrophilic nature of poly(ethylene glycol) (PEG) inhibits its encapsulation through this method.[74,75]

2.4.2.4 Spray drying

The methods discussed thus far all result from concurrent polymerization and encapsulation of the PCM. The processes of spray drying results instead in microencapsulation after the synthesis of the polymer. Spray drying occurs by first creating a homogenous solution or stable suspension of polymer droplets and PCM in a good solvent. The carrier gas, such as nitrogen, atomizes the solution, forming tiny droplets that result in solid microcapsules after drying.[76] Borreguero et al. performed this technique in order to coat commercial paraffin, Rubitherm RT27, with a low-density polyethylene and ethyl vinyl acetate copolymer. This produces shells with increased uniformity and higher thermal stability than the PS microcapsules created through the suspension polymerization technique.[12] While a large body of work focuses on this technique in the pharmaceutical and food industry, its use in the microencapsulation of PCM only began recently.[76] Patents regarding this area are present but focus primarily on the use of emulsion polymerization technique.[56]

2.4.2.5 Coacervation

Other post-polymerization microencapsulation techniques include coacervation. This method incorporates the strong attraction between polyanions and polycations with phase separation to afford spherical aggregates. Emulsification of the PCM takes place in an aqueous solution of the neutralized polycation. Addition of the polyanion then occurs and subsequent lowering of the mixtures pH induces a positive charge on the polycation to result in electrostatic interaction between the oppositely charged polymers. This interaction neutralizes the charges affording phase separation in the oil layer enveloping the PCM droplets in a shell. [77] The unique ability of some natural polymers, such as gelatin and gum arabic, to easily convert from a charged to neutral state with a relatively small pH change enables their use in this technique.[77,78] Studies on polymers with variations in the number of charge sites along the backbone demonstrates the necessity to form strong ionic interactions. Introduction of crosslinks results in shells with better coverage, and scientists have considered the addition of crosslinking agents, such as formaldehyde, to improve shell coverage and create a more complete network.[78] The reduced universality of this method, in comparison to the previously described techniques, limits its use in industry, but the possible application of biorenewable materials makes it an area of interest. In all of these cases, the shell material exhibits minimal effects on the transition temperature of the PCM it encloses. Effects from the shell instead results from capsule size, as well as the amount of PCM, which plays a role in the energy absorbed by the system.[77]

2.4.3 Solid-Solid Phase Change Materials

In a few cases, scientists studied the application of polymers for use directly as the active phase change material rather than as an encapsulation material. This limited number of studies reflects the lower enthalpy of fusion (ΔH_f) during the melt transition, which directly influences the energy storage properties of the materials. The lower ΔH_f results from a higher number of imperfections within the crystal growth of polymers. Difficulty also arises due to the large difference between the crystallization and melting temperature (supercooling) as well as the limitation due to the fact that few polymers possess melting points within the working temperatures of a home. Poly(ethylene glycol) demonstrates one of the few polymers that can be utilized for these types of application as a result of its high ΔH_f (>150 kJ/kg) and melting/crystallization temperatures within the working range of a traditional PCM.[79,80] This enthalpy value is comparable to traditional organic molecules, which on average exhibit latent heat values of 190 kJ/kg.[81] Benefits from the utilization of polymers as PCMs arise from the higher thermal stability and enhanced mechanical stability in comparison to a small molecule.

The largest benefit from polymer-based PCMs arise through the development of solid-solid phase change materials (SSPCM). These types of PCMs exploit crosslinking (physical/chemical) to create a network that provides dimensional stability, even as the active PCM segment melts. Covalent bonding of the PCM to the crosslinked matrix differentiates these from composite materials. Initial studies into the development of these systems focused on the crosslinking of PEG with a urethane matrix. Li et al. studied the crosslinking of PEG (M_n=10,000 g/mol) with 4,4′-diphenylmethane diisocyanate (MDI) and pentaerythritol (PE) to create a solid-solid phase change material (**Scheme 2.1**). The group discovered that as they restricted the mobility of the PEG chains through

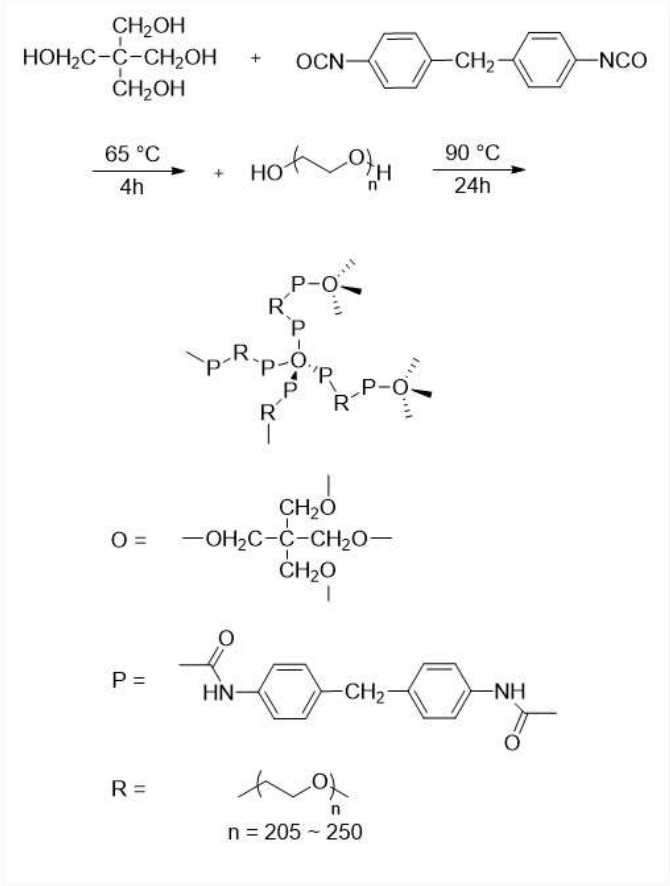

Scheme 2.1. Synthesis of a polyethylene glycol containing solid-solid phase change material. Adapted from Li et al.[82]

crosslinking, a reduction of the ΔH_f from 189 kJ/kg to 153 kJ/kg occurs. This reduction stems from the restricted motion in the PEG chains, which limits crystallization and lowers the total energy adsorption possible.[82] Even so, this value demonstrates a marked improvement over previously reported SSPCM that employed a physically crosslinked hard-soft segmented block copolymer. In this research, the segmented polymer, comprised of a PEG soft segment and PU hard segment, observed a reduction in the ΔH_f to 139 kJ/kg and a reduction in the size of the spherulites. This indicated that the hard segment restricted the growth of crystalline domains.[83]

Cao et al. in 2017 even demonstrated that reducing hydrogen bonding between the soft and hard segments through chain extension with N-methyldiethanolamine only

afforded a maximum ΔH_f 140 kJ/kg relative to 180 kJ/kg achieved by the PEG homopolymer.[84] Other architectures, such as utilizing hyperbranched polymers as the mechanically stabilizing component, still resulted in significant loss of ΔH_f . Du et al in 2017, developed a hyperbranched polyol with a 2,2'-bishydroxymethyl propionic acid chain extender and PEG as the core molecule. This unique system still only achieved a ΔH_f of about 120 kJ/kg.[85] Further study of hyperbranched systems by Sundararajan et al., afforded an increase in the ΔH_f to 146 kJ/kg through the use of PEG in the arms of the hyperbranched structure rather than in the core. The groups utilized a $A_2 + B_3$ approached in which PEG, terminated with an isocyanate moiety, acted as the branching unit.[86] Chen et al. extensively compared current PU-PEG based SSPCMs and demonstrated that in most cases the polymer only maintained 80% of the original enthalpy value after bonding the PCM to the polymer matrix.[87]

The major issue observed with these types of SSPCMs results from the lower volume of PEG per volume of the total material in comparison to the homopolymer of PEG, through the introduction of additional monomers. The maximization of the volume of PCM within the total material exhibits beneficial improvements to the overall adsorption of energy. In an effort to maximize this volume, researchers moved to the area of brush and graft polymers, in which a superior volume of PCM is achieved in comparison to other polymer components. These experiments primarily utilize different derivatives of PEG reacted with chain-growth-based polymer backbones or monomers. Xi et al. designed one example of these polymers by synthesizing a methacrylic monomer derivatized with a PEG tail. A highly reactive isocyanate group (2,4-toluenediisocyante) linked the varying molecular weights of PEG monomethyl ether (MPEG) and N-

hydroxymethylacrylamide. Copolymerization then occurred between the novel monomer and styrene through free radical polymerization. Unfortunately, since this material relied on styrene incorporation to stabilize the mechanical properties, specifically requiring a ratio of 1:2 PEG:PS to maintain the solid-solid transition. As a result, a reduction in the ΔH_f occurred in comparison to the matrix based systems (109 kJ/kg).[88] Sari et al. improved upon this system by grafting directly to PS and utilizing a higher molecular weight PEG. This grafting process occurred through the bromination of PS at different weight % bromine then performing a copper-mediated nucleophilic aromatic substitution

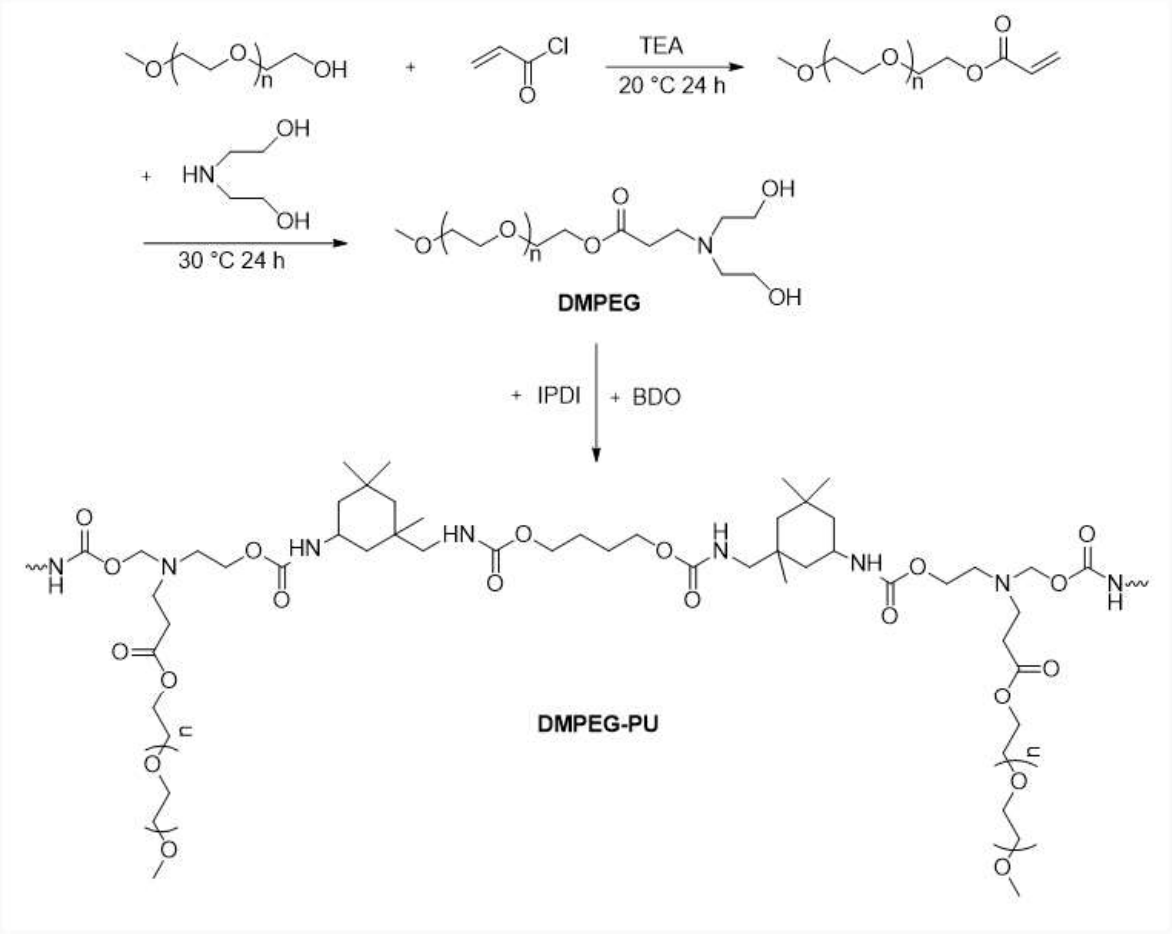

Scheme 2.2. Synthesis a novel solid–solid phase change material with a comb-PU block copolymer structure. Adapted from Du et al.[90]

with PEG (M_n = 6,000 g/mol). The ΔH_f was significantly improved as the wt % PEG increased. At the highest concentration of brominated styrene (1:1 wt% styrene:brominated styrene), the grafted polymer achieved a ΔH_f values (180 kJ/kg) comparable to the homopolymer of PEG.[89] The development of grafted PCMs occurred as well using step-growth polymerization. Du et al. studied the synthesis of a PU-based brush copolymer utilizing a novel diol monomer, diethanolamine modified monomethoxy PEG (**Scheme 2.2**). The higher restriction of chain mobility due to hydrogen bonding in these polymers resulted in a lower ΔH_f value of 123 kJ/kg.[90] Aside from relying on PEG as the PCM in these novel polymeric materials, analysis of other long alkane chain compounds occurred. Two examples include octadecanol and palmitic acid grafted to polymer backbones. The restriction of mobility through attachment to the backbone of a polymer impacted these low molecular weight compounds greater than PEG resulting in severe drops of the ΔH_f.[91,92]

2.5 Conclusion

Advanced applications of polymeric materials show great promise to further energy reduction and inherently CO_2 emissions in the building sector. The key to scientific improvement and large-scale application in these two fields includes understanding the limitations and necessary areas of growth. Nanoporous foams demonstrated that CO_2 solubility and the T_g drastically impact the ability to achieve small pore size and low density. Synthesis of novel polymers with the specific intent to control these two factors demonstrates the next step to expanding the working range of polymers that achieve nanoporous foams. Microencapsulation technologies of phase change materials

demonstrate that wide varieties of polymers may be utilized in the development of shells. The focus of current and future work includes the development of solid-solid phase change materials. Placing more focus on improving the energy adsorption of these materials must occur in order to achieve comparable materials to the current microencapsulation technologies. Such synthetic studies should consider the phase separation of the active PCM and crosslinking segment in an attempt to reduce restrictions of the crystallizable group. The successful design of these materials will greatly increase the rate at which PCMs become common in commercial building materials. Further studies into polymers for both of these applications substantially aid in the efforts toward decreasing greenhouse gas emissions.

References

(1) Kaklauskas, A.; Pacheco Torgal, F.; Grafakos, S.; Lapinskiene, V., In *Nearly Zero Energy Building Refurbishment*; Pacheco Torgal, F., Mistretta, M., Kaklauskas, A., Granqvist, C. G., Cabeza, L. F., Eds.; Springer London: 2013, p 61.

(2) Gao, Y.; Gao, X.; Zhang, X., The 2 °C Global Temperature Target and the Evolution of the Long-Term Goal of Addressing Climate Change—From the United Nations Framework Convention on Climate Change to the Paris Agreement, *Engineering* **2017**, *3*, 272.

(3) Office of, S.; Technology, P. *First State of the Carbon Cycle Report (SOCCR): North American Carbon Budget and Implications for the Global Carbon Cycle : U.S. Climate Change Science Program: Synthesis and Assessment Products;2007 ASI 426-1.3;Synthesis and Assessment Product 2.2*, 2007.

(4) Lechtenböhmer, S.; Schüring, A., The potential for large-scale savings from insulating residential buildings in the EU, *Energy Efficiency* **2011**, *4*, 257.

(5) Thiers, S.; Peuportier, B., Energy and environmental assessment of two high energy performance residential buildings, *Building and Environment* **2012**, *51*, 276.

(6) Trubiano, F., *Design and construction of high-performance homes: building envelopes, renewable energies and integrated practice*; Routledge: Abingdon, Oxon [England]; New York, NY, 2013.

(7) Nowakowski, P., In *Universal Access in Human-Computer Interaction. Intelligent and Ubiquitous Interaction Environments*; Stephanidis, C., Ed.; Springer Berlin Heidelberg: 2009; Vol. 5615, p 100.

(8) Ebert, H.-P., In *Nearly Zero Energy Building Refurbishment*; Pacheco Torgal, F., Mistretta, M., Kaklauskas, A., Granqvist, C. G., Cabeza, L. F., Eds.; Springer London: 2013, p 457.
(9) Jelle, B. P., Traditional, state-of-the-art and future thermal building insulation materials and solutions – Properties, requirements and possibilities, *Energy and Buildings* **2011**, *43*, 2549.
(10) Asdrubali, F.; D'Alessandro, F.; Schiavoni, S., A review of unconventional sustainable building insulation materials, *Sustainable Materials and Technologies* **2015**, *4*, 1.
(11) Cuce, E.; Cuce, P. M.; Wood, C. J.; Riffat, S. B., Toward aerogel based thermal superinsulation in buildings: A comprehensive review, *Renewable and Sustainable Energy Reviews* **2014**, *34*, 273.
(12) Borreguero, A. M.; Valverde, J. L.; Rodríguez, J. F.; Barber, A. H.; Cubillo, J. J.; Carmona, M., Synthesis and characterization of microcapsules containing Rubitherm®RT27 obtained by spray drying, *Chemical Engineering Journal* **2011**, *166*, 384.
(13) Zhang, C.; Zhu, B.; Li, D.; Lee, L. J., Extruded polystyrene foams with bimodal cell morphology, *Polymer* **2012**, *53*, 2435.
(14) Cabeza, L.; Fernández, A. I., In *Nearly Zero Energy Building Refurbishment*; Pacheco Torgal, F., Mistretta, M., Kaklauskas, A., Granqvist, C. G., Cabeza, L. F., Eds.; Springer London: 2013, p 537.
(15) Torgal, F. P., *Nanotechnology in eco-efficient construction*; Woodhead Publishing Limited: Cambridge, UK; Philadelphia, PA, 2013.
(16) Ziman, J. M., *Principles of the theory of solids*; University Press: Cambridge [Eng.], 1972; Vol. 2d.
(17) Incropera, F. P., *Introduction to heat transfer*; Wiley: Hobokenm NJ, 2007; Vol. 5th.
(18) Powell, R. W.; Ho, C. Y.; Liley, P. E., *Thermal conductivity of selected materials*; U.S. Dept. of Commerce, National Bureau of Standards; for sale by the Superintendent of Documents, U.S. Govt. Print. Off: Washington, 1966.
(19) Gibson, L. J.; Ashby, M. F., *Cellular solids : structure and properties*; 2nd ed. ed.; Cambridge University Press: Cambridge ;, 1997.
(20) Papadopoulos, A. M., State of the art in thermal insulation materials and aims for future developments, *Energy and Buildings* **2005**, *37*, 77.
(21) Vo, C. V.; Bunge, F.; Duffy, J.; Hood, L., Advances in Thermal Insulation of Extruded Polystyrene Foams, *Cellular Polymers* **2011**, *30*, 137.
(22) Jelle, B. P.; Gustavsen, A.; Baetens, R., The path to the high performance thermal building insulation materials and solutions of tomorrow, *Journal of Building Physics* **2010**, *34*, 99.
(23) Rousseau, E.; Siria, A.; Jourdan, G.; Volz, S.; Comin, F.; Chevrier, J.; Greffet, J.-J., Radiative heat transfer at the nanoscale, *Nature Photonics* **2009**, *3*, 514.
(24) Notario, B.; Pinto, J.; Solorzano, E.; de Saja, J. A.; Dumon, M.; Rodríguez-Pérez, M. A., Experimental validation of the Knudsen effect in nanocellular polymeric foams, *Polymer* **2015**, *56*, 57.
(25) Costeux, S., CO2-blown nanocellular foams, *Journal of Applied Polymer Science* **2014**, *131*, n/a.

(26) Forest, C.; Chaumont, P.; Cassagnau, P.; Swoboda, B.; Sonntag, P., Polymer nano-foams for insulating applications prepared from CO2 foaming, *Progress in Polymer Science* **2015**, *41*, 122.
(27) Ruiz, J. A. R.; Pedros, M.; Tallon, J.-M.; Dumon, M., Micro and nano cellular amorphous polymers (PMMA, PS) in supercritical CO2 assisted by nanostructured CO2-philic block copolymers – One step foaming process, *The Journal of Supercritical Fluids* **2011**, *58*, 168.
(28) Pinto, J.; Reglero-Ruiz, J. A.; Dumon, M.; Rodriguez-Perez, M. A., Temperature influence and CO2 transport in foaming processes of poly(methyl methacrylate)–block copolymer nanocellular and microcellular foams, *The Journal of Supercritical Fluids* **2014**, *94*, 198.
(29) Guo, H.; Nicolae, A.; Kumar, V., Solid-state microcellular and nanocellular polysulfone foams, *Journal of Polymer Science, Part B: Polymer Physics* **2015**, *53*, 975.
(30) Bernardo, V.; Martín-de León, J.; Rodríguez-Pérez, M. A., Production and characterization of nanocellular polyphenylsulfone foams, *Material Letters* **2016**, *178*, 155.
(31) Miller, D.; Chatchaisucha, P.; Kumar, V., Microcellular and nanocellular solid-state polyetherimide (PEI) foams using sub-critical carbon dioxide I. Processing and structure, *Polymer* **2009**, *50*, 5576.
(32) Krause, B.; Sijbesma, H. J. P.; Münüklü, P.; van der Vegt, N. F. A.; Wessling, M., Bicontinuous Nanoporous Polymers by Carbon Dioxide Foaming, *Macromolecules* **2001**, *34*, 8792.
(33) Pinto, J.; Notario, B.; Verdejo, R.; Dumon, M.; Costeux, S.; Rodriguez-Perez, M. A., Molecular confinement of solid and gaseous phases of self-standing bulk nanoporous polymers inducing enhanced and unexpected physical properties, *Polymer* **2017**, *113*, 27.
(34) Syurik, J.; Schwaiger, R.; Sudera, P.; Weyand, S.; Johnsen, S.; Wiegand, G.; Holscher, H., Bio-inspired micro-to-nanoporous polymers with tunable stiffness, *Beilstein Journal of Nanotechnology* **2017**, *8*, 906.
(35) Wen, N.; Lei, Y. J.; Luo, S. K., Porous Structural Transformation from Closed Microcellular to Bicontinuous Nanoporous Based on Poly(phthalazinone ether sulfone ketone) Containing Biphenyl Moieties by Carbon Dioxide Foaming, *Industrial & Engineering Chemistry Research* **2018**, *57*, 4721.
(36) Lopez-Periago, A. M.; Domingo, C., Features of supercritical CO2 in the delicate world of the nanopores, *Journal of Supercritical Fluids* **2018**, *134*, 204.
(37) Sandler, J. K. W.; Francis, T.; Lopes, P. M. S., Nanoporous polymer foams. US 8529808 B2, September 10, 2013.
(38) Kazarian, S. G.; Vincent, M. F.; Bright, F. V.; Liotta, C. L.; Eckert, C. A., Specific Intermolecular Interaction of Carbon Dioxide with Polymers, *Journal of American Chemical Society* **1996**, *118*, 1729.
(39) Ewing, A. V.; Gabrienko, A. A.; Semikolenov, S. V.; Dubkov, K. A.; Kazarian, S. G., How Do Intermolecular Interactions Affect Swelling of Polyketones with a Differing Number of Carbonyl Groups? An In Situ ATR-FTIR Spectroscopic Study of CO2 Sorption in Polymers, *The Journal of Physical Chemistry C* **2015**, *119*, 431.

(40) Tomasko, D. L.; Li, H.; Liu, D.; Han, X.; Wingert, M. J.; Lee, L. J.; Koelling, K. W., A Review of CO2 Applications in the Processing of Polymers, *Industrial & Engineering Chemistry Research* **2003**, *42*, 6431.
(41) Guo, H.; Nicolae, A.; Kumar, V., Solid-state poly(methyl methacrylate) (PMMA) nanofoams. Part II: Low-temperature solid-state process space using CO2 and the resulting morphologies, *Polymer* **2015**, *70*, 231.
(42) Zirkel, L.; Jakob, M.; Münstedt, H., Foaming of thin films of a fluorinated ethylene propylene copolymer using supercritical carbon dioxide, *The Journal of Supercritical Fluids* **2009**, *49*, 103.
(43) Ruiz, J. A. R.; Cloutet, E.; Dumon, M., Investigation of the nanocellular foaming of polystyrene in supercritical CO2 by adding a CO2-philic perfluorinated block copolymer, *Journal of Applied Polymer Science* **2012**, *126*, 38.
(44) Costeux, S.; Jeon, H. K.; Bunker, S. P.; Khan, I., Nanocellular Foams from Acrylic Polymers: Experiments and Modeling, *FOAMS 2012 conference (Barcelona)* **2012**.
(45) Zhou, C.; Vaccaro, N.; Sundarram, S. S.; Li, W., Fabrication and characterization of polyetherimide nanofoams using supercritical CO2, *Journal of Cellular Plastics* **2012**, *48*, 239.
(46) Notario, B.; Pinto, J.; Rodriguez-Perez, M. A., Nanoporous polymeric materials: A new class of materials with enhanced properties, *Progress in Materials Science* **2016**, *78–79*, 93.
(47) Costeux, S.; Bunker, S. P.; Jeon, H. K., Homogeneous nanocellular foams from styrenic-acrylic polymer blends, *Journal of Materials Research* **2013**, *28*, 2351.
(48) Yokoyama, B. H.; Li, L.; Nemoto, T.; Sugiyama, K., Tunable Nanocellular Polymeric Monoliths Using Fluorinated Block Copolymer Templates and Supercritical Carbon Dioxide, *Advanced Materials* **2004**, *16*, 1542.
(49) Yokoyama, H.; Sugiyama, K., Nanocellular Structures in Block Copolymers with CO2-philic Blocks Using CO2 as a Blowing Agent: Crossover from Micro- to Nanocellular Structures with Depressurization Temperature, *Macromolecules* **2005**, *38*, 10516.
(50) Forest, C.; Chaumont, P.; Cassagnau, P.; Swoboda, B.; Sonntag, P., Generation of nanocellular foams from ABS terpolymers, *European Polymer Journal* **2015**, *65*, 209.
(51) Wang, G. L.; Zhao, J. C.; Mark, L. H.; Wang, G. Z.; Yu, K. J.; Wang, C. D.; Park, C. B.; Zhao, G. Q., Ultra-tough and super thermal-insulation nanocellular PMMA/TPU, *Chemical Engineering Journal* **2017**, *325*, 632.
(52) Pinto, J.; Morselli, D.; Bernardo, V.; Notario, B.; Fragouli, D.; Rodriguez-Perez, M. A.; Athanassiou, A., Nanoporous PMMA foams with templated pore size obtained by localized in situ synthesis of nanoparticles and CO2 foaming, *Polymer* **2017**, *124*, 176.
(53) Krause, B.; Mettinkhof, R.; van der Vegt, N. F. A.; Wessling, M., Microcellular Foaming of Amorphous High-Tg Polymers Using Carbon Dioxide, *Macromolecules* **2001**, *34*, 874.
(54) Aher, B.; Olson, N. M.; Kumar, V., Production of bulk solid-state PEI nanofoams using supercritical CO2, *Journal of Materials Research* **2013**, *28*, 2366.

(55) Schröder, J.; Gawron, K., Latent heat storage, *International Journal of Energy Research* **1981**, *5*, 103.
(56) Kalnæs, S. E.; Jelle, B. P., Phase change materials and products for building applications: A state-of-the-art review and future research opportunities, *Energy and Buildings* **2015**, *94*, 150.
(57) Chen, X.; Yang, H.; Lu, L., A comprehensive review on passive design approaches in green building rating tools, *Renewable & Sustainable Energy Reviews* **2015**, *50*, 1425.
(58) Cabeza, L. F.; Castell, A.; Barreneche, C.; de Gracia, A.; Fernández, A. I., Materials used as PCM in thermal energy storage in buildings: A review, *Renewable and Sustainable Energy Reviews* **2011**, *15*, 1675.
(59) Muthuvel, S.; Saravanasankar, S.; Sudhakarapandian, R.; Muthukannan, M., Passive cooling by phase change material usage in construction, *Building Services Engineering Research & Technology* **2015**, *36*, 411.
(60) Tyagi, V. V.; Kaushik, S. C.; Tyagi, S. K.; Akiyama, T., Development of phase change materials based microencapsulated technology for buildings: A review, *Renewable and Sustainable Energy Reviews* **2011**, *15*, 1373.
(61) Ma, S.; Song, G.; Li, W.; Fan, P.; Tang, G., UV irradiation-initiated MMA polymerization to prepare microcapsules containing phase change paraffin, *Solar Energy Materials and Solar Cells* **2010**, *94*, 1643.
(62) Su, J.-F.; Wang, L.-X.; Ren, L., Synthesis of polyurethane microPCMs containing n-octadecane by interfacial polycondensation: Influence of styrene-maleic anhydride as a surfactant, *Colloids and Surfaces A: Physicochemical and Engineering Aspects* **2007**, *299*, 268.
(63) Torini, L.; Argillier, J. F.; Zydowicz, N., Interfacial Polycondensation Encapsulation in Miniemulsion, *Macromolecules* **2005**, *38*, 3225.
(64) Tseng, Y. H.; Fang, M. H.; Tsai, P. S.; Yang, Y. M., Preparation of microencapsulated phase-change materials (MCPCMs) by means of interfacial polycondensation, *Journal of Microencapsulation* **2005**, *22*, 37.
(65) De Castro, P. F.; Shchukin, D. G., New Polyurethane/Docosane Microcapsules as Phase-Change Materials for Thermal Energy Storage, *Chemistry-a European Journal* **2015**, *21*, 11174.
(66) Costa, V.; Nohales, A.; Félix, P.; Guillem, C.; Gutiérrez, D.; Gómez, C. M., Structure–property relationships of polycarbonate diol-based polyurethanes as a function of soft segment content and molar mass, *Journal of Applied Polymer Science* **2015**, *132*, n/a.
(67) Brownt, E. N.; Kessler, M. R.; Sottos, N. R.; White, S. R., In situ poly(urea-formaldehyde) microencapsulation of dicyclopentadiene, *Journal of Microencapsulation* **2003**, *20*, 719.
(68) Li, W.; Geng, X. Y.; Huang, R.; Wang, J. P.; Wang, N.; Zhang, X. X., Microencapsulated Comb-Like Polymeric Solid-Solid Phase Change Materials via In-Situ Polymerization, *Polymers* **2018**, *10*.
(69) Yin, D.; Liu, H.; Ma, L.; Zhang, Q., Fabrication and performance of microencapsulated phase change materials with hybrid shell by in situ polymerization in Pickering emulsion, *Polymers for Advanced Technology* **2015**, *26*, 613.

(70) Jin, Z.; Wang, Y.; Liu, J.; Yang, Z., Synthesis and properties of paraffin capsules as phase change materials, *Polymer* **2008**, *49*, 2903.
(71) Al Shannaq, R.; Farid, M. M., In *Advances in Thermal Energy Storage Systems*; Cabeza, L. F., Ed.; Woodhead Publishing: 2015, p 247.
(72) Al-Shannaq, R.; Farid, M.; Al-Muhtaseb, S.; Kurdi, J., Emulsion stability and cross-linking of PMMA microcapsules containing phase change materials, *Solar Energy Materials and Solar Cells* **2015**, *132*, 311.
(73) Wang, Y.; Shi, H.; Xia, T. D.; Zhang, T.; Feng, H. X., Fabrication and performances of microencapsulated paraffin composites with polymethylmethacrylate shell based on ultraviolet irradiation-initiated, *Materials Chemistry and Physics.* **2012**, *135*, 181.
(74) Sánchez, L.; Sánchez, P.; de Lucas, A.; Carmona, M.; Rodríguez, J., Microencapsulation of PCMs with a polystyrene shell, *Colloid and Polymer Science* **2007**, *285*, 1377.
(75) Sari, A.; Alkan, C.; Doguscu, D. K.; Bicer, A., Micro/nano-encapsulated n-heptadecane with polystyrene shell for latent heat thermal energy storage, *Solar Energy Materials and Solar Cells* **2014**, *126*, 42.
(76) Hawlader, M. N. A.; Uddin, M. S.; Khin, M. M., Microencapsulated PCM thermal-energy storage system, *Applied Energy* **2003**, *74*, 195.
(77) Bayés-García, L.; Ventolà, L.; Cordobilla, R.; Benages, R.; Calvet, T.; Cuevas-Diarte, M. A., Phase Change Materials (PCM) microcapsules with different shell compositions: Preparation, characterization and thermal stability, *Solar Energy Materials and Solar Cells* **2010**, *94*, 1235.
(78) Onder, E.; Sarier, N.; Cimen, E., Encapsulation of phase change materials by complex coacervation to improve thermal performances of woven fabrics, *Thermochimica Acta* **2008**, *467*, 63.
(79) Chen, C.; Liu, W.; Wang, H.; Peng, K., Synthesis and performances of novel solid–solid phase change materials with hexahydroxy compounds for thermal energy storage, *Applied Energy* **2015**, *152*, 198.
(80) Andriamitantsoa, R. S.; Dong, W. J.; Gao, H. Y.; Wang, G., PEG encapsulated by porous triamide-linked polymers as support for solid-liquid phase change materials for energy storage, *Chemical Physics Letters* **2017**, *671*, 165.
(81) Farid, M. M.; Khudhair, A. M.; Razack, S. A. K.; Al-Hallaj, S., A review on phase change energy storage: materials and applications, *Energy Conversion Management* **2004**, *45*, 1597.
(82) Li, W.; Ding, E., Preparation and characterization of cross-linking PEG/MDI/PE copolymer as solid–solid phase change heat storage material, *Solar Energy Materials and Solar Cells* **2007**, *91*, 764.
(83) Su, J.; Liu, P., A novel solid–solid phase change heat storage material with polyurethane block copolymer structure, *Energy Conversion Management* **2006**, *47*, 3185.
(84) Cao, H. W.; Qi, F. X. Y.; Liu, R. W.; Wang, F. T.; Zhang, C. X.; Zhang, X. N.; Chai, Y. Y.; Zhai, L. L., The influence of hydrogen bonding on N-methyldiethanolamine-extended polyurethane solid-solid phase change materials for energy storage, *RSC Advances* **2017**, *7*, 11244.

(85) Du, X. S.; Wang, H. B.; Wu, Y.; Du, Z. L.; Cheng, X., Solid-solid phase-change materials based on hyperbranched polyurethane for thermal energy storage, *Journal of Applied Polymer Science* **2017**, *134*.
(86) Sundararajan, S.; Samui, A. B.; Kulkarni, P. S., Thermal Energy Storage Using Poly(ethylene glycol) Incorporated Hyperbranched Polyurethane as Solid-Solid Phase Change Material, *Industrial & Engineering Chemistry Research* **2017**, *56*, 14401.
(87) Chen, C.; Liu, W.; Wang, H.; Zhu, L., Synthesis and characterization of novel solid-solid phase change materials with a polyurethaneurea copolymer structure for thermal energy storage, *RSC Advances* **2016**, *6*, 102997.
(88) Xi, P.; Gu, X.; Cheng, B.; Wang, Y., Preparation and characterization of a novel polymeric based solid–solid phase change heat storage material, *Energy Conversion Management* **2009**, *50*, 1522.
(89) Sarı, A.; Alkan, C.; Biçer, A., Synthesis and thermal properties of polystyrene-graft-PEG copolymers as new kinds of solid–solid phase change materials for thermal energy storage, *Materials Chemistry and Physics* **2012**, *133*, 87.
(90) Du, X.; Wang, H.; Cheng, X.; Du, Z., Synthesis and thermal energy storage properties of a solid-solid phase change material with a novel comb-polyurethane block copolymer structure, *RSC Advances* **2016**, *6*, 42643.
(91) Shi, H.; Li, J.; Jin, Y.; Yin, Y.; Zhang, X., Preparation and properties of poly(vinyl alcohol)-g-octadecanol copolymers based solid–solid phase change materials, *Materials Chemistry and Physics* **2011**, *131*, 108.
(92) Sarı, A.; Alkan, C.; Biçer, A.; Karaipekli, A., Synthesis and thermal energy storage characteristics of polystyrene-graft-palmitic acid copolymers as solid–solid phase change materials, *Solar Energy Materials and Solar Cells* **2011**, *95*, 3195.

Chapter 3: Segmented Liquid Crystalline Copolyesters

(Published in *Liquid Crystalline Polymers,* Mittal, V., Ed.; Central West Publishing: Australia, 2018, p. 205)

Katherine V. Heifferon and Timothy E. Long

Macromolecules Innovation Institute, Department of Chemistry, Virginia Tech, Blacksburg, VA 24061

Keywords: liquid crystalline, polyesters, phase separated, segmented

3.1 Introduction

Over the last 30 years, the field of segmented liquid crystalline (LC) copolyesters expanded significantly. IUPAC defines segmented copolymers as "copolymers containing phase domains of microscopy or smaller size, with the domains constituted principally of single types of structural units".[1] The understanding of the expanse of polymer architectures and structures that facilitate phase separation into nanodomain morphologies experienced great growth since its inception along with the expansion of knowledge in the role that LC properties play in this phase separation. This chapter explores the synthesis and characterization of segmented liquid crystalline copolyesters, delving into the parameters required for phase separation and the impact of the domain morphology.

3.1.1 History of Polyesters

The first exploration and fundamental understanding of step-growth polymers began with the work of Carothers at DuPont in the 1930's. These studies began with the most well-known step-growth polymers, polyesters.[2,3] This work elucidated the fundamental processes of step-growth polymerization (condensation) through the intentional study of aliphatic polyesters. The authors identified important characteristics,

such as functionality, degree of polymerization, and conversion, among others. Unfortunately, these polymers remained unsuitable for commercialization due to low melting temperatures and other unfavorable properties like a sensitivity to hydrolysis.

In the 1940's, the introduction of a rigid aromatic monomer into the polymer backbone revealed stiffening in the polymer chains resulting in high melting temperature fibers. This polyester, synthesized from terephthalic acid and ethylene glycol and known as poly(ethylene terephthalate) (PET), pushed polyesters into commercialization. Further variation of ethylene glycol with a wide variety of aliphatic diols led to an extensive family of polymers.[4,5] Today, PET production encompasses 70 % of all PP&A (polyester, polyamide, and acrylic) fiber production and 7 % of the world's plastic.[6] The food packaging industry extensively uses PET in blow molded and biaxially oriented bottles, accounting for 30 % of its global demand.[7] Aside from the apparent usefulness of PETs semi-crystalline nature and rigidity, one of the major benefits arose from its recyclability back to the monomeric state. This depolymerization uses techniques, such as methanolysis, to break the polymer chain and reform oligomer/monomers. Reuse of these products in repolymerization represents a large field of study for companies, such as Eastman Chemical Company, DuPont, and Hoechst-Celanese Company.[8] As research of polyesters grew in the 1970's, exploration into a wide range of unique morphologies and structures provided the scientific community with block copolymers and liquid crystalline polyesters. The relevancy of the polyester field of chemistry continues to this day and demonstrates roots in a deep history of industrial development.

3.1.2 History of Liquid Crystalline Polymers

A liquid crystal refers to molecules that undergo an intermediate phase that lies between a solid and a liquid state. These molecules exhibit more order than an isotropic liquid but less than a 3-dimensional crystal structure and their presence in nature provides many unique and useful materials.[9] Friedrich Reinitzer, an Austrian botanist, first discovered liquid crystals while experimenting with cholesterol in 1888. Otto Lehmann (his collaborator) and Reintzer coined the term mesophase, after the Greek word mesos meaning intermediate, to represent this unique phase.[10] In 1922, Georges Freidel further presented a classification scheme for the three possible morphological phases of this state; nematic, smectic, and cholesteric phases.[11,12] Freidel's paper sealed the acceptance of liquid crystals in the scientific community, debunking previous contradictory articles. Further study of synthetic molecules confirmed that LC properties arose from small molecules comprised of rod- or disk-like shapes, or amphiphilic molecules exhibiting anisotropy in their structure.[11,13] Rod- and disk-shaped rigid molecules encompass the field of thermotropic LC molecules which induce the formation of a mesophase through thermal means. These materials exhibit a LC mesophase at temperatures above the melting point of the crystal structure (T_m). The isotropic temperature (T_i) represents the upper limit to the mesophase at which complete disorder occurs. Amphiphilic molecules transition into a mesophase through the dissolution of the molecule upon introduction of a solvent, termed lyotropic. While not the focus of this review, these materials intersect with many aspects of our daily lives, such as the dissolution of soap into water as well as in our cell membranes (dissolution of phospholipids in water). Small molecule LC's facilitated the development of a wide range of applications including LC displays in television, spatial light modulators, and temperature sensors.[14,15]

In 1956, Paul Flory hypothesized the ability to incorporate LC molecules into polymers.[16,17] Flory deemed the key parameters impacting LC properties as geometry and molecular structure utilizing lattice theories. This study proposed an aspect ratio (length/diameter) of 6 or greater was necessary for polymers to achieve LC properties. Utilizing this understanding of the aspect ratio, Dupont scientists developed one of the first commercialized polymeric LC, Kevlar, which exhibited lyotropic properties. Further study produced the first thermotropic LCPs from a select group of companies including Eastman-Kodak, Amoco, Dupont, and Celanese.[14,18] Thermotropic main-chain polymers excelled in industry due to the useful thermoplastic properties, such as shear thinning, high chemical and thermal resistance, low dielectric constants, and low moisture uptake.[14] During this time, main-chain LC structures took the form of fully-aromatic polymers (polyarylates) due to their high rigidity. Vectra®, poly(6-hydroxy-2-napthoic acid-co-4-hydroxybenzoic acid), emerged as one of the first LC polyesters, developed by Ticona/ Celanese, that achieved commercialization despite its high cost.[19] The primary uses of this polymer include electronic parts and high-performance fibers.[10] Eastman-Kodak also explored the reaction of p-acetoxybenzoic acid with PET to form the first aromatic-aliphatic copolyester exhibiting thermotropic properties.[10,20-22] As this field grew, the next logical scientific step became the synthesis of LC block copolymers which could incorporate LC properties into other polymers through phase separated morphologies.

3.1.3 History of Segmented Copolymers

Polyurethanes comprised many of the first reported phase separated copolymers.[23-25] These polymers formed segregated domains considered hard- and soft-segments that

impart stiffness from the physical crosslinking of the hard-block and elasticity from the flexibility of the soft-block. Poly(styrene-*b*-isoprene-*b*-styrene) demonstrates another widely studied thermoplastic elastomer synthesized through a more controlled anionic polymerization technique in the 1960's.[26,27] Most of these early works focused on eliminating macroscale phase separation but maintaining microscale phase separated domains utilizing a block copolymer architecture to impart physical properties from both polymeric units into the final polymer.

In the field of polyesters, the 1970's represented a boom in block copolymer research though it was DuPont's Hytrel (poly(oxytetramethylene)-*b*-poly(butylene terephthalate)) that eventually found commercial success as a thermoplastic elastomer.[28] Segmented copolymers rose to prominence in LC polymers as blend compatibilizers and mechanical property adaptors.[29,30] The advent of controlled polymerization techniques, such as anionic polymerization, enabled much smaller dispersity in block size opening the door for well-controlled morphologies including lamellae, hexagonal cylinders, bicontinuous gyroid, and body-centered cubic arrays of spherical micelles.[31] These morphological structures facilitated the development of a wide variety of applications including but not limited to drug delivery, soft lithography, and the development of porous materials. This area of research exploded over the last 60 years and continues to develop with the synthesis of new polymers. LC segmented copolymers represent a rapidly growing field in which many interesting orientation properties lie.

3.2 Synthetic Overview

The synthetic methods required to synthesize segmented LC copolyesters incorporate a range of techniques from polycondensation to controlled radical and other chain-growth

methods. The basics of polymer synthesis within the areas of polyesters and LC polymers acts as a platform for understanding the synthetic requirements of segmented LC copolyesters.

3.2.1 Basics of Polyester Synthesis

The family of polymers known as polyesters contains at least one ester functionality in every repeating unit. The formation of an ester occurs through a variety of different carbonyl reactions, most commonly transesterification or esterification, as expanded upon in **Figure 3.1**. These reactions occur through attack on the carbonyl carbon resulting in the production of a tetrahedral intermediate. Reforming the carbonyl causes elimination of a leaving group and inevitably the formation of the ester functionality.[28] Polymerization to form polyesters, in all cases except ring-opening polymerization, follows step-growth kinetics. As with all step-growth polymerizations, there are six

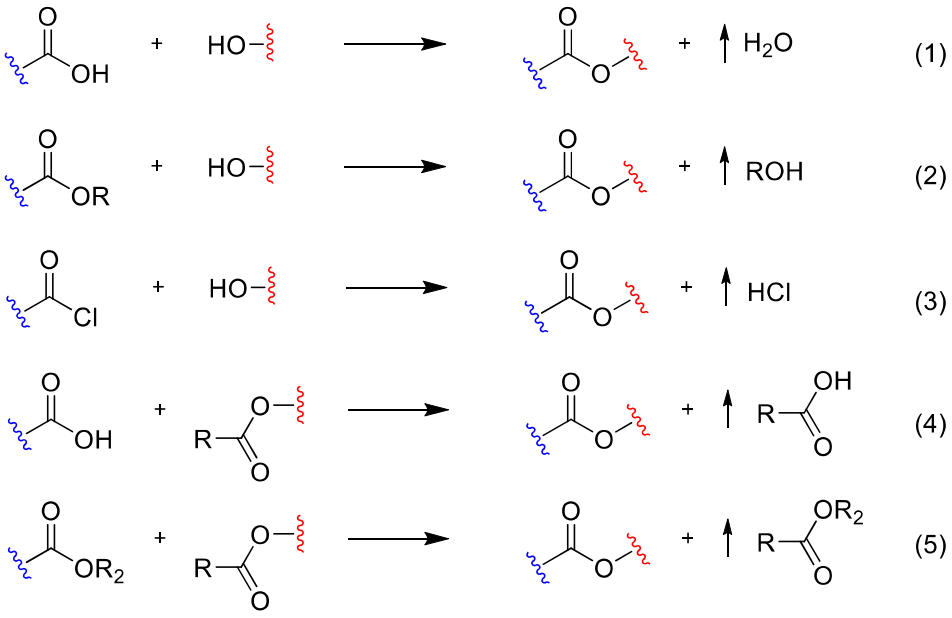

Figure 3.1. Examples of reactions utilized in the synthesis of polyesters. Adapted from Rogers et al.[28]

essential criteria that must be achieved in order for the polymerization of a linear polymer to reach high molecular weight (MW).[28,32]

1. Stoichiometry of the functional groups forming the polymer must equal 1.0
2. Monomer functionality (*f*) must equal 2.0 to maintain linearity and prevent branching
3. Absence of side-reactions
4. Efficient removal of condensates formed during polymerization (when applicable)
5. High reaction conversions (>99.9 %)
6. Accessibility of reactive end-groups

These essential criteria all relate back to the Carothers equation, representing the kinetics of MW growth in a step-growth polymer, as outlined in **Equation 3.1**, where X_n represents the degree of polymerization, f_{avg} the average functionality, and ρ the extent of conversion.

$$X_n = \frac{2}{2 - \rho f_{avg}} \qquad \textbf{(3.1)}$$

AB or AA/BB monomers build MW through the initial formation of oligomers, such as dimers, trimers, etc. This occurs through coupling of small molecules after complete monomer consumption. The final stage of MW growth occurs only at > 90 % conversion and results in the formation of linear high MW polymers, as demonstrated in **Figure 3.2**.

The most common type of polymerization for polyesters utilizes high temperature bulk reactions known as melt polycondensation. When utilized in the synthesis of PET, this occurs through either direct polyesterification, as illustrated in **Figure 3.1.1,** or transesterification represented in **Figure 3.1.2**. These reactions proceed under solventless conditions upon heating the monomers above their respective T_m resulting in a homogenous melt. Slow increase of the reaction temperature affords monomer consumption while maintaining a homogenous solution and allowing time for oligomer formation to prevent distillation of the growing chains. The final stage of the reaction

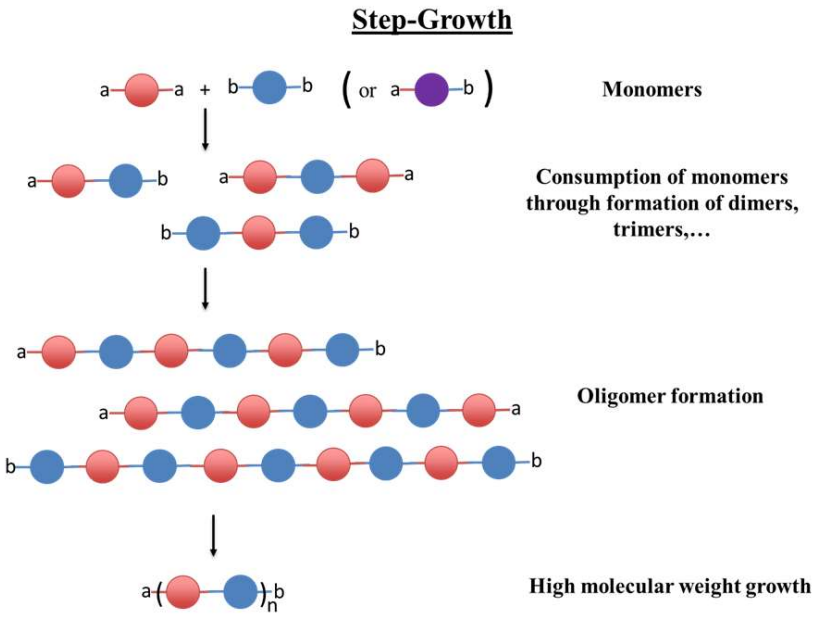

Figure 3.2. Graphical illustration of the mechanism of molecular weight growth for step-growth polymers.

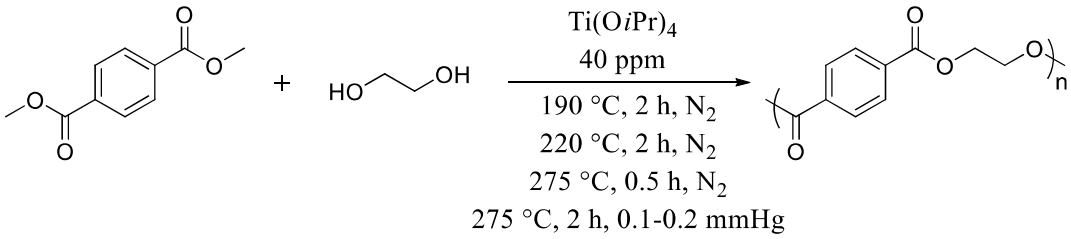

Scheme 3.1. Common lab scale synthesis of poly(ethylene terephthalate) with melt transesterification and polycondensation. Adapted from Lin et al.[33]

includes the application of vacuum to distill off the condensate and form high MW polymers through Le Chatelier's principle resulting in a drastic viscosity increase.[8,28,32] Commonly, excess diol, such as ethylene glycol in the case of PET, is initially added to the polymerization then removed during the final vacuum stage to bring the stoichiometry of the reaction back to the necessary 1:1. This limits error that occurs from early distillation or inaccuracies while measuring monomers. **Scheme 3.1** illustrates a common high temperature bulk procedure utilized in the synthesis of PET.[33]

Both transesterification and direct esterification exhibit slow reaction conditions at room temperature and therefore require high temperatures to push the reaction to completion. Catalyst incorporation increases reaction rates and ensures the formation of high MW polymers. Organometallics compounds and metal alkoxides comprise some of the most widely used catalysts for polyesterification reactions. The study of these catalytic mechanisms led to the understanding that Lewis acids, such as zinc and manganese, activate the ester group through complexation with the carbonyl oxygen. This complexation favors nucleophilic attack lowering the activation energy for these reactions. In contrast, Weingart et al. elucidated that antimony and titanium alkoxide catalysts undergo ligand exchange reactions, as illustrated in **Figure 3.3**.[34] Titanium alkoxides demonstrate a high efficiency in the catalysis of both esterification and

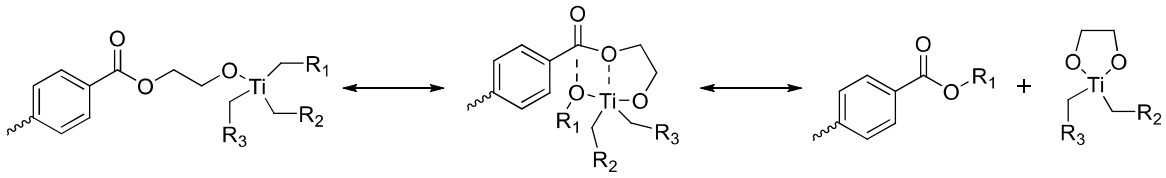

Figure 3.3. Mechanism of ligand exchange during polymerization using titanium catalysts. Proposed by Weingart and adapted from Schiers et al.[8,34]

transesterification (polycondensation) reactions resulting in their addition at the start of the reaction.[8] On the contrary, antimony trioxide (Sb_2O_3) exhibits a higher activity toward polycondensation (the final reaction stage) than esterification resulting in its addition just before the vacuum stage to assist in MW growth. The deleterious toxicity of antimony catalysts influenced the shift toward titanium based catalysts and novel organocatalysts.[35]

In the case of less reactive alcohols, like phenols, slow reaction rates limit the use of ester/carboxylic acid functional groups. The conversion of phenolic monomers to the acetoxy functionality promotes the reaction between a carboxylic acid and phenol enabling their polymerization in the bulk. The one-pot method utilizes the addition of anhydrides, like acetic anhydride and pivalic anhydride, to form a mixed anhydride *in-situ* with the carboxylic acid monomer improving the leaving groups of the functional group. The pre-acetylation of phenolic monomers results in the same formation of mixed anhydrides through a two-step route. Han et al. studied the mechanism of this reaction and attributed the improved reactivity to the carboxy-ester interchange reaction between acetoxyaryl groups and carboxylic acid functional groups resulting in the elimination of acetic acid, illustrated in **Figure 3.1.4**. [36,37] The temperature of these reactions must be at least 20 °C greater than the T_m of the monomers and increased stepwise to maintain a low viscosity during the polymerization. Common polymers synthesized with this technique

include fully-aromatic polyesters, such as LC copolymer Vectra® and amorphous polyarylate poly(bisphenol-terephthalate).

Melt polycondensation exhibits a very useful and industrially relevant technique towards the synthesis of polyesters. The environmentally friendly nature of this reaction due to the lack of solvent and minimal post-polymerization work up, drove it to prominence. Unfortunately, high temperature reactions are more prone to side-reactions which can impact the final polymer backbone structure and MW. A few examples of this include the formation of diethylene glycol through etherification of ethylene glycol in the synthesis of PET or the formation of THF during synthesis of PBT.[8] These high temperature conditions also inhibit polymerization with any thermally sensitive monomers, such as those utilized in unsaturated polyesters. The conversion of monomers to more activated carbonyls with better leaving groups and the use of solvents facilitate lower temperature reactions.[8]

The polyester synthesis between acid chlorides and alcohols typically takes place in solution to reduce side-products resulting from the formation of HCl, as illustrated in **Figure 3.1.3**. Due to the better leaving group, these reactions occur at lower temperatures than those necessary for esters and carboxylic acids. The solvent selection plays a key role in reaction rate; more polar solvents facilitated fast reaction rates.[38] It is important that the final polymer remain soluble in the solvent selected to prevent precipitation from stunting MW growth. HCl evolution enables reaction tracking and end-point determination.[39] Catalysts in this technique often take on the form of tertiary amines, such as pyridine or triethylamine, which also act as a HCl scavengers.[28,40-44] The tertiary amine forms a quaternary ammonium salt in the presence of HCl inhibiting reverse-

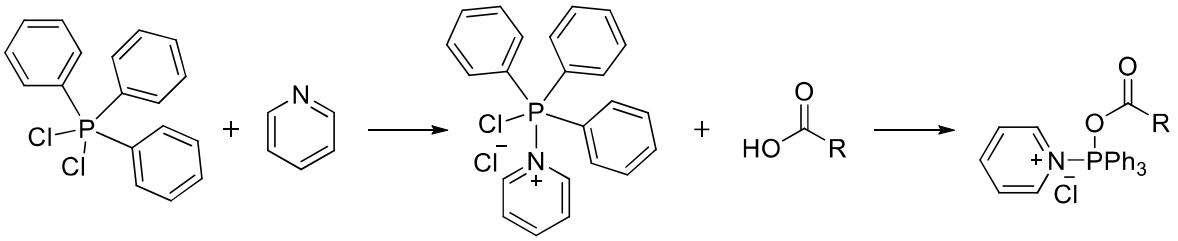

Scheme 3.2. Formation of triphenyl phosphine salts in the presence of pyridine and the resulting carbonyl activation. Adapted from Rogers et al.[28]

reactions and side-reactions from occurring during the polymerization or post-processing.[28] In many cases, solution polymerization at high temperatures occur to improve solubility of polymers/monomers that do not dissolve well at room temperature or exhibit crystallinity. During these polymerizations, the use of high boiling point solvents prevents distillation.

Solution polymerizations using activating agents stimulate higher monomer reactivity but their consumption during the reaction limits the label catalysts. Phosphorus derivates represent a large portion of activating agents, triphenyl phosphine and diphenylchlorophosphate representing the most effective. These compounds form salts in the presence of pyridine in turn enabling the activation of carboxylic acids, as demonstrated in **Scheme 3.2**. Rogers et al. described a wide range of other activating agents that can be utilized in polyester synthesis. [28]

The use of interfacial polymerization with acid chloride functionalized monomers has been demonstrated in a few cases within the segmented LC copolyester literature. This technique restricts the alcohol to a phenolic monomer due to the required formation of an alcoholate ion in aqueous solutions; impossible for aliphatic diols. The reaction conditions for this technique requires a two-phase solvent system (aqueous/organic), surfactant, water-soluble base, and organic-soluble monomers/final polymer. The

alcoholate ion of the aromatic phenol forms through a reaction with alkali bases, such as NaOH. Surfactants (phase-transfer agents) increase the interfacial area between the two solvents where the reaction occurs helping to control the reaction rate.[28] Examples of possible surfactants include fatty acid sulfates, and quaternary ammonium salts, such as benzyltributylammonium bromide or tetrabutylammonium hydrogensulfate.[28,45-47]

These polymerization techniques utilize step-growth kinetics resulting in broad MW dispersity (Đ), equivalent to 2. Ring-opening polymerization exhibits the only polymerization technique for polyesters that achieves narrow Đ as it follows chain-growth kinetics. Examples of this synthesis include polymerization of lactides or glycolides.[48,49] This polymerization occurs in bulk or solution at temperatures typically ranging from room temperature to > 100 °C. Catalysis for this technique ranges from standard metallic systems, like titanium alkoxides and Sb_2O_3, to novel organocatalysts that Kiesewetter et al. describes in depth.[49]

3.2.2 Synthesis of Thermotropic LC Polymers

Classification of LC polymers initiates with the differentiation between lyotropic and thermotropic. This chapter focuses on the area of thermotropic LC polyesters which comprise materials that transition into the LC state through application of thermal energy. Three main morphologies of LC mesophases form from thermotropic LCPs; nematic, smectic, and cholesteric.[14,50,51] Nematic exhibits one-dimensional order within the microscopic unit element (domain) in the polymer matrix. The molecules arrange themselves in a specific direction within the domain and the limited intermolecular forces enable the molecules to easily pass each other, allowing mobility in the system. As illustrated in **Figure 3.4**, other than orientation the molecules arrange randomly. Smectic

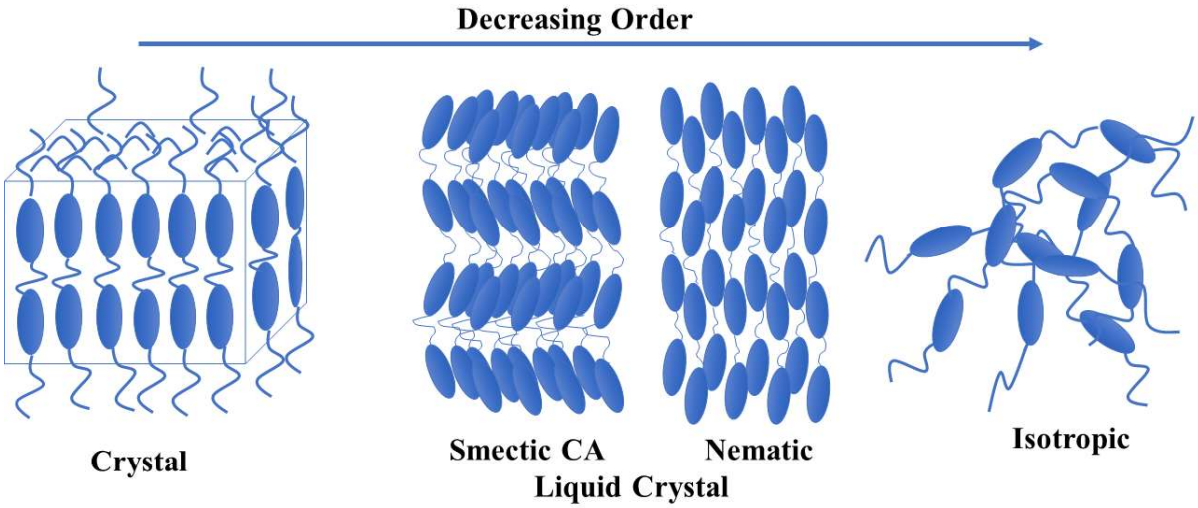

Figure 3.4. Basic graphical illustration of the differences between crystalline, liquid crystalline, and isotropic states for main-chain LC polymers.

LCPs possess "two-dimensional" ordering within the domains. In this case the mesogenic monomers arrange to form layers or planes. The direction or orientation of the mesogens within these layers enable differentiation between a variety of unique smectic LC phases. The Smectic A (S_A) mesophase possesses orientation in which the long axis of the rod shaped mesogen lies perpendicular to plane of the layer.[14,50,51] Smectic mesophases that exhibit tilting of the mesogens with respect to the layer encompasses a Smectic C (S_C) but if the tilt of the mesogen flips its direction with each new layer, as illustrated in **Figure 3.4**, the mesophase would identify as Smectic CA (S_{CA}).[14,50-52] Cholesteric LCPs exhibit similarities to nematic phases in that layers do not form but rather the molecules only possess an orientation director. The difference between cholesteric and nematic lies in the twist of the director resulting in a helical path, like DNA. The origin of this phase results from a chiral bond within the chemical structure of the polymer repeat unit.[14,50,51] Chung et al and Ciferri et al. describe a wide range of other classifications depending on the packing structure within the mesophase.[14,53]

3.2.2.1 Main-Chain LC Polymers (MCLCP)

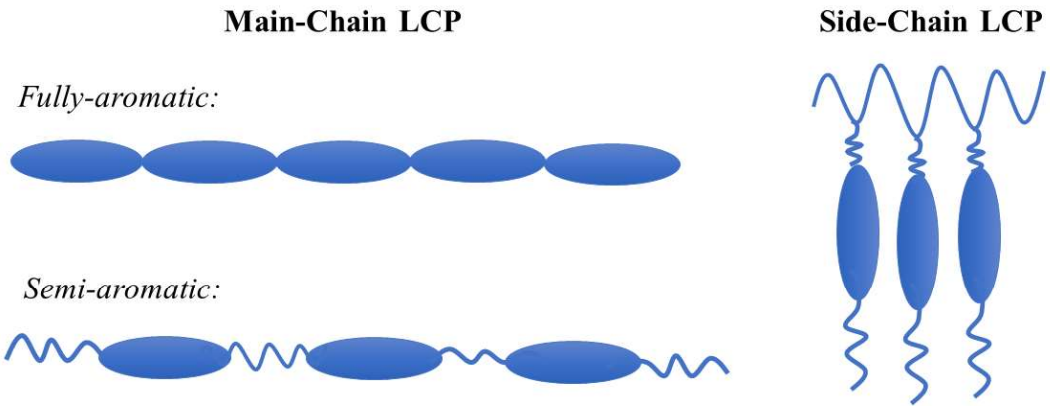

Figure 3.5. Basic architectural differences between main-chain and side-chain LCPs. Ovals represent mesogenic units while the wavy lines represent flexible chains.

The thermotropic family of LCPs comprise two main polymer architectures; side-chain (SCLCP) and main-chain polymers (MCLCP). Main-chain polymers possess the mesogenic unit (monomer/ structure imparting LC properties) within the backbone of the polymer. These linear polymers, often synthesized through step-growth methods, take on molecular structures such as polyesters and polyamides. Side-chain differs from main-chain due to the mesogenic unit hanging off the backbone of the polymer, as illustrated in **Figure 3.5**. Side-chain polymers commonly utilize controlled chain-growth polymerization techniques, such as anionic polymerization and RAFT. Their ability to align easily under magnetic or electric fields fostered SCLCPs use in lithographic fields. MCLCPs most notably exhibit high mechanical properties, significant shear thinning in the melt, and orientation under mechanical deformations promoting their use in high strength fibers and injection molded structural applications.[28]

LC polyesters fall into the field of main-chain LCPs and take on two different backbone structures, semi-aromatic and fully-aromatic. The first polyesters found with LC characteristics utilized fully-aromatic structures. Flory's original computational hypothesis indicated that the formation of LC properties in a polymer requires a structure

with a high degree of rigidity and linearity.[16,17] As a result, scientists initially synthesized very rigid aromatic backbones but quickly discovered that completely linear backbones resulted in T_m*'s* greater than the polymer degradation temperature making it impossible to form a stable LC state. Neither poly(4-hydroxybenzoic acid) (Ekonol) or poly(1,4-terephthalate) melt before there degradation temperature at 600 °C.[54-56] Scientist use four main approaches to reduce the melting temperature of LCPs in order to achieve a melt-processable polymer that benefits from the significant shear thinning prominent in the LC state.

1) Copolymerization with different linear monomers (mesogens).
2) Copolymerization with non-mesogenic monomers.
3) Polymerization of monomers with bulky lateral substituents.
4) Introduction of flexible aliphatic spacers. [20,28]

Copolymerization of different rigid linear (*para*) monomers, such as terephthalic acid, 4-hydroxybenzoic acid, 2,6-hydroxynapthoic acid, and hydroquinone, comprises common industrially processes.[14,28] This type of LCP maintains the linearity required to produce LC order but disrupts the regularity required for crystalline chain packing through randomization of the structure. Vectra® and Xydar®, two commercially available fully-aromatic LCPs, both utilize this approach to achieve T_m < 300 °C.[19,57,58] The copolymerization of linear mesogenic repeat units with non-mesogenic monomers represents another method to reduce T_m. Typically, these non-mesogenic monomers use kinked aromatic structures due to functional groups placed *meta* on the ring. Examples of this include isophthalic acid, resorcinol, and 2,5-substituted thiophene. These structures disrupt the lateral interactions of the chains affording T_m reduction but unfortunately also

exhibit a disruption of the LC properties through interruption of the chain rectilinearity.[14,28] The addition of a bulky lateral group represents a very successful method for disrupting lateral interactions without impacting the rectilinearity of the chain. These monomers take on the structure of various p-aromatic monomers with the addition of benzyl rings or halide groups in the *ortho* or *meta* positions. Roger et al. provides an extensive list of various bulky substituent based monomers utilized in LCPs. Fully-aromatic LCPs, such as those described here, form nematic mesophases because of their rigid/linear but non-regular structure impeding the formation of smectic layers.[14,28]

The addition of flexible spacers between mesogenic monomers results in the formation of semi-aromatic LCPs. The structural architecture of semi-aromatic LCPs, illustrated in **Figure 3.5,** result in significant decreases in transition temperatures. Unfortunately, the polymer degradation temperature also reduces. Watanabe et al. and other groups extensively studied the structure-property-relationships of semi-aromatic LCPs utilizing the mesogenic monomer, dimethyl 4,4'-bibenzoate (4,4'BB).[59-63] Considering only linear aliphatic spacers, Watanabe elucidated that a spacer length greater than three but less than 9 methylene units exhibit LC properties. These polymers afford T_m < 250 °C and T_i < 300 °C and decrease in their endothermic transitions as the aliphatic spacer length increases revealing an odd-even oscillation. The chain flexibility and regularity of the 4,4'BB based semi-aromatic polyesters with linear spacers result in the formation of smectic mesophases. Specifically, aliphatic spacers with an odd number of methylene units result in a S_{CA} mesophase morphology while those with even numbered spacers form S_A morphologies.[59-62] This effect results from the extended chain confirmation that occurs in LCPs with odd and even spacers, as demonstrated in **Figure**

3.6 through the extended chain structures of poly(pentamethylene 4,4'-bibenzoate) and poly(hexamethylene 4,4'-bibenzoate).[64] Utilizing spacers with additional R-groups off the backbone disrupts the close packing of the polymer chains resulting in a disruption of crystallinity and, under specific circumstances, a transition to a nematic mesophase rather than smectic.[65] In most cases, the addition of R-groups off the chain result in the formation of a LC glass due to the complete inhibition of crystallization but the continued presence of a S_A mesophase. Poly(4,4'BB-2-methyl propylene) (poly(BB-5(3-Me)) represents an example of a LC glass.[66-71] Copolyesters of poly(ethylene terephthalate) with hydroxybenzoic acid represent a non-traditional semi-aromatic LCP which utilizes

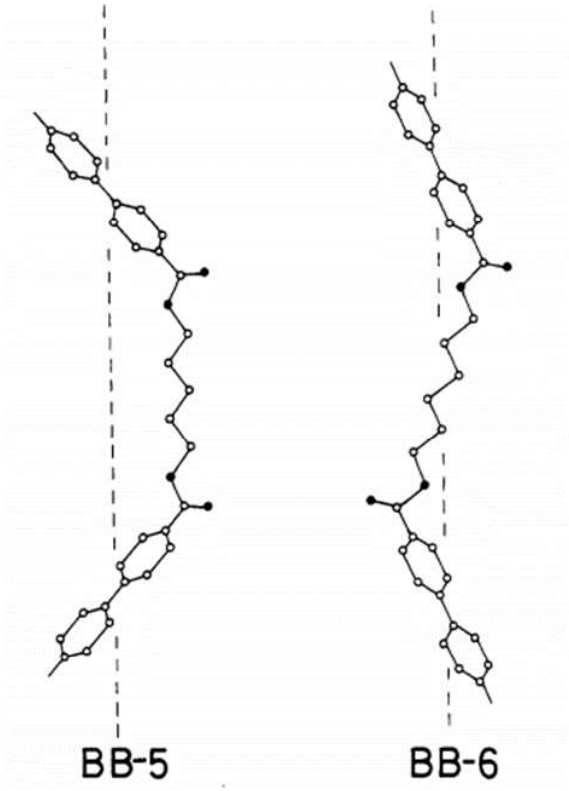

Figure 3.6. Extended chain structure of poly(hexamethylene 4,4'-bibenzoate) (BB-6) and poly(pentamethylene 4,4'-bibenzoate) (BB-5). Reprinted with permission from Watanabe, J.; Hayashi, M., *Macromolecules* **1989**, *22*, 4083. Copyright © 1989 American Chemical Society.[64]

PET as the spacer between the rigid mesogens. Similar to fully-aromatic polymers, the randomized structure due to copolymerization results in a nematic mesophase.[72-74] Other mesogenic monomers utilized in the synthesis of semi-aromatic LCP include 4,4'-biphenol, stilbene, 4,4'-dihydroxy-2,2'-dimethyl-azoxy-benzene, and many more outlined by Demus et al. These monomers form a highly versatile family of structures able to achieve different mesophase morphologies while maintaining processable melting/isotropic temperatures.[8,47,51]

All the methods mentioned so far, with the exception of semi-aromatic LCPs, utilize phenolic monomers. As described in the previous section, phenolic monomers require more reactive functional groups than carboxylic acids and alcohols in order to polymerize. Acidolysis polymerization represents a widely utilized polymerization method for the formation of fully-aromatic LCPs.[75-77] Fully-aromatic LCPs often polymerize in a turbid state because of the presence of nematic LC phases at the polymerization temperatures.[10,14] This melt polycondensation technique often utilizes no solvent or catalyst and still achieves high MW polymers. Other groups, such as Chain-Shu et al, show that the introduction of catalysts, like dibutyl tin oxide, improve reaction rates between less reactive/nucleophilic monomers.[78,79] Unfortunately, due to the monomer choice this technique often requires high temperatures (>250 °C) limiting thermally sensitive monomers due to degradation and side reactions. Also, the acetoxy functionality introduces side-reactions through the formation of ketenes or acetolysis which other polymerization methods eliminate.[80] This technique represents an uncommon polymerization method for semi-aromatic polymers but is vastly utilized for fully-aromatic LCPs. In the segmented LCP literature, Jannesari et al. represents the only work

to utilize acidolysis for semi-aromatic polyesters due to the choice of a phenolic mesogenic monomer and a aliphatic diacid.[81]

The use of acid chloride functionalities instead of carboxylic acid moieties represents a more widely utilized monomer in the polymerization of main-chain LCPs throughout the segmented LCP literature. The greater reactivity of these monomers in esterification reactions occurs from the better leaving group, chloride, on the carbonyl. This functional group enables reactions with phenolic monomers without the need for acetylation. A few studies on LCPs demonstrate the possibility of solvent-less melt polycondensation methods using these monomers but side-reactions and the need for lower temperatures direct many scientists to prefer solution polymerizations.[28,82-84] Solution polymerizations for fully-aromatic polymers often occur at temperatures higher than those utilized for aliphatic polyesters (50-250 °C) due to the limited solubility of these polymers/monomers[29,85-92] A few segmented LCP studies have also utilized the addition of activating agents, such as triphenylphosphine dichloride (TPPC) and diphenylchlorophosphate (DPCP), as described for polyester synthesis.[93] Angeloni et al. represent the first group to utilize interfacial polymerization in the synthesis of segmented LC polyesters.[94] The benefit of this polymerization method came from the use of a lower reaction temperature, to prevent a thermally unstable monomer from degrading during the polymerization. LC polymers that utilize these techniques comprise both semi-aromatic and fully-aromatic LCPs.[45,46,95-97]

Melt transesterification represents the most utilized synthesis method for semi-aromatic LC polyesters. Most 4,4'BB based LCPs use this polymerization method with a range of different aliphatic diols.[59,68,98-100] The versatility of this technique and the low

processing temperatures of the structures formed with this method resulted in its use often in the formation of segmented LCP. The Long group utilized this polymerization method on several occasions for the synthesis of semi-aromatic LC polyesters and segmented LCP.[99,101-103] Nelson et al. synthesized high-performance segmented LC copolyesters utilizing this technique. The authors heated the monomers and 40 ppm of titanium isopropoxide catalyst from 190-275 °C over the course of 4.5 h under N_2 flow. A final vacuum step (0.15 mmHg) at 275 °C for 2 h enabled the formation of high MW polyesters. The use of titanium alkoxide catalysts has been most prevalent in these studies due to the non-toxic nature of this catalyst and its high activity. [28,35]

3.2.2.2 Side-Chain LC Polymers (SCLCP)

A flexible polymeric backbone, mesogenic monomer, spacer, and tail comprise the structure of a SCLCP. The polymer backbone in segmented systems range from flexible amorphous polymers, to semi-crystalline or LC polymers. Flexible backbones give rise to easier ordering of the mesogenic units, therefore the most widely used backbones include polymethacrylates, polyphosphazenes, polysiloxanes, ethylene oxides, and different polyacrylate derivates.[9,51] In order to ensure the polymer coiling does not influence the LC properties of the mesogenic unit it must be decoupled from the polymer backbone through use of a spacer.[9] This allows the mesogen to exhibit long-range order and orientation while promoting entropy in the backbone to balance the flexibility of the chain. The length of the spacer and tail drastically alters the mesophase morphology. For SCLCP with rod-like mesogens, short tails/spacers result in a nematic mesophase while long tails and long spacers allow enough decoupling from the backbone to order into a smectic mesophase.[104] Altering the structure of the tail from an aliphatic unit to

perfluorinated consistently alters the mesophase to S_A due to the greater rigidity of the chain.[104] Cyano and nitro moieties impart positive dielectric anisotropy when used in tails.[9] Emmerling et al. demonstrated the synthesis of a novel SCLCP utilizing a nitro tail which afforded multiple smectic and nematic phases.[105]

The mesogenic unit choice depends on whether the small molecules analog exhibits LC properties due to the axial ratio and polarity of the molecule. The molecular geometry usually comprises a rod-shape, disk-shape, or amphiphile (lyotropic). In comparison to main-chain LCPs, the mesogenic monomer unit does not change its axial ratio when polymerized. As a result, SCLCP ordering properties resemble the low MW LC much closer than main-chain LCPs. Rigid rod mesogenic units usually comprise combinations of two or three aromatic rings, as Demus et al comprehensively lists.[51] Disk-shaped (Discotic) mesogens usually link aromatic rings to form structures like triphenylene exhibiting a planar rigid disk shape.[9,106] Discotic SCLCP are quite uncommon in the segmented LC copolyester literature, therefore they will not be focused on in this review. Semi-fluorinated alkyl side chains represent a non-phenyl based mesogen that exhibits high rigidity in comparison to CH_2 units and better molecular organization resulting from their low surface energy.[107,108] Al-Hussein et al. synthesized diblock copolymers of polyacrylate derivates with semi-fluorinated side chains and poly(methyl methacrylate) (PMMA) utilizing atom transfer radical polymerization (ATRP).[68]

Figure 3.7 illustrates the three key synthetic pathways to the production SCLCP**.** **Figure 3.7.1** uses chain-growth polymerization of a LC monomer to form the SCLCP. As seen for the polymerization of styrene or methacrylate-based monomers, polymerization

occurs through the vinyl functionality on the monomer while the mesogenic monomer hangs off the vinyl group. **Figure 3.7.2** illustrates the design of a difunctional monomer for polycondensation polymerization. The final scheme (**Figure 3.7.3**) exemplifies post-functionalization to attach a mesogenic monomer after the polymerization is complete.[53]

Chain-growth polymerizations use vinyl functionality to achieve high MW through a wide variety of techniques. Though often resulting in polymers with higher dispersity than controlled polymerization methods, free-radical polymerization remains the most commonly used method of polymerization through a vinyl moiety. This method begins the polymerization through thermal or photodecomposition of an initiator to form a radical. This radical propagates through the double bond of the monomer, transferring the activated site. The activated site then goes on to react with another vinyl group and the radical continues transferring and reacting until a termination step neutralizes the radical or two chains combine in a coupling mechanism inhibiting further chain growth.[109] A number of controlled polymerization techniques regulate the kinetics of

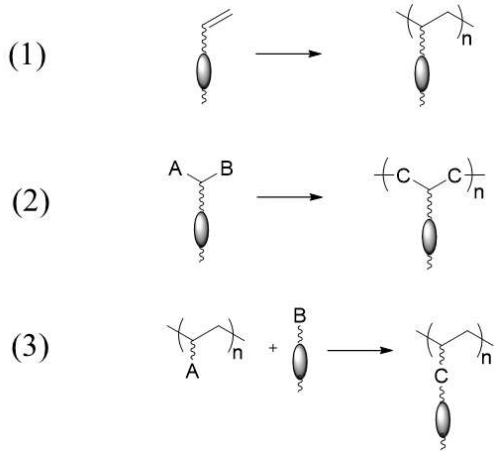

Figure 3.7. Polymerization of SCLCPs using 1) chain-growth polymerization 2) step-growth polymerization 3) post-polymerization modification. Adapted from Ciferri et al.[53]

free-radical polymerizations, such as atom transfer radical polymerization and reversible addition-fragmentation chain transfer polymerization.[32] These methods along with anionic and cationic polymerizations facilitate the polymerization of SCLCP and the selection of polymerization type depends on monomer choice and the desired control over Đ and MW.[32]

Ring-opening polymerization also possess chain-growth kinetics and enables the polymerization of SCLCPs. While not a vinyl group, the double bond in a cyclic norbornene monomer facilitates polymerization through ring-opening metathesis polymerization. Derivation of these monomers with mesogenic units, like n-alkyloxycyanobiphenyl groups, reveals LC properties upon polymerization.[110] Del Campo et al. also demonstrated ring-opening polymerization of epoxide derivates through cationic polymerization also facilitates the formation of SCLCPs.[111]

The design of monomers with AA or AB molecular geometries functionalized with SCLCs facilitate their use in step-growth polymerization methods, as demonstrated in **Figure 3.7.2**. Mesogenic side-chains located off a rigid aromatic diacid/diester enables their use in polyesters. Pospiech et al. explored the use of such monomers in a segmented copolymer with a poly(sulfone) secondary block. This study synthesized a LC polyester segment containing a derivatized isophthalate unit with semi-fluorinated alkyl chain located *meta* to the diacid functionalities. This represents one of the few polyester side-chain LCP examples as this polymer family primarily comprises main-chain LCP structures.[73] Emmerling et al. achieved another example of SCLCP through polycondensation polymerization when 4-(4-nitrobenzyloxy)biphenyl-4'-ol underwent etherification with diethyl 6-bromohexylmalonate to form diethyl 6-[4-(4-

nitrobenzyloxybiphenyl-4'-oxy]hexylmalonate. This SCLCP, polymerized through melt transesterification with various diols, exhibited multiple smectic and nematic mesophases.[105] Mandal et al. further revealed a novel synthetic method toward the formation of SCLCP involving the combination of both polycondensation polymerization and post-processing. This study synthesized aliphatic polyesters through solution polymerization between acyl chloride moieties and derivatized diols, as illustrated in **Scheme 3.3**. The diols contained pendant propargyl groups affording a clickable functionality on the polymer enabling the attachment of a semi-fluorinated alkyl mesogen.[39] Post-processing ensured that the mesogenic unit did not inhibit polymerization through impacting solubility or introduction of side-reactions. Anionic polymerization is notoriously sensitive to monomer choice therefore post-polymerization affords a wider range of final achievable polymer structures. Manfred et al. utilized the protected monomer, 2-(trimethylsiloxy)ethyl methacrylate (SHEMA), to polymerize SCLCP using anionic polymerization. Deprotection of SHEMA after polymerization

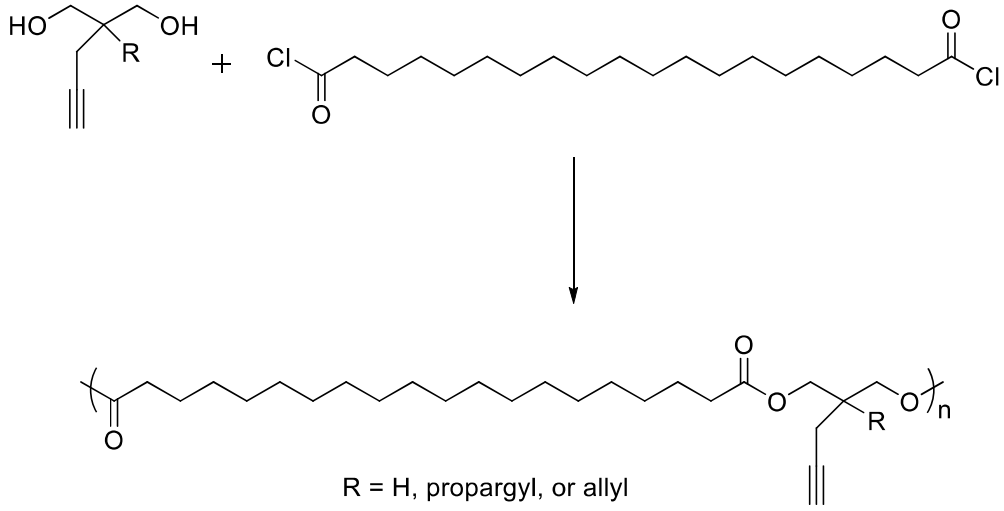

Scheme 3.3 Polymerization of a periodically clickable polyester utilized in the synthesis of a SCLCP. Adapted from Mandal et al.[39]

afforded 2-hydroxyethyl methacrylate (HEMA) which, when reacted with cholesteryl chloroformate, afforded the SCLCP illustrated in **Scheme 3.4**.[112]

3.2.3 Synthesis of Segmented LC Copolyesters

Segmented LC copolyesters must consist of three main features. First, the polymer must phase separate through synthesis of block or multiblock architectures. Secondly, one of the blocks must contain a LC polymer. Finally, one block must contain a polyester though the second and third requirements may be combined through use of a LC polyester. Design of these materials occurs using a wide range of block copolymer structures and architectures that result in discrete blocks of monomer units along the polymer chain. This includes linear diblocks (AB), triblock (ABA), pentablock (ABABA), and multiblock (segmented, $(AB)_n$), or non-linear graft and star block copolymers. Synthesis of these structures occur through both step-growth and chain-growth polymerization methods. Due to the presence of polyesters in these (co)polymers,

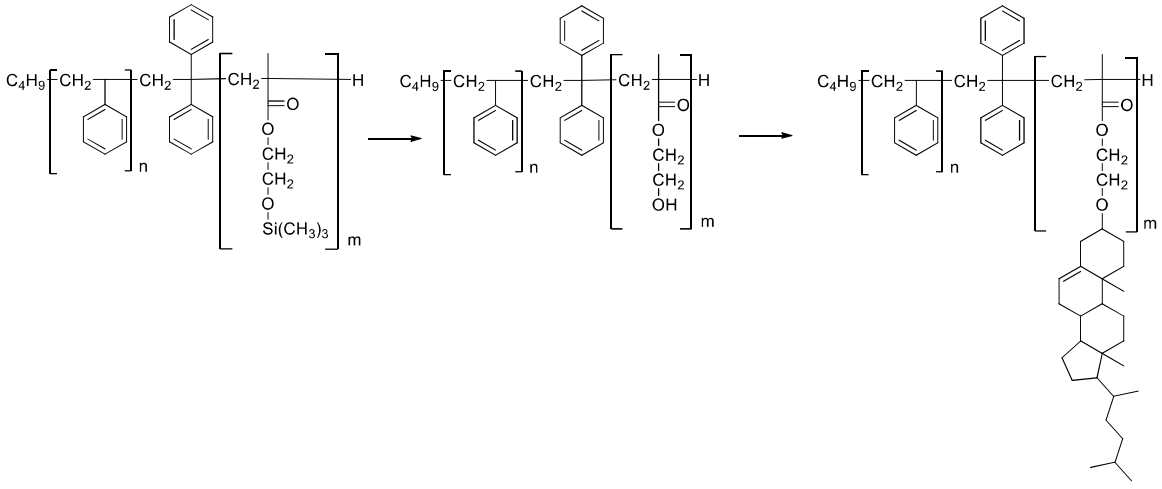

Scheme 3.4. Post-polymerization deprotection of 2-(trimethylsiloxy)ethyl methacrylate and subsequent reaction with cholesteryl chloroformate to form a SCLCP. Adapted from Manfred et al. [112]

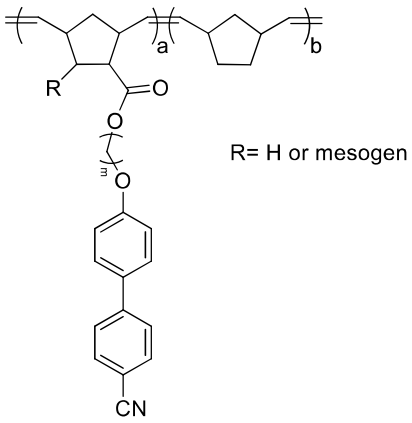

Figure 3.8. Structure of a segmented LC copolyester utilizing only chain-growth polymerization. Adapted from Deshmuk et al.[110]

synthesis occurs through either entirely step-growth polymerization or a hybridization of step-growth and chain-growth polymerization. Only one account of a segmented LC (co)polyester through entirely chain-growth polymerization has been located. In this polymerization, Deshmukh et al. functionalized norbornene with either one or two cyanobiphenyl mesogens, illustrated in **Figure 3.8**. A secondary norbornene monomer was functionalized with poly(lactide) (PLA) through ring-opening polymerization. Ring-opening metathesis polymerization afforded the grafted block copolymer with 75 % liquid crystalline content in order to achieve a hexagonally packed cylindrical phase separated cylindrical morphology.[110]

3.2.3.1 Segmented LC Copolyesters Synthesized via Step-Growth Polymerization

Polymerization methods utilizing entirely step-growth reactions comprise half of all the literature on segmented LC copolyesters. Considering the history of multiblock copolymers in the thermoplastic elastomer field, it is not surprising that this architecture possesses the largest literature presence. While uncommon in more recent literature, early studies into LC block copolyesters analyzed block-copolymers containing only

polyesters. Mathew et al. studied the copolymerization of PET with 4-acetoxybenzoic acid (ABA) through melt esterification. Kinetics studies indicated that the DP limit for the ABA monomers reached 5 and DSC studies support a random block structure.[113] Although it is difficult to determine whether phase separation occurred in these early studies, an understanding was formed that in order to create block copolymers transesterification between the segments must be limited.[40,113] In 1991, Tsai et al. attempted to control the transesterification between two polyester oligomers to afford block copolyesters. This study utilized the immiscible poly(butylene terephthalate) and poly(butylene adipate) and copolymerized these oligomers through melt mixing with the addition of 1,4-butanediol (BD). The amount of BD added and reaction time controlled the degree of randomization that occurred.[114] Novack et al. and Yan et al. utilized the natural randomization that occurs through transesterification to introduce LC blocks into commercial PET. Yan et al. coupled two HBA molecules with terephthaloyl chloride (TPC) to form a LC triad acid chloride which was incorporated into commercial PET chains through solution polymerization with a triethylene amine/pyridine catalyst.[42] Novack et al. performed a similar analysis in which the monomers, 4,4'-dihydroxy-α,ω-diphenoxy decamethylene and TPC, reacted with PET using solution polymerization.[90] In 1994, Ignatious et al. further explored this area but utilized PBT instead of PET and different diad and triad LC acid chloride monomers.[43] In all these cases, high temperature solution polymerization was performed instead of melt transesterification in an effort to control sequence randomization. Unfortunately, the disperse nature of the blocks made the microphase separated morphology difficult to discern in all studies. Only a blocky

structure was truly confirmed due to the presence of endothermic transitions for both the semi-crystalline and LC blocks and optical microscopy analysis.[42,43,90]

These analyses enabled the observation that randomization control demonstrates a less practical method in the formation of multiblock copolymers. In order to introduce more control into the polymerization, scientists began utilizing reaction methods and secondary copolymers that inhibited transesterification. Tsai et al. utilized methylene-4,4'-diphenylene diisocyanate to link oligomers of a semi-aromatic LCP, poly(pentamethylene 4,4'BB), with poly(tetramethylene adipate) through coupling in DMF in the presence of dibutyltin dilaurate. While this successfully produced high MW phase separated multiblock copolymers, the presence of hydrogen bonding resulted in conformation restrictions which limited the LC properties.[115]

Over the years, segmented LC copolyesters with multiblock architectures incorporated a large variety of high-performance polymers in the form of oligomers, such as polysulfones (PSU), poly(ether ether ketone) (PEEK), poly(phenylene sulfide) (PPS), and poly(phenylene oxide) (PPO). These high-performance materials utilize step-growth polymerization methods, such as nucleophilic aromatic substitution.[32] Due to the structural differences between these polymers and polyesters, randomization through transesterification becomes impossible. The extensive use of these types of phase separated copolymers in the area of blend compatibilization arises from the incompatibility between these polymers and commercial LC polyesters.[86]

PSU represent the most widely studied of these high-performance polymers for segmented LC copolymers. Copolymerization of PSU oligomers with LC polyesters occurs through coupling with LC polyester oligomers or polymerization of mesogenic

monomers in the presence of PSU oligomers. Auman et al. first synthesized PSU-LCP (co)polyesters in 1988 utilizing an acetoxy terminated PSU. Melt acidolysis polymerization with chlorohydroquinone diacetate and trans-1,4-cyclohexanedicarboxylic acid afforded high MW block copolymers with phase separated properties. The immiscibility of the amorphous PSU (MW > 2300 g/mol) with the LC phase of the monomers at the reaction temperatures resulted in chain extended structures while lower MW PSU (M_n = 1400 g/mol) facilitated the formation of multiblock copolymers.[116] Chain-Shu et al. followed this study and synthesized PSU-LCP copolymers utilizing the LC monomers, p-acetoxybenzoic acid (ABA), terephthalic acid, and hydroquinone diacetate. This copolymer utilized melt acidolysis polymerization from the acetoxy terminated poly(ether sulfone) at different weight % relative to LC monomers. This method revealed a significant amount of unreacted PSU oligomers remaining at the end of reaction that required removal as to not affect the final properties.

In 1994, Brenda et al. moved to a high temperature (180-250 °C) solution polycondensation utilizing diphenyl ether as the solvent in order to improve the reaction with the oligomers. This study analyzed poly(ether ether sulfone) oligomers (10,000, 7000, and 2500 g/mol) copolymerized with either a semi-crystalline LC polyester, an amorphous LC polyester (LC glass), or a non-LC amorphous polyester, as illustrated in **Figure 3.9**. This polymerization technique enabled the formation of phase separated block copolymers utilizing much higher MW PSU oligomers than previously reported because it no longer relied on solubility in the melt.[85] Chang et al. utilized solution polymerization with an activating agent, triphenylphosphine/pyridine, in hexachloroethane to polymerize block copolymers from hydroxy terminated PSU

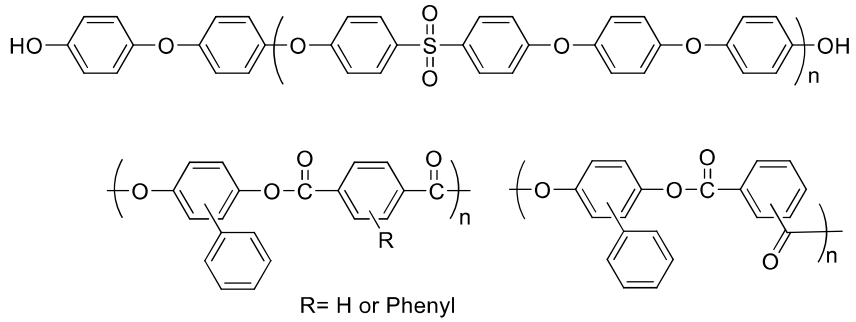

Figure 3.9. Structure of poly(ether ether) sulfone multiblock copolymers with different LC polyester segments. Adapted from Brenda et al.[85]

oligomers and HBA/HNA LC monomers.[97] Unfortunately, fractionating the polymer with different solvent systems revealed that the use of an activating agent still left unreacted PSU oligomers in the final polymer. A later study by Wang et al. using a wide MW range of hydroxy terminated PSU (30,000 – 10,000 g/mol) reconfirmed what Brenda et al. indicated early on, that high temperature solution polymerization utilizing diacid chloride and diphenol functional groups consistently produces multiblock copolymers. This study utilized 2-(3'-trifluoromethylphenyl) hydroquinone (TFMPH) and TPC to produce the LC segment.[29] Pospiech et al. in 1996 and 2001 reported the synthesis of PSU-LC block copolymers through the coupling of both a PSU oligomer and LC polyester oligomers rather than polymerization from monomers.[73,83] These polymerization studies utilized melt acidolysis to couple acetoxy terminated PSU with carboxylic acid terminated PET/HBA copolymers. This method produced homogenous multiblock copolymers eliminating the presence of unreacted oligomers.[83] Other LC systems, such as carboxylic acid terminated semi-fluorinated side-chain polyesters were polymerized utilizing this same method.[73]

Yang et al. and Zeng et al. both produced segmented LC copolymers utilizing poly(ether ether ketone) segments of different backbone structures.[30,86] Yang et al synthesized BPA based PEEK with hydroxy terminal groups through nucleophilic aromatic substitution achieving an M_n = 7797 g/mol and Đ = 1.2. This oligomer facilitated the formation of block copolymers through high temperature (180-250 °C) solution polymerization using TFMPH and TPC to form the LC segments. Alternatively, Zeng et al. polymerized multiblock copolymers using carboxylic acid terminated Vectra® oligomers and acetoxy terminated PEEK, exhibited in **Scheme 3.5**, at an equimolar ratio through melt acidolysis using a zinc acetate/diantimony trioxide (co)catalyst.[30] Heyde et al. utilized high temperature solution polymerization to produce block copolymers of PPO and LC polyester segments. Telechelic functionality was added to poly(oxy-1,4-phenylene) post-polymerization using potassium 4-bromophenolate and 4,4'-isopropylidenediphenol (BPA). Following similar methods demonstrated for PSU and PEEK, LC monomers (TPC or bromoterephthaloyl dichloride and biphenyl-2,5-diol)

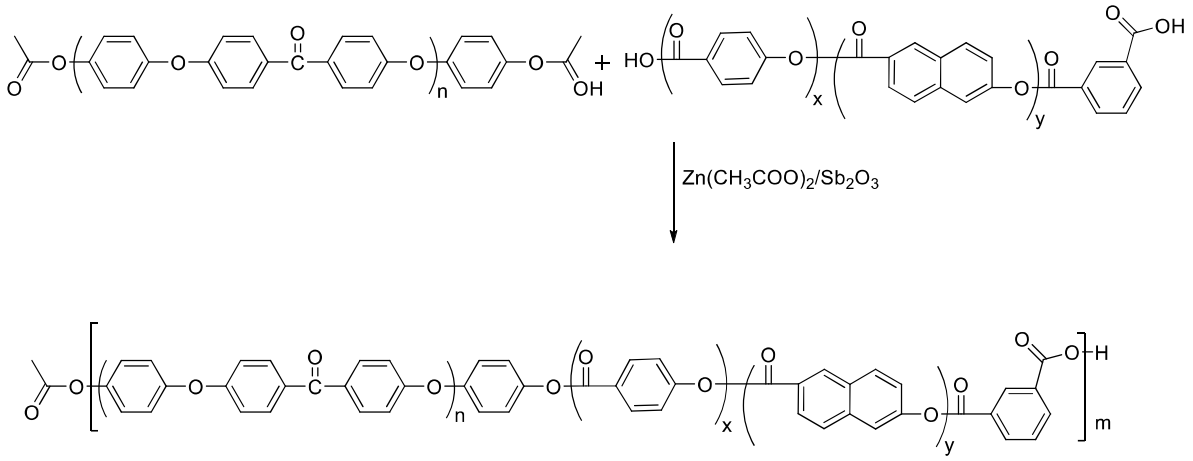

Scheme 3.5. Synthetic route to multiblock copolymers containing PEEK and Vectra® segments. Adapted from Zeng et al.[30]

polymerized off poly(oxy-1,4-phenylene) to produce multiblock copolymers.[91] Heitz demonstrated the synthesis of PPO-LC block copolymer as well as PPS-LC block copolymers in 1989. [117] Synthesis of poly(oxy-2,6-dimethyl-1,4-phenylene) and poly(oxy-1,4-phenylene) through Cu catalyzed oxidation of either 2,6-dimethylphenol or bromophenol with a diphenol monomer produced telechelic phenol groups. Reacting 1,4-dichlorobenzene and sodium sulfate produced poly(phenylene sulfide) which encountered functionalization during the second stage of the reaction converting the thiolate end groups to carboxylic acids moieties with chlorobenzoic acid. These oligomers were reacted with the monomers of semi-aromatic LC polyesters (TA and 4,4'-alkylenediphenols) using different carbon spacers through solution polymerization in pyridine at 120 °C.[117] In a more recent study, Gopakumar et al. copolymerized carboxylic acid terminate PPS with PET-co-oxybenzoate (PET/HBA) using uncatalyzed melt transesterification at 300 °C.[74]

Two different groups synthesized LC copolymers with non-traditional architectures producing phase separated morphologies using entirely step-growth polymerization methods. Nießner et al. synthesized novel PPO macromonomers, α-(2,5-dimethoxyphenyl)-ω-bromooligo(oxy-l,4-phenylene), through Ullmann reactions with potassium 4-bromophenolate and 1-bromo-2,5-dimethoxybenzene proceeding cleavage of the ether bond with boron tribromide. This macromonomer polymerized with trifluoromethylterephthaloyl dichloride and t-butylhydroquinone through solution polycondensation in diphenyl ether to form a graft copolymer, illustrated in **Figure 3.10**.[92] Mandal et al. produced aliphatic polyesters with propargyl side groups enabling a click reaction with semi-flourinated SCLCP. This graft copolymer utilized solution

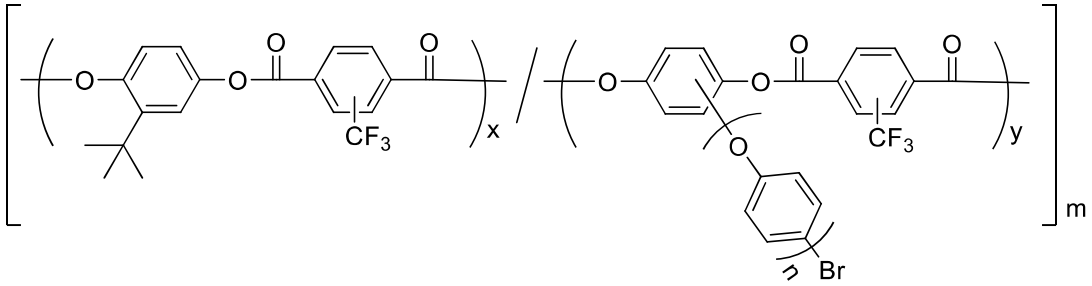

Figure 3.10. Structure of LC copolyester with PPO grafts. Adapted from Norbert et al.[92]

polymerization, as mentioned in a previous section, and the foldable aliphatic section promoted phase separation and ordering of the LC side chain groups.[39]

3.2.3.2 Segmented LC Copolyesters Synthesized via Combination of Step-Growth/ Chain-Growth Polymerization

The combination of step-growth and chain-growth polymerization to form segmented LC copolyesters enables the synthesis of some of the most well-known thermoplastic elastomers, multiblock copoly(ether-ester)s. The incompatibility between polyethers and polyesters results in macro phase separation for blended systems but forms beneficial nanoscopic phase separation for block copolymers. Thermoplastic elastomers form from multiblock copoly(ether-esters) due to the ability to combine properties from the flexible ether soft-segment and the tough physical crosslinks of the LC polyester hard-segment. The choice of polymerization technique used to synthesize these polymer systems depends heavily on the type of LC polyester. In all cases oligomers of poly(ether)s, such as polytetramethlyene oxide (PTMO or PTHF) and poly(ethylene oxide) (PEO or PEG), were synthesized or bought ahead of time at a variety of MWs. The synthesis of these poly(ethers) occurs through ring-opening polymerization using a variety of reaction conditions, as Hertzberger et al. describes.[118]

Hydroxy terminated poly(ethers) enables the oligomer to participate in transesterification reactions.

On one occasion, Pospiech et al. converted the hydroxy terminal group to a trimellitimide functionality to prevent the characteristic degradation that had been reported for PTMO with hydroxy, acetoxy, or acetamido end-groups.[78] Similar to the PSU block copolymers, incorporation of these oligomers into different polymerizations occurred through introduction as a reactive starting material, to become a repeat unit segmented within the final polymer backbone. Due to the lower reactivity of phenol monomers, fully-aromatic LCP used melt acidolysis or reactions between acyl chloride and alcohols either in the melt or in solution. One of the first studies of these polymers in 1991, utilized solution polymerization of TPC and methylhydroquinone with pyridine in 1,1,2,2-tetrachloromethane to polymerize phase separated copoly(ether-esters) with fully-aromatic LC segments.[44] For two different polymeric studies, Sonpatki et al. utilized melt transesterification with acyl chloride moieties to synthesize multiblock copolymers with PTMO segments and fully-aromatic LC segments from TPC and different hydroquinone derivatives (hydroquinone, methylhydroquinone, or chlorohydroquinone).[82,84] The trimillitimide terminated PTMO (750, 1000, and 2000 g/mol) mentioned previously utilized melt-acidolysis polymerization with acetoxy terminated HBA and an acetoxy terminated trimer, illustrated in **Scheme 3.6**.[78]

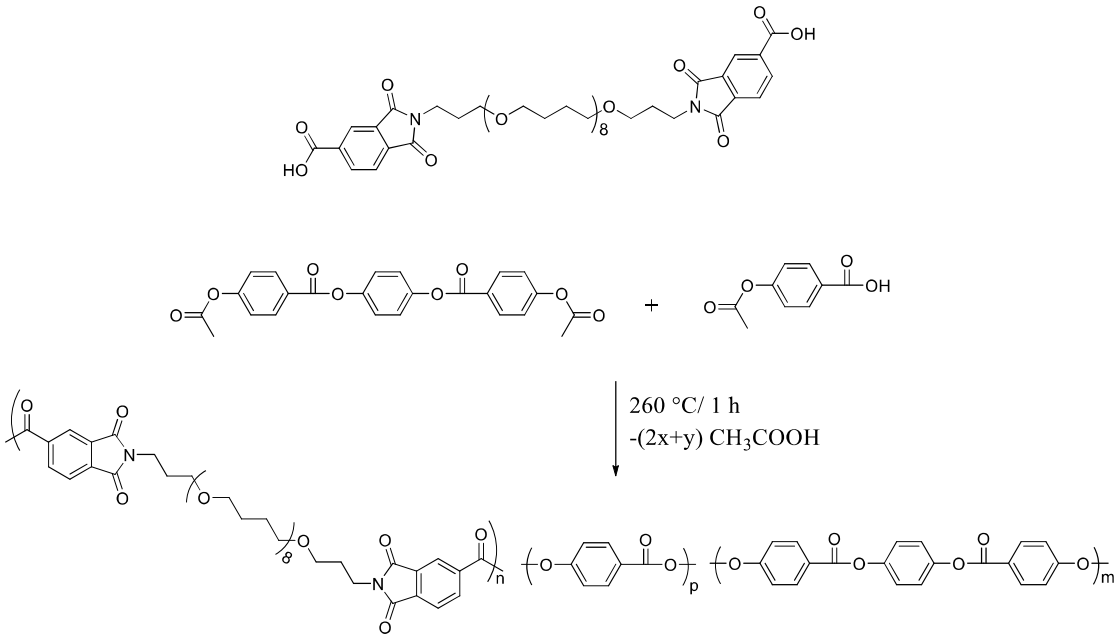

Scheme 3.6. Melt acidolysis polymerization for the synthesis of segmented LC polyester with PTMO soft-segment. Adapted from Pospiech et al.[78]

Semi-aromatic LCPs exhibit successful polymerization through melt transesterification of diester-diol monomers. Successful application of this polymerization method to multiblock copoly(ether-esters) resulted in an array of polymer structures. Tsai et al. extensively studied the incorporation of PTMO oligomers into multiblock copolymers with a series of 4,4'BB based LCP featuring different alkyl spacers through melt-transesterification.[119-121] Within the same group, Hsuie et al. synthesized multiblock copolymers with PEO soft-blocks and either poly(hexamethylene-4,4'BB) or poly(pentamethylene-4,4'BB) utilizing melt-transesterification. These studies focused on the change in hydrophilicity of the final polymers through the incorporation of a hydrophilic soft-segment.[122,123] Nelson et al. synthesized novel multiblock copolymers using pluronic oligoethers (poly(propylene glycol)-*block*-poly(ethylene glycol)-*block*-poly(propylene glycol). The polymer synthesis used one-pot melt-

transesterification with a titanium tetraisopropoxide catalyst, as illustrated in **Scheme 3.7**.[99]

Internal macroinitiators represent an innovative method to synthesize multiblock copolymers of LC polyesters and radically polymerizable segments. Angeloni et al. first proposed this technique in 1993. This work synthesized a semi-aromatic LC polyester through interfacial polymerization of 4,4'-octamethylene dioxydibenzoyl chloride, pentamethylene di(4-hydroxybenzoate) and 4,4'-azobis(4-cyanopentanoyl chloride). Upon thermal decomposition of the azo moiety in the polymer backbone, a radical initiation of styrene occurred. This resulted in a multiblock structure due to the different termination mechanisms for PS.[94]

Figure 3.11 demonstrates a schematic of this polymerization occurring. Chiellini et al. and Galli et al. further analyzed the block formation of this polymerization in

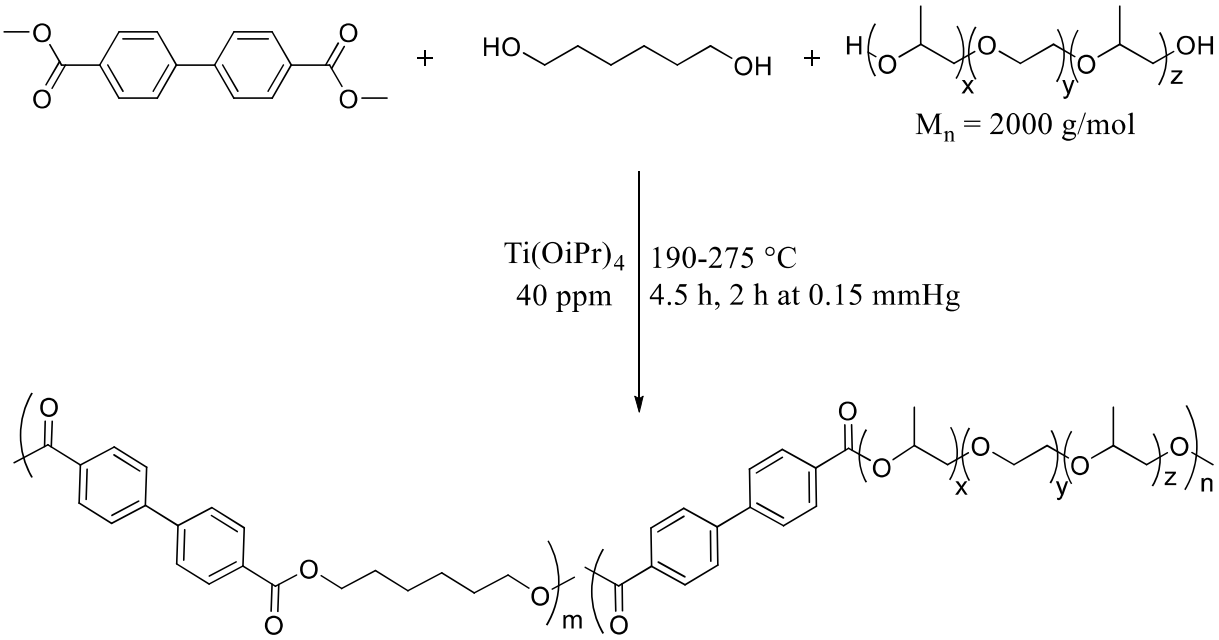

Scheme 3.7. Synthesis of segmented LC polyester with pluronic soft-segment using melt transesterification polymerization. Adapted from Nelson et al.[99]

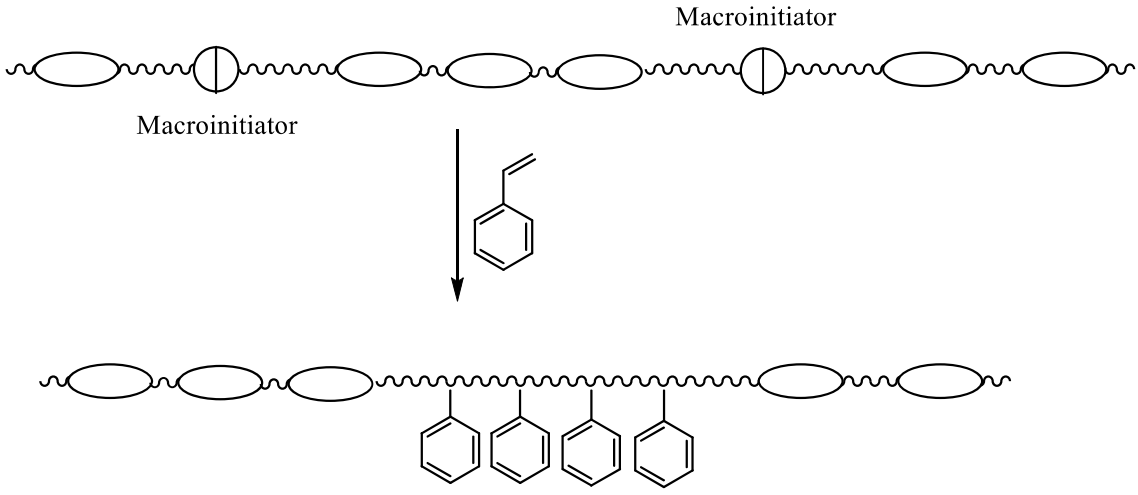

Figure 3.11. Graphical schematic of multiblock copolymers utilizing an internal macroinitiator. Adapted from Chiellini et al.[46]

1994.[46,96] Galli et al. and Laus et al. both demonstrated the use of this approach to synthesize multiblock copolymers with a combination of side-chain and main-chain LCsP. In both cases, the same semi-aromatic LCP macroinitiator initiated free radical polymerization with two different PMMA based side-chain LCPs.[45,95,124] While this method represents a creative technique to combine step-growth and chain-growth polymerization, Lin et al. recently demonstrated a much simpler approach to achieving multiblock copolymers with PS and LC polyesters. This approach functionalized PS oligomers with carboxylic acid end groups then underwent high temperature solution polymerization with HBA and HNA using the activating agent, triphenylphosphine dichloride/pyridine. Acidolysis polymerization of these PS segments would be impossible due to the ceiling temperature residing at 280 °C. The limitation of this approach resulted from the mixture of final products (PS oligomer, LC oligomer, segmented copolymer) requiring fractionation to remove unreacted oligomers.[125] Rather than polymerizing PS off of LC oligomers, Reichelt et al. coupled hydroxy terminated oligomers of PS in

solution with acid chloride terminated poly(2,2'-dimethyl-4,4'-biphenylene phenylterephthalate) at a 2:1 ratio to produce triblock copolymers.[89] The same group replaced PS with PEG to further study this coupling reaction and form hydrophilic triblock copolymers.[87]

Functionalizing the terminal group of LC polyester into macroinitiators, rather than dispersion through the backbone, enables the polymerization of copolymers with controlled architectures such as triblock copolymers. A grouping of studies performed using a semi-aromatic LC polyester (poly(4,4'BB-5(3-Me))) functionalized through post-polymerization modification with a 2-bromo-2-methylpropionyl end-group formed a terminal macroinitiator. This macroinitiator facilitated ATRP off the ends of the LCP chains forming triblock copolymers with a variety of outer blocks. Some of these outer blocks include PMMA, PEMA, and derivatized PMMA functionalized with either a semi-fluorinated or phenylbenzoate based SCLCP.[66,68,70,71,126] This method was further utilized with fully-aromatic LC polyester comprised of diphenyl-4,4'-(decane-1,10-diylbis(oxy)dibenzoate) and tert-butylhydroquinone monomers with PS outer blocks.[127]

Two examples of graft copolymers utilizing a hybrid chain/step-growth polymerization method have been studied. Heitz et al. reported the synthesis of PS graft copolymers in which macromonomers of PS bearing either a 4,4'-methylenediphenol or hydroquinone functional group were synthesized using free-radical polymerization. A two-stage solution condensation first endcapped these macromonomers with derivatives of TPC then enable the polymerization with more TPC and tert-butylhydroquinone to form graft copolymers.[128] Sato et al. synthesized a diphenolic OH-terminated PS macromonomer to expand upon this work. The Higashi method of DPCP in pyridine

with lithium chloride polymerized this macromonomer into a LC polyester.[93] Studies into the synthesis of segmented LC copolyesters span a huge range of polymer architectures and structural characteristics. These unique structures impart many interesting physical properties from magnetic orientation to blend compatibilization.

3.3 Properties of Segmented LC Copolyesters

The unique properties of segmented LC copolyesters arise from nanoscopic scale phase separations enabling the bulk properties to encompass a combination of properties from the two types of polymer segments. Unlike block copolymers, random copolymers with non-mesogenic units eventually results in a complete disruption of LC properties, such as is the case with many copolyesters. The phase separated domains of block copolymers maintain the order of the segments within those domains enabling LC or crystalline packing.

$$\chi_{AB} = \frac{V_{AB}}{RT}(\delta_A - \delta_B)^2 \quad with\ V_{AB} = (V_A - V_B)/2 \qquad (3.2)$$

In order to achieve phase separated morphologies once copolymerized, the solubility of each polymer segment within the other along with MW must be considered. The χ-parameter represents the interaction parameter between two different materials and was originally applied to studies of polymers in solution to determine the interaction between the solvent and the polymer. **Equation 3.2** expresses the parameter in mathematical form illustrating that the interaction parameter comprises the Hildebrand solubility parameters (δ) of each polymer as well as the volume (V_{AB}) of each polymer segment related to MW.[129] This basic parameter helps to determine the MW necessary to cause phase separation during the polymerization of block copolymers. Pospiech et al. demonstrated the use of this parameter in the synthesis of multiblock copolymers of

polysulfones (PSU) with a range of secondary blocks. The group calculated the χ-parameter between PSU and each composition, as illustrated in **Figure 3.12**, ranging from 0.89 to 13.68. This study fostered the understanding that for multiblock copolymers with lower χ, higher MW PSU oligomers were necessary to induce phase separation in comparison to copolymers with higher χ, such as the fluorinated SCLCP block.[73] A non-phase separated (co)polymer commonly forms with low MW PSU oligomers.

The dispersity of the polymer segments greatly affects the types of phase separated morphologies observed. Unlike multiblock copolymers, which exhibit large PDI between the segments, the narrow dispersity of controlled architectures, such as diblock/triblock copolymers, promote phase separation into ordered long range morphologies. The phase morphology of block copolymers relies heavily on the fractional composition of each block, as illustrated in **Figure 3.13**, and take 3D

Polymer	Non-PSU structure in block copolymer	χ
PSU-poly(tetramethylene oxide)	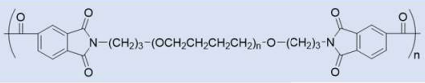	0.89
PSU-poly(ethylene terephthalate-co-oxybenzoate)	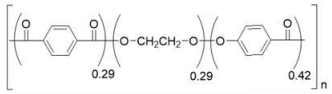	0.07
PSU-poly(ethylene terephthalate-co-polyester imide)	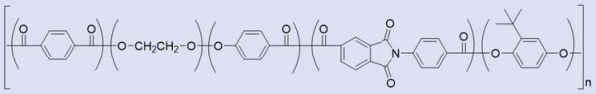	1.61
PSU-poly(ester imide) R= t-butyl or phenyl substituent	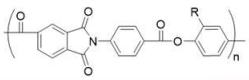	0.75 or 2.22
PSU-poly(phenyl-p-phenylene terephthalate)	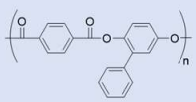	0.45
PSU-semifluorinated polyester multiblock copolymer	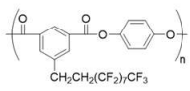	13.68

Figure 3.12. Segmented copolysulfones utilizing a range of secondary block structures exhibiting different χ parameters. Adapted from Pospiech et al.[73]

structures, such as lamellar, cylindrical, and spherical.[130-132] The development of X-Ray scattering to analyze well-ordered morphologies led to in depth understanding of molecular orientation within layers. These structures exhibit significant use in nanotemplating for lithographic applications. Many applications deem controlled morphologies unnecessary and a multiblock copolymer produces proper phase separation to achieve the properties desired.

Microphase separated block copolymers maintain the properties of each polymer segment within the domain of that material. As a result, the thermal properties of block copolymers generally exhibit the same transitions observed for each separate

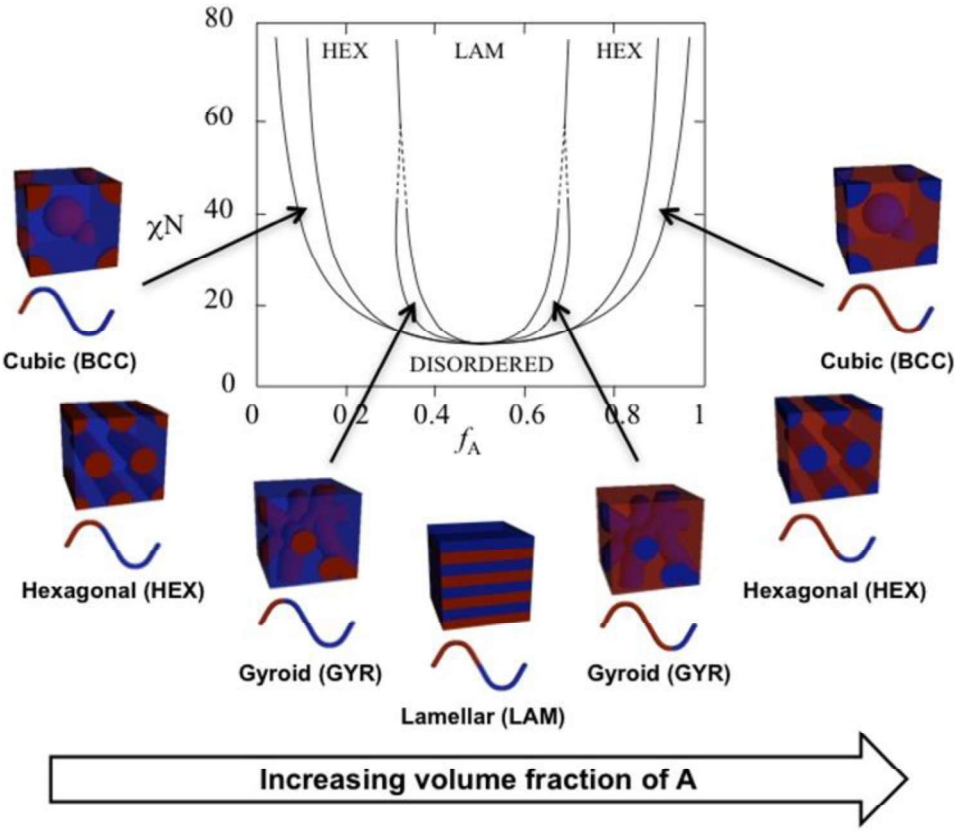

Figure 3.13. Phase diagram of morphological changes within the compositional range of a block copolymer. Reprinted with permission from Swann, J. M. G.; Topham, P. D., *Polymers* **2010**, *2*, 454.[132]

homopolymer. For example, two glass transition temperatures (T_g) corresponding to the T_g for each separate segment occurs in both multiblock copolymers and well-defined morphologies. Ishige et al. observed two T_g's for the well-ordered tri-block copolymer.[68] If the homopolymer of the segment exhibits a LC mesophase, ordering occurs within the domains of the LC segment. This results in the observation of a T_i in the block copolymers with the ΔH_i relying on the volume of the segment. The ability to form a LC mesophase within the phase separated domain boundary exhibits a length scale limit. An early study reported that the confinement of a nematic material within a droplet of 350 nm exhibited a well-defined T_i while reduction of the droplet to less than 35 nm resulted in loss of LC order.[133] Polymer segments also exhibit crystallization with the phase separated domain and a T_m associated with segregated domain melting occurs. In all cases, unless intermixing happens between the segments, the crystalline packing structure and mesophase morphology remains the same between the homopolymers and the block copolymers. The difference in ΔH and slight shifts in the T_m/T_i are attributed to MW differences between the segment lengths and the high MW homopolymer as well as the overall volume change of the ordered segments within the copolymer throughout the series.

The mechanical properties of the bulk materials also comprise a combination of each block's properties. This represents the basis for the development of thermoplastic elastomers. The hard-segment, usually a semi-crystalline or LC polymer, acts as a physical crosslink while the low T_g amorphous segment imparts flexibility. Scientists studying TPEs exhibited interest in LC polyesters because of their high tensile properties. Pospiech et al. demonstrated the formation of a TPE with LC hard-segments through the

combination of an acetoxy terminated LC trimer with a p-acetoxybenzoic acid chain extender and trimellitimide terminated PTMO. The group noted that when utilizing PTMO, a degree of polymerization between 8-13 afforded phase separation resulting in elastic properties while higher MW soft-segments overwhelmed the HS resulting in LC domain disruption.[78] Sonpatki et al. also noted elastomeric properties in their multiblock copoly(ether ester).[82] These systems impart inherent tunability onto the bulk mechanical properties during the synthesis through a balance between number of crosslinks and amount of flexibility. In dynamic mechanical analysis, these types of polymers exhibit an extended plateau after the soft-segment T_g and a flow temperature consistent with the disruption of the hard-segment.

For multiblock copolymers utilizing high-performance polymers, thermoplastic elastomers were not the primary goal of copolymerizing. Instead, other benefits arose from blend compatibilization and shear flow modulation. Blend compatibilizing occurs through lowering the surface tension at the interface between two polymers. Block copolymers act as a bridge between the two polymers resulting in a lower degree of phase separation in the blend.[29] Yang et al. synthesized multiblock copolymers from a thermotropic LC polyester and PEEK segments to act as a compatibilizer between blends of the homopolymers. The non-compatibilized blends exhibited a strong interface at the surface between the two blends during SEM of the fracture surface. Incorporating different phase separated block copolymers compatibilized the blend resulting in a undiscernible interface.[86]

PEEK and PSU high performance polymers exhibit high melt viscosities causing difficulties when processing these materials. Uniquely, LC alignment facilitates

significant shear thinning in the melt which resulted in their success/commercialization as composites in injection molded parts. The phase separation of LC segments enables the bulk properties to benefit from the reduced viscosity of the LC polymers resulting in an overall decrease in melt viscosity. Studies demonstrated that the bulk melt viscosity ranges between the values of the two homopolymers in a compositional range of block copolymers.[73]

For tri/di block copolymers exhibiting well-ordered morphologies, extensive studies determined the orientation of the LC mesophase within the phase separated domains. These studies utilized a non-crystalline smectic center block and various outer blocks ranging from amorphous to SCLCPs. Koga et al. determined that for a triblock copolymer series using PEMA outer blocks, as the fraction of amorphous polymer increased the lamellar thickness remained stable until transitioning into cubes and finally disordered spheres at $\delta > 68$ %. The smectic mesophases form chain folding lamella with extend chain conformations in which the folding surface oriented parallel to the phase separated lamellae boundary. As the amorphous domain in the lamellae increased, the LC

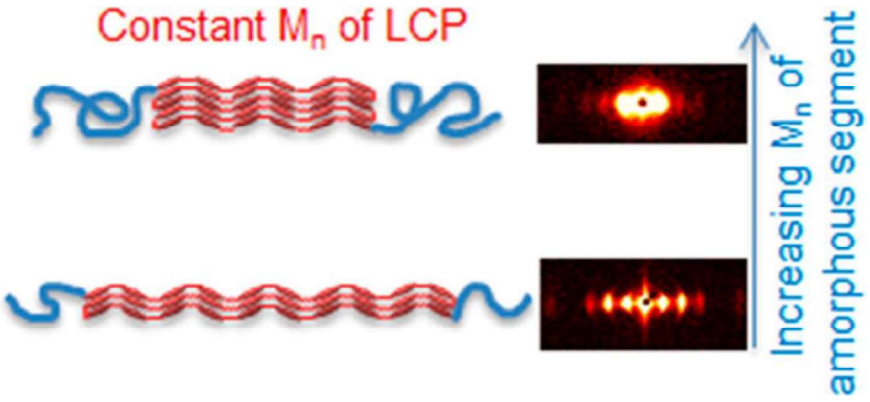

Figure 3.14. Change in lamellar thickness of smectic phase as amorphous domain increases in a triblock copolymer. Reprinted with permission from Koga, M.; Ishige, R.; Sato, K.; Ishii, T.; Kong, S.; Sakajiri, K.; Watanabe, J.; Tokita, M., *Macromolecules* **2012**, *45*, 9383. Copyright © 2012 American Chemical Society.[98]

phase counterbalanced by increasing the number of folds that occurred and extending the phase boundary between the LC and PEMA maintaining the lamellar thickness, as observed in **Figure 3.14**.[70,98] Studies utilizing another amorphous outer block, PMMA, corroborated this reported ordering.[126] WAXS proved in both cases that within the phase boundaries a S_{CA} mesophase remained.[70,98,126] SAXS at temperatures greater than the center block T_i indicated that lamellar phase separation relies on the volume fraction of the outer block. Polymers with < ~ 40 % PMMA/ PEMA resulted in disruption of microphase separated structure above the T_i of the LC block. [98]

The exchange of the outer block to a side-chain LCP did not impact the ordering of the internal S_{CA} polyester. Both a semi-fluorinated and a phenyl benzoate based SCLCP resulted in primarily lamellar phase separated morphologies. The phenyl benzoate based SCLCP exhibited lamellar morphology with volume fractions ranging from 22-56 % outer block then transitioned into a hexagonally packed cylinder at 65 %, finally achieving spherical domains at 81 % of the SCLCP. The mesophases of each block stayed the same regardless of the phase separated morphology. Unlike the internal block, the SCLCP exhibited a S_A mesophase and in both domains the smectic layers lay parallel to the lamellar interface while the LC director lay perpendicular, as seen in **Figure 3.15**. This homeotropic LC anchoring at the interface demonstrates the fact that

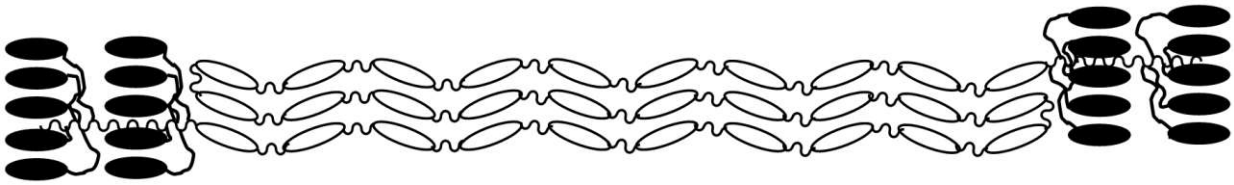

Figure 3.15. Simplified two-phase model of microdomain phase separated structure within a triblock copolymer made up of a MCLCP inner block and SCLCP outer block. Open oval indicative of main-chain LCP structure while filled oval indicates side-chain LCP structure. Adapted from Koga et al.[66]

the LC morphology of the internal block influences the outer block as this ordering contradicts previous studies in which non-LC internal blocks exhibited planar anchoring of the SCLCP at the interface.[66] The exchange of the phenyl benzoate SCLCP for a semi-fluorinated block results in a change in the outer block morphology to tilted hexatic with a bilayer structure, likely S_F or S_I. Higher immiscibility between the fluorinated block and the polyester resulted in a well-controlled lamellar morphology from 11-70 % outer block, as well as the maintenance of the lamellar structure at temperatures above the T_i of the SCLCP mesophase. Unlike the aromatic SCLCP, the DP of the outer block impacts the direction of the LC director (long-axis of mesogen). In depth SAXS/WAXS studies elucidated that short outer block chains result in the LC director of the SCLCP laying parallel to the MCLCP and perpendicular to the microphase interface. Increasing the

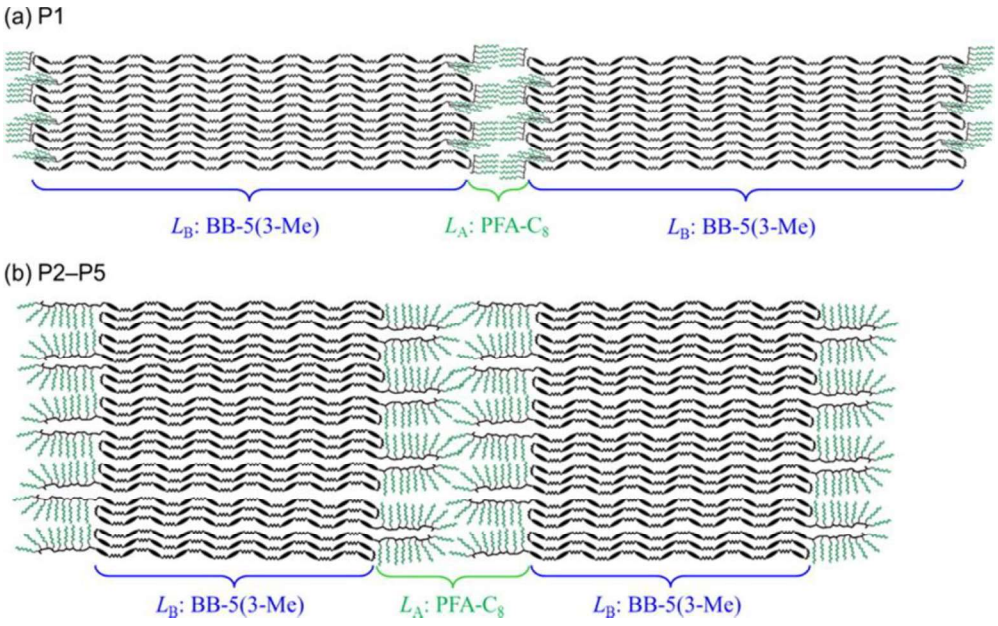

Figure 3.16. Two-phase model of microdomain phase separated structure within a triblock copolymer made up of a MCLCP inner block and fluorinated SCLCP outer block. Reprinted with permission from Ishige, R.; Ohta, N.; Ogawa, H.; Tokita, M.; Takahara, A., *Macromolecules* **2016**, *49*, 6061. Copyright © 2016 American Chemical Society.[68]

chain length resulted in the opposite orientation to the interface, as seen in **Figure 3.16**. This suggests a counterplay between the need to match the interfacial area and the energetic favoring to match smectic layer orientation.[68] Due to the low surface free energy of the semi-fluorinated chains, block copolymers with high outer block content (70 %) resulted in a perpendicular lamellar structure relative to the silicone surface without extra processing steps.[68]

Sato et al. studied the ordering of an ABA triblock copolyester with a nematic internal block utilizing a fully-aromatic copolyester and an amorphous PS outer block. Unlike smectic mesophases, the nematic ordering results in the LC director laying parallel to the microphase interface. The lamellar spacing in this polymer increases reversibly with increasing temperature, associated with an increase in chain folding, then disrupts completely upon isotropization of the LC segment, as illustrated in **Figure 3.17**.[127]

3.3.1 Orientation of Segmented LC Copolyesters

Orientation of block copolymers enables the formation of nanostructured morphologies over large length scales. Direction of the LC phases within the block

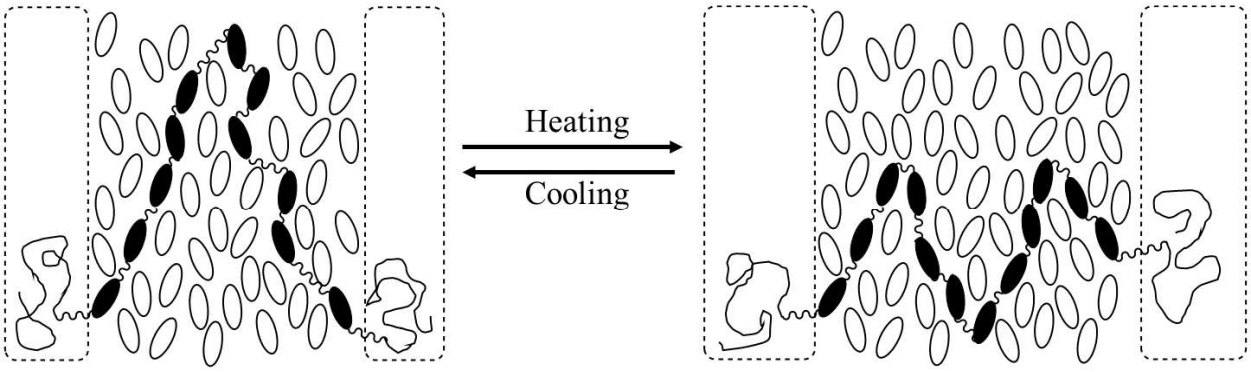

Figure 3.17. Two-phase model of microdomain phase separated structure within a triblock copolymer made up of a nematic LCP inner block and amorphous outer block. Adapted from Sato et al.[127]

copolymer significantly impacts this orientation. Orientation of segmented LC polyesters occurs both through application of mechanical (shear/tensile) strain or in the presence of a magnetic field. Electrical orientation has yet to be examined for these systems.

Mechanical orientation of LC polyesters in commercial processes usually occurs through fiber drawing. Nematic polymers, such as fully-aromatic polyesters, orient the LC director with the pull direction therefore in line with the fiber length resulting in the high tensile properties associated with these materials.[20] Smectic polymer orientation relies on the speed of mechanical deformation. Osada et al. showed through WAXS analysis of drawn fibers that fast drawing speeds result in orientation of the smectic layers perpendicular to the fiber axis while slow speeds result in parallel layer orientation. This is attributed to flow within the smectic layer when rate of strain is slow enough to prevent domains disruption.[134,135] Koga et al. studied the orientation of fibers comprised of a PEMA-[BB-5(3-Me)]-PEMA triblock. The orientation of the phase separated structure and mesophase packing changed depending on the thermal history of the fiber. Fibers that were spun at temperatures above the T_i and quickly quenched resulted in the LC director of the smectic polymer parallel with the microdomain interface due to the polymer chains aligning in the direction of the orientation. Annealing the spun fiber below T_i maintained the chain alignment but the phase separate morphology migrated so that the lamellae interface returned to the energetically favored position perpendicular to LC director (parallel with smectic layers). As a result, the phase separated lamella structure lay perpendicular to the fiber axis. Heating the spun fiber above the T_i resulted in disruption of the internal block but maintained the phase separated morphology. Cooling back down below T_i resulted in homeotropic anchoring of the mesogens at the

interface to the energetically favored orientation and final lamellar microstructure orienting parallel with the fiber axis.[71] **Figure 3.18** illustrates this unique orientation behavior. On the contrary orientation of a triblock copolymer with an internal nematic block resulted in the lamellar layers and the LC director of the nematic polymer parallel to the fiber direction as expected.[127]

Magnetic orientation of segmented LC copolyesters has only been demonstrated in one study. Deshmukh et al. synthesized novel brush-like block copolymers with SCLCP and PLA grafted blocks, which exhibited a hexagonally packed cylindrical morphology.[110] The SCLCP chosen exhibited the required magnetic anisotropy. Previous studies indicated that orientation of a LC block copolymer under a magnetic field relies on orientation of the mesogen relative to the microphase interface, while the kinetics of the alignment rely on the viscosity of the material. In the case of the cylindrical morphologies, the mesogens anchored planar to the interface of the cylinder resulting in

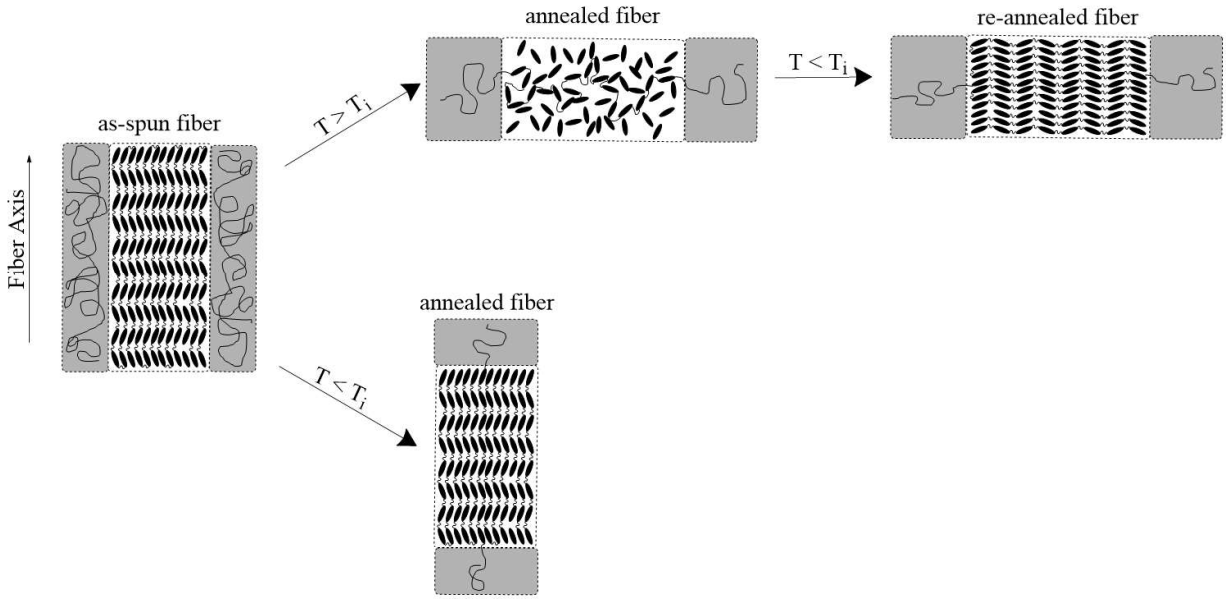

Figure 3.18. Orientation of lamellar and smectic layer structures in fibers with different thermal histories. Fiber axis is vertical. Adapted from Koga et al.[71]

parallel alignment relative to the magnetic field. [136-138] Orientation occurs upon cooling the sample through its mesophase while in the presence of the magnetic field. The driving force for alignment results from the ordering of the mesophase below the T_i. In a material which is weakly segregated, the LC order drives phase separation resulting in a disorder temperature of the phases separated morphology equivalent to the T_i. This enables better alignment due to the low viscosity above the T_i and a drastic decrease in mobility below the T_i freezing the orientation into place. The increased mobility of the material imparted through the addition of plasticizers resulted in effective orientation of cylinders and smectic layer normal parallel to the magnetic field. X-ray scattering elucidated the order parameter revealing a value of P= 0.98 where 0 indicates complete disorder and 1 completely ordered systems.[110]

3.4 Conclusions

Segmented LC copolyesters represent a field of block copolymers encompassing intricately controlled architectures to multiblock copolymers utilized in commercial applications. These materials exhibit phase separated morphologies that incorporate the beneficial properties of each polymer and combine them into all-inclusive materials. The choice of segments stems from the desired final properties, as drastically different materials can be synthesized. The combination of flexible ether soft-segments with rigid main-chain LC polyesters form thermoplastic elastomers while exchanging these soft-blocks with high-performance polymers results in high tensile materials that exhibit low melt viscosities and act as compatibilizers to blends. Controlling the synthetic methods to reduce Đ of the blocks enables the formation of well-ordered phase separated structures that form long range nanostructures in fibers and films through mechanical and magnetic

orientation. This area of long-range nanostructures will benefit greatly from increased research and could be incredibly beneficial to the field of lithography bringing scientists one step closer to the computers and phones of the future.

References

(1) Work, W. J.; Horie, K.; Hess, M.; Stepto, R. F. T. In *Pure Applied Chemistry* 2004; Vol. 76, p 1985.

(2) Carothers, W. H.; Arvin, J. A., Studies on Polymerization and Ring Formation. II. Poly-esters, *Journal of American Chemical Society* **1929**, *51*, 2560.

(3) Carothers, W. H., Studies on Polymerization and Ring Formation. I. An Introduction to the General Theory of Condensation Polymers, *Journal of American Chemical Society* **1929**, *51*, 2548.

(4) Whinfield, J. R.; Dickson, J. T., British Patent 578,079, June 16, 1946.

(5) Whinfield, J. R., Chemistry of 'Terylene', *Nature* **1946**, *158*, 930.

(6) Geyer, R.; Jambeck, J. R.; Law, K. L., Production, use, and fate of all plastics ever made, *Science Advances* **2017**, *3*.

(7) Ji, L. N., Study on Preparation Process and Properties of Polyethylene Terephthalate (PET), *Applied Mechanics and Materials* **2013**, *312*, 406.

(8) Scheirs, J.; Long, T. E., *Modern polyesters: chemistry and technology of polyesters and copolyesters*; John Wiley: Hoboken, NJ;Chichester, England;, 2003.

(9) Collings, P. J.; Hird, M.; Huang, C. C., Introduction to Liquid Crystals: Chemistry and Physics, *American Journal of Physics* **1998**, *66*, 551.

(10) Tai-Shung, C., The recent developments of thermotropic liquid crystalline polymers, *Polymer Engineering & Science* **1986**, *26*, 901.

(11) Hussein, M. A.; Abdel-Rahman, M. A.; Asiri, A. M.; Alamry, K. A.; Aly, K. I., Review on: liquid crystalline polyazomethines polymers. Basics, syntheses and characterization, *Designed Monomers and Polymers* **2012**, *15*, 431.

(12) Friedel, G., Les états mésomorphes de la matière, *Ann. Phys.* **1922**, *9*, 273.

(13) Collings, P. J., *Liquid Crystals: Nature's Delicate Phase of Matter*; 2nd Ed. ed.; Princeton University Press, 1947.

(14) Chung, T., *Thermotropic liquid crystal polymers: thin-film polymerization, characterization, blends, and applications*; Technomic Pub. Co: Lancaster, Pa, 2001.

(15) In *Handbook of Liquid Crystals*.

(16) Flory, P. J., Phase Equilibria in Solutions of Rod-Like Particles, *Proceedings of the Royal Society of London. Series A, Mathematical and Physical Sciences* **1956**, *234*, 73.

(17) Flory, P. J., In *Recent Advances in Liquid Crystalline Polymers*; Chapoy, L. L., Ed.; Springer Netherlands: Dordrecht, 1985, p 99.

(18) Cowie, J. M. G., Liquid crystal polymers: From structures to applications. Edited by A. A. Collyer. Elsevier Science Publishers, London, 1992. pp. xvi + 474, price £110.00. ISBN 1-85166-797-0, *Polymer International* **1994**, *34*, 122.

(19) Calundann, G. W., Polyester of 6-Hydroxy-2-naphthoic Acid and Para-hydroxy Benzoic Acid Capable of Readily Undergoing Melt Processing. U.S. Patent 4,161,470, October, 20 1977.
(20) Jackson, W. J., Liquid Crystal Polymers. IV. Liquid Crystalline Aromatic Polyesters, *British Polymer Journal* **1980**, *12*, 154.
(21) Jackson, W. J.; Kuhfuss, H. F., Liquid crystal polymers. I. Preparation and properties of p-hydroxybenzoic acid copolyesters, *Journal of Polymer Science: Polymer Chemistry Edition* **1976**, *14*, 2043.
(22) Jackson, W. J.; Kuhfuss, H. F., Liquid crystal polymers. III. Preparation and properties of poly(ester amides) from p-aminobenzoic acid and poly(ethylene terephthalate), *Journal of Applied Polymer Science* **1980**, *25*, 1685.
(23) Speckhard, T. A.; Miller, J. A.; Cooper, S. L., Monte Carlo simulation study of the polymerization of polyurethane block copolymers. 1. Natural compositional heterogeneity under ideal polymerization conditions, *Macromolecules* **1986**, *19*, 1558.
(24) Peebles, L. H., Sequence Length Distribution in Segmented Block Copolymers, *Macromolecules* **1974**, *7*, 872.
(25) Miller, J. A.; Speckhard, T. A.; Cooper, S. L., Monte Carlo simulation study of the polymerization of polyurethane block copolymers. 2. Modeling of premature phase separation during reaction using the two-phase ideal reaction model, *Macromolecules* **1986**, *19*, 1568.
(26) G., H.; T., B. E.; R., L. N., Thermoplastic elastomers, *Journal of Polymer Science Part C: Polymer Symposia* **1969**, *26*, 37.
(27) Szwarc, M.; Levy, M.; Milkovich, R., Polymerization Initiated by Electron Transfer to Monomer. A New Method of Formation of Block Polymers, *Journal of American Chemical Society* **1956**, *78*, 2656.
(28) Rogers, M. E.; Long, T. E., *Synthetic Methods in Step-Growth Polymers*.
(29) Wang, T. T.; Wang, H. B.; Liu, Z. Z.; Liu, T.; Zhang, H.; Yang, Y. H., Synthesis and characterization of liquid crystalline copolymers containing poly (ether sulfone) segments, *High Performance Polymers* **2012**, *24*, 289.
(30) Zeng, L. X.; Li, R. S.; Chen, P.; Xu, J. J.; Liu, P. Q., Synthesis and characterization of thermotropic liquid crystalline polyarylate with ether ether ketone segments in the main chain, *Journal of Applied Polymer Science* **2016**, *133*.
(31) Lodge, T. P., Block Copolymers: Past Successes and Future Challenges, *Macromolecular Chemistry and Physics* **2003**, *204*, 265.
(32) Odian, G. G., *Principles of polymerization*; Wiley: New York, 1991.
(33) Kang, H.; Lin, Q.; Armentrout, R. S.; Long, T. E., Synthesis and Characterization of Telechelic Poly(ethylene terephthalate) Sodiosulfonate Ionomers, *Macromolecules* **2002**, *35*, 8738.
(34) Weingart, F., Thesis, Type, University of Stuttgart, 1994.
(35) Nachtergael, A.; Coulembier, O.; Dubois, P.; Helvenstein, M.; Duez, P.; Blankert, B.; Mespouille, L., Organocatalysis Paradigm Revisited: Are Metal-Free Catalysts Really Harmless?, *Biomacromolecules* **2015**, *16*, 507.

(36) Choi, W. S.; Padias, A. B.; Hall, H. K., LCP aromatic polyesters by esterolysis melt polymerization, *Journal of Polymer Science, Part A: Polymer Chemistry* **2000**, *38*, 3586.
(37) Calundann, G. W.; Charbonneau, L. F.; Benicewicz, B. C., Melt Processing Polyester Capable of Forming an Anisotropic Melt Comprising a Relatively Low Concentration of 6-oxy-2-naphthoyl moiety, 4-benzoyl moiety, 1,4-dioxyphenylene moiety, isophthaloyl moiety, and terephthaloyl moiety. U.S. Patent 4,522,974, June 11, 1985.
(38) Valery, A. V.; Svetlana, V. V., Advances in Acceptor-catalytic Polyesterification, *Russian Chemical Reviews* **1979**, *48*, 16.
(39) Mandal, J.; Prasad, S. K.; Rao, D. S. S.; Ramakrishnan, S., Periodically Clickable Polyesters: Study of Intrachain Self-Segregation Induced Folding, Crystallization, and Mesophase Formation, *Journal of American Chemical Society* **2014**, *136*, 2538.
(40) Higashi, F.; Ong, C. H.; Kim, J. H., Attempt to control monomer sequences in copolycondensations of IPA, TPA, BPA, and PHB, *Journal of Polymer Science, Part A: Polymer Chemistry* **1999**, *37*, 2371.
(41) Meng, F. B.; Zhang, B. Y.; Xu, Y.; Liu, J. Y., Main-chain liquid-crystalline ionomers bearing potassium sulfonate groups, *Journal of Applied Polymer Science* **2005**, *96*, 2021.
(42) Yan, Q.; He, J., Segmented liquid crystalline copolyesters and blending with poly(ethylene terephthalate), *Polymer Bulletin* **1995**, *34*, 441.
(43) Ignatious, F.; Lenz, R. W.; Kantor, S. W., Synthesis and Characterization of Block-Copolymers Containing Rigid Liquid-Crystalline and Flexible Butylene Terephthalate Segements, *Macromolecules* **1994**, *27*, 5248.
(44) Wang, J.; Lenz, R. W., Preparation and properties of a liquid crystalline segmented block copolyester, *Polymer Engineering & Science* **1991**, *31*, 739.
(45) Galli, G.; Chiellini, E.; Laus, M.; Bignozzi, M. C.; Angeloni, A. S.; Francescangeli, O., Synthesis and thermal behavior of liquid-crystalline block copolymers containing both main-chain and side-chain mesomorphic blocks, *Macromolecular Chemistry and Physics* **1994**, *195*, 2247.
(46) Chiellini, E.; Galli, G.; Angeloni, A. S.; Laus, M.; Bignozzi, M. C.; Yagci, Y.; Serhatli, E. I., Hybrid Thermotropic Liquid-Crystalline Block-Copolymers, *Macromolecular Symposia* **1994**, *77*, 349.
(47) Huang, J. M.; Kuo, J. F.; Chen, C. Y., Synthesis and Characterization of Segmented Liquid-Crystal Poly(azoxy polyester-co-polyoxypropylene), *Journal of Polymer Science, Part A: Polymer Chemistry* **1995**, *33*, 165.
(48) Dove, A. P., Organic Catalysis for Ring-Opening Polymerization, *ACS Macro Letters* **2012**, *1*, 1409.
(49) Kiesewetter, M. K.; Shin, E. J.; Hedrick, J. L.; Waymouth, R. M., Organocatalysis: Opportunities and Challenges for Polymer Synthesis, *Macromolecules* **2010**, *43*, 2093.
(50) Liquid Crystals. Vol. 3: Topics in Physical Chemistry, *Zeitschrift Für Kristallographie* **1995**, *210*, 976.
(51) Demus, D., *Handbook of liquid crystals*; Weinheim ; New York : Wiley-VCH, c1998., 1998.

(52) Tokita, M.; Funaoka, S.-i.; Watanabe, J., Study on Smectic Liquid Crystal Glass and Isotropic Liquid Glass Formed by Thermotropic Main-Chain Liquid Crystal Polyester, *Macromolecules* **2004**, *37*, 9916.
(53) Ciferri, A., *Liquid crystallinity in polymers: principles and fundamental properties*; VCH Publishers: New York, 1991.
(54) James, E.; S., S. R.; I., M. V.; G., C. S.; E., N. B., Synthesis and structure of the p-hydroxybenzoic acid polymer, *Journal of Polymer Science: Polymer Chemistry Edition* **1976**, *14*, 2207.
(55) Jin, J.-I.; Kang, C.-S., Thermotropic main chain polyesters, *Progress in Polymer Science* **1997**, *22*, 937.
(56) Economy, J.; Goranov, K., Thermotropic Liquid-Crystalline Polymers for High-Performance Applications, *Advanced Polymer Science* **1994**, *117*, 221.
(57) Cottis, S. G.; Economy, J.; Nowak, B. E., U.S. Patent 3,637,595, January 25, 1972.
(58) Cottis, S. G.; Economy, J.; Wohrer, L. C., US Patent 3,975,487, August 17, 1976.
(59) Tokita, M.; Watanabe, J., Several Interesting Fields Exploited through Understanding of Polymeric Effects on Liquid Crystals of Main-Chain Polyesters, *Polymer Journal* **2006**, *38*, 611.
(60) Watanabe, J.; Hayashi, M.; Nakata, Y.; Niori, T.; Tokita, M., Smectic liquid crystals in main-chain polymers, *Progress in Polymer Science* **1997**, *22*, 1053.
(61) Watanabe, J.; Hayashi, M.; Morita, A.; Tokita, M., Thermotropic Liquid Crystals of Main-Chain Polyesters Having a Mesogenic 4,4'-Biphenyldicarboxylate Unit. 6. Chiral Mesophases of Polyesters with a (S)-2-Methylbutylene Spacer, *Macromolecules* **1995**, *28*, 8073.
(62) Watanabe, J.; Hayashi, M., Thermotropic liquid crystals of polyesters having a mesogenic p,p'-bibenzoate unit. 1. Smectic A mesophase properties of polyesters composed of p,p'-bibenzoic acid and alkylene glycols, *Macromolecules* **1988**, *21*, 278.
(63) Krigbaum, W. R.; Asrar, J.; Toriumi, H.; Ciferri, A.; Preston, J., Aromatic polyesters forming thermotropic smectic mesophases, *Journal of Polymer Science: Polymer Letters Edition* **1982**, *20*, 109.
(64) Watanabe, J.; Hayashi, M., Thermotropic liquid crystals of polyesters having a mesogenic p,p'-bibenzoate unit. 2. X-ray study on smectic mesophase structures of BB-5 and BB-6, *Macromolecules* **1989**, *22*, 4083.
(65) Perez, E.; Fernandez-Blazquez, J. P.; Martinez-Gomez, A.; Bello, A.; Cerrada, M. L.; Benavente, R.; Perena, J. M., In *Applications of Synchrotron Light to Scattering and Diffraction in Materials and Life Sciences*; Ezquerra, T. A., GarciaGutierrez, M. C., Nogales, A., Eds. 2009; Vol. 776, p 157.
(66) Koga, M.; Sato, K.; Kang, S.; Tokita, M., Microphase-Separated Morphology and Liquid Crystal Orientation in Block Copolymers Comprising a Main-Chain Liquid Crystalline Central Segment Connected to Side-Chain Liquid Crystalline Segments at Both Ends, *Macromolecular Chemistry and Physics* **2018**, *219*, 1700332.
(67) Tokita, M.; Sugimoto, A.; Takahashi, C.; Yoshihara, S.; van de Watering, R.; Kang, S., Extended Chain Lamella Formation Characteristics of Main-Chain

Smectic Liquid Crystalline Copolyesters Comprising Different Length Units, *Macromolecules* **2016**.
(68) Ishige, R.; Ohta, N.; Ogawa, H.; Tokita, M.; Takahara, A., Fully Liquid-Crystalline ABA Triblock Copolymer of Fluorinated Side-Chain Liquid-Crystalline A Block and Main-Chain Liquid-Crystalline B Block: Higher Order Structure in Bulk and Thin Film States, *Macromolecules* **2016**, *49*, 6061.
(69) Koga, M.; Tokita, M., Micro-Phase Separated Structures of Block Copolymers Having a Semiflexible Liquid Crystalline Main-Chain Polyester Block, *Kobunshi Ronbunshu* **2014**, *71*, 501.
(70) Koga, M.; Abe, K.; Sato, K.; Koki, J.; Kang, S.; Sakajiri, K.; Watanabe, J.; Tokita, M., Self-Assembly of Flexible–Semiflexible–Flexible Triblock Copolymers, *Macromolecules* **2014**, *47*, 4438.
(71) Koga, M.; Sato, K.; Kang, S. M.; Sakajiri, K.; Watanabe, J.; Tokita, M., Influence of Smectic Liquid Crystallinity on Lamellar Microdomain Structure in a Main-Chain Liquid Crystal Block Copolymer Fiber, *Macromolecular Chemistry and Physics* **2013**, *214*, 2295.
(72) Amendola, E.; Carfagna, C.; Netti, P.; Nicolais, L.; Saiello, S., The Influence of a Copolymer as Adhesion Promoter for Polycarbonate and Liquid-Crystralline Polymer Blends, *Journal of Applied Polymer Science* **1993**, *50*, 83.
(73) Pospiech, D.; Haussler, L.; Eckstein, K.; Komber, H.; Voigt, D.; Jehnichen, D.; Friedel, P.; Gottwald, A.; Kollig, W.; Kricheldorf, H. R., Synthesis and phase separation behaviour of high performance multiblock copolymers, *High Performance Polymers* **2001**, *13*, S275.
(74) Gopakumar, T. G.; Ponrathnam, S.; Rajan, C. R.; Fradet, A., Block copolymers of telechelic poly(phenylene sulfide) and semiaromatic thermotropic liquid crystalline polyester segments, *Journal of Polymer Science, Part A: Polymer Chemistry* **1998**, *36*, 2707.
(75) Suenaga, J.-i.; Owaki, T.; Egawa, M., Wholly Aromatic Heat-Stable Liquid Crystalline Polyester Resin Composition with Improved Melt Flowability. US Patent 6,656,386 B2, December 2, 2003.
(76) Cottis, S. G.; Layton, R.; Field, N. D., Injection Moldable Aromatic Polyesters Compositions and Method of Preparation. US Patent 4,563,508, January 7, 1986.
(77) Jackson Jr., W. J.; Morris, J. C., Liquid Crystal Copolyesters Containing Terephthalic Acid and 2,6-Napthalenedicarboxylic Acid. US Patent 4,169,933, October 2, 1979.
(78) Pospiech, D.; Komber, H.; Voigt, D.; Häußler, L.; Meyer, E.; Schauer, G.; Jehnichen, D.; Böhme, F., Thermotropic elastomers with poly(oxy-1,4-butanediyl) units in the main chain, *Macromolecular Chemistry and Physics* **1994**, *195*, 2633.
(79) Chain-Shu, H.; Ling-Bar, C., Synthesis and characterization of block copolymers of polyether sulfone with liquid crystalline polyesters, *Materials Chemistry and Physics* **1993**, *34*, 28.
(80) Stinson, S., Polyesterification mechanism study, *Chemical & Engineering News Archive* **1997**, *75*, 29.

(81) Jannesari, A.; Ghaffarian, S. R.; Molaei, A., The effect of curing reaction on mesophase-rich islands of segmented main chain liquid crystalline oligoesters, *Reactive & Functional Polymers* **2006**, *66*, 1250.
(82) Sonpatki, M. M.; Ravindranath, K.; Ponrathnam, S., Random thermotropic elastomers: effect of hard/soft-segment lengths on the properties of liquid-crystalline copoly(ether ester)s, *Polymer* **1995**, *36*, 3127.
(83) Pospiech, D.; Haussler, L.; Komber, H.; Voigt, D.; Jehnichen, D.; Janke, A.; Baier, A.; Eckstein, K.; Bohme, F., LC multiblock copolymers containing polysulfone segments .1. Synthesis and morphology, *Journal of Applied Polymer Science* **1996**, *62*, 1819.
(84) Sonpatki, M. M.; Ravindranath, K.; Ponrathnam, S., Segmented copoly(ether-ester) elastomers - influence of hard segment length and substitutions on mesophase formation, *Polymer Journal* **1994**, *26*, 804.
(85) Brenda, S.; Heitz, W.; Karbach, A.; Wehrmann, R., Block-Copolymers of Poly(ether-ether-sulfones) with Liquid Crystalline Non-Liquid-Crystalline Polyesters, *Macromolecular Chemistry and Physics* **1994**, *195*, 1327.
(86) Yang, Y. H.; Zhu, W. C.; Jiang, D.; Ma, R. T.; Jiang, Z. H., Synthesis of multi-block copolymer and its compatibilization to the blends of poly(ether ether ketone) with thermotropic liquid crystalline polymer, *Journal of Applied Polymer Science* **2007**, *104*, 35.
(87) Schulze, U.; Schmidt, H. W., Synthesis and characterization of ABA-triblock copolymers with poly(ethylene glycol) segments and LC-segments, *Polymer Bulletin* **1998**, *40*, 159.
(88) Lin, L. L.; Hong, J. L., Multiple melting behavior of a thermotropic copolyester containing spirobicromane moiety, *Polymer* **2000**, *41*, 7471.
(89) Reichelt, N.; Schulze, U.; Schmidt, H. W., Synthesis and characterization of ABA-triblock copolymers with polystyrene and main-chain liquid crystalline polyester segments, *Macromolecular Chemistry and Physics* **1997**, *198*, 3907.
(90) Novack, K. M.; Martins, J. C. A.; Gomes, A. S., Block copolymers with poly(ethylene terephthalate) and liquid crystalline polyester segments: Effect of reaction time, *Polymer. Bulletin* **1996**, *37*, 603.
(91) Heyde, G.; Heitz, W.; Karbach, A.; Wehramann, R., Block copolymers with poly(oxy-1,4-phenylene) and liquid crystalline polyester segments, *Die Makromolekulare Chemie* **1993**, *194*, 2741.
(92) Norbert, N.; Walter, H., Poly(oxy-1,4-phenylene) macromonomers for polycondensation, *Die Makromolekulare Chemie* **1990**, *191*, 1463.
(93) Moriyuki, S.; Takashi, M.; Kazue, N.; Ken-ichi, M.; Fumihiko, Y.; Yasushi, O., Thermotropic liquid-crystalline polyester-graft-polystyrene copolymers from a polystyrene macromonomer with amido linkage, *Macromolecular Rapid Communications* **1994**, *15*, 243.
(94) Angeloni, A. S.; Bignozzi, M. C.; Laus, M.; Chiellini, E.; Galli, G., Hybrid liquid-crystalline block copolymers based on polystyrene and polyester blocks, *Polymer Bulletin* **1993**, *31*, 387.
(95) Laus, M.; Bignozzi, M. C.; Angeloni, A. S.; Francescangeli, O.; Galli, G.; Chiellini, E., Hybrid Liquid-Crystalline Block Copolymers I. Synthesis and

Mesomorphic Behavior of Polyester–Polymethacrylate Block Copolymers, *Polymer Journal* **1995**, *27*, 993.
(96) Galli, G.; Chiellini, E.; Laus, M.; Angeloni, A. S.; Bignozzi, M. C.; Francescangeli, O., Hybrid Liquid-Crystalline Block Copolymers with Polystyrene and Polyester Blocks, *Molecular Crystals and Liquid Crystals Science and Technology. Section A. Molecular Crystals and Liquid Crystals* **1994**, *254*, 429.
(97) Chang, Y. M.; Hsu, C. S.; Liu, M. C., Synthesis and characterization of segmented copolymers of aromatic polyether sulfone and thermotropic liquid crystalline poly(oxy-1,4-phenylenecarbonyl-co-oxy-2,6-naphthaloyl), *Materials Chemistry and Physics* **1996**, *43*, 250.
(98) Koga, M.; Ishige, R.; Sato, K.; Ishii, T.; Kong, S.; Sakajiri, K.; Watanabe, J.; Tokita, M., Well-Ordered Lamellar Microphase-Separated Morphology of an ABA Triblock Copolymer Containing a Main-Chain Liquid Crystalline Polyester as the Middle Segment 2: Influence of Amorphous Segment Molecular Weight, *Macromolecules* **2012**, *45*, 9383.
(99) Nelson, A. M.; Fahs, G. B.; Moore, R. B.; Long, T. E., High-Performance Segmented Liquid Crystalline Copolyesters, *Macromolecular Chemistry and Physics* **2015**, *216*, 1754.
(100) Tokita, M.; Takahashi, T.; Hayashi, M.; Inomata, K.; Watanabe, J., Thermotropic Liquid Crystals of Polyesters Having a Mesogenic p,p‘-Bibenzoate Unit. 7. Chain Folding in the Smectic Phase of BB-6, *Macromolecules* **1996**, *29*, 1345.
(101) Herzberger, J.; Meenakshisundaram, V.; Williams, C. B.; Long, T. E., 3D Printing All-Aromatic Polyimides Using Stereolithographic 3D Printing of Polyamic Acid Salts, *ACS Macro Letters* **2018**, 493.
(102) Lin, Q.; Pasatta, J.; Long, T. E., Synthesis and characterization of chiral liquid-crystalline polyesters containing sugar-based diols via melt polymerization, *Journal of Polymer Science, Part A: Polymer Chemistry* **2003**, *41*, 2512.
(103) Lin, Q.; Pasatta, J.; Wang, Z.-H.; Ratta, V.; Wilkes, G. L.; Long, T. E., Synthesis and characterization of sulfonated liquid crystalline polyesters, *Polymer International* **2002**, *51*, 540.
(104) Jeu, W. H. d.; ebrary, I., *Liquid crystal elastomers: materials and applications*; Springer: New York;Berlin;, 2012; Vol. 250.
(105) Emmerling, U.; Diele, S.; Schmalfuss, H.; Werner, J.; Kresse, H.; Lindau, J., Thermal phase behavior of homologous liquid crystalline side group polyesters in dependence on the polymethylene main chain spacer length, *Macromolecular Chemistry and Physics* **1998**, *199*, 1529.
(106) Mu, B.; Wu, B.; Pan, S.; Fang, J.; Chen, D., Hierarchical Self-Organization and Uniaxial Alignment of Well Synthesized Side-Chain Discotic Liquid Crystalline Polymers, *Macromolecules* **2015**, *48*, 2388.
(107) Katano, Y.; Tomono, H.; Nakajima, T., Surface Property of Polymer Films with Fluoroalkyl Side Chains, *Macromolecules* **1994**, *27*, 2342.
(108) Hare, E. F.; Shafrin, E. G.; Zisman, W. A., Properties of Films of Adsorbed Fluorinated Acids, *The Journal of Physical Chemistry* **1954**, *58*, 236.

(109) Matroniani, R.; Wang, S. H., Thermal degradation of polymer systems having liquid crystalline oligoester segment, *Polimeros-Ciencia E Tecnologia* **2017**, *27*, 280.
(110) Deshmukh, P.; Gopinadhan, M.; Choo, Y.; Ahn, S.-k.; Majewski, P. W.; Yoon, S. Y.; Bakajin, O.; Elimelech, M.; Osuji, C. O.; Kasi, R. M., Molecular Design of Liquid Crystalline Brush-Like Block Copolymers for Magnetic Field Directed Self-Assembly: A Platform for Functional Materials, *ACS Macro Letters* **2014**, *3*, 462.
(111) del Campo, A.; Bello, A.; Perez, E., Synchrotron X-ray study of liquid crystalline polyoxetanes containing two mesogenic groups connected by a flexible spacer in the side chain, *Macromolecular. Chemistry and Physics* **2003**, *204*, 682.
(112) Manfred, A.; Sven, P.; Hartmut, F.; Willy, F.; Hermann, U., Liquid-crystalline side chain block copolymers — synthesis, morphology and LC behaviour, *Macromolecular Rapid Communications* **1994**, *15*, 487.
(113) Mathew, J.; Ghadage, R. S.; Ponrathnam, S.; Prasad, S. D., Catalytic Synthesis of Poly(ethylene terephthalate-co-oxybenzoate) systems via the melt polyesterification route-copolyesterification kinetics., *Macromolecules* **1994**, *27*, 4021.
(114) Tsai, H.-B.; Li, H.-C.; Chang, S.-J.; Yu, H.-H., Copolyesters, *Polymer Bulletin* **1991**, *27*, 141.
(115) Tsai, R. S.; Lee, Y. D.; Tsai, H. B., Block copolyesters of poly(pentamethylene p,p '- bibenzoate) and poly(tetramethylene adipate), *Journal of Polymer Science, Part A: Polymer Chemistry* **2002**, *40*, 2626.
(116) Auman, B. C.; Percec, V., Synthesis and Characterization of Segmented Copolymers of Aromatic Polyether sulfone and a thermotropic Liquid-Crystalline Polyester, *Polymer* **1988**, *29*, 938.
(117) Heitz, W., Block copolymers with LC-segments, *Makromolekulare Chemie. Macromolecular Symposia* **1989**, *26*, 1.
(118) Herzberger, J.; Niederer, K.; Pohlit, H.; Seiwert, J.; Worm, M.; Wurm, F. R.; Frey, H., Polymerization of Ethylene Oxide, Propylene Oxide, and Other Alkylene Oxides: Synthesis, Novel Polymer Architectures, and Bioconjugation, *Chemical Reviews* **2016**, *116*, 2170.
(119) Tsai, H. B., Characterization of thermotropic block copolyetheresters by x-ray diffraction and DSC, *Journal of Macromolecular Science-Physics* **1997**, *B36*, 175.
(120) Tsai, H.-B.; Lee, C.; Chang, N.-S., Synthesis and Thermal Properties of Thermotropic Block Copolyetheresters, *Polymer Journal* **1992**, *24*, 157.
(121) Tsai, H.-B.; Lee, D.-K.; Liu, J.-L.; Tsao, Y.-S.; Tsai, R.-S.; You, J.-W., Block copolyetheresters, *Polymer Bulletin* **1995**, *35*, 743.
(122) Hsiue, L. T.; Ma, C. C. M.; Tsai, H. B., Hydrophilic Thermotropic Block Copolyetheresters with Poly(pentamethylene p,p'-bibenzoate) Segments, *Macromolecular Chemistry and Physics* **1995**, *196*, 3459.
(123) Hsiue, L. T.; Ma, C. C. M.; Tsai, H. B., Synthesis and Characterization of Hydrophilic Thermotropic Block Copolyetheresters, *Journal of Polymer Science, Part A: Polymer Chemistry* **1995**, *33*, 1153.

(124) Ferri, D.; Wolff, D.; Springer, J.; Francescangeli, O.; Laus, M.; Angeloni, A. S.; Galli, G.; Chiellini, E., Phase and orientational behaviors in liquid crystalline main-chain/side-group block copolymers, *Journal of Polymer Science, Part B: Polymer Physics* **1998**, *36*, 21.
(125) Lin, C. H., Synthesis and characterization of segmented copolymers of polystyrene and thermotropic liquid crystalline poly(4-oxybenzoate-co-2,6-oxynaphthoate), *Designed Monomers and Polymers* **2013**, *16*, 537.
(126) Ishige, R.; Ishii, T.; Tokita, M.; Koga, M.; Kang, S. M.; Watanabe, J., Well-Ordered Lamellar Microphase-Separated Morphology of an ABA Triblock Copolymer Containing a Main-Chain Liquid Crystalline Polyester as the Middle Segment, *Macromolecules* **2011**, *44*, 4586.
(127) Sato, K.; Koga, M.; Kang, S.; Sakajiri, K.; Watanabe, J.; Tokita, M., Lamellar Morphology of an ABA Triblock Copolymer with a Main-Chain Nematic Polyester Central Block, *Macromolecular Chemistry and Physics* **2013**, *214*, 1089.
(128) Heitz, T.; Rohrbach, P.; Höcker, H., Rigid rods with flexible side chains — A route to molecular reinforcement?, *Die Makromolekulare Chemie* **1989**, *190*, 3295.
(129) Burchard, W., In *Chemistry and Technology of Water-Soluble Polymers*; Finch, C. A., Ed.; Springer US: Boston, MA, 1983, p 125.
(130) Matsen, M. W.; Schick, M., Self-assembly of block copolymers, *Current Opinion in Colloid & Interface Science* **1996**, *1*, 329.
(131) Ciach, A.; Pekalski, J.; Gozdz, W. T., Origin of similarity of phase diagrams in amphiphilic and colloidal systems with competing interactions, *Soft Matter* **2013**, *9*, 6301.
(132) Swann, J. M. G.; Topham, P. D., Design and Application of Nanoscale Actuators Using Block-Copolymers, *Polymers* **2010**, *2*, 454.
(133) Fischer, H.; Poser, S., Liquid crystalline block and graft copolymers, *Acta Polymer* **1996**, *47*, 413.
(134) Osada, K.; Koike, M.; Tagawa, H.; Hunaoka, S.-i.; Tokita, M.; Watanabe, J., Two Distinct Types of Orientation Process Observed in Uniaxially Elongated Smectic LC Melt, *Macromolecules* **2005**, *38*, 7337.
(135) Tokita, M.; Tokunaga, K.; Funaoka, S.-i.; Osada, K.; Watanabe, J., Parallel and Perpendicular Orientations Observed in Shear Aligned SCA Liquid Crystal of Main-Chain Polyester, *Macromolecules* **2004**, *37*, 2527.
(136) Osuji, C.; Ferreira, P. J.; Mao, G.; Ober, C. K.; Vander Sande, J. B.; Thomas, E. L., Alignment of Self-Assembled Hierarchical Microstructure in Liquid Crystalline Diblock Copolymers Using High Magnetic Fields, *Macromolecules* **2004**, *37*, 9903.
(137) Gopinadhan, M.; Majewski, P. W.; Choo, Y.; Osuji, C. O., Order-Disorder Transition and Alignment Dynamics of a Block Copolymer Under High Magnetic Fields by In Situ X-Ray Scattering, *Phys. Rev. Lett.* **2013**, *110*, 078301.
(138) Gopinadhan, M.; Majewski, P. W.; Beach, E. S.; Osuji, C. O., Magnetic Field Alignment of a Diblock Copolymer Using a Supramolecular Route, *ACS Macro Letters* **2012**, *1*, 184.

Chapter 4: Tailoring the glassy mesophase range of thermotropic polyesters through copolymerization of 4,4'-bibenzoate and kinked isomer

(Published in *Polymer,* **2019**, *163*, 125)

Katherine V. Heifferon, Ryan J. Mondschein, Samantha J. Talley, Robert B. Moore, S. Richard Turner, and Timothy E. Long

Macromolecules Innovation Institute, Department of Chemistry, Virginia Tech, Blacksburg, VA 24061

Keywords: polyester, liquid crystalline, copolymerization, bibenzoate, regioisomers

4.1 Abstract:

The substitution of a linear biphenyl monomer with its *meta* isomer in liquid crystalline polyesters affords (co)polyesters with tunable liquid crystalline (LC) and thermomechanical properties. Melt transesterification afforded two (co)polyester series based on the semi-aromatic homopolymers poly(diethylene glycol 4,4' bibenzoate) and poly(butylene 4,4' bibenzoate) at high molecular weights. In each series, the linear dimethyl 4,4'-bibenzoate (4,4'BB) was systematically exchanged with its kinked isomer, dimethyl 3,4'-bibenzoate (3,4'BB). The incorporation of the *meta* isomer resulted in tunable crystalline and LC properties. Differential scanning calorimetry (DSC), wide angle X-ray scattering (WAXS), X-ray diffraction (XRD), and polarized optical microscopy (POM) elucidated that the kinked structure of 3,4'BB disrupted crystallization at low incorporations, significantly lowering the melting transition temperature (> 50 °C) in each series. The LC properties were less impacted due to the biphenyl structure resulting in LC glasses with wide mesogenic windows. Dynamic mechanical analysis (DMA) further demonstrated the tunable nature of the thermomechanical properties resulting from the (co)polymerization of these isomers.

4.2 Introduction:

Thermotropic liquid crystalline polyesters (LCPs) possess high thermal stability (> 300 °C) and good mechanical properties making them interesting candidates for high strength fibers, electronic parts, or light weight medical instruments.[1-3] In contrast to other high-performance polymers, thermotropic LCPs uniquely exhibit anisotropic properties in an extended temperature window above the crystalline melting temperature (mesogenic window). Rigid rod type (mesogenic) monomer segments, either in the backbone or as side-chains cause this anisotropy. The unique properties within this window result from molecular/chain alignment and provide significant viscosity reductions with shear as well as high levels of chain orientation during fiber drawing. As a result, processing of these materials frequently occurs within the mesogenic window, therefore broadening this temperature region is ultimately beneficial.[4]

Commonly, main-chain LCPs consist of a fully-aromatic backbone that require harsh polymerization conditions, including high temperatures and acidolysis producing acidic condensates. Also, their highly rigid structure, depending on composition, leads to high degrees of crystallinity and melting temperatures (T_m) above the respective degradation temperature. Efforts to lower the T_m often focus on copolymerization using aromatic monomers with *para* (linear) bond structures, such as terephthalate and 2,6-naphthalate, to randomize polymer chain packing.[5,6] Another viable method of disrupting packing includes the incorporation of flexible spacers into the polyester backbone, such as aliphatic diols, producing a class of polyesters known as semi-aromatic LCPs.[4,7,8] The use of aliphatic diols enables milder reaction conditions compared to fully aromatic LCPs, mimicking polymerization techniques commonly utilized in the synthesis of

poly(ethylene terephthalate) (PET), such as melt transesterification and polycondensation.[7,9,10] These synthetic techniques present advantages compared to acidolysis due to lower reaction temperatures and inert condensate byproducts, such as methanol.

Many semi-aromatic LCPs contain the mesogenic monomer, dimethyl 4,4'-bibenzoate (4,4'BB). The combination of 4,4'BB with a variety of aliphatic diols imparts a wide range of morphologies and thermal transitions onto the final polymers while enabling more facile processing conditions in comparison to their fully aromatic precursors.[7,11] Previous studies revealed that the length of the diol plays a key role in both of these properties. As the diol length is increased, the melting temperature systematically decreases.[12] Further, Watanabe *et al*. reported a unique odd-even effect relative to the T_ms.[8] Aliphatic diols with an odd number of atoms commonly exhibit a smectic CA (S_{CA} or S_{CAlt}) mesophase in which the mesogenic monomers arrange tilted relative to the layers and the tilt direction reverses between each consecutive layer.[8,13] In contrast, even numbered diols formed a smectic A (S_A) mesophase with better chain packing due to the mesogenic monomers orienting perpendicular to the layer direction. This resulted in a systematically higher T_m over their odd numbered counterparts.[8] Copolymerization of 4,4'BB with an aromatic comonomer represented another strategy to control thermal and mechanical properties.[13-16] However, examples of kinked monomers often exhibit complete disruption of the LC phase, attributed to the reduction in the aspect ratio (persistence length/ chain diameter ratio) due to the increased curvature of the chains.[2,13,15] Consequently, researchers seek alternative strategies to lower the T_m while maintaining the unique LC properties.[13,15]

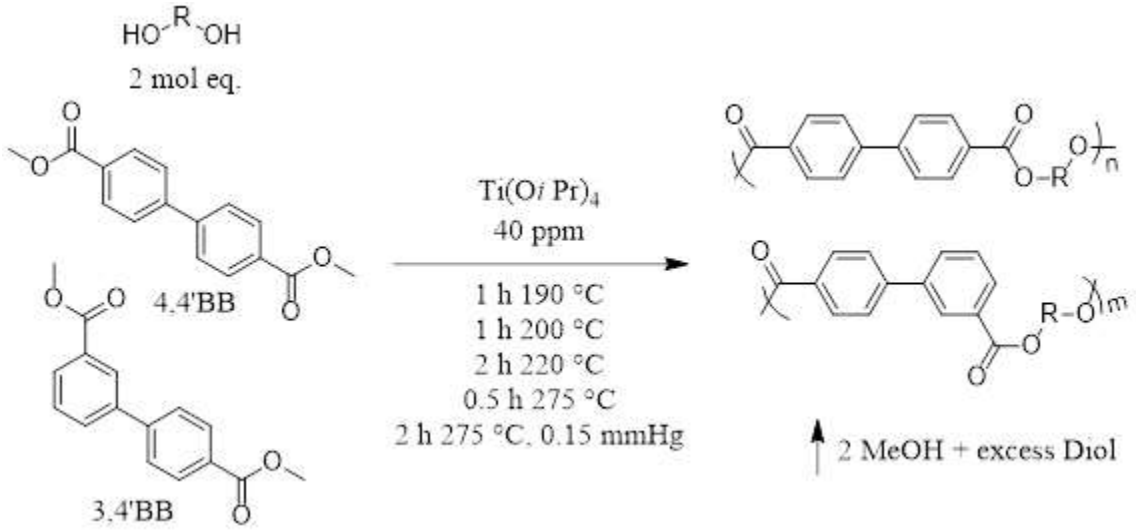

Scheme 4.1. Synthesis of poly(R-4,4'-bibenzoate-co-3,4'-bibenzoate) (co)polyesters through conventional melt transesterification of bibenzoate isomers with either diethylene glycol (R = $CH_2CH_2OCH_2CH_2$) or butylene (R = $(CH_2)_4$).

Here, we discuss the use of a kinked monomer, dimethyl 3,4'-bibenzoate (3,4'BB), to partially substitute 4,4'BB in LCP (co)polymers as demonstrated in **Scheme 4.1**. Previously, 3,4'BB, which was incorporated into semi-aromatic non-LC polyesters, indicated the monomer imparts desirable mechanical, gas permeability, and thermal properties compared to terephthalate based comonomers.[17,18] The kinked biphenyl structure of 3,4'BB reduces the impact of the single *meta* unit on the LC order while preferentially disrupting the crystalline packing of the polyester chains. This enabled tunable LC properties and bibenzoate-based polyesters with LC glass morphologies. As a result, mesogenic windows as broad as 140 °C were obtained enabling a desirable wide range of processing temperatures.

4.3 Experimental:

4.3.1 Materials.

Dimethyl 3,4'-biphenyldicarboxylate (3,4'BB) and dimethyl 4,4'-biphenyldicarboxylate (4,4'BB) were provided by ExxonMobil and used as received.

Diethylene glycol (DEG) (Fisher Scientific, Reagent Grade), 1,4-butanediol (BD) (Sigma Aldrich, ≥ 99%), chloroform-*d* ($CDCl_3$) (Cambridge Isotope Laboratories, 99.8% atom D) and trifluoroacetic acid-*d* (Sigma Aldrich, 99.5% atom D) were used as received. A 0.01g/mL solution of titanium tetra(isopropoxide) (Sigma Aldrich, 99%) in 1-butanol (Sigma Aldrich, anhydrous 99.8%) was prepared following a previously described procedure.[19] All solvents were purchased from Spectrum and used as received. Nitrogen gas (99.999%) was purchased from Praxair.

4.3.2 Analytical Methods.

^{1}H nuclear magnetic resonance (NMR) spectroscopy was performed at 23 °C using a Varian Unity 400 at 400 MHz. Deuterated chloroform served as solvent for all polymers containing DEG units. Polymers with butanediol segments required a ratio of 1:1 $CDCl_3$: d-TFA. Waters Acquity Advanced Permeation Chromatography (APC) was used to characterize molecular weights (MW) of these polymers at 35 °C against polystyrene standards. Acquity APC XT columns were utilized at a flow rate of 1 mL/min with a sample concentration of 1 mg/mL. Thermogravimetric analysis (TGA) was performed from 25 to 600 °C at 10 °C/min using a TA Instruments Q50 under constant N_2 flow. Differential scanning calorimetry (DSC) was conducted using a TA instruments Q1000 DSC under a 50 mL/min nitrogen flow. The instrument was calibrated using indium (T_m = 156.60 °C) and zinc (T_m = 419.47 °C) standards. For the poly(DEG-4,4'BB-*co*-3,4'BB) (co)polyesters, an initial heating rate of 10 °C/min was used followed by a quench cool of 100 °C/min to remove thermal history. The second heat cycle at 10 °C/min was used to calculate thermal transitions. For the annealing study utilized for the phase diagram shown in **Figure 4.7**, samples were placed in a vacuum oven at (760 mmHg) 90 °C for 9

d. Subsequently, DSC measurements were conducted and the first heat cycle with a heating rate of 10 °C/min determined the respective thermal transitions. A slow cool at 10 °C/min was conducted for all poly(BD-4,4'BB-*co*-3,4'BB) (co)polyesters. Data analysis was performed by using the inflection point of the glass transition temperature (T_g) and the maximum of the melting point (T_m). Compression molding was performed using aluminum plates, 400 μm thick stainless-steel shims, and Kapton™ sheets coated with a Rexco Partall® Power Glossy Liquid mold release agent. Samples were pressed at temperatures above their T_m and immediately quench cooled in an ice bath. Dynamic mechanical analysis (DMA) was conducted in tension mode at a frequency of 1 Hz, an oscillatory amplitude of 15 μm, and a static force of 0.01 N. Experimentation was performed on a TA Instruments Q800 DMA with a heating rate of 3 °C/min and an average starting specimen length of 11 ± 2 mm. Wide-angle X-ray scattering (WAXS) experiments were performed using a Rigaku S-Max 3000 3 pinhole SAXS system, equipped with a rotating anode emitting X-rays with a wavelength of 0.154 nm (Cu Kα). The sample-to-detector distance was 110 mm and the q-range was calibrated using a silver behenate standard. Two-dimensional diffraction patterns were obtained using an image plate with an exposure time of 1 h. WAXS data were analyzed using the SAXSGUI software package to obtain radially integrated WAXS intensity versus the scattering vector, 2θ, where $q=(4\pi/\lambda)\sin(\theta)$, θ is one half of the scattering angle and λ is the wavelength of X-ray. X-ray diffraction (XRD) patterns were obtained on a Rigaku MiniFlex II Desktop X-ray powder diffractometer. The radiation source was Cu Kα radiation, with a wavelength of 0.154 nm. The angular scanning range was 2θ = 5−40°, with 0.01° steps. Polarized optical microscopy (POM) was performed on a Zeiss

Axioplan polarizing optical microscope with a THMS 600 hot stage. Samples were pressed between glass slides while isotropic and cooled at 10 °C/min. Sample nomenclature consists of poly(DEG-N-4,4'BB-M-*co*-3,4'BB) or poly(BD-N-4,4'BB-*co*-M-3,4'BB) where N and M refer to the mol % of 4,4'BB and 3,4'BB, respectively.

4.3.3 Synthesis of poly(DEG-4,4'BB-*co*-3,4'BB) (co)polyester series.

For the synthesis of poly(DEG-4,4'BB-*co*-3,4'BB), a previously demonstrated melt transesterification procedure was suitable.[9,20] (Co)polyesters with ratios ranging from 100:0 to 0:100 mol % 4,4'BB:3,4'BB were prepared. Two mol equiv. of diethylene glycol was consistently used relative to the total moles of diester. In the case of poly(DEG-75-4,4'BB-*co*-25-3,4'BB), 18.527 g 4,4'BB (0.068 mol), 6.179 g 3,4'BB (0.022 mol) and 19.429 g DEG (0.183 mol) were weighed into a dry 100-mL round-bottomed flask, followed by addition of 40 ppm titanium isopropoxide catalyst. The reactor comprised a t-neck adaptor, metal stir-rod, glass stir-rod adaptor, distillation tube with round-bottomed flask to collect condensate, and an overhead mechanical stirrer. The reaction was evacuated and back-filled with N_2 three times to ensure an inert atmosphere. The reaction was heated from 190 °C to 275 °C under N_2 flow for 6 h. After the reaction mixture had reached 275 °C, reduced pressure (0.15 mmHg) was applied for 2 h to remove excess diol from the melt. The reaction yielded a viscous polymer, which was used without further purification.

4.3.4 Synthesis of poly(BD-4,4'BB-*co*-3,4'BB) (co)polyester series.

The synthesis of poly(BD-4,4'BB-*co*-3,4'BB) was performed analogous to poly(DEG-4,4'BB-*co*-3,4'BB). In the case of poly(BD-75-4,4'BB-*co*-25-3,4'BB), 19.47 g 4,4'BB (0.072 mol), 6.49 g 3,4'BB (0.024 mol) and 17.33 g BD (0.192 mol) were

weighed into a dry 100-mL, round-bottomed flask followed by addition of the titanium isopropoxide catalyst (40 ppm). The reactor set-up was identical to the DEG series and the flask was evacuated and back-filled with N_2 three times to ensure an inert atmosphere. The round-bottomed flask was heated from 190 °C to 275 °C under nitrogen flow for 6 h. Subsequently, the temperature was increased to 220 °C for 2 h and followed by 0.5 h at 275 °C. In the last step, vacuum (0.15 mmHg) was applied for 2 h at 275 °C. The resulting polymer was used without further purification.

4.4 Results and Discussion:

4.4.1 Synthesis and Structural Determination.

Scheme 4.1 depicts the traditional melt transesterification procedure used in the synthesis of (co)polyesters. Excess diol assists in the initial transesterification of the diesters. Tracking the generation of methanol enabled following the reaction progress and indicated completion of the transesterification. High temperature and vacuum facilitated removal of the excess diol, initiated polycondensation and drove the reaction to high conversion (>99.9%).[9,18,20-23] In all cases except two, polymers maintained a homogenous

Table 4.1. SEC molecular weight in chloroform and ^{1}H NMR characterization in $CDCl_3$ of the poly(DEG-4,4'BB-*co*-3,4'BB) (co)polyester series.

Targeted 4,4'BB:3,4'BB Molar Ratio	4,4' BB: 3,4'BB Molar Ratio[a]	M_n[b] (kg/mol)	M_w[b] (kg/mol)	Đ M_w/M_n
100:0	100:0	26.6	48.3	1.82
95:5	93:7	20.7	38.1	1.84
90:10	89:11	36.5	64.6	1.77
80:20	79:21	30.8	57.2	1.86
75:25	75:25	28.3	52.4	1.85
70:30	70:30	33.0	50.0	1.51
60:40	61:39	43.7	80.8	1.85
50:50	45:55	26.2	48.8	1.86
25:75	27:73	35.1	66.4	1.89
0:100	0:100	45.4	85.1	1.87

a. Calculated by ^{1}H NMR spectroscopy
b. Calculated by SEC ($CHCl_3$, DRI detector, PS standards)

Table 4.2. SEC molecular weight in chloroform and ^{1}H NMR characterization in *d*-TFA of poly(BD-4,4'BB-*co*-3,4'BB) (co)polyester series. Insoluble samples indicated with N/A.

Reaction Feed: 4,4'BB:3,4'BB Molar Ratio	NMR: 4,4' BB: 3,4'BB Molar Ratio	M_n (kg/mol)	M_w (kg/mol)	Đ M_w/M_n
100:0	N/A	N/A	N/A	N/A
90:10	N/A	N/A	N/A	N/A
75:25	73:27	N/A	N/A	N/A
50:50	47:53	N/A	N/A	N/A
40:60	39:61	N/A	N/A	N/A
30:70	28:72	43.6	62.9	1.44
25:75	23:77	38.5	70.7	1.83
0:100	0:100	54.2	69.8	1.29

melt during the entire reaction. Poly(BD-4,4'BB) and poly(BD-90-4,4'BB-*co*-10-3,4'BB) became opaque and solidified rapidly upon application of vacuum during the final stage of the reaction resulting from their high T_m's. This solidification limited the molecular weight growth of these polymers and resulted in brittle products. DEG-based (co)polyesters exhibited higher solubility in organic solvents compared to the BD-based (co)polyesters, thus enabling SEC characterization.[15] **Table 4.1** shows the molecular weights for the poly(DEG-4,4'BB-*co*-3,4'BB) series, which range from 20 – 45 kg/mol with polydispersities near 1.80.[24] Three polymers with high 3,4'BB content (100, 77, and 72 mol % 3,4'BB) in the poly(BD-4,4'BB-*co*-3,4'BB) series were also soluble in chloroform. These polymers exhibited M_n values from 38 – 54 kg/mol, as illustrated in **Table 4.2**. While insoluble in chloroform, all polymers in the BD series from 73:27 – 0:100 mol % 4,4'BB:3,4'BB formed ductile films upon compression molding, suggestive of high molecular weight polymers.[9,25,26]

Analysis of the ^{1}H NMR spectra determined 4,4'BB:3,4'BB molar ratios of the (co)polyesters. Calculations from ^{1}H NMR spectroscopy listed in **Table 4.1** and **4.2** revealed good correlation between targeted and obtained monomer molar ratios. For accuracy, calculated ratios were utilized for further polymer analysis.

4.4.2 Thermal Analysis.

Thermotropic LCPs based on bibenzoates can exhibit high melting temperatures (> 250 °C for semi-aromatic LCPs) close to the polymer degradation temperatures making melt processing difficult.[8] Processing of these polymers typically occurs between the T_m and the LC to isotropic transition (T_i), often referred to as the mesogenic window. Extending this range to lower temperatures enables easier processing. TGA measurements revealed a one-step degradation for both (co)polyester series. Weight-loss ($T_{d,5\%}$) occurred above 370 °C, independent of the used diol (**Table 4.3** and **4.4**), correlating well with previous studies of 4,4'BB based LCPs.[18,27]

Table 4.3. Characterization data obtained from differential scanning calorimetry and dynamic mechanical analysis of poly(DEG-4,4'BB-co-3,4'BB) (co)polyester series.

Poly(diethylene glycol 4,4'-bibenzoate-*co*-3,4'-bibenzoate)					
4,4'BB: 3,4'BB Molar Ratio	$T_{g,LC}$ (°C)[a]	T_i (°C)[a]	ΔH_i (J/g)	$T_{g,LC}$ (°C)[b]	$T_{d,5\%}$ (°C)
100:0	-	204	15.9	57	392
93:7	51	192	16.5	-	398
89:11	52	176	13.3	58	391
79:21	53	148	11.8	57	382
75:25	53	134	10.6	54	389
70:30	53	116	7.9	67	395
	$T_{g,a}$ (°C)			$T_{g,a}$ (°C)	
61:39	58	-	-	64	400
45:55	59	-	-	65	388
27:73	59	-	-	64	388
0:100	59	-	-	64	385

[a]Determined from DSC second heat, [b]Calculated from DMA using quenched films

Table 4.4. Characterization data obtained from differential scanning calorimetry and dynamic mechanical analysis of poly(BD-4,4'BB-*co*-3,4'BB) (co)polyester series.

Poly(butylene 4,4'-bibenzoate-*co*-3,4'-bibenzoate)							
4,4'BB: 3,4'BB Molar Ratio	$T_{g,LC}$ (°C)[a]	T_m (°C)[a]	ΔH_m (J/g)	T_i (°C)[a]	ΔH_i (J/g)	$T_{g,LC}$ (°C)[b]	$T_{d,5\%}$ (°C)
100:0	-	260	19.6	295	25.8	-	390
90:10	-	244	12.3	275	11.0	-	390
73:27	-	200	3.7	229	7.2	72	375
47:53	52	-	-	153	2.2	79	378
39:61	59	-	-	118	0.8	80	378
	$T_{g,a}$ (°C)					$T_{g,a}$ (°C)	
28:72	65	-	-	-	-	78	391
23:77	68	-	-	-	-	80	376
0:100	63	-	-	-	-	76	392

[a]Determined from DSC second heat, [b]Calculated from DMA using quenched films

Unlike their degradation characteristics, these two series exhibit varying crystallization properties. Previous studies on poly(DEG-4,4'BB) revealed a slow rate of crystallization for these polyesters.[13,28] This enables the development of a LC glass with a smectic CA mesophase when quenched from the melt. This phenomenon occurs when a LC polymer is cooled below the T_g prior to growth of crystalline domains and results in a glassy polymer exhibiting only a LC

mesophase. The mesogenic window is widened through the development of a LC glass since the lack of a T_m results in a processing window ranging from the T_g to the T_i. In our study, DSC measurements of the (co)polyesters indicated only one endothermic peak associated with the smectic to isotropic transition (T_i).[13,15] The substitution of 4,4'BB with 3,4'BB resulted in a systematic decrease of the T_i from 204 °C to 116 °C and decrease in enthalpy ΔH_i from 16.5 J/g to 7.9 J/g. Polymers with ≥ 40 mol % 3,4'BB showed no T_i, indicating the formation of amorphous polymers. Annealing at 90 °C for 4 d allowed for slow crystallization of poly(DEG-4,4'BB) and poly(DEG-95-4,4'BB-*co*-5-3,4'BB). These polymers exhibited a second endothermic transition (T_m) at 124 and 116

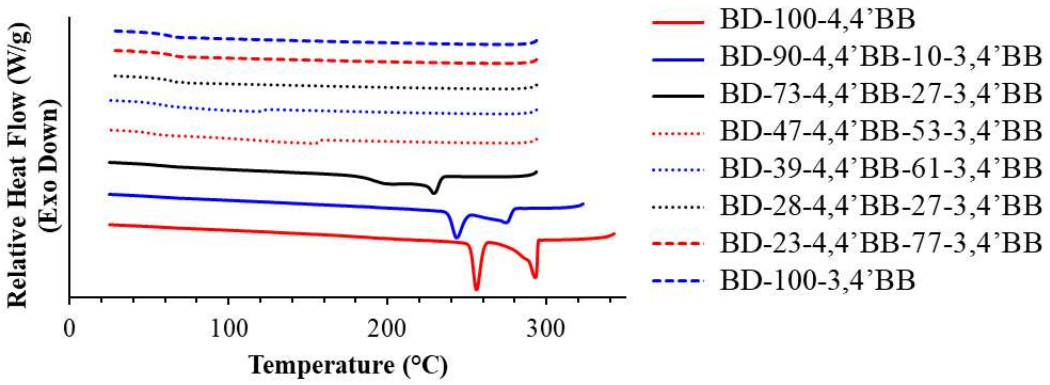

Figure 4.1. Cooling curves of poly(BD-4,4'BB-co-3,4'BB) (co)polyester series showing decreasing T_m and T_i with increasing 3,4'BB incorporation. BD-X-4,4'BB-Y-3,4'BB where X and Y indicate the molar ratios of corresponding 4,4'BB and 3,4'BB repeating units.

°C, respectively. Polymers with higher 3,4'BB content (≥ 61 mol %) showed an inability to crystallize within the time frame of annealing.

The exchange of DEG for BD in these polymers resulted in a homopolymer, poly(BD-4,4'BB), that exhibited two endothermic transitions at 260 °C and 295 °C correlating with the crystalline to smectic A (S_A) transition and S_A to isotropic transition, respectively.[8] The effects resulting from the exchange of carbon for oxygen atoms in aliphatic spacers have been extensively studied in the literature.[29,30] These experiments demonstrated that all-carbon spacers exhibit fewer confirmations and increased chain stiffness relative to their oxygen bearing counterparts resulting in increased crystallinity and higher T_m's.[29,30] The transition from DEG to BD in these polymers reiterated this trend therefore enabling the study of how the increased mol % of 3,4'BB impacts both crystalline and LC order. Unlike repeating units with one aromatic ring (e.g. isophthalate), the biphenyl structure of 3,4'BB results in a significant decrease of the polymer crystallinity but does not impact the LC order as drastically, resulting in the formation of LC glasses. For example, a T_m is not observed after incorporating > 27 mol

% 3,4'BB, but LC order is maintained up to the incorporation of 61 mol % 3,4'BB. This polymer shows a drop in T_m of 95 °C while the 3,4'BB content is systematically increased. Over the compositional range of the (co)polyesters, the T_i decreased by 192 °C, illustrated in **Figure 4.1**. Consequently, incorporation of higher amounts of 3,4'BB is possible before the LC order is lost in comparison to the poly(DEG-4,4'BB-*co*-3,4'BB) series due to the higher rigidity of BD relative to the flexible DEG spacer.[29]

Both (co)polyester series showed non-traditional changes in T_g that do not follow the Fox equation for random copolymers. Due to the consistency in the DSC test parameters for the copolymers in each series, these discrepancies were not attributed to differences in thermal history. Unexpectedly, the polymers with LC properties possess a lower T_g relative to the amorphous polymers in the same series. This is contradictive to previous studies that indicated an increase in T_g with increasing 3,4'BB content.[17,18] While uncommon for semi-crystalline materials, this trend has been repeatedly observed in LC polymers.[31,32] In particular, smectic polymers, which exhibited directional order and layering of the rigid monomers in the mesophase, demonstrate restricted translational motion within these layers. For a smectic glass, the primary segmental motion occurring above the T_g but below the T_i is limited to translational motion. This is unlike amorphous polymers, which must undergo full segmental motion. As a result, the LC glass requires less energy to undergo segmental motion than their amorphous counterparts, thus resulting in lower T_gs, which are identified specially as $T_{g,LC}$.

4.4.3 Morphological Characterization.

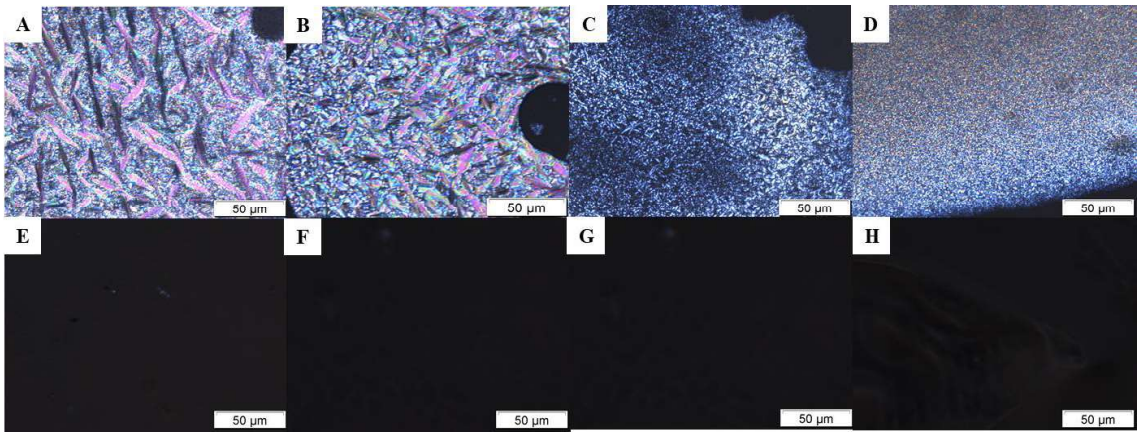

Figure 4.2. Polarized optical microscopy images of poly(DEG-4,4'BB-*co*-3,4'BB) samples at temperatures below the T_i and above T_g. A) DEG-100-4,4'BB B) DEG-89-4,4'BB-11-3,4'BB C) DEG-79-4,4'BB-21-3,4'BB D) DEG-75-4,4'BB-25-3,4'BB E) DEG-61-4,4'BB-39-3,4'BB F) DEG-45-4,4'BB-55-3,4'BB G) DEG-27-4,4'BB-73-3,4'BB H) DEG-100-3,4'BB.

POM and WAXS analysis elucidated the LC properties of the poly(DEG-4,4'BB-*co*-3,4'BB) series. Previous studies indicated that poly(DEG-4,4'BB) possesses a smectic CA (S_{CA}) mesophase.[15,28,33] Under polarized light the S_{CA} mesophase often exhibits focal conic fan-shape textures with stripe domains.[1] Slow cooling a sample of poly(DEG-4,4'BB) at 10 °C/min from an isotropic melt revealed this specific texture in **Figure 4.2A**. As the mol % 3,4'BB increased, the texture domain size decreased until POM exhibited only fine-scale optical textures reaching the resolution limit of the microscope therefore restricting texture identification (**Figure 4.2B-D)**.[1] Further increasing the 3,4'BB content resulted in loss of birefringence (**Figure 4.2E-H)** as the polymers became amorphous. Due to the presence of the mesophase and the absence of crystallinity, WAXS performed at room temperature validated the morphology observed through POM. Following procedures from previous literature, 400 µm thick films were oriented using a draw rate of 1 mm/sec at 75 °C until 25 mm extension of the film was achieved. This procedure oriented the LC polydomains allowing the ordered morphology

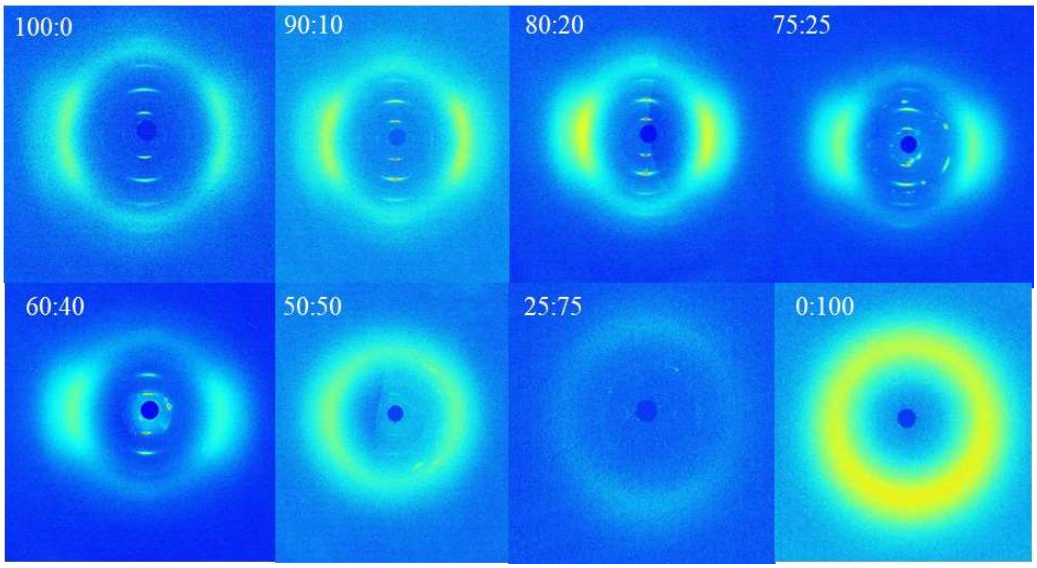

Figure 4.3. 2D WAXS profiles of the poly(DEG-4,4'BB-co-3,4'BB) (co)polyester series. Orientation direction is vertical relative to these images.

of the mesophase to be characterized.[13,15] **Figure 4.3** depicts the 2D WAXS scattering profiles of the poly(DEG-4,4'BB-*co*-3,4'BB) series. The two intensity maxima straddling the equator in the broad order reflections confirmed the presence of a S_{CA} mesophase. These maxima revealed the switching tilt of the mesogenic groups relative to the orientation direction, along with the switching of the tilt direction between each layer of the mesophase, common for this morphology.[13] The reflections along the vertical axis, indicative of the mesogenic unit layer, demonstrate that the layer normal lies parallel to the orientation direction. As mol % 3,4'BB increased, these scattering profiles lost the clear maxima and revealed fewer higher ordered reflections. The incorporation of 3,4'BB disrupts the packing and reduces the LC order; orientation becomes more difficult under the same conditions resulting in scattering separate from the ordered reflections and fewer overall higher ordered reflections. At the incorporation of ≥ 53 mol % 3,4'BB, the LC order is no longer observed, and an amorphous halo remains. Unlike the POM data which exhibited isotropic properties for DEG-61-4,4'BB-39-3,4'BB, drawing this sample

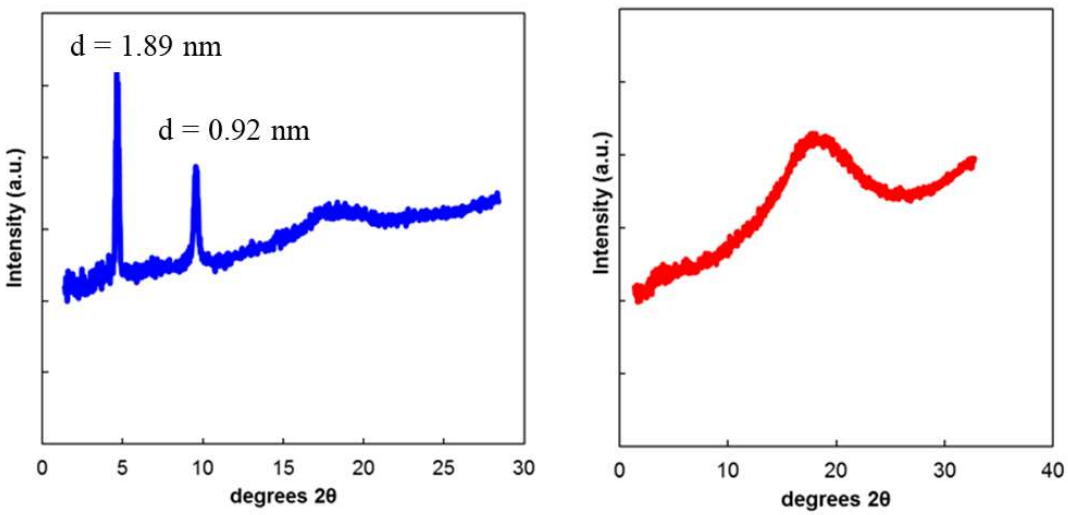

Figure 4.4. WAXS profiles of the poly(DEG-80-4,4'BB-*co*-20-3,4'BB) (left) and poly(DEG-3,4'BB) (right).

revealed reflections along the y-axis in the WAXS studies. This indicates that the sample still exhibit enough linearity to order upon application of external stimuli, such as tension, and without this stimulus the polymer is amorphous. A series of poly(diethylene glycol 4,4'-bibenzoate-*co*-isophthalate) exhibited similar trends.[15] However, in contrast to copolyesters with isophthalate (IA), higher mol % 3,4'BB maintain LC properties. Spacing of the smectic layers at high 4,4'BB content was calculated and shown in **Figure 4.4.** The d-spacing values are similar to the fully extended repeat unit, common for oriented LC materials.[15]

The poly(BD-4,4'BB-*co*-3,4'BB) series revealed similar changes to the LC morphology upon incorporation of 3,4'BB. The observation of a fan-shaped texture in POM correlates with the presences of a S_A mesophase.[1,34-36] The homopolymer, poly(BD-4,4'BB), revealed the fan-shape texture in **Figure 4.5A**. Focal conics within the image also indicate S_A morphology correlating with the smectic layers laying perpendicular to the substrate plane and arranging in Dupin cyclides.[36] As the mol % of 3,4'BB increased,

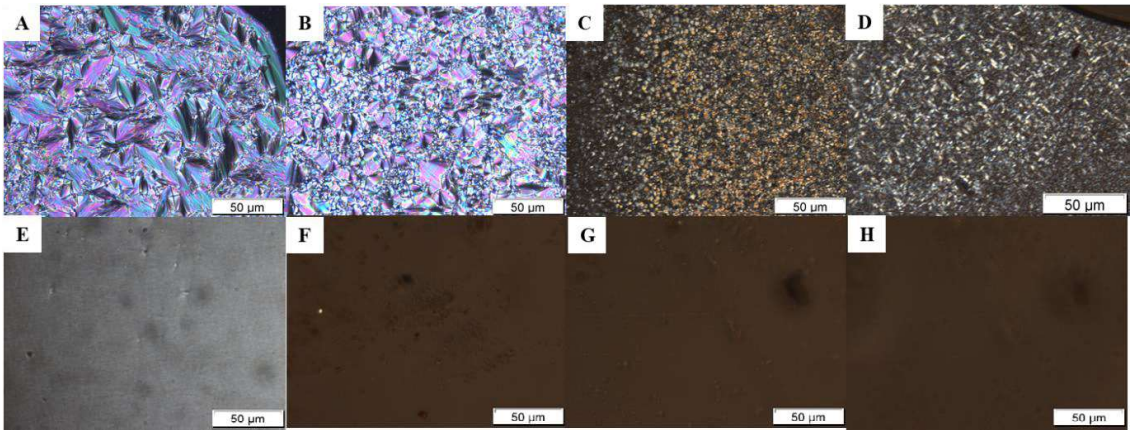

Figure 4.5. Polarized optical microscopy images of poly(BD-4,4'BB-*co*-3,4'BB) samples at temperatures below the T_i and above T_g. A) BD-100-4,4'BB B) BD-90-4,4'BB-10-3,4'BB C) BD-73-4,4'BB-27-3,4'BB D) BD-47-4,4'BB-53-3,4'BB E) BD-39-4,4'BB-61-3,4'BB F) BD-28-4,4'BB-72-3,4'BB G) BD-23-4,4'BB-77-3,4'BB H) BD-100-3,4'BB.

the size of the fans and focal conics decreased, and the texture became harder to detect until loss of order occurred completely in **Figure 4.5F-H.** Hu et al. hypothesized, in the study of poly(DEG-4,4'BB-*co*-IA) (co)polymers, that the incorporation of the kinked IA monomers did not impact the basic morphological structure of the polymer due to exclusion from the LC domains into the amorphous regions. The restriction of the 3,4'BB monomer to the amorphous domains could explain why the extent of LC character is reduced upon incorporation of 3,4'BB, as observed through a decrease in the ΔH_i over both series, but the morphology remains the same aside from the reduction in domain size in POM.[15]

XRD analysis of the polymer series, in **Figure 4.6**, at room temperature further examined the morphological behavior. Homopolymer, poly(BD-4,4'BB), exhibits sharp crystalline reflections at 19.0, 20.9, 22.7, 25.6, 27.7, and 29.3 ° 2θ.[37,38] The crystalline component of the diffraction pattern decreases with increasing 3,4'BB content until 53 mol % 3,4'BB, where no crystalline reflections are observed. As the incorporation of

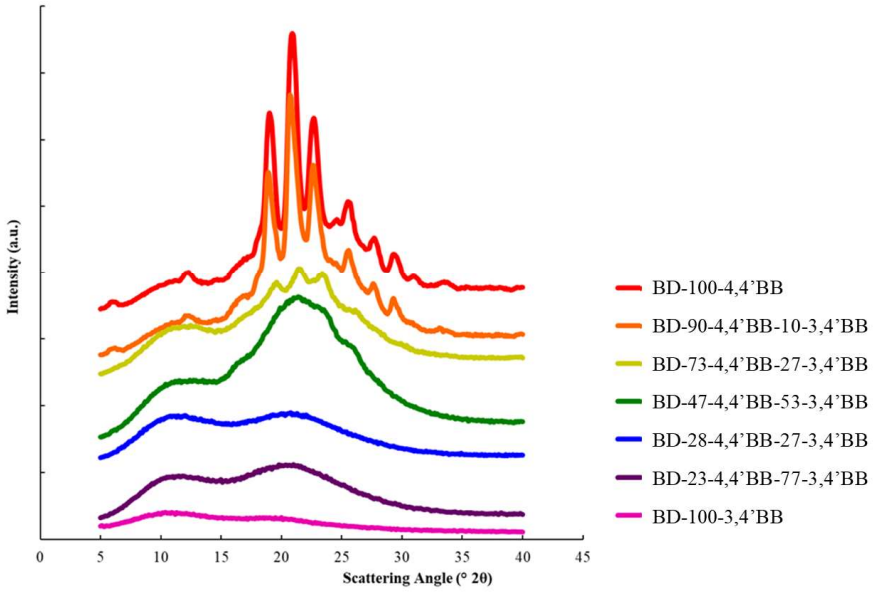

Figure 4.6. XRD scattering profile of the poly(BD-4,4'BB-co-3,4'BB) (co)polyester series.

3,4'BB increases to 73 mol %, the crystalline component of the scattering profile decreases. This specifies that the crystal lattice structure remains the same in the copolyesters. Other (co)polyester systems, such as poly(HD-4,4'BB-*co*-IA) and poly(DEG-4,4'BB-*co*-IA), afford the same phenomenon attributing it to the exclusion of the kinked monomer from the crystal structure into the amorphous domains.[15,37,39]

Poly(BD-4,4BB) and poly(BD-90-4,4'BB-*co*-10-3,4'BB) also exhibit reflections at 6 and 12.3 ° 2θ corresponding with the smectic layer spacing reported for the homopolymer (S_A).[37] Due to distortion through crystallization, this spacing of 14.7 Å is significantly smaller than the fully extended repeating unit of homopolymer (15.8 Å). The scattering angle (2θ) corresponding to this dimension does not change upon incorporation of the kinked monomer. In the case of 27 mol % 3,4'BB, smectic layer reflections are not observed and crystalline reflections remain. Increasing the incorporation of 3,4'BB to 53 mol %, results in the total loss of smectic layer reflections

and crystallinity as observed by XRD. This is contradictory to polarized optical microscopy analysis of BD-47-4,4'BB-53-3,4'BB, which exhibits birefringence indicative of persistent LC character. This combination of properties between the XRD and POM analysis is consistent with a LC glass. Previous analysis justified the loss of smectic peaks (6 and 12.3 ° 2θ) in XRD as a polymer exhibiting lateral ordering but a disruption in longitudinal registry.[15,39,40] This disruption in part occurs through decreased concentration of linear sequences in the polymer during increasing 3,4'BB incorporation and as a result, decreased volume of ordered domains. Previous investigation of poly(HD-4,4'BB-*co*-IA) utilizing AFM demonstrated that copolyesters exhibiting high IA content and loss of smectic layer peaks in WAXS move from a well-ordered lamellar packed morphology to short curving lamellae.[39] These copolymers retain some smectic order but lost the long range periodicity that produces ordered domains and enables the

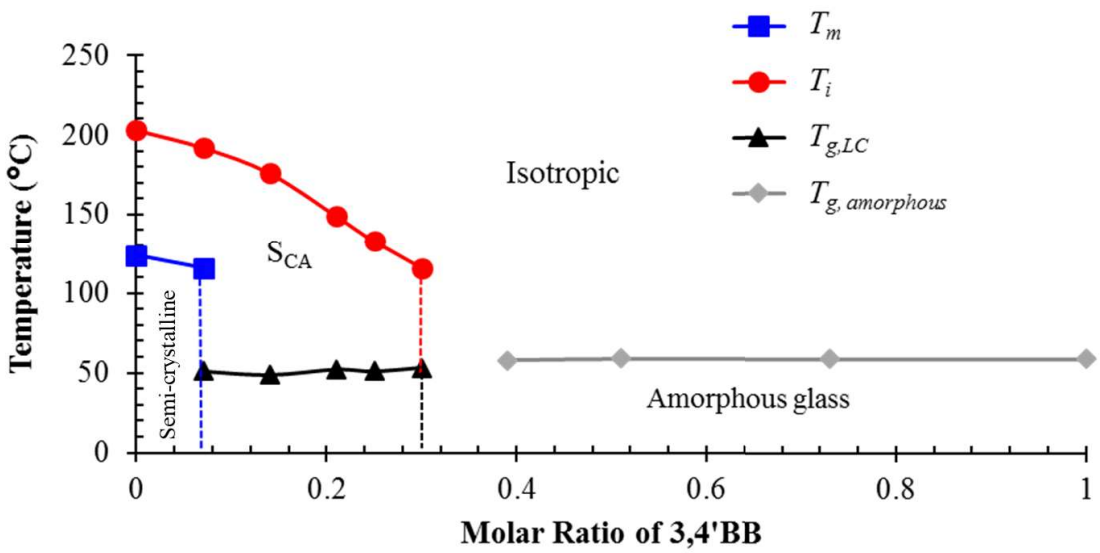

Figure 4.7. Phase diagram of (co)polyester series describing the change in thermal transitions as a function of increasing 3,4'BB molar ratio in poly(DEG-4,4'BB-*co*-3,4'BB). Samples annealed for 9 d at 90 °C.

peaks to be observed in WAXS. Smectic layer assembly becomes impossible as the runs of linear polymer are at too low of a concentration as 3,4'BB content is increased >47 mol %. As a result, all polymers with > 47 mol % 3,4'BB produce only broad amorphous scattering peaks in XRD. In summary, increasing the 3,4'BB content does not alter the crystal and LC structures but disrupts linearity of the backbone in turn inhibiting chain alignment.

Data from the WAXS, POM, DSC, and NMR measurements for these two series collectively enabled the generation of phase diagrams to better understand the range of properties each polymer series achieved. **Figure 4.7** illustrates the phase-diagram plotted for poly(DEG-4,4'BB-*co*-3,4'BB), while **Figure 4.8** depicts the phase-diagram for poly(BD-4,4'BB-*co*-3,4'BB). In both series, the phase diagrams reiterate the transition from a semi-crystalline polymer to a LC glass upon incorporation of the kinked 3,4'BB comonomer. This unique stabilization of the LC phase into a LC glass has not been previously observed in similar systems, such as poly(pentamethylene 4,4'- bibenzoate-

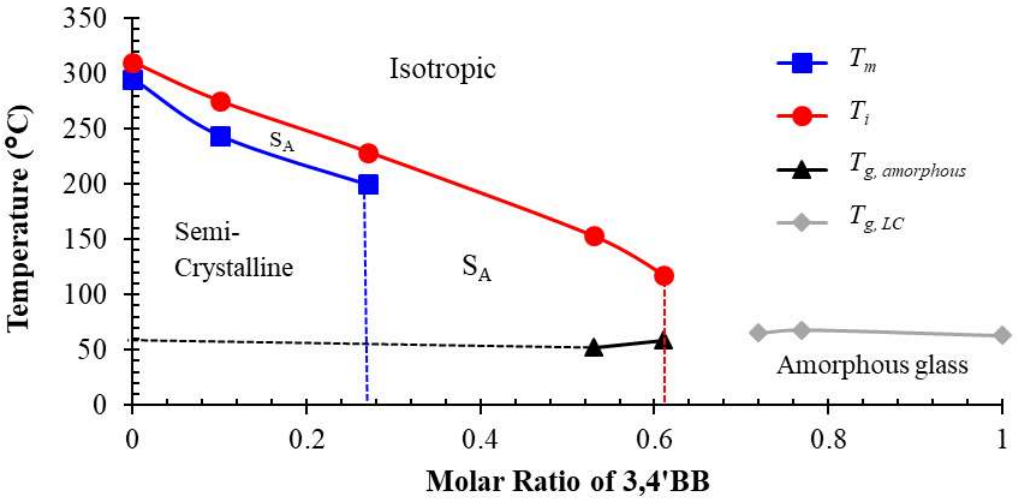

Figure 4.8. Phase diagram of (co)polyester series describing the change in thermal transitions as a function of increasing 3,4'BB molar ratio in poly(BD-4,4'BB-*co*-3,4'BB).

co- 2,6-napthalene dicarboxylates).[32] The rigidity of the aliphatic spacer effects the amount of 3,4'BB necessary to induce this transition. (Co)polyesters with high incorporation of 3,4'BB result in amorphous polymers with T_g's around 60 °C. The morphology of the LC phase relies on the linear spacer between the 4,4'BB mesogens and remains unaltered after copolymerization with 3.4'BB.

4.4.4 Thermomechanical Characterization.

DMA provided thermomechanical characterization of both (co)polyester series. Poly(DEG-4,4'BB-*co*-3,4'BB) series showed T_gs following the same trend as those evaluated from DSC (Table 2). The difference between the values for T_g determined from DSC and DMA are attributed to the different physical characteristic being probed within each analytical method, as well as the different heating rates utilized.[41] For (co)polyesters with high 4,4'BB mol %, an extended plateau modulus occurred without the presence of crystalline domains. This demonstrated the physical crosslinking capability of the smectic

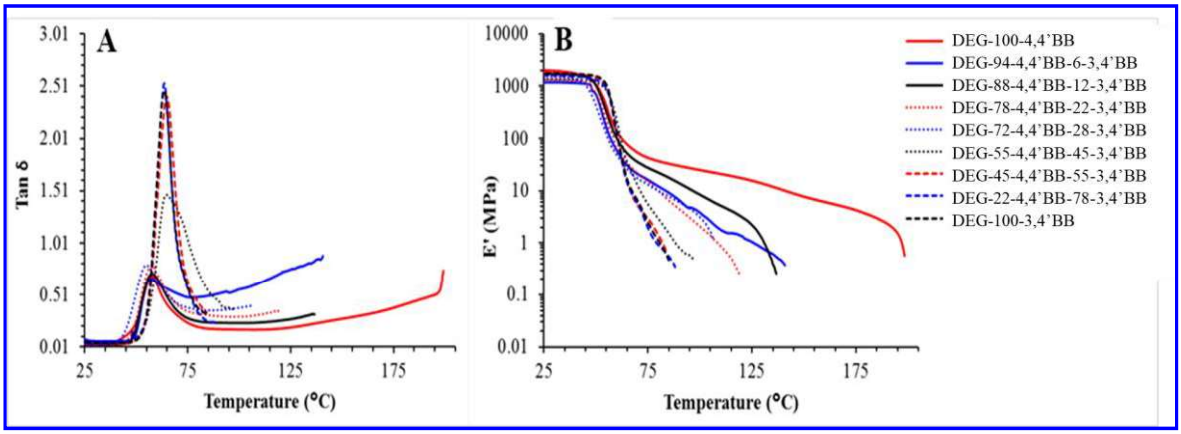

Figure 4.9. Dynamic mechanical analysis temperature ramp of poly(DEG-4,4'BB-*co*-3,4'BB) (co)polyester series as a function of increasing 3,4'BB content. Graph B shows storage modulus versus temperature while graph A portrays the corresponding tan δ versus temperature. DEG-X-4,4'BB-Y-3,4'BB where X and Y indicate the molar ratios of corresponding 4,4'BB and 3,4'BB repeat units.

mesophase within the polymer matrix. The T_{flow} occurs prior to the observed T_i due to the ability of translational motion within the smectic layers, and T_{flow} decreased with decreasing 4,4'BB content. The plateau moduli converge for all polymers that exhibited amorphous properties, as illustrated in **Figure 4.9**. The (co)polymers transition from LC glass to amorphous morphology also afforded an increase in the area of the tan delta attributed to increased amorphous character of the polymers.

DMA on poly(BD-4,4'BB-*co*-3,4'BB) samples containing ≤ 73 mol % 4,4'BB content exhibited similar properties to the DEG series, (**Figure 4.10**). The three polymers in this series that exhibited LC ordering (27, 53, and 61 mol % 3,4'BB) showed extended plateau moduli. These curves ended in viscous flow slightly below the T_i. For compositions possessing amorphous properties, the T_{flow} converge and minimal plateau moduli are detected along with a stronger tan delta peak. The T_gs for all polymers exhibit analogous properties to the T_gs observed by DSC.

4.5 Conclusion:

Melt transesterification containing kinked 3,4'BB comonomer generated, for the first time, two LC (co)polyester series. ^{1}H NMR spectroscopy confirmed the consistency

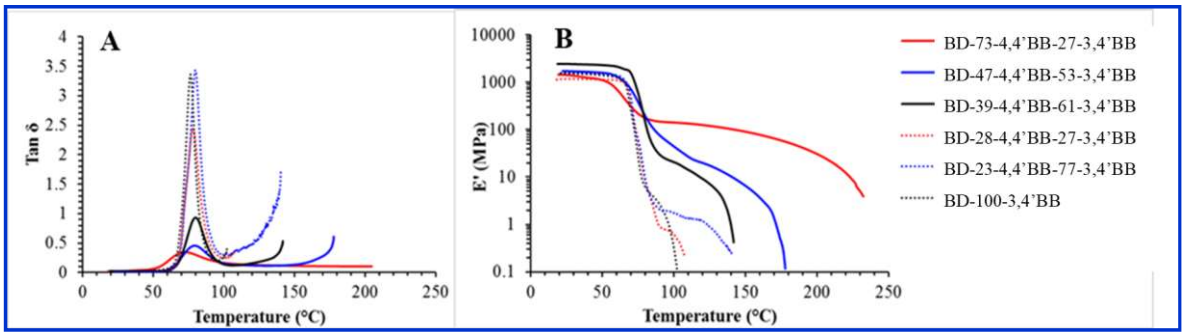

Figure 4.10. Dynamic mechanical analysis temperature ramp of poly(BD-4,4'BB-*co*-3,4'BB) (co)polyester series as a function of increasing 3,4'BB content. Graph B shows storage modulus versus temperature while graph A portrays the corresponding tan δ versus temperature. BD-X-4,4'BB-Y-3,4'BB where X and Y indicate the molar ratios of corresponding 4,4'BB and 3,4'BB repeat units.

of (co)polyester compositions to the targeted monomer ratios. SEC of soluble compositions established that the polymerizations achieved high molecular weights. DSC, POM, and WAXS confirmed the presence of a smectic CA mesophase over the LC compositions of the poly(DEG-4,4'BB-*co*-3,4'BB) series and the inhibition of crystallization. In contrast, DSC, POM and XRD revealed a smectic A mesophase and crystalline ordering in the poly(BD-4,4'BB-*co*-3,4'BB) series. Both series demonstrated disruption of crystalline order prior to LC order disruption resulting in the formation of LC glasses. These LC glasses exhibit a much broader mesogenic window than their semi-crystalline counterpart affording an increased temperature window for the orientation of these materials. This stabilization of the LC phase has not commonly been observed in other studies, such as copolymerization with dimethyl-2,6-naphthalene dicarboxylate or isophthalate, and could be uniquely beneficial toward applications in the electronics or fibers industry. Finally, DMA confirmed the ability of the smectic mesophase to act as physical crosslinks in a LC glass providing a tunable plateau modulus with T_{flow} close to the T_i. Future work will probe properties achieved upon incorporation of this kinked monomer into fully-aromatic LCPs.

Acknowledgements:

The authors thank Dr. Maruti Hegde in the Department of Applied Physical Sciences at University of North Carolina at Chapel Hill for insightful discussions. The morphology characterization is supported by the National Science Foundation under Grant No. DMR-1507245 and DMR-0923107.

Funding:

This work was supported by ExxonMobil Chemical Company.

References:

(1) Donald, A. M.; Windle, A. H.; Hanna, S., *Liquid crystalline polymers*; 2nd ed.; Cambridge University Press: Cambridge, 2006.

(2) Windle, A. H., In *Liquid Crystalline and Mesomorphic Polymers*; Shibaev, V. P., Lam, L., Eds.; Springer New York: New York, NY, 1994, p 26.

(3) Dobb, M. G.; McIntyre, J. E., In *Liquid Crystal Polymers II/III*; Platé, N. A., Ed.; Springer Berlin Heidelberg: Berlin, Heidelberg, 1984, p 61.

(4) Chung, T., *Thermotropic liquid crystal polymers: thin-film polymerization, characterization, blends, and applications*; Technomic Pub. Co: Lancaster, Pa, 2001.

(5) Ma, H.; Hibbs, M.; Collard, D. M.; Kumar, S.; Schiraldi, D. A., Fiber Spinning, Structure, and Properties of Poly(ethylene terephthalate-co-4,4‘-bibenzoate) Copolyesters, *Macromolecules* **2002**, *35*, 5123.

(6) Pérez-Manzano, J.; Fernández-Blázquez, J. P.; Bello, A.; Pérez, E., Liquid-crystalline copolymers of bibenzoate and terephthalate units, *Polymer Bulletin* **2006**, *56*, 571.

(7) Jackson, W. J.; Morris, J. C., In *Liquid-Crystalline Polymers*; American Chemical Society: 1990; Vol. 435, p 16.

(8) Watanabe, J.; Hayashi, M.; Nakata, Y.; Niori, T.; Tokita, M., Smectic liquid crystals in main-chain polymers, *Progress in Polymer Science* **1997**, *22*, 1053.

(9) Nelson, A. M.; Fahs, G. B.; Moore, R. B.; Long, T. E., High-Performance Segmented Liquid Crystalline Copolyesters, *Macromolecular Chemistry and Physics* **2015**, *216*, 1754.

(10) Watanabe, J.; Hayashi, M.; Morita, A.; Tokita, M., Thermotropic Liquid Crystals of Main-Chain Polyesters Having a Mesogenic 4,4'-Biphenyldicarboxylate Unit. 6. Chiral Mesophases of Polyesters with a (S)-2-Methylbutylene Spacer, *Macromolecules* **1995**, *28*, 8073.

(11) Krigbaum, W. R.; Asrar, J.; Toriumi, H.; Ciferri, A.; Preston, J., Aromatic polyesters forming thermotropic smectic mesophases, *Journal of Polymer Science: Polymer Letters Edition* **1982**, *20*, 109.

(12) Tokita, M.; Watanabe, J., Several Interesting Fields Exploited through Understanding of Polymeric Effects on Liquid Crystals of Main-Chain Polyesters, *Polymer Journal* **2006**, *38*, 611.

(13) Hu, Y. S.; Schiraldi, D. A.; Hiltner, A.; Baer, E., Structural Model for Oxygen Permeability of a Liquid Crystalline Polymer, *Macromolecules* **2003**, *36*, 3606.

(14) Wendling, J.; Gusev, A. A.; Suter, U. W.; Braam, A.; Leemans, L.; Meier, R. J.; Aerts, J.; Heuvel, J. v. d.; Hottenhuis, M., Crystal Morphology and Thermodynamics of Poly(ethylene-4,4‘-biphenyl dicarboxylate) and Related Copolymers with Ethylene-2,6-naphthalene Dicarboxylate, *Macromolecules* **1999**, *32*, 7866.

(15) Hu, Y. S.; Liu, R. Y. F.; Schiraldi, D. A.; Hiltner, A.; Baer, E., Solid-State Structure of Copolyesters Containing a Mesogenic Monomer, *Macromolecules* **2004**, *37*, 2128.

(16) Hu, Y. S.; Liu, R. Y. F.; Schiraldi, D. A.; Hiltner, A.; Baer, E., Oxygen Barrier Properties of Copolyesters Containing a Mesogenic Monomer, *Macromolecules* **2004**, *37*, 2136.
(17) Edling, H. E.; Liu, H.; Sun, H.; Mondschein, R. J.; Schiraldi, D. A.; Long, T. E.; Turner, S. R., Copolyesters based on bibenzoic acids, *Polymer* **2017**.
(18) Mondschein, R. J.; Dennis, J. M.; Liu, H.; Ramakrishnan, R. K.; Nazarenko, S.; Turner, S. R.; Long, T. E., Synthesis and Characterization of Amorphous Bibenzoate (Co)polyesters: Permeability and Rheological Performance, *Macromolecules* **2017**, *50*, 7603.
(19) Kang, H.; Lin, Q.; Armentrout, R. S.; Long, T. E., Synthesis and Characterization of Telechelic Poly(ethylene terephthalate) Sodiosulfonate Ionomers, *Macromolecules* **2002**, *35*, 8738.
(20) Dennis, J. M.; Fahs, G. B.; Moore, R. B.; Turner, S. R.; Long, T. E., Synthesis and Characterization of Polysulfone-Containing Poly(butylene terephthalate) Segmented Block Copolymers, *Macromolecules* **2014**, *47*, 8171.
(21) Dennis, J. M.; Enokida, J. S.; Long, T. E., Synthesis and Characterization of Decahydronaphthalene-Containing Polyesters, *Macromolecules* **2015**, *48*, 8733.
(22) Kelsey, D. R.; Scardino, B. M.; Grebowicz, J. S.; Chuah, H. H., High Impact, Amorphous Terephthalate Copolyesters of Rigid 2,2,4,4-Tetramethyl-1,3-cyclobutanediol with Flexible Diols, *Macromolecules* **2000**, *33*, 5810.
(23) Zhang, M.; Zhang, M.; Moore, R. B.; Long, T. E., Influence of charge placement on the thermal and morphological properties of sulfonated segmented copolyesters, *Polymer* **2013**, *54*, 3521.
(24) Scheirs, J.; Long, T. E., *Modern polyesters: chemistry and technology of polyesters and copolyesters*; John Wiley: Hoboken, NJ;Chichester, England;, 2003.
(25) Arnold, F. E.; Van Deusen, R. L., Preparation and Properties of High Molecular Weight, Soluble Oxobenz[de]imidazobenzimidazoisoquinoline Ladder Polymer, *Macromolecules* **1969**, *2*, 497.
(26) Yeh, J.-M.; Liou, S.-J.; Lai, C.-Y.; Wu, P.-C.; Tsai, T.-Y., Enhancement of Corrosion Protection Effect in Polyaniline via the Formation of Polyaniline−Clay Nanocomposite Materials, *Chemistry Materials* **2001**, *13*, 1131.
(27) Jin, J.-I.; Kang, C.-S., Thermotropic main chain polyesters, *Progress in Polymer Science* **1997**, *22*, 937.
(28) Pérez, E.; Benavente, R.; Cerrada, M. L.; Bello, A.; Pereña, J. M., Synchrotron X-ray and DSC Studies of the Phase Behaviour of Poly(diethylene glycol p,p′-bibenzoate), *Macromolecular Chemistry and Physics* **2003**, *204*, 2155.
(29) Bello, P.; Bello, A.; Riande, E.; Heaton, N. J., Thermotropic Polyesters with Flexible Spacers Bearing Ether Bonds in Asymmetric Position, *Macromolecules* **2001**, *34*, 181.
(30) Bello, A.; Riande, E.; Perez, E.; Marugan, M. M.; Perena, J. M., Influence of the spacer on the thermotropic and conformational properties of poly[oxybis(trimethylene) p,p'-bibenzoate] and poly(heptamethylene p,p'-bibenzoate), *Macromolecules* **1993**, *26*, 1072.

(31) Spies, C.; Zachmann, H. G., Investigation of the molecular mobility in a ternary copolyester in the liquid crystalline and isotropic states by means of deuteron n.m.r, *Polymer* **1994**, *35*, 3816.
(32) Tokita, M.; Osada, K.; Watanabe, J., Thermotropic Liquid Crystals of Main-Chain Polyesters Having a Mesogenic 4,4′-Biphenyldicarboxylate Unit XI. Smectic Liquid Crystalline Glass, *Polymer Journal* **1998**, *30*, 589.
(33) Martínez-Gómez, A.; Pérez, E.; Bello, A., Synthesis of copolybibenzoates with thioether and ether groups in the flexible spacers, *Polymer International* **2005**, *54*, 1196.
(34) Pereira, F. V.; Borsali, R.; Ritter, O. M. S.; Gonçalves, P. F.; Merlo, A. A.; Silveira, N. P. d., Structure-property relationships of smectic liquid crystalline polyacrylates as revealed by SAXS, *Journal of the Brazilian Chemical Society* **2006**, *17*, 333.
(35) Cook, A. G.; Wardell, J. L.; Brooks, N. J.; Seddon, J. M.; Martínez-Felipe, A.; Imrie, C. T., Non-symmetric liquid crystal dimer containing a carbohydrate-based moiety, *Carbohydrate Research* **2012**, *360*, 78.
(36) Dierking, I., In *Textures of Liquid Crystals*; Wiley-VCH Verlag GmbH & Co. KGaA: 2004, p 91.
(37) Hu, Y. S.; Wang, H. P.; Schiraldi, D. A.; Hiltner, A.; Baer, E., Oxygen-transport properties of liquid-crystalline polyesters based on 4,4′-bibenzoic acid, *Journal of Applied Polymer Science* **2007**, *105*, 30.
(38) Watanabe, J.; Hayashi, M., Thermotropic liquid crystals of polyesters having a mesogenic p,p'-bibenzoate unit. 1. Smectic A mesophase properties of polyesters composed of p,p'-bibenzoic acid and alkylene glycols, *Macromolecules* **1988**, *21*, 278.
(39) Hu, Y. S.; Hiltner, A.; Baer, E., Solid state structure and oxygen transport properties of copolyesters based on smectic poly(hexamethylene 4,4′-bibenzoate), *Polymer* **2006**, *47*, 2423.
(40) Polyakova, A.; Liu, R. Y. F.; Schiraldi, D. A.; Hiltner, A.; Baer, E., Oxygen-barrier properties of copolymers based on ethylene terephthalate, J*ournal of. Polymer Science, Part B: Polymer Physics* **2001**, *39*, 1889.
(41) Campbell, D.; Pethrick, R. A.; White, J. R., *Polymer characterization: physical techniques*; Stanley Thornes: Cheltenham, Glos., United Kingdom, 2000.

Supporting Information

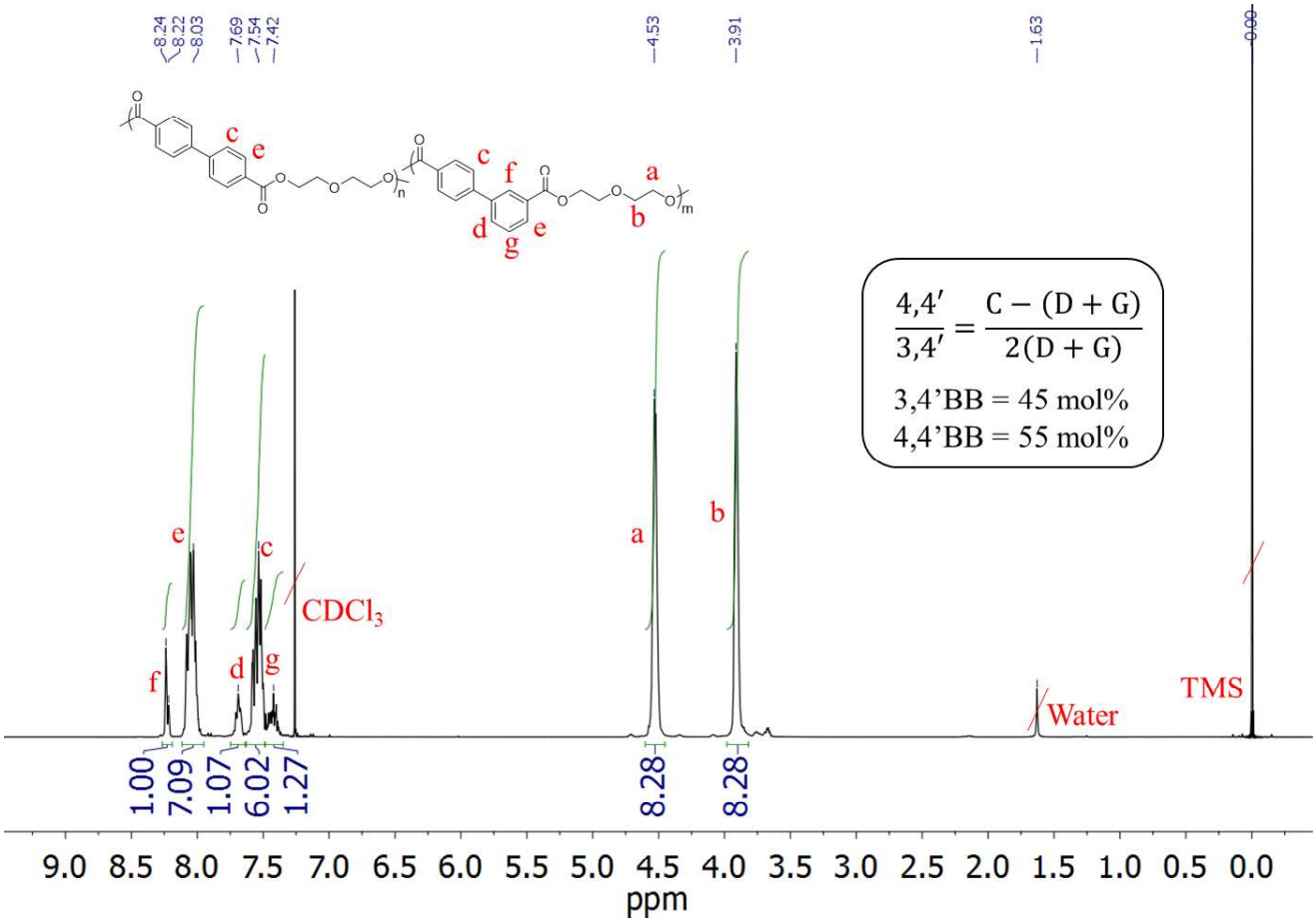

Figure S4.1. ^{1}H NMR spectrum of poly(DEG-45-4,4'BB-*co*-55-3,4'BB) copolyester with targeted ratio of 50:50 4,4'BB:3,4'BB. Isomeric ratios determined from calculations using peaks c, d, and g, as shown in equation.

.

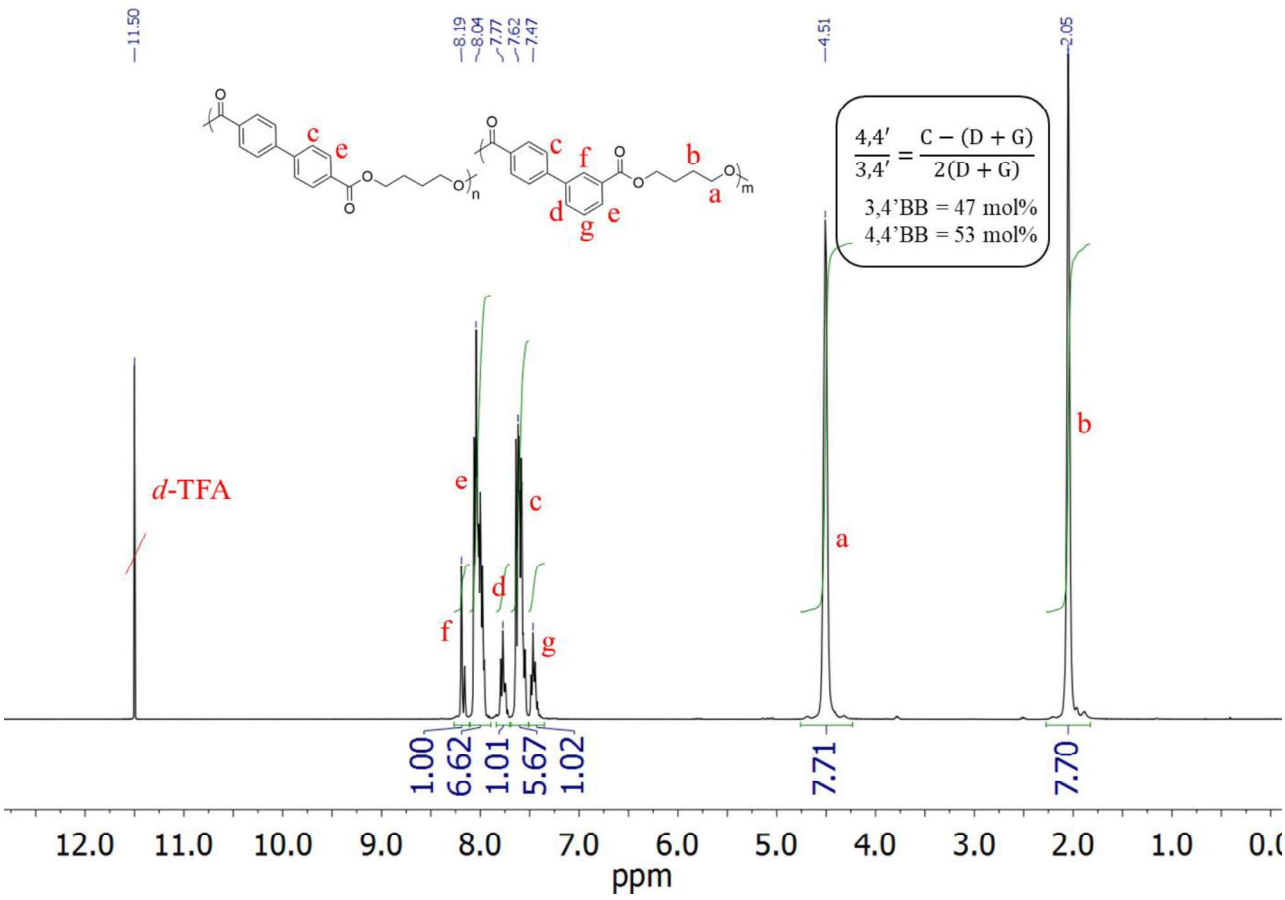

Figure S4.2. ^{1}H NMR of poly(BD-47-4,4'BB-*co*-53-3,4'BB) copolyester with incorporation targeted ratio of 50:50 4,4'BB:3,4'BB. Isomeric ratios determined from calculations using peaks c, d, and g, as shown in equation.

Chapter 5: Structure-property-morphology relationships of liquid crystalline telechelic ionomers

Katherine V. Heifferon and Timothy E. Long*

Macromolecules Innovation Institute, Department of Chemistry, Virginia Tech, Blacksburg, VA 24061

Keywords: liquid crystalline, polyesters, ionomer, telechelic

5.1 Abstract:

The α,ω-functionalization of a liquid crystalline polyester, poly(hexamethylene 4,4' bibenzoate), with sodium 3-sulfomethylbenzoate (SSMB) provides a series of telechelic ionomers with varying molecular weight and ionic content. Melt transesterification with 0 to 10 mol % monofunctional ionic or non-ionic end group (*m*-toluic acid) enabled the polymerization of the ionomers with systematically lower degree of polymerization and as well as generating a non-ionic control. Thermogravimetric analysis revealed insignificant differences between the two series of polymers, all exhibiting $T_{d,5\%}$ of 360 ± 5 °C. Differential scanning calorimetry exhibited insignificant changes in the thermal transitions until 10 mol % incorporation of SSMB at which a 3 °C decrease in the melting temperature (T_m) and an 8 °C decrease in the isotropic temperature (T_i) occurred. Polarized optical microscopy corroborated the decrease in the T_i with an observed reduction in the texture size relative to the other polymers. Dynamic mechanical analysis identified a slight increase in the T_g of the ionic endcapped polymer relative to the non-ionic samples. Finally, melt rheology using a frequency sweep demonstrated an increase in the zero-shear viscosity for the ionomers in comparison to the non-ionic polymer of similar molecular weight.

5.2 Introduction:

Thermotropic liquid crystalline polyesters (LCP) represent a field of high-performance polymers typically exhibiting high tensile strength, high flame resistance, and high chemical resistance. Applications as high strength fibers, miniature insulators in electronic parts, and stainless-steel replacements in the medical industry exploit these beneficial properties.[1-3] Thermotropic LCP exhibit a transition into a liquid crystalline mesophase upon application of heat, typically transitioning from a crystalline solid (3D) to a smectic (2D) or nematic (1D) mesophase. These mesophase exhibit varying degrees of translational and orientational order.[2,4,5] Within the temperature window of this liquid crystalline (LC) phase, molecular alignment imparts high levels of chain orientation and significant decreases in viscosity under shear, thus enabling better melt processability through injection molding and the formation of highly oriented fibers or molded parts.[5-8]

Synthesis of these polymers often requires the use of rigid rod type monomers which exhibit LC properties prior to polymerization (mesogenic monomers), such as dimethyl 4,4'-bibienzoate (4,4'BB). Most polymers using 4,4'BB in a main-chain configuration incorporate a flexible spacer between the mesogenic monomers forming a semi-aromatic polymer. This structure imparts a lower processing temperature relative to their fully-aromatic counterpart and enables the use of melt-transesterification polycondensation, identical to the synthesis of polyethylene terephthalate (PET), rather than high-temperature acidolysis polymerization techniques. Watanabe et al. synthesized a wide-range of 4,4'BB based polymers with different aliphatic diols demonstrating an odd-even effect on the thermal transitions of the polymers, as well as their LC morphology.[9-13] This work demonstrated that polymers with an odd number of atoms in

the spacer achieved a smectic CA (S_{CA}) morphology while those with an even number of atoms obtained a smectic A morphology within the LC temperature range.[13] Specifically, poly(hexamethylene- 4,4' bibenzoate) revealed a smectic A morphology with a crystalline to smectic transition (T_m) at 169 °C and the smectic to isotropic transition (clearing temperature, T_i) at 229 °C.[11]

Two major shortcomings of LCPs arise from their weak transverse properties which often exhibit 1-2 order of magnitude drop relative to the axial properties, as well as their poor miscibility and interfacial adhesion with other thermoplastics.[1,14] Incorporation of functional groups within LCPs which interact intramolecularly as self-supporting physical crosslinks or intermolecularly with other polymer structures represent an approach to improving these deficits. The application of ionic functional groups has garnered some success within this area. The term ionomer refers to a charged polymer with the incorporation of ionic groups in polymers at less than 15 mol %. The ionic groups within these polymers form thermo-reversible physical crosslinks through ionic aggregation that result from the Coulombic interactions between the ionic moieties.[15] These physical interactions facilitate increases in mechanical strength, as well as directly impacting the solution/melt rheological and morphological properties of the polymers.[16-18]

Sulfonate based ionic groups, such as sodium 5-sulfoisophthalate, comprise one of the most common ionic moieties utilized in step-growth ionomers. DuPont's patents of sulfonated PET (SPET) utilizing sulfonate ionic groups to improve the dyeability of these textile fibers represents an early example of the industrial use of ionomers.[19,20] Further studies of SPET demonstrated that the polymer lowered the interfacial tension

between PET and various polyamides through interactions between the ionic group and the polar amide units improving blend miscibility.[21-25]

Both side-chain and main-chain LCPs have demonstrated success in the synthesis of LC ionomers. Side-chain LCPs (SCLCPs) synthesized LC ionomers through attaching ionic moieties and mesogenic monomers pendant to the backbone of flexible polymers, such as polysiloxanes or polyacrylates.[26-31] These afford LC polymers with a variety of smectic and nematic morphologies. Zhang et al. demonstrated the ability of one SCLCP ionomer to act as a compatibilizer between blends of polyamide-1010 and polypropylene.[29]

Main-chain LCP incorporate ionic groups either through random placement throughout the backbone of the polymer or as terminal groups (telechelic ionomer).[14,26,32-42] A wide number of these polymers utilized the ionic monomer, Brilliant Yellow (2,2'-(1,2-ethenediyl)bis[5-[(4-hydroxyphenyl)azo]-benzenesulfonic acid disodium salt), which contains sodium sulfonate groups to generate LC ionomers through interfacial polymerization.[40-43] This strategy created nematic LC ionomers which recently showed promise as a compatibilizing agent between montmorillonite nanocomposites and PEO/PLA blends for application in solid polymer electrolytes.[41] Xue and Hara's work on LC ionomers randomly copolymerized sodium 5-sulfoisophthalate with naphthalene based fully-aromatic polyesters using melt polymerization methods. The *meta* linkage in combination with the ionic aggregation resulted in a reduction of the T_m while a nematic morphology persisted for all compositions (0-20 mol % ionic content).[14] Long et al. conducted a similar study utilizing a semi-aromatic LCP, poly(hexamethylene 4,4'-bibenzoate, and dimethyl-5-sodiumsulfoisophthalate at concentrations from 0-20 mol %.

This polymers smectic mesophase exhibit destabilization when utilizing > 15 mol % ionic group.[33]

The terminal attachment of ionic groups to form α,ω-telechelic ionomers stems from the ability to incorporate these units while limiting the drastic increase in melt viscosity. This polymer structure enables electrostatic chain extension which results in lower melt viscosities at the same molecular weight as a random ionomer and lower impact on the polymer crystallinity due to less disruption in the structures symmetry.[44,45] LC telechelic ionomers primarily focus around the use of monofunctional dye, 4-hydro-phenylazobenzene sulfonic acid, through interfacial polymerization. These nematic polymers exhibit minimal impact of the ionic group on the thermal transitions of the polymer while demonstrating successful compatibilization of poly(butylene terephthalate) and polypropylene.[38,39]

Herein, this manuscript discusses the synthesis and characterization of a series of novel LC telechelic ionomers. The backbone structure comprises the semi-aromatic polymer, poly(hexamethylene 4,4' bibenzoate), while the terminal moiety, synthesized from sodium 3-sulfomethylbenzoate (SSMB), provided the ionic charge. A secondary terminal group, from *m*-toluic acid (*m*-TA), enabled the synthesis of a series of non-ionic standards with which to compare properties. The ionic aggregation resulted in minimal changes to the thermal transitions of the LCP while maintaining the smectic A mesophase. Polarized optical microscopy displayed a significant decrease in domain size upon incorporation of greater than 5 mol % SSMB. Melt viscosity also demonstrates a higher zero-shear viscosity for polymers with 10 mol % SSMB relative to the 10 mol % *m*-TA.

5.3 Experimental:

5.3.1 Materials.

Dimethyl 4,4'-biphenyldicarboxylate (4,4'BB) (Sigma-Aldrich, 99%), *m*-toluic acid (Sigma-Aldrich, 99%), sodium 3-sulfobenzoate (Sigma-Aldrich, 97%), 1,6-hexanediol (Sigma-Aldrich, 97%), trifluoroacetic acid-*d* (*d*-TFA) (Sigma-Aldrich, 99.5% atom D), sodium acetate (Sigma-Aldrich, ≥ 99%), and chloroform-*d* ($CDCl_3$) (Cambridge Isotope Laboratories, 99.8% atom D) were used as received. Preparation of the catalyst solution, 0.01g/mL solution of titanium tetra(isopropoxide) (Sigma-Aldrich, 99%) in 1-butanol (Sigma-Aldrich, anhydrous 99.8%), occurred following a previously described procedure.[45] All solvents were used as received after purchase from Spectrum.

5.3.2 Analytical Methods:

A Varian Unity 400 at 400 MHz (23 °C) afforded both the ^{1}H and ^{13}C nuclear magnetic resonance (NMR) spectroscopy of the polymers utilizing *d*-TFA as solvent. A TA Instruments Q50 thermogravimetric analyzer (TGA) revealed the weight loss profiles of the polymers, under constant N_2 flow, at a rate of 10 °C/min from 25 to 600 °C. A heat/cool cycle with a rate of 10 °C/min for both cycles on a TA Instruments Q1000 differential scanning calorimeter (DSC) afforded the thermal transitions of the polymers. Analysis was performed on the cooling cycle using the maximum of the melting temperature (T_m) and the isotropic temperature (T_i). Indium (T_m = 156.60 °C) and zinc (T_m = 419.47 °C) standards calibrated the instrument prior to analysis. Compression molding formed free-standing polymer films after melting at 275 °C between a sandwich of aluminum plates, Kapton™ sheets coated with a Rexco Partall® Power Glossy Liquid mold release agent, and 150 μm thick stainless-steel shims. Quenching in an ice bath cooled the packet rapidly to room temperature. Dynamic mechanical analysis studies

occurred in tension mode on a TA Instruments Q800 DMA with a 0.01 N static force, frequency of 1 Hz, amplitude of 0.1% strain, and a heating rate of 3 °C/min. The maximum of the DMA tan delta provided the T_g measurements from this test. An Olympus BX51 polarizing optical microscope with a Linkham TMS 94 hot stage provided the polarized optical microscopy (POM) images of the endcapped polymers. The polymer samples were melted between the glass slides at 275 °C then cooled at a rate of 10 °C/min to reveal the birefringent textures. Melt rheological characterization was performed on a TA instruments Discovery Hybrid Rheometer-2 using 25 mm disposable parallel plates under N_2. A strain-sweep from 0.0125 to 12.5% strain using 1 Hz at 275 °C afforded the linear viscoelastic region for the polymers. A frequency-sweep from 0.1 to 100 rad/s using 1.25% strain generated the analysis of complex viscosity as a function of frequency. Zero-shear viscosity measurements occurred from 0.1 rad/s. The polymer back bone remained the same for all samples, poly(hexamethylene 4,4'-bibenzoate) (poly(HD-4,4'BB)). The end groups varied between the two series and are identified by the mol % added to the reaction as well as the type of end group, sodium 3-sulfomethylbenzoate (SSMB) or *m*-toluic acid (*m*-TA).

5.3.3 Esterification of sodium 3-sulfobenzoate.

Sodium 3-sulfobenzoate (16.95 g, 0.0756 mol), toluene sulfonic acid (2.86 g, 0.0166 mol), and methanol (150 mL) were measured into a 250-mL round-bottomed flask attached to a condenser. Refluxing the reaction mixture at 80 °C overnight (15 h) afforded a homogenous clear solution. Concentration *via* a rotary evaporator removed the MeOH forming a white solid. Stirring the solid in DCM followed by filtration removed the salts. Recrystallization in ethanol, filtration, and drying *in vacuo* at 50 °C afforded a pure sodium salt form as a white solid.

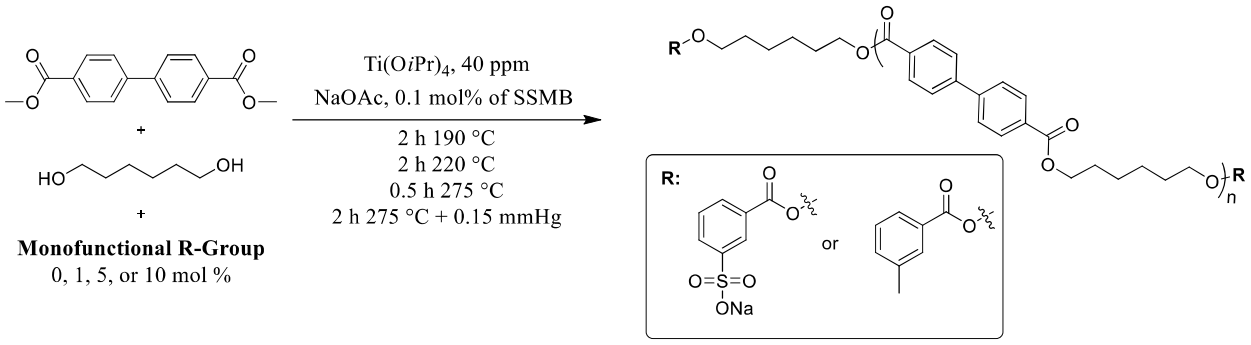

Scheme 5.1. Synthesis of poly(hexamethylene 4,4' bibenzoate) endcapped with either sodium 3-sulfomethylbenzoate or m-toluic acid

^{1}H NMR (400 MHz, DMSO-d$_6$): δ 8.21 (t, 1H), 7.90 (d, 1H), 7.86 (d, 1H), 7.50 (t, 1H), and 3.87 (s, 3H) ppm.

5.3.4 Synthesis of endcapped polymers.

Melt transesterification and polycondensation afforded the synthesis of poly(HD-4,4'BB) endcapped with SSMB. 4,4'BB (16.04 g, 0.059 mol) and HD (14.32 g, 0.118 mol) were weighted into a dry 100-mL round-bottomed flask. Addition of 1, 5, or 10 mol % of the SSMB (0.74 g, 0.003 mol, 5 mol %) based on the final polymer occurred depending on the reaction. Dry NaOAc (0.025 g, 0.0003 mol) was added the reaction flask at a 0.1 mol % concentration based on SSMB. Addition of the titanium isopropoxide catalyst (40 ppm) was quickly followed by evacuation of the flask and backfilling with N_2 three times to ensure an inert atmosphere. The reaction set-up included a t-neck adaptor, distillation tube, 100-mL round-bottomed collection flask, overhead mechanical stirrer, glass stir-rod adaptor, and metal stir-rod. Heating the reaction at 190 °C for 2 h, 220 °C for 2 h, and 275 °C for 0.5 h under N_2 flow afforded a homogenous melt and collection of the condensate. The final application of vacuum (0.15 mmHg) for 2 h at 275 °C facilitated a significant increase in the product viscosity. The final polymer was removed from the 100-mL round-bottomed flask, after the reaction

cooled, by breaking away the glass flask and clipping the resulting material from the metal stir-rod. The polymer was then used without further purification.

Synthesis of *m*-TA endcapped polymers occurred through the same method. Addition of 0, 1, 5, or 10 mol % of the *m*-TA (0.89 g, 0.007 mol, 10 mol %) based on the final polymer was chosen depending on the reaction. No NaOAc was utilized due to elimination of the ionic group.

5.4 Results and Discussion:

5.4.1 Synthesis and Structural Characterization.

Melt transesterification and polycondensation afforded the polymerization of all polymers within this study, as illustrated in **Scheme 5.1**. The procedure followed methods previously described in the literature from our group.[44-46] Unlike *m*-TA which created a homogenous solution during the polymerization, sodium 3-sulfobenzoate's

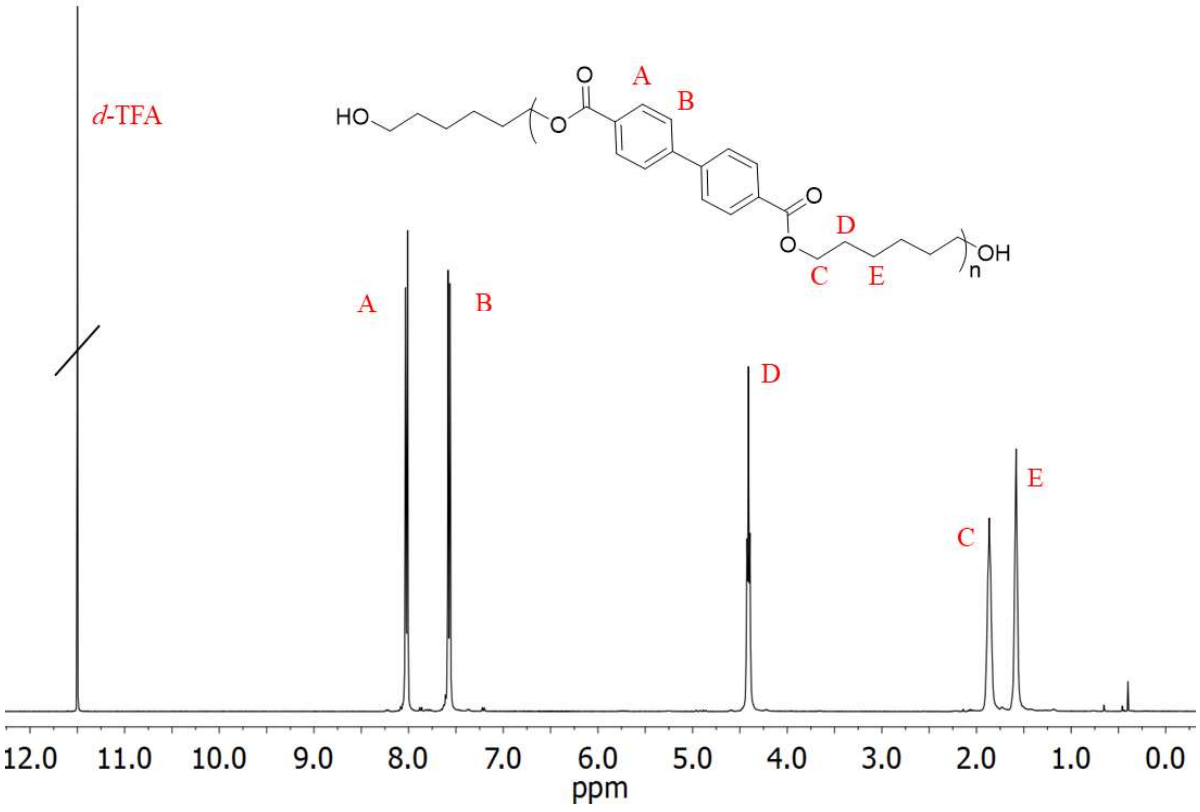

Figure 5.1. ^{1}H NMR spectroscopy (*d*-TFA, 400 MHz) of poly(hexamethylene 4,4' bibenzoate) without sulfonate end groups.

insolubility in the monomers resulted in a heterogenous reaction mixture inhibiting its polymerization. Esterification of the carboxylic acid on the ionic end group to the methyl ester prior to the polymerization reduced the polarity of the monomer facilitating a homogenous reaction when incorporated into the polymerization mixture. ^{1}H NMR spectroscopy confirmed full conversion of the carboxylic acid to the ester prior to use in the polymerization. The maintained peak locations between the starting material and final product, as well as unobserved broad peak associated with the proton on a sulfonic acid, confirmed the presence of the ionic salt form of the new monofunctional endgroup.

Synthesis of a non-endcapped poly(HD-4,4'BB) occurred as a standard (0 mol % *m*-TA/SSMB) and ^{1}H NMR spectroscopy confirmed the structure of this polymer in **Figure 5.1**. Peaks associated with the formation of the possible 6,6'-oxybis-1-hexanol side-product within the polymer backbone were not observed in the ^{1}H NMR studies. Separation of the SSMB peaks within the ^{1}H NMR spectroscopy of the ionomer series enabled the calculation of the ionic group concentration within the polymer, as illustrated in **Figure 5.2. Table 5.1** reveals that the calculated concentrations follows the values initially charged at the start of the polymerizations closely. Unfortunately, overlap with the backbone peaks inhibited the same analysis for the *m*-TA samples. Insolubility in

Table 5.1. Molecular weight and end group analysis of poly(hexamethylene 4,4' bibenzoate) endcapped with sodium 3-sulfomethylbenzoate (SSMB) using ^{1}H NMR spectroscopy.

End-Group	Targeted mol % end group	Estimated M_n (g/mol)	Mol % end group[a]
SSMB	Non-endcapped	-	-
	1	34,000	1
	5	7,000	4
	10	4,000	9

[a] Calculated from ^{1}H NMR spectroscopy

standard SEC solvents, such as chloroform or THF, inhibited molecular weight analysis through this method with these two polymer series.

5.4.2 Thermal and Thermomechanical Analysis.

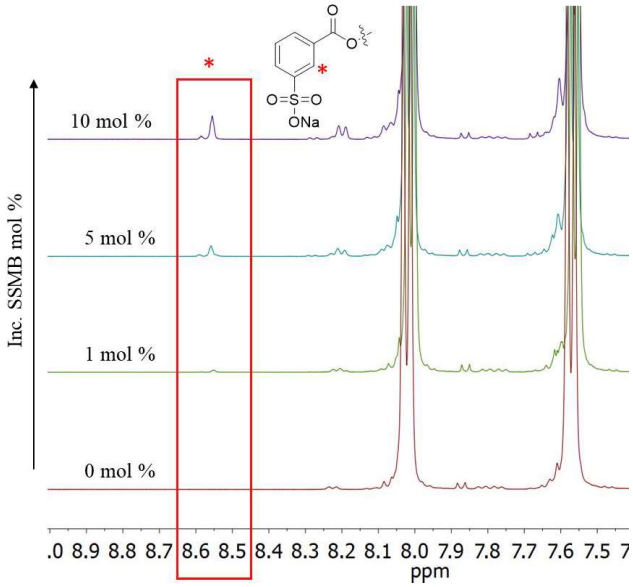

Figure 5.2. ^{1}H NMR spectroscopy (*d*-TFA, 400 MHz) of poly(hexamethylene 4,4' bibenzoate) endcapped with increasing mol % sodium 3-sulfomethylbenzoate.

Thermogravimetric analysis was performed on the two series to determine the effect of end groups on the weight loss profile of the polymers. All polymers exhibited a one-step weight loss profile with $T_{d,5\%}$ of 360 ± 5 °C (**Figure 5.3**), consistent with previous literature on poly(HD-4,4'BB).[47]

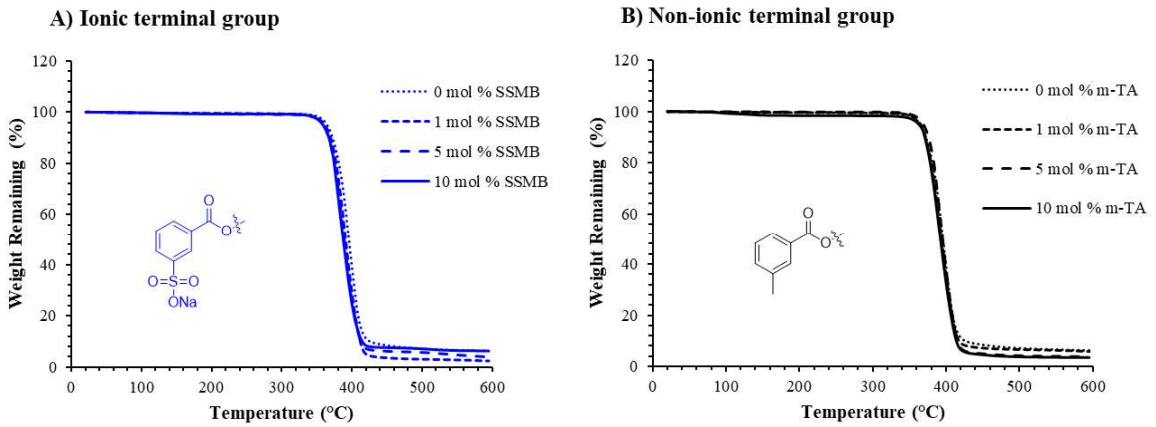

Figure 5.3. TGA analysis of poly(HD-4,4'BB) endcapped with either A) sodium 3-sulfomethylbenzoate (SSMB), or B) m-toluic acid (m-TA).

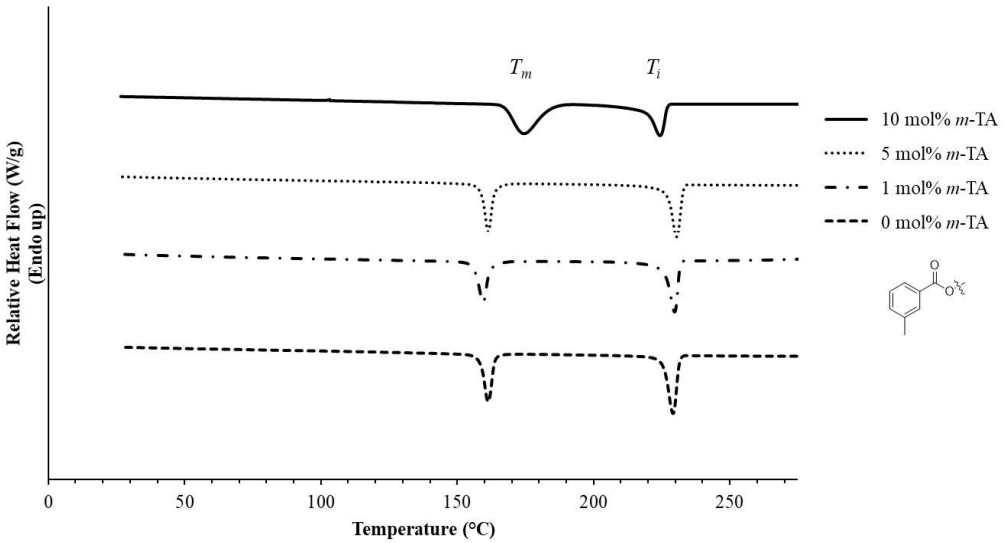

Figure 5.4. Cooling curves of poly(HD-4,4'BB) at a rate of 10 °C/min endcapped with increasing mol % m-toluic acid (m-TA).

DSC revealed the thermal transitions for ionic and non-ionic polymers. The standard, poly(HD-4,4'BB) with 0 mol % end groups, resulted in two exothermic transitions upon cooling the sample at 10 °C/min from 280 °C. These transitions occurred at 230 °C and 159 °C associated with morphological transitions from isotropic into a Smectic A mesophase (T_i) and the transition from Smectic A to semi-crystalline morphology (T_m), respectively.[10,11] The highly ordered nature of this polymer between the LC and crystalline domains limits the observance of a T_g. The series of non-ionic endcapped polymers exhibits no substantial change to the thermal transitions until the 10 mol % *m*-TA sample (**Figure 5.4**). At this concentration, the end groups become much more prevalent in the system as the molecular weight experiences an estimated drop of about 4,000 g/mol, as calculated using the modified Carothers equation. As a result, the T_m increases from 159 °C to 175 °C with an increase in the heat of fusion from 21.1 to 35.1 J/g. Chen et al. observed similar trends in a study of the effect of molecular weight on the crystallization of poly(trimethylene terephthalate) indicating that T_m and ΔH_m increase as molecular weight decreases. Higher molecular weight resulted in decreased

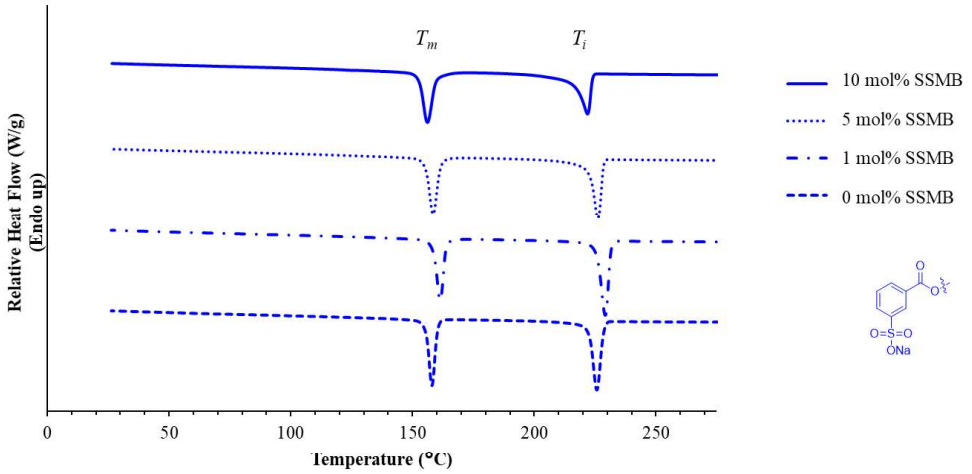

Figure 5.5. Cooling curves of poly(HD-4,4'BB) at a rate of 10 °C/min with increasing mol % sodium 3-sulfomethylbenzoate (SSMB) terminal groups.

crystallizability as well as a decreased rate of crystallization upon cooling.[48] In contrast, the T_i decreased slightly from 230 °C to 224 °C with a 6.6 J/g drop in the ΔH_i in the 10 mol % *m*-TA sample. Tsai et al. demonstrated a molecular weight effect on poly(hexamethylene 4,4'-bibenzoate), which determined that the smectic order decreases with decreasing molecular weight. Also while not the focus of the study, an increase in the T_m was also observed with decreasing molecular weight.[49]

Figure 5.5 illustrates the DSC profiles of the ionic endcapped polymers. The changes in the T_m and T_i across the concentration range did not follow the same trend as the *m*-TA polymers. Insignificant changes in these values occurred prior to the 10 mol % SSMB polymer which resulted in a 3 °C decrease in the T_m as well as an 8 °C decrease in the T_i. Telechelic ionomers of poly(ethylene terephthalate) in previous studies exhibited a decrease in T_m with increasing concentration of the ionic end groups. [45] Kang et al. attributed this shift to a decrease in the crystallization rate due to slower polymer chain mobility as a function of the ionic end groups.[45] The reduced T_i presumably could be attributed to this retarded chain mobility limiting the ability to form a smectic mesophase.

Table 5.2. Thermal characterization of the two series of endcapped poly(HD-4,4'BB) utilizing thermogravimetric analysis, differential scanning calorimetry, and dynamic mechanical analysis.

End-Group	mol % end group	T_m (°C)[a]	ΔH_m (J/g)[a]	T_i (°C)[a]	ΔH_i (J/g)[a]	$T_{d,5\%}$ (°C)	Char Yield at 600 °C (%)	T_g (°C)[b]
SSMB	Non-endcapped	159	21.1	230	25.9	365	6	55
	1	158	20.0	226	26.0	361	2	58
	5	159	22.6	226	25.1	359	4	N/A
	10	156	23.7	222	21.5	359	6	N/A
m-TA	1	161	21.3	229	27.3	365	6	52
	5	164	22.1	233	27.5	369	4	N/A
	10	175	35.1	224	19.3	363	4	N/A

[a] Determined from cooling cycle of DSC
[b] Determined from DMA of compression molded films

These telechelic ionomers differed significantly from previous random copolymerization ionomers synthesized using poly(HD-BB) with various concentrations of dimethyl-5-sodiumsulfoisophthalate. The previous copolymers exhibit an initial drop in the T_i upon incorporation of the ionic monomer followed by a subsequent increase resulting in a maximum value at 10 mol % incorporation. Addition greater than 15 mol % ionic monomers disrupted the LC morphology entirely resulting in a semi-crystalline polymer.

Compression molding at 275 °C afforded free standing films of poly(HD-BB) and the 1 mol % end group samples. Films based on the 5 and 10 mol % *m*-TA/SSMB polymers were brittle and crumbled upon clamping into the tension geometry of the DMA preventing analysis. The 0 mol % sample, poly(HD-BB), afforded a T_g at 55 °C with flow occurring close to 225 °C near the T_i of the polymer (**Figure 5.6** and **Table 5.2**). Unlike nematic polymers, a smectic mesophase exhibits limited flow within the mesogenic window due to the 2D ordered structure. The 1 mol % *m*-TA polymer exhibited a slightly lower T_g of 52 °C associated with the assumed reduced molecular weight of this polymer. In contrast, 1 mol % SSMB garnered an increase in the T_g to 58 °C. Previous literature on the telechelic ionomers of poly(butylene terephthalate) also

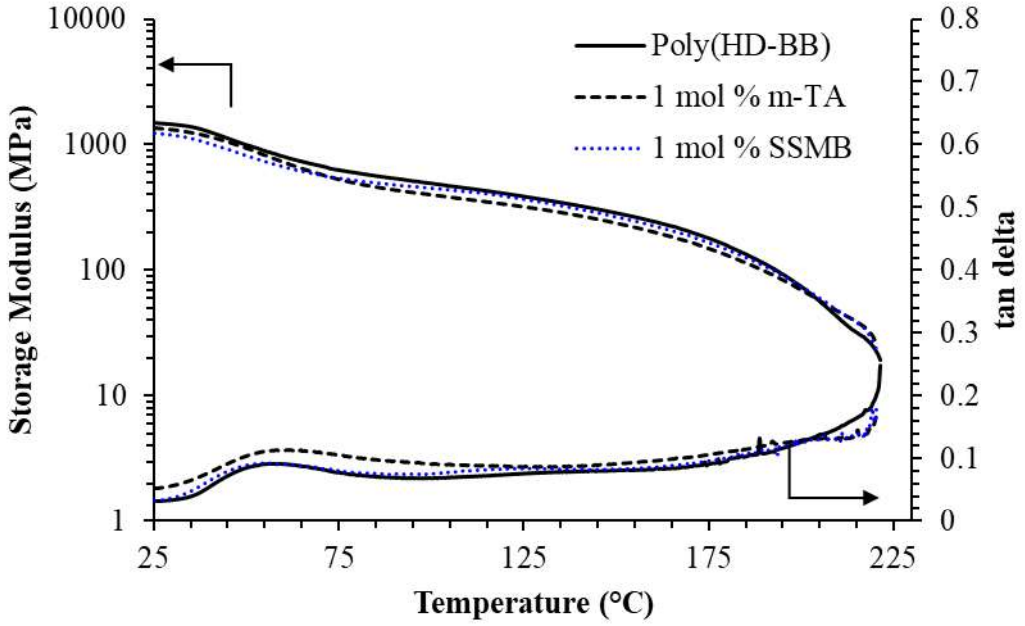

Figure 5.6. Dynamic mechanic analysis of compression molded films of poly(HD-4,4'BB) either alcohol, m-TA, or SSMB terminated.

demonstrated a slight increase in T_g with increase in the ionic concentration associated with the formation of ionic aggregates between the polymer chains. Insignificant differences in the plateau modulus were observed between the three polymers.

5.4.3 Rheological Analysis.

Melt rheology was performed on the two sets of polymers at 275 °C in order to compare the effects of ionic aggregation on the zero-shear viscosity of these polymers. **Figure 5.7** illustrates representative curves from the complex viscosity sweep using 1.25% strain while **Figure 5.8** shows the zero-shear complex viscosity (determined at 0.1 rad/s) as a function of mol % end group**.** The 1 mol % *m*-TA/SSMB samples exhibited equivalent zero-shear viscosity within error of each other. The high concentration of end groups and subsequent low molecular weight for the 10 mol % samples afforded the most drastic difference between the two equivalent polymers. At this concentration, the ionomer achieved a higher melt viscosity relative to the non-ionic polymer resulting from the ionic aggregate present with these telechelic ionomers even at 275 °C. This follows

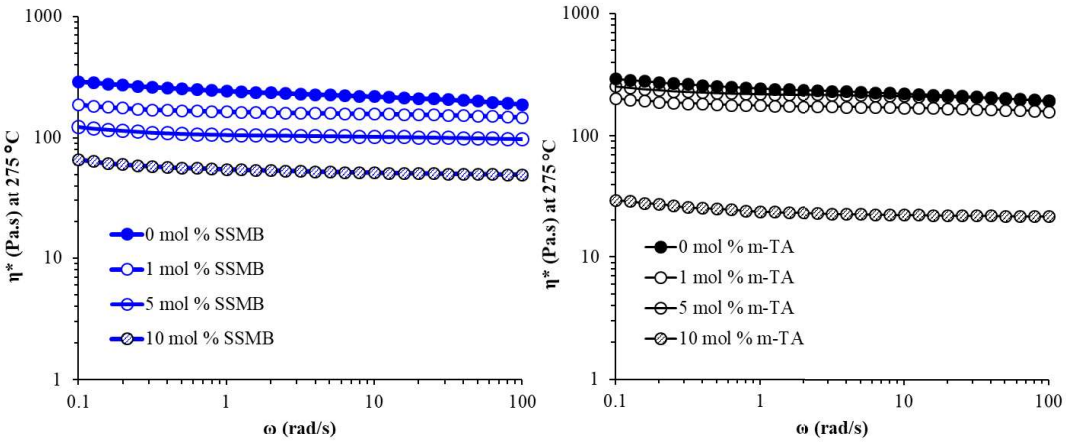

Figure 5.7. Complex viscosity sweep from 0.1-100 rad/s utilizing 1.25% strain of the two series of endcapped polymers.

observations from previous literature on telechelic and non-telechelic ionomers in which the presence of ionic aggregation results in an increase in melt viscosity.[45] While the SSMB series exhibits a systematic decrease in zero-shear viscosity as a function of

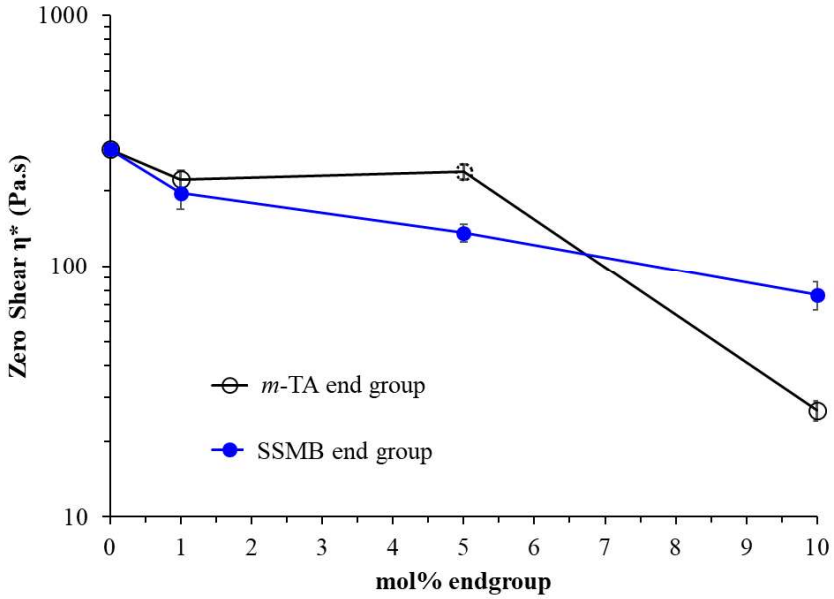

Figure 5.8. Zero-shear viscosity measured at 0.1 rad/s represented as a function of concentration of end groups for the two series of poly(HD-4,4'BB).

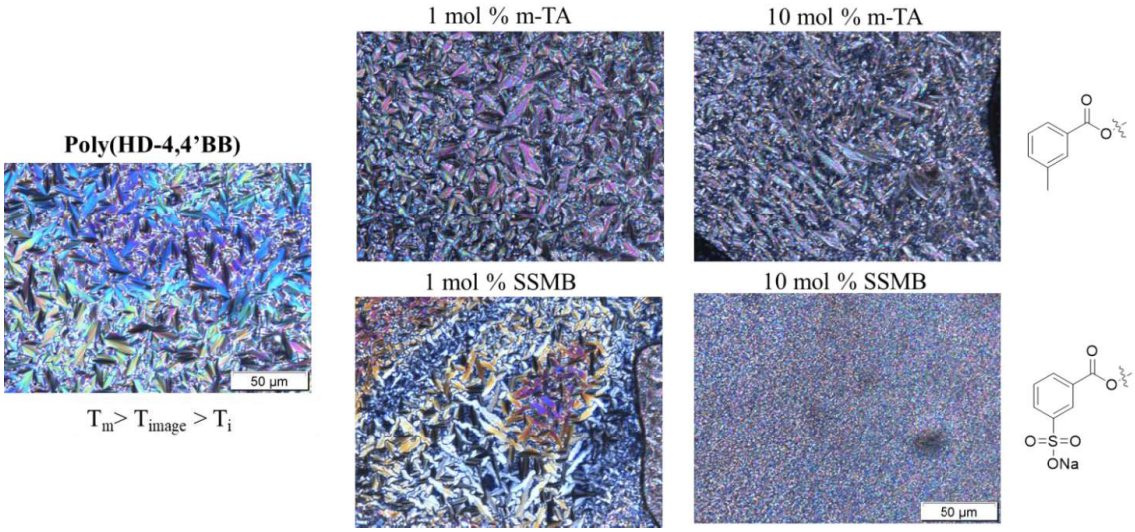

Figure 5.9. Polarized optical microscopy of poly(HD-4,4'BB) synthesized with increasing concentration of ionic or non-ionic end groups.

decreasing molecular weight (increasing mol % end group), *m*-TA exhibited an outlier in the 5 mol % end group sample which revealed a melt viscosity similar to the non-endcapped polymer. Further analysis will need to be performed to confirm whether the 5 mol % *m*-TA sample was a true value or possibly an unsuccessful attachment of the end group during the polymerization resulting in a higher molecular weight polymer.

5.4.4 Morphological Characterization.

Polarized optical microscopy characterized the mesophase morphology of the 0 and 10 mol % end group samples in order to characterize the effect that the ionic and non-ionic end groups (**Figure 5.9**). Cooling non-endcapped poly(HD-BB) from the isotropic state (275 °C) below the T_i resulted in the formation of a birefringent texture. This fan-shaped texture with focal conics correlates with the formation of smectic A morphology arranging into Dupin cyclides enabling the smectic layers to orient perpendicular to the substrate.[46,50] Previous X-Ray scattering analysis further confirmed

this smectic A morphology.[49,51] The addition of 1 mol % *m*-TA or SSMB did not drastically impact the birefringent texture enabling the formation of clear focal conics and fan shapes. Increasing the end group concentration to 10 mol % afford the first significant difference in the textures. The 10 mol % *m*-TA still generated a fan shape texture of similar size to the 0 and 1 mol % *m*-TA samples. In contrast, 10 mol % SSMB resulted in a fine-scale optical texture with no obvious fans. This presumably relates to the ionic aggregates disrupting the packing structure of the smectic A mesophase resulting much smaller domain sizes than for the non-ionic polymer. The fact that the 10 mol % *m*-TA still observes a clear fan-shaped texture indicates that the smaller domain was unassociated with the decreasing molecular weight. Further SAXS and WAXS analysis would be needed to confirm the effect of ionic aggregates on the smectic morphology.

5.5 Conclusions:

Melt transesterification and polycondensation enabled the synthesis of two series of novel telechelic LC polymers with ionic or non-ionic end groups. Poly(HD-BB) comprised the semi-aromatic LC backbone while *m*-TA and SSMB made up the non-ionic and ionic end groups, respectively. The non-ionic comparison replaced the *meta* sulfonate unit with a methyl substituent in order to create a direct analogue to the telechelic ionomer. While TGA exhibited insignificant impact of the end group on the polymer's thermal stability, DSC revealed shifts in the T_m and T_i dependent on end group and molecular weight. Ionic aggregates slowed chain mobility resulting in a slight decrease in both the T_m and T_i. DMA exhibited slight changes in the T_g of the 1 mol % samples associated with lower molecular weights and ionic aggregation. Unfortunately, the higher concentration of the ionic end groups could not overcome the decreased molecular weight to form creasable films. Rheological testing demonstrated higher melt

viscosities for the 10 mol % ionic end group polymer relative to its non-ionic analogue. Finally, morphological analysis using polarized optical microscopy illustrated a significant decrease in the domain size of the LC texture within the mesophase as a result of disruption through the ionic aggregation. Following the applications observed for other telechelic LC ionomers, this novel system could find use as compatibilizers in blends or nanocomposites.

Acknowledgments:

The authors thank Dr. Ryan Mondschein, Dr. Justin Sirrine, and Dr. Ashley Nelson for insightful discussions.

Notes:

The authors declare no competing financial interest

Funding:

This work was sponsored by Solvay.

References:

(1) Donald, A. M.; Windle, A. H.; Hanna, S., *Liquid crystalline polymers*; 2nd ed.; Cambridge University Press: Cambridge, 2006.
(2) Windle, A. H., In *Liquid Crystalline and Mesomorphic Polymers*; Shibaev, V. P., Lam, L., Eds.; Springer New York: New York, NY, 1994, p 26.
(3) Dobb, M. G.; McIntyre, J. E., In *Liquid Crystal Polymers II/III*; Platé, N. A., Ed.; Springer Berlin Heidelberg: Berlin, Heidelberg, 1984, p 61.
(4) Lenz, R. W., In *Recent Advances in Liquid Crystalline Polymers*; Chapoy, L. L., Ed.; Springer Netherlands: Dordrecht, 1985, p 3.
(5) Chung, T., *Thermotropic liquid crystal polymers: thin-film polymerization, characterization, blends, and applications*; Technomic Pub. Co: Lancaster, Pa, 2001.
(6) Blackwell, J.; Biswas, A., In *Developments in Oriented Polymers—2*; Ward, I. M., Ed.; Springer Netherlands: Dordrecht, 1987, p 153.
(7) Bhattarcharya, S. K.; Misra, A., Rheological properties of a liquid crystalline copolyester, *Polymer Engineering & Science* **1990**, *30*, 124.
(8) Romo-Uribe, A.; Windle, A. H., "Log-Rolling" Alignment in Main-Chain Thermotropic Liquid Crystalline Polymer Melts under Shear: An In-Situ WAXS Study, *Macromolecules* **1996**, *29*, 6246.

(9) Tokita, M.; Watanabe, J., Several Interesting Fields Exploited through Understanding of Polymeric Effects on Liquid Crystals of Main-Chain Polyesters, *Polymer Journal* **2006**, *38*, 611.
(10) Watanabe, J.; Hayashi, M., Thermotropic liquid crystals of polyesters having a mesogenic p,p'-bibenzoate unit. 1. Smectic A mesophase properties of polyesters composed of p,p'-bibenzoic acid and alkylene glycols, *Macromolecules* **1988**, *21*, 278.
(11) Watanabe, J.; Hayashi, M., Thermotropic liquid crystals of polyesters having a mesogenic p,p'-bibenzoate unit. 2. X-ray study on smectic mesophase structures of BB-5 and BB-6, *Macromolecules* **1989**, *22*, 4083.
(12) Watanabe, J.; Hayashi, M.; Morita, A.; Tokita, M., Thermotropic Liquid Crystals of Main-Chain Polyesters Having a Mesogenic 4,4'-Biphenyldicarboxylate Unit. 6. Chiral Mesophases of Polyesters with a (S)-2-Methylbutylene Spacer, *Macromolecules* **1995**, *28*, 8073.
(13) Watanabe, J.; Hayashi, M.; Nakata, Y.; Niori, T.; Tokita, M., Smectic liquid crystals in main-chain polymers, *Progress in Polymer Science* **1997**, *22*, 1053.
(14) Xue, Y.; Hara, M., Ionic Naphthalene Thermotropic Copolyesters: Effect of Ionic Content, *Macromolecules* **1997**, *30*, 3803.
(15) Eisenberg, A.; Hird, B.; Moore, R. B., A new multiplet-cluster model for the morphology of random ionomers, *Macromolecules* **1990**, *23*, 4098.
(16) Chisholm, B. J.; Moore, R. B.; Barber, G.; Khouri, F.; Hempstead, A.; Larsen, M.; Olson, E.; Kelley, J.; Balch, G.; Caraher, J., Nanocomposites Derived from Sulfonated Poly(butylene terephthalate), *Macromolecules* **2002**, *35*, 5508.
(17) Kang, H.; Armentrout, R. S.; Wang, J.; Long, T. E., In *Functional Condensation Polymers*; Carraher, C. E., Swift, G. G., Eds.; Springer US: Boston, MA, 2002, p 249.
(18) Lin, Q.; Unal, S.; Fornof, A. R.; Armentrout, R. S.; Long, T. E., Synthesis and characterization of telechelic phosphine oxide polyesters and cobalt(II) chloride complexes, *Polymer* **2006**, *47*, 4085.
(19) Hansen, S. M.; Howell, J. M.; Reese, C. E., Sulfonate-Containing Polyesters Dyeable with Basic Dyes. US005607765A, 1997.
(20) Horn, C. F., Acyloxymetallosulfophthalate containing dyeable polyesters. US 3,185,671, 1965.
(21) Gemeinhardt, G. C.; Moore, A. A.; Moore, R. B., Influence of ionomeric compatibilizers on the morphology and properties of amorphous polyester/polyamide blends, *Polymer Engineering & Science* **2004**, *44*, 1721.
(22) Hu, Y. S.; Prattipati, V.; Mehta, S.; Schiraldi, D. A.; Hiltner, A.; Baer, E., Improving gas barrier of PET by blending with aromatic polyamides, *Polymer* **2005**, *46*, 2685.
(23) Iyer, S.; Schiraldi, D. A., Role of ionic interactions in the compatibility of polyester ionomers with poly(ethylene terephthalate) and nylon 6, *Journal of Polymer Science, Part B: Polymer Physics* **2006**, *44*, 2091.
(24) Ng, C. W. A.; MacKnight, W. J., Ionomeric Blends of Poly(ethyl acrylate-co-4-vinylpyridine) with Metal-Neutralized Sulfonated Poly(ethylene terephthalate). 4. Effects of Counterions, *Macromolecules* **1996**, *29*, 2421.

(25) Özen, İ.; Bozoklu, G.; Dalgıçdir, C.; Yücel, O.; Ünsal, E.; Çakmak, M.; Menceloğlu, Y. Z., Improvement in gas permeability of biaxially stretched PET films blended with high barrier polymers: The role of chemistry and processing conditions, *European Polymer Journal* **2010**, *46*, 226.
(26) Wilbert, G.; Zentel, R., Liquid crystalline main-chain polymers containing the ferrocene unit as a side group, *Macromolecular Chemistry and Physics* **1996**, *197*, 3259.
(27) Hu, J.; Zhang, B.; Feng, Z.; Wang, H.; Zhou, A., Synthesis and characterization of chiral smectic side-chain liquid crystalline polysiloxanes and ionomers containing sulfonic acid groups, *Journal of Applied Polymer Science* **2001**, *80*, 2335.
(28) Tong, B.; Zhang, B.; Hu, J.; Dai, R.; Deng, Y., Synthesis and characterization of side-chain liquid-crystalline ionomers containing quaternary ammonium salt groups, *Journal of Applied Polymer Science* **2003**, *90*, 2879.
(29) Li, Y.; Zhang, B. Y.; Feng, Z.; Zhang, A., Compatibilization of side-chain, thermotropic, liquid-crystalline ionomers to blends of polyamide-1010 and polypropylene, *Journal of Applied Polymer Science* **2002**, *83*, 2749.
(30) Zhang, B.; Guo, S.; Shao, B., Synthesis and characterization of liquid crystalline ionomers with polymethylhydrosiloxane main-chain- and side-chain-containing sulfonic acid groups, *Journal of Applied Polymer Science* **1998**, *68*, 1555.
(31) Zang, B.-L.; Hu, J.-S.; Meng, F.-B.; Zhang, B.-Y., New side-chain liquid-crystalline ionomers. I. Synthesis and characterization of a homopolymer derived from ionic mesogenic groups, *Journal of Applied Polymer Science* **2004**, *93*, 2511.
(32) Jin, H.; Wang, Y., Synthesis and characterization of the novel meta-modified aramid fibers with liquid crystalline properties, *Polymer Composites* **2012**, *33*, 1620.
(33) Lin, Q.; Pasatta, J.; Wang, Z.-H.; Ratta, V.; Wilkes, G. L.; Long, T. E., Synthesis and characterization of sulfonated liquid crystalline polyesters, *Polymer International* **2002**, *51*, 540.
(34) Meng, F.-B.; Zhang, B.-Y.; Xu, Y.; Liu, J.-Y., Main-chain liquid-crystalline ionomers bearing potassium sulfonate groups, *Journal of Applied Polymer Science* **2005**, *96*, 2021.
(35) Sordi, D.; De Ruijter, C.; Orlanducci, S.; Picken, S. J.; Sudhölter, E. J. R.; Terranova, M. L.; de Smet, L. C. P. M.; Dingemans, T. J., Sulfonated liquid crystalline polyesters as resin matrix for single wall carbon nanotube and nanodiamond composites, *Journal of Polymer Science, Part A: Polymer Chemistry* **2011**, *49*, 1079.
(36) Tian, M.; Zhang, B.-Y.; Meng, F.-B.; Zang, B.-L., Main-chain chiral smectic liquid-crystalline ionomers containing sulfonic acid groups, *Journal of Applied Polymer Science* **2006**, *99*, 1254.
(37) Xu, X. Y.; Zhang, B. Y.; Gu, W. M.; Wang, L. X., Synthesis, structure, and mesomorphic properties of main-chain liquid-crystalline ionomers containing sulfonate groups, *Journal of Materials Science* **2009**, *44*, 1787.
(38) Zhang, A.; Zhang, B.; Feng, Z., Compatibilization by main-chain thermotropic liquid crystalline ionomer of blends of PBT/PP, *Journal of Applied Polymer Science* **2002**, *85*, 1110.

(39) Zhang, B.; Weiss, R. A., Liquid crystalline ionomers. II. Main chain liquid crystalline polymers with terminal sulfonate groups, *Journal of Polymer Science, Part A: Polymer Chemistry* **1992**, *30*, 989.
(40) Zhang, B.; Weiss, R. A., Liquid crystalline lonomers. I. Main-chain liquid crystalline polymer containing pendant sulfonate groups, *Journal of Polymer Science, Part A: Polymer Chemistry* **1992**, *30*, 91.
(41) Zhang, N.; Zhang, A.-l.; Liu, Q.-f.; Zhang, M.; Li, Q.; Li, F.-f., Effect of liquid crystal ionomer intercalated montmorillonite nanocomposites on PEO/PLA solid polymer electrolytes, *Ionics* **2018**, *24*, 3805.
(42) Zhi, J.; Zhang, B.; Wu, Y.; Feng, Z., Study on a series of main-chain liquid–crystalline ionomers containing sulfonate groups, *Journal of Applied Polymer Science* **2001**, *81*, 2210.
(43) Zhang, A.-l.; Cao, F.-y.; Na, G.-z.; Wang, S.; Li, S.-x.; Liu, J.-c., A novel PEO-based blends solid polymer electrolytes doping liquid crystalline ionomers, *Ionics* **2016**, *22*, 2103.
(44) Berti, C.; Colonna, M.; Binassi, E.; Fiorini, M.; Karanam, S.; Brunelle, D. J., Telechelic ionomeric poly(butylene terephthalate): Synthesis, characterization and comparison with random ionomers, *Reactive Functional Polymers* **2010**, *70*, 366.
(45) Kang, H.; Lin, Q.; Armentrout, R. S.; Long, T. E., Synthesis and Characterization of Telechelic Poly(ethylene terephthalate) Sodiosulfonate Ionomers, *Macromolecules* **2002**, *35*, 8738.
(46) Heifferon, K. V.; Mondschein, R. J.; Talley, S. J.; Moore, R. B.; Turner, S. R.; Long, T. E., Tailoring the glassy mesophase range of thermotropic polyesters through copolymerization of 4,4'-bibenzoate and kinked isomer, *Polymer* **2019**, *163*, 125.
(47) Nelson, A. M.; Fahs, G. B.; Moore, R. B.; Long, T. E., High-Performance Segmented Liquid Crystalline Copolyesters, *Macromolecular Chemistry and Physics* **2015**, n/a.
(48) Chen, X.; Hou, G.; Chen, Y.; Yang, K.; Dong, Y.; Zhou, H., Effect of molecular weight on crystallization, melting behavior and morphology of poly(trimethylene terephalate), *Polymer Testing* **2007**, *26*, 144.
(49) Tsai, H.-B.; Lee, D.-K.; Chen, H.-W.; Chang, J.-Y.; Liu, J.-L.; Chang, C.-H.; Du, I.-C.; Lei, S.-Y.; You, J.-W., Effect of molecular weight on two smectic polyesters, *Journal of Polymer Research* **1996**, *3*, 59.
(50) Dierking, I., In *Textures of Liquid Crystals*; Wiley-VCH Verlag GmbH & Co. KGaA: 2004, p 91.
(51) Tokita, M.; Takahashi, T.; Hayashi, M.; Inomata, K.; Watanabe, J., Thermotropic Liquid Crystals of Polyesters Having a Mesogenic p,p'-Bibenzoate Unit. 7. Chain Folding in the Smectic Phase of BB-6, *Macromolecules* **1996**, *29*, 1345.

Supporting Information:

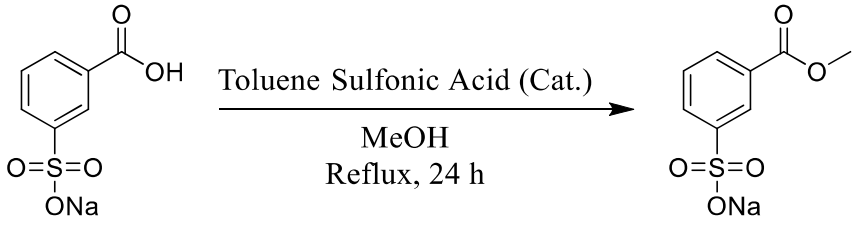

Scheme S5.1. Esterification of sodium sulfobenozoic acid to form sodium 3-sulfomethylbenzoate for improved solubility in melt-polycondensation polymerization of poly(HD-4,4'BB).

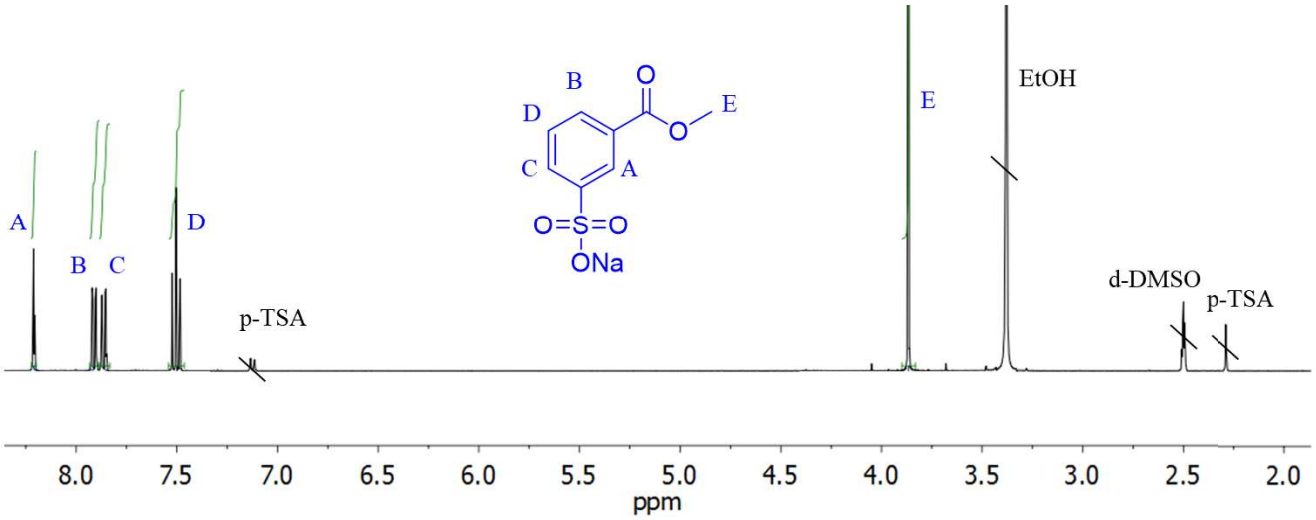

Figure S5.1. ^{1}H NMR spectroscopy of sodium 3-sulfomethylbenzoate confirming the successful esterification.

Chapter 6: Synthesis and characterization of a nematic fully aromatic polyester based on biphenyl 3,4'-dicarboxylic acid

(Manuscript submitted for publication)

Katherine V. Heifferon[1], Glenn A. Spiering[1], Samantha J. Talley[1], Maruti Hegde[1,2], Robert B. Moore[1], S. Richard Turner[1], and Timothy E. Long[1]

[a]*Macromolecules Innovation Institute, Department of Chemistry, Virginia Tech, Blacksburg, VA 24061*
[b]*Department of Applied Physical Sciences, University of North Carolina, Chapel Hill, NC, 27599-3050*

Keywords: polyester, liquid crystalline, melt polymerization, bibenzoate

6.1 Abstract:

Melt acidolysis polymerization of hydroquinone with a kinked monomer, biphenyl 3,4'-bibenzoate, afforded the synthesis of a novel liquid crystalline polymer (LCP), poly(*p*-phenylene 3,4'-bibenzoate) (poly(HQ-3,4'BB)). Selection of hydroquinone diacetate (HQ_a) or hydroquinone dipivilate (HQ_p) facilitated either a tan or white final polymer, respectively. ^{1}H NMR spectroscopy confirmed consistent polymer backbone structure for polymers synthesized with either derivative of hydroquinone. Poly(HQ-3,4'BB) exhibited an onset of weight loss at about 480 °C, similar to commercially available Vectra® LCP. Differential scanning calorimetry (DSC) and dynamic mechanical analysis (DMA) revealed a glass transition temperature (T_g) of 190 °C and an isotropic temperature (T_i) near 330 °C. The observation of a melting temperature (T_m) depended upon the thermal history of the polymer. Wide-angle X-ray scattering (WAXS) and polarized optical microscopy (POM) confirmed the formation of a nematic glass morphology after quench-cooling from the isotropic state. Subsequent annealing at 280 °C or mechanical deformation induced crystallization of the polymer. Rheological studies demonstrated similar shear thinning behavior for poly(HQ-3,4'BB)

and Vectra® RD501 in the power law region at 340 °C. Zero-shear viscosity measurements indicated that HQ_a afforded higher melt viscosities after identical polymerization conditions relative to HQ_p, suggesting higher molecular weights.

6.2 Introduction:

Thermotropic liquid crystalline polyesters (LCPs) represent a unique field of high-performance polymers with properties that enable electronic and automotive parts, high strength fibers, and stainless-steel replacements in the medical industry. These applications demand a complement of high thermal stability, dielectric strength, and chemical resistance.[1-4] Thermotropic LCPs exhibit anisotropic ordering when heated above the melting temperature, transitioning the morphology into a LC phase. This LC phase exhibits various degrees of translational and orientational order that reside between 3D crystallinity and a completely amorphous melt (isotropic).[4,5] The LC mesophase facilitates enhanced levels of chain orientation during fiber formation, as well as drastic viscosity reductions under shear.[6] As a result of these beneficial properties, melt processing and polymerization often occurs in the presence of a LC phase, between the melting temperature (T_m) and the isotropic temperature (T_i), commonly referred to as the mesogenic window.

Small molecule liquid crystals, originally discovered by an Austrian botanist in 1888, often comprise rod- or disk-like shapes synthesized from aromatic rigid structures with an aspect ratio (length/diameter ratio) of ~ 6.[5,7] In 1956, Flory hypothesized that incorporation of these small molecules into a polymer could impart LC properties to polymers.[8] The incorporation of the LC monomer typically occurs through polymerization into the backbone (main-chain) or incorporation as a pendant unit (side-chain).[5] Polyesters primarily utilize main-chain structures, and early patents in this field

focus on acidolysis polymerization to synthesize polymers with fully aromatic backbones (polyarylates), such as the commercially available polymer Vectra®.[9-11] Homopolymers of these rigid linear molecules, such as poly(*p*-phenylene terephthalate) or poly(*p*-hydroxybenzoic acid), resulted in very high melting temperatures (> 600 °C), rendering them improcessable with the exception of forging techniques.[12-14] Efforts to reduce T_m and improve processability focused on random copolymerization to disrupt translational symmetry. The focus on symmetrical aromatic comonomers (*para*: 180° bond angle) afforded the reduction in T_m while maintaining a stable LC phase, broadening the mesogenic window. In contrast, asymmetric or "kinked" aromatic comonomers (*meta*: 120° bond angle), although effectively reduce the T_m, often result in destabilization of the LC phase, which was attributed to disruption of chain linearity.[4,13,15] The linearity of the polymer plays an important role in the stability of the LC phase as a reduction of linearity results in decreasing the polymer aspect ratio (persistence length/diameter ratio), which needs to exhibit a value of > 6 to achieve a LC phase. As a result, homopolymers such as poly(*p*-phenylene isophthalate) or poly(*m*-hydroxybenzoic acid) do not exhibit LC properties despite their rigidity due to loss of rectilinearity.[4,13,16] Although exchanging an aromatic unit in the backbone with a flexible aliphatic spacer also reduces T_m, the thermal stability of polymer is compromised, as demonstrated in the earlier literature.[17-19]

In this manuscript, we describe the synthesis and characterization of a novel kinked polymer, poly (*p*-phenylene 3,4' bibenzoate) (poly(HQ-3,4'BB)). This wholly aromatic homopolymer is derived from biphenyl 3,4'-dicarboxylic acid (3,4'BB), which is the regioisomer of the common mesogenic monomer biphenyl 4,4'-dicarboxylic acid. Previous copolymerization of 4,4'BB based semi-aromatic polymers with 3,4'BB

afforded a range of polymer morphologies from LC to amorphous with a trend of reduced melting temperatures upon increased incorporation of 3,4'BB.[19] In contrast to previous kinked homopolymers such isophthalates, the biphenyl unit of 3,4'BB forms a longer kinked structure, which facilitates formation a nematic mesophase and limits polymer crystallization. This manuscript describes the first instance, to the best of our knowledge, of a fully aromatic homopolyester without pendant substituents that achieves LC behavior over an accessible temperature window for melt processing.

6.3 Experimental:

6.3.1 Materials.

Dimethyl 3,4'-biphenyldicarboxylate (dimethyl 3,4'-bibenzoate: 3,4'BB), Vectra® A950, and Vectra® RD501 samples were generously provided by ExxonMobil and used as received. Hydroquinone (HQ) (Sigma-Aldrich, ≥ 99%) and hydroquinone diacetate (HQ_{dac}) (Sigma-Aldrich, 98%) were recrystallized from ethanol (EtOH) (Decon Labs, 200 proof). Pivalic anhydride, also known as trimethylacetic anhydride, (Acros Organics, 99%), chloroform-*d* (*$CDCl_3$*) (Cambridge Isotope Laboratories, 99.8% atom D), trifluoroacetic acid-*d* (*d*-TFA) (Sigma-Aldrich, 99.5% atom D), dimethyl sulfoxide-*d_6* (*DMSO-d_6*) (Cambridge Isotope Laboratories, 99.9% atom D), tetrahydrofuran (THF) (Fisher Chemical), and sodium hydroxide (NaOH) (Fisher Chemical) were used as received.

6.3.2 Analytical Methods.

A Varian Unity 400 at 400 MHz (23 °C) generated the ^1H and ^{13}C nuclear magnetic resonance (NMR) spectra of the monomers, in $CDCl_3$ and DMSO-*d_6,* and the polymer required *d*-TFA. A TA Instruments Q50 thermogravimetric analyzer (TGA),

under constant N_2 flow, afforded the weight loss profile of the polymers during a ramp from 25 to 600 °C with a rate of 10 °C/min. A heat/cool/heat cycle using a rate of 10 °C/min, 100 °C/min, and 10 °C/min, respectively, on a TA Instruments Q1000 differential scanning calorimeter (DSC) with a 50 mL/min nitrogen flow, revealed the thermal transitions for the polymer. Indium (T_m = 156.60 °C) and zinc (T_m = 419.47 °C) standards calibrated the instrument prior to analysis. Data analysis occurred on the second heat cycles using the inflection point of the T_g and the maximum of the T_i and T_m. Compression molding of the polymers utilized a sandwich of aluminum plates, Kapton® sheets coated with a Rexco Partall® Power Glossy Liquid mold release agent, and 400 μm thick stainless-steel shims between which the samples were placed. Heating above the T_i of the polymer at 340 °C generated films upon molding and an immediate quench in an ice bath quickly cooled the sample. Dynamic mechanical analysis (DMA) utilized an oscillatory amplitude of 15 μm, a frequency of 1 Hz, and a static force of 0.01 N while in tension mode. The TA Instruments Q800 DMA used a heating rate of 3 °C/min until reaching 300 °C, and subsequently the sample was rapidly cooled to room temperature prior to restarting the run. Analysis of the DMA measurement occurred on the second heat and maximum of the tan delta afforded the T_g of the polymers.

Wide-angle X-ray scattering (WAXS) experiments were performed using a Rigaku S-Max 3000 3 pinhole SAXS system, equipped with a rotating anode emitting X-rays with a wavelength of 0.154 nm (Cu Kα). The sample-to-detector distance was 110 mm and the q-range was calibrated using a silver behenate standard. Two-dimensional diffraction patterns were obtained using an image plate with an exposure time of 1 h. WAXS data were analyzed using the SAXSGUI software package to obtain radially

integrated WAXS intensity versus the scattering vector, 2θ, where $q=(4\pi/\lambda)\sin(\theta)$, θ is one half of the scattering angle and λ is the wavelength of X-ray. Polarized optical microscopy (POM) was performed by placing the samples between crossed polarizers of a Nikon LV100 Eclipse optical microscope equipped with a Linkham TMS 94 hot stage and a Nikon DXM1200 digital camera. Samples were pressed between glass slides after heating past the T_i and cooled at an approximate rate of either 10 °C/min or 75 °C/min. Melt rheology was performed on a TA instruments DHR-2 rheometer at 340 °C using a 1.25% strain with an 8 mm disposable parallel-plate geometry under N_2 flow. A hole punch generated circular disks of the sample from a compression molded film, which were stacked 8 tall on the bottom geometry. The sample was heated to 340 °C then compressed together by lowering the top geometry into place. The linear viscoelastic region was determined prior to each frequency sweep using a strain sweep from 0.01 to 10% oscillatory strain at 1 rad/s in order to guarantee melding of the films. Frequency sweeps ranging from 1 to 100 rad/s afforded complex viscosity values and standard deviations from a minimum of three runs. Sample nomenclature comprises poly(HQ_a-3,4'BB) or poly(HQ_p-3,4'BB) where **a** and **p** refer to the use of acetylated or pivilated hydroquinone, respectively. The added identifier poly(HQ-3,4'BB): **X** min vac refers to the length of time of the vacuum stage during the polymers (X = 1, 30, or 60 min).

6.3.3 Synthesis of biphenyl 3,4'-dicarboxylic acid.

Dimethyl-3,4' bibenzoate (3,4'BB) (39.94 g, 0.148 mol) refluxed for 24 h in 400 mL of a 1M sodium hydroxide solution of 1:1 DI water:THF based on previous literature (**Scheme S6.1**).[20] Filtration removed unreacted 3,4'BB, subsequent rotary evaporation removed the remaining THF. The final product, 3,4'BB-COOH, precipitated from the

remaining aqueous solution upon the addition of concentrated HCl. Filtration and rinsing with distilled water neutralized the product, which was dried *in vacuo* at 120 °C overnight to remove residual water, resulting in a fine white powder (34.69 g, 97% yield).

^{1}H NMR (400 MHz, DMSO-d_6): δ 13.12 (s, 2H), 8.24 (s, 1H), 8.05(d, 2H), 7.99 (d, 2H), 7.84 (d, 2H), and 7.64 (t, 1H) ppm.

^{13}C NMR (400 MHz, DMSO-d_6): δ 167.51, 143.73, 139.78, 132.03, 131.73, 130.51, 129.90, 129.44, 127.96, and 127.36 ppm.

Melting Point (DSC): 103 °C

6.3.4 Synthesis of hydroquinone dipivilate.

Hydroquinone (5.1g, 0.046 mol) and pivalic anhydride (20 mL, 0.135 mol) were weighed into a dry 100-mL, round-bottomed, flask equipped with a t-neck adaptor, distillation tube, a round-bottomed collection flask, glass stir-rod adaptor, mechanical stir-rod, and an overhead mechanical stirrer. Evacuation and back-filling of the reaction vessel occurred three times with N_2 and a vacuum pump to ensure an inert atmosphere. Heating the reaction at 170 °C under constant N_2 flow removed the pivalic acid condensate into a distillation flask (**Scheme S6.2)**. According to thin layer chromatography, the reaction achieved full conversion after 1 h, which prompted cooling to room temperature. The product crystallized from the resulting solution upon cooling, and filtration from the remaining pivalic anhydride and further washes with EtOH facilitated purification. A white crystalline solid resulted after drying the resulting product, hydroquinone dipivilate (HQ_{dpv}), *in vacuo* overnight at 100 °C.

^{1}H NMR (400 MHz, $CDCl_3$): δ 7.04 (s, 4H) and 1.33 (s, 18H) ppm.

^{13}C NMR (400 MHz, $CDCl_3$): δ 176.91, 148.29, 122.20, 39.04, and 27.09 ppm

Melting Point (DSC): 104 °C

6.3.5 Synthesis of poly(*p*-phenylene 3,4'-bibenzoate).

Acidolysis polymerization afforded a liquid crystalline, fully aromatic, polymer as illustrated in **Scheme 6.1**.[10,11,21] 3,4'BB-COOH (6.237 g, 0.026 mol) and either HQ_a (5 g, 0.026 mol) or HQ_p (7.167 g, 0.026 mol) were weighed into an oven dried, 100-mL, round-bottomed flask. The reactor comprised a t-neck adaptor, distillation tube with a 100-mL round-bottomed collection flask, glass stir-rod adaptor, mechanical stir-rod, and an overhead mechanical stirrer. Evacuation and back-filling of the reaction set-up with vacuum and N_2 three-times ensured an inert atmosphere. Heating the reaction from 300 to 360 °C under N_2 flow for 1.5 h afforded a homogenous clear melt. Finally, application of reduced pressure (0.15 mmHg) for 0.5 h at 360 °C produced a highly viscous tan or white polymer, as illustrated in **Figure 6.1**, which was utilized without further purification.

For the polymerization studies, three equivalent reactions using HQ_a and HQ_p separately (6 total) were stopped after different lengths of time under vacuum during the

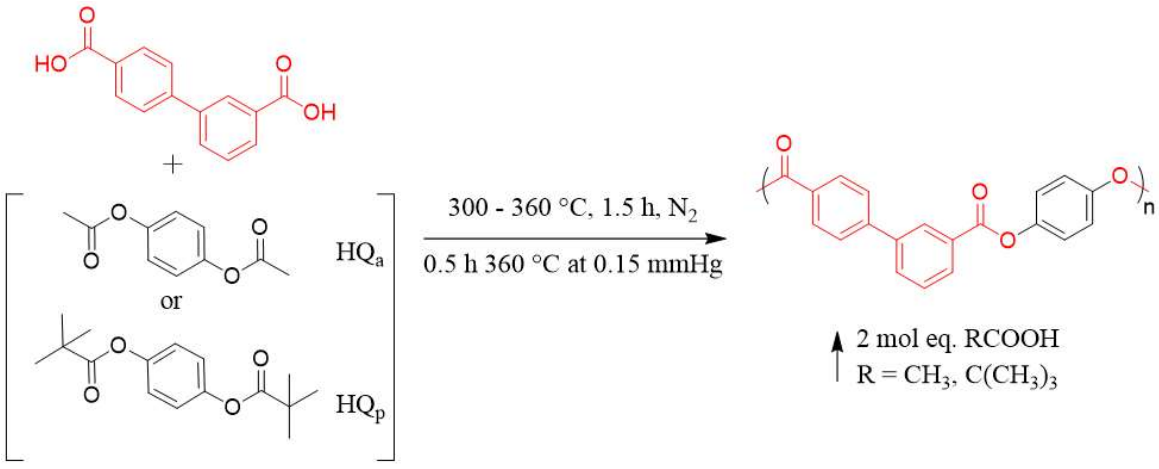

Scheme 6.1. Synthesis of poly(hydroquinone-3,4'-bibenzoate) through acidolysis polycondensation utilizing either hydroquinone diacetate (poly(HQ_a-3,4'BB)) or hydroquinone dipivilate (poly(HQ_p-3,4'BB)).

final stage of the reaction (1 min, 30 min, or 60 min). Rheological properties of the resulting polymers were measured without further purification.

6.4 Results and Discussion:

6.4.1 Synthesis and Structural Characterization.

Scheme 6.1 illustrates the polymerization of poly(*p*-phenylene 3,4' bibenzoate) (poly(HQ-3,4'BB) utilizing an acidolysis strategy. Hydrolysis of dimethyl 3,4'-bibenzoate generated the diacid derivative using procedures from Stock et al. earlier, to enable the acidolysis polymerization.[20] ^{1}H and ^{13}C NMR spectroscopy confirmed the structure of this monomer after purification. For the second monomer, this work investigated the two derivatives of hydroquinone: hydroquinone diacetate (HQ_a) and hydroquinone dipivilate (HQ_p). Early patents and publications, which described fully aromatic LCPs, demonstrated success through the *in-situ* generation of these hydroquinone derivatives during the polymerization. This synthesis progressed through a one-pot reaction of the diacid, diphenol, and acetic/pivalic anhydride.[9-11,22] While this synthetic pathway represents a more commercially viable polymerization method to generate LCPs, pre-acetylated/pivilated hydroquinone enabled consistent polymerization conditions throughout all reactions studied. This strategy guaranteed accurate

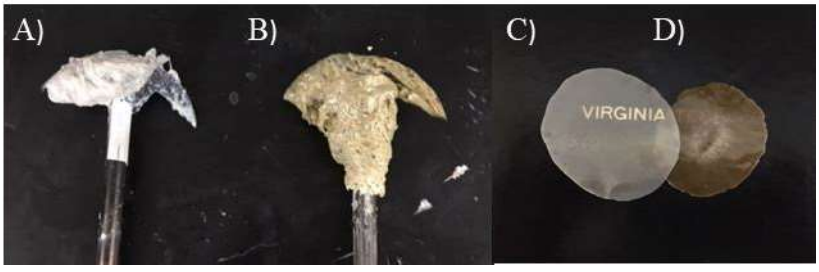

Figure 6.1. Poly(hydroquinone-3,4'-bibenzoate) before (A/B) and after (C/D) compression molding utilizing hydroquinone dipivilate (A/C) or hydroquinone diacetate (B/D).

stoichiometries of acetylated/pivilated phenolic monomers at the onset of the polymerization and ensured identical reaction times and temperatures for all polymerizations.[7,21,23]

Recrystallization of the commercially available hydroquinone diacetate from EtOH afforded a pure starting material. Synthesis of hydroquinone dipivilate occurred in a solvent-free reaction between HQ and pivalic anhydride, similar to *in-situ* polymerization conditions. The synthetic method utilized 3 eq. excess pivalic anhydride, which generated pivalic acid upon reaction with hydroquinone at 170 °C. The high temperature and nitrogen flow facilitated removal of the by-product, driving the reaction toward completion. Upon cooling, HQ_p recrystallized from the remaining pivalic anhydride and afforded a pure product after rinsing with EtOH. ^{1}H and ^{13}C NMR spectroscopy confirmed the structure and purity of the monomer prior to polymerization.

Acidolysis polymerization generated poly(HQ-3,4'BB) using a high temperature heating ramp from 300 to 360 °C, and the monomers maintained a transparent homogenous melt. During the final step of the reaction, the application of vacuum drove the reaction to high conversion and achieved a high viscosity polymer melt, which wrapped the metal stir-rod. Due to the high viscosity of the final polymer, as well as the subsequent removal of a large amount of condensate (acetic acid or pivalic acid), the application of vacuum resulted in foaming, which is common for these polymerizations.[24] ^{1}H NMR spectroscopy in a 1:1 mixture of $CDCl_3$:d-TFA (**Figure S6.4**) confirmed the structure of poly(HQ_a-3,4'BB) and poly(HQ_p-3,4'BB), verifying insignificant backbone differences between the polymers due to the different condensate. The two polymers exhibited very limited solubility in standard solvents, such as THF and $CHCl_3$, preventing

the use of size exclusion chromatography to determine molecular weights. However, ductile films through compression molding suggested the formation of polymers above the molecular weight of entanglement.[25-28]

Hall et al. previously studied ketene formation in the model compounds *p-tert*-butyl phenyl acetate and *p-tert*-butyl phenyl pivilate. This study linked ketene production with color-forming side-reactions, which result in the persistent tan color observed in most fully aromatic LCPs synthesized through high temperature acidolysis.[29] Hall also found that the lack of an α-hydrogen on the pivilate compound prevented ketene formation at high temperatures, therefore reducing color formation with respect to the acetate.[29] Comparison of HQ_a and HQ_p in the polymerization of poly(HQ-3,4'BB) corroborated this earlier study, resulting in a considerably less colored polymer from the pivilated monomer, as illustrated in **Figure 6.1.** These side reactions, which cause color

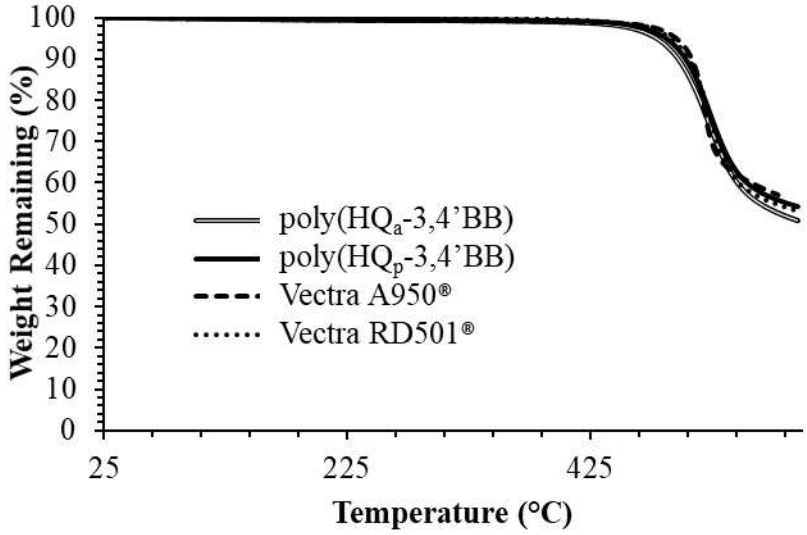

Figure 6.2. Thermogravimetric analysis of poly(HQ_a-3,4'BB), poly(HQ_p-3,4'BB), and two unfilled Vectra® industrial standards.

formation, occur at concentrations below the detection limit of NMR spectroscopy and therefore were not analyzed through this method.

6.4.2 Thermal Characterization.

Thermogravimetric analysis characterized the thermal stability of the polymer as a function of temperature, as illustrated in **Figure 6.2.** Poly(HQ_a-3,4'BB) and poly(HQ_p-3,4'BB) exhibited one-step weight loss profiles with overlapping $T_{d,5\%}$ values of 480 and 487 °C, respectively. These polymers exhibit nearly identical weight-loss profiles to the two unfilled industrial standards, Vectra® A950 and Vectra® RD501. Vectra® A950's structure consists of a comonomer composition of 6-hydroxy-2-naphthoic acid (HNA) and para-hydroxybenzoic acid (*p*-HBA). Vectra® RD501 consists of four different monomeric units (HNA, *p*-HBA, terephthalic acid (TA), and HQ).[30-32] The Vectra® and poly(HQ-3,4'BB) samples exhibited an insignificant difference between their char yield or the $T_{d,5\%}$ due to the similar bond stability in these backbone structures.

Differential scanning calorimetry revealed the thermal transitions for these four polymers, as illustrated in **Figure 6.3A** and **Table 6.1**. The DSC of Vectra® A950 and

Table 6.1. Thermal characterization of poly(HQ_a-3,4'BB), poly(HQ_p-3,4'BB), and two Vectra® standards utilizing TGA and DSC.

Sample	$T_{d,5\%}$ (°C)	Char yield (%)	T_g (°C)	ΔC_p (W/g)	T_m (°C)	ΔH_m (J/g)	T_i (°C)	ΔH_i (J/g)
Poly(HQ_a-3,4'BB)	480	51	191	0.05	320[a]	N/A	332	26.7
Poly(HQ_p-3,4'BB)	487	54	188	0.05	315[a]	N/A	324	20.4
Vectra A950	496	57	93[b]	0.03[b]	280	1.63	> 500[b]	N/A
Vectra RD501	491	53	112[b]	N/A	220	1.82	> 500[b]	N/A

[a] Only observed after slow cool at 10 °C/min
[b] Value determined from reference materials
N/A indicates unable to measure value accurately

Vectra® RD501 revealed an endothermic transition at 280 and 220 °C, respectively, with ΔH_m of 1.63 and 1.82 J/g. These transitions correspond to the T_m of these polymers as the polymer transitions from a semi-crystalline to a nematic morphology. The T_i was not observed for these polymers as it resides above the degradation temperature, resulting in processing and polymerization occurring in the desirable nematic state.[33] DSC did not reveal T_g's for these two standards, but references identify these values as 93 and 112 °C, respectively.[32] In sharp contrast to the Vectra® samples, both poly(HQ_a-3,4'BB) and poly(HQ_p-3,4'BB) exhibited obvious T_g's at 191 °C and 188 °C, respectively, which was within error of each other with a ΔC_p of 0.05 W/g. The more obvious T_g possibly correlates with a higher amorphous content in the novel polymer due to the kinked structure relative to the more linear structure of Vectra®.[34]

Both poly(HQ_a-3,4'BB) and poly(HQ_p-3,4'BB) also revealed one large endothermic transition respectively at 332 and 324 °C during the heat cycle following a quench-cool (100 °C/min from 360 °C) in the DSC, as illustrated in **Figure 6.3A**. In

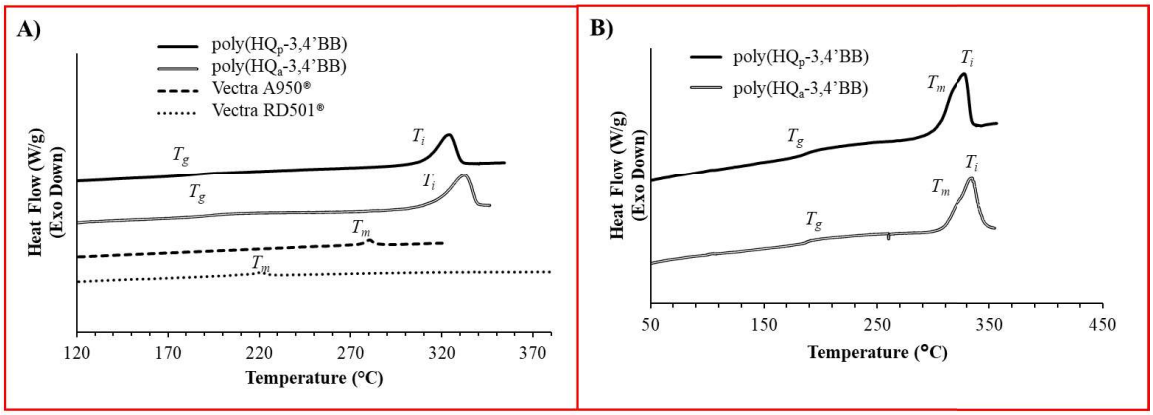

Figure 6.3. Second heating traces in DSC after A) quench cool or B) slow cool for poly(HQ_a-3,4'BB) and poly(HQ_p-3,4'BB).

contrast to the Vectra® samples, this transition represented the T_i (LC to isotropic transition) with a larger ΔH_i of 26.7 and 20.4 J/g, respectively. In contrast, processing the polymer through a slow cool (10 °C/min) from 360 °C facilitated the formation of a shoulder on the T_i at 315 °C and 320 °C, respectively, during the following heat cycle (**Figure 6.3B**). This new transition presumably represents the T_m of this LC polymer. This overlap of the peaks inhibited accurate measurement of the enthalpy values for this transition. The inability to observe the T_m under quench-cooling suggests that this system forms a LC glass, which hinders the formation of 3D crystalline packing structure while maintaining a LC mesophase below the T_g. This would significantly broaden the mesogenic window of the polymer. Polarized optical microscopy and WAXS further probed the morphological changes to determine LC phase and crystallization properties.

6.4.3 Morphological Characterization.

Polarized optical microscopy facilitated the initial characterization of the morphology of poly(HQ-3,4'BB). The lowest viscosity sample from the molecular weight study, poly(HQ_p-3,4'BB): 1 min vac, enabled significant flow between the glass slides forming a thin section. This allowed the formation of a clear image of the LC phase. Heating the polymer above the endothermic transition to 350 °C formed an isotropic melt without birefringence. Cooling the sample at a rate of 10 °C/min facilitated the transition into a birefringent texture at 320 °C, observed in **Figure 6.4A-2.** Cooling to 175 °C, below the T_g, maintained the same texture**.** Optical comparison of this texture to previous literature of other LCPs classifies the birefringence as a schlieren texture, common for nematic LC's.[35,36] The images in **Figure 6.4B** represent a quench-cooled sample using a rate of 75 °C/min from isotropic (350 °C) to 200 °C. The study revealed

that the polymer possessed birefringence after quenching without an easily identifiable texture. This confirms that quenching the sample does not eliminate LC phase resulting possibly in a LC glass. Slow cooling the sample from 350 °C to 280 °C, in **Figure 6.4C**, and subsequently holding for 10 min did not promote significant texture change as is often observed during crystallization.[4,37] While this is contradictory to the DSC results, it was presumed that at a low % crystallinity, a change in texture may not be observed. Attempts to analyze higher molecular weight samples enabled the observation of

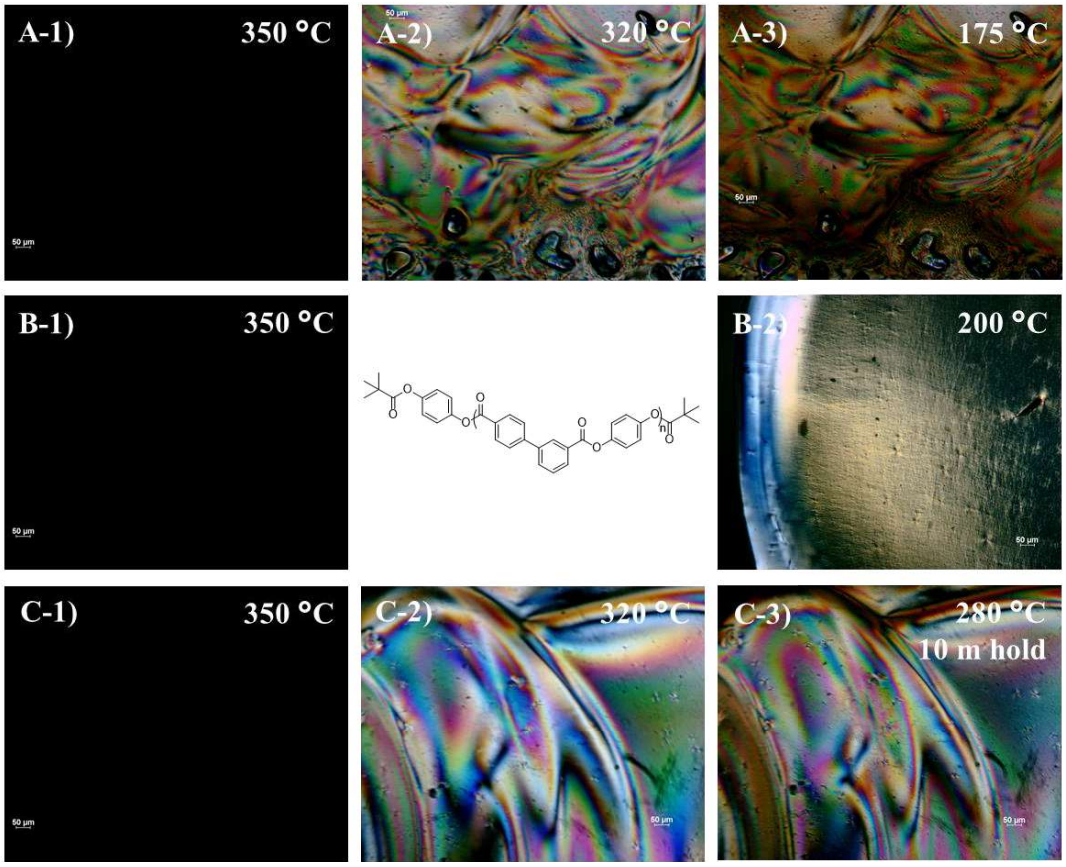

Figure 6.4. Polarized optical microscopy of poly(HQ_p-3,4'BB) reveals birefringence with schlieren texture under different thermal treatments. A) Cooling at 10 °C/min from isotropic B) Cooling at 75 °C/min from isotropic C) Cooling at 10 °C/min from 350-280 °C then isotherm for 10 m.

birefringence below the T_i, but the high viscosity resulted in samples too thick for obvious LC textures (**Figure S6.5**). Even so, these samples did not demonstrate an obvious difference in texture between poly(HQ_a-3,4'BB) and poly(HQ_p-3,4'BB).

Performing WAXS on a compression molded film of poly(HQ_p-3,4'BB) after different thermal treatments verified the polarized optical microscopy. Rapidly cooling the initial compression molded film from the isotropic state (340 °C) in an ice bath provided a quench-cooled sample for analysis. The single diffuse scattering peak (**Figure 6.5 and 6.6**) indicates the absence of a 2D layer structure that often forms lamellar morphologies prevalent in smectic mesophases; the data also confirms the absence of the packing structure of crystalline domains.[38-40] The few minor peaks occurring in the quenched film may indicate insufficient quenching of the thick film in comparison to the much thinner polarized optical microscopy sample. Upon heating the polymer film for 5 min at 280 °C, sharp angular reflections emerged at 5.2, 6.1, 13.1, 14.2, 18.6, 19.6, 24.6,

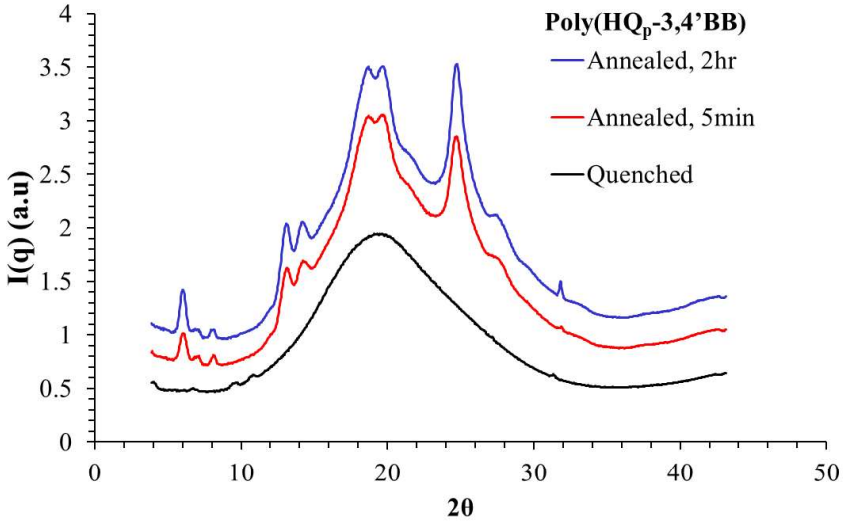

Figure 6.5. WAXS integration analysis of poly(HQ_p-3,4'BB) after different thermal history. Curves vertically shifted for clarity.

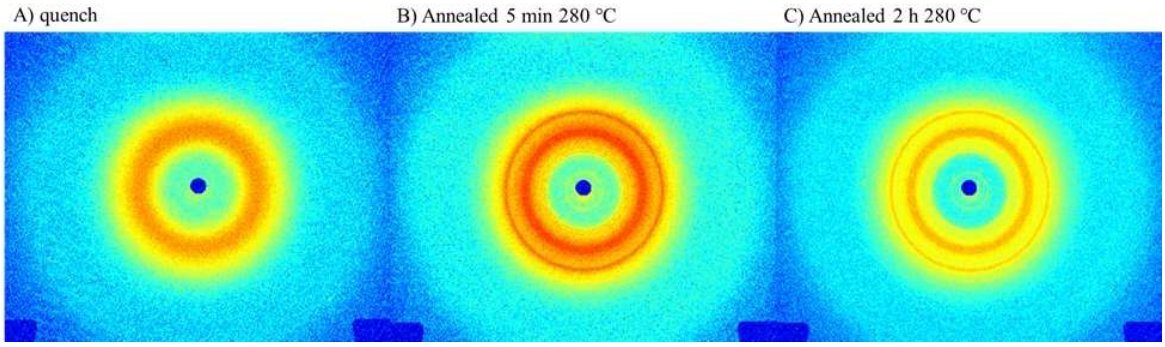

Figure 6.6. 2D WAXS profiles of poly(HQ_p-3,4'BB) after different thermal history. A) quench cooled from isotropic B) quenched film annealed for 5 m at 280 °C C) quenched film annealed for 2 h at 280 °C.

and 31.7° 2θ indicative of a semi-crystalline morphology forming in the polymer film corroborating the secondary shoulder observed in the DSC analysis. These sharp reflections increased slightly in intensity after longer annealing times (2 h at 280 °C). This limited crystallinity may have hindered the observation of a textural change in the optical microscopy after 10 min of annealing. Attempts to orient the quench-cooled sample below the T_i (310 °C) resulted in strain-induced crystallization rather than orientation (**Figure S6.6**). While the crystallization during orientation limits the ability to confirm the mesophase morphology for the polymer, the observation of a schlieren texture using polarized optical microscopy highly suggests a nematic morphology.

From the overall morphological characterization, poly(HQ_p-3,4'BB) appears to form a nematic LC mesophase below the main endothermic transition, identified as the T_i. Processing the material through a quench-cool, imparts a LC glass morphology in which the LC mesophase exists below the T_g of the material without the presence of crystalline domains. Confirmation of the LC glass was achieved with the observation of a birefringent texture after a quench cool. Polarized optical microscopy coupled with room temperature diffraction patterns (**Figure 6.5 and 6.6A**), consisting of a single diffuse

scattering peak centered about 20° 2θ, is typically indicative of an amorphous polymer. Both thermal treatments (annealing and slow cooling) and mechanical deformation promote crystallization of the polymer films. This crystallization results in a second endothermic transition, near the T_i, resulting in the commonly shown multipeak DSC curve for LC polymers. This crystallization remains consistent with other kinked non-LC fully aromatic polyesters, such as poly(*m*-HBA) and poly(IA-HQ), which exhibit semi-crystalline morphologies.[15] In contrast to these earlier examples, to the best of our knowledge this represents the first fully-aromatic polyester homopolymer that exhibits a stable LC mesophase without requiring copolymerization or pendant substituents from the backbone to achieve melt processability. The difference between these polymers lies in the longer kink structure of the biphenyl monomer which may increase the persistence length of the polymer fostering an aspect ratio within the required range for liquid crystallinity (>6).[8,41] However, future work is necessary to confirm this hypothesis.

6.4.4 Thermomechanical Characterization.

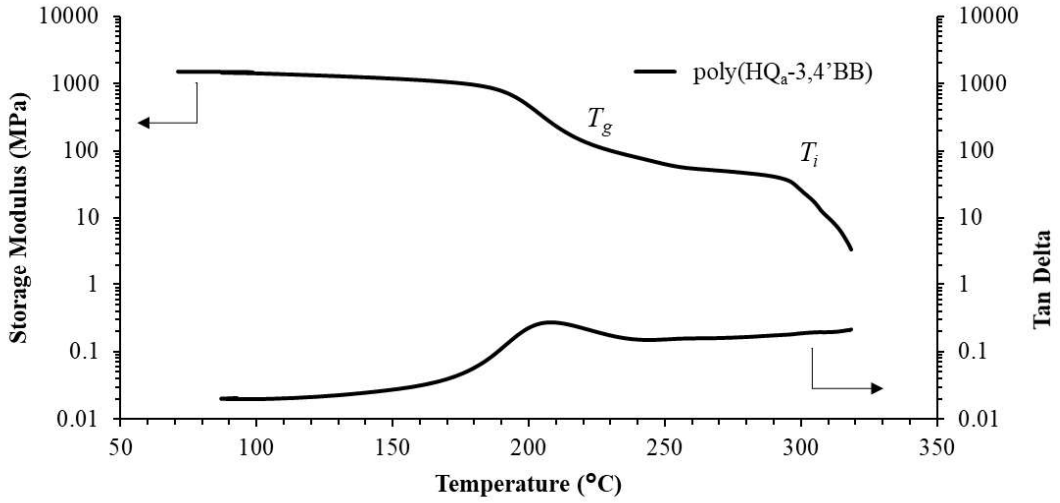

Figure 6.7. Dynamic mechanical analysis temperature ramp of poly(HQ$_a$-3,4'BB) at a frequency of 1 Hz.

Dynamic mechanical analysis (DMA) probed the thermomechanical properties of poly(HQ_a-3,4'BB). During the first heat cycle, the DMA heated the film under tension mode through the α-transition until 300 °C at which an increase in the modulus occurred and reached a maximum. Due to the temperature at which the maximum occurs, this is believed to be attributed to a combination of crystallization and improvement of the nematic ordering. Deconvolution of these two mechanisms will require further characterization. Quickly cooling the sample to room temperature and rescanning is depicted in **Figure 6.7.** The DMA curve exhibited a T_g at 208 °C, slightly higher than the DSC value. The onset of flow began at 298 °C and continued until after the measured T_i (332 °C). Nematic LCPs commonly flow within the mesogenic window (T_m – T_i) allowing for polymerization and processing when an isotropic state cannot be achieved.[12] DMA of Vectra® A950exhibits the onset of flow near the T_m due to the semi-crystalline morphology.[42] This inhibition of flow below the T_i for poly(HQ-3,4'BB) presumably resulted from crystallization. Thus, poly(HQ-3,4'BB) achieves processability in the isotropic state at 340 °C, impossible for Vectra® which never achieves an isotropic state.

The importance of characterizing the viscous flow properties of LC polymers stems from the significant use of the shear thinning properties for LCPs. The power law coefficient represents a value for comparison of the shear thinning behavior of a polymer, expressed as n in **Equation 6.1**. This equation outlines the viscosity (η) change in the power law region of a polymer during melt rheology as a function of the consistency index (m) and shear rate (γ) to the power law coefficient minus 1. The values of n range

$$\eta = m(x)\gamma^{(n-1)} \qquad \textbf{(6.1)}$$

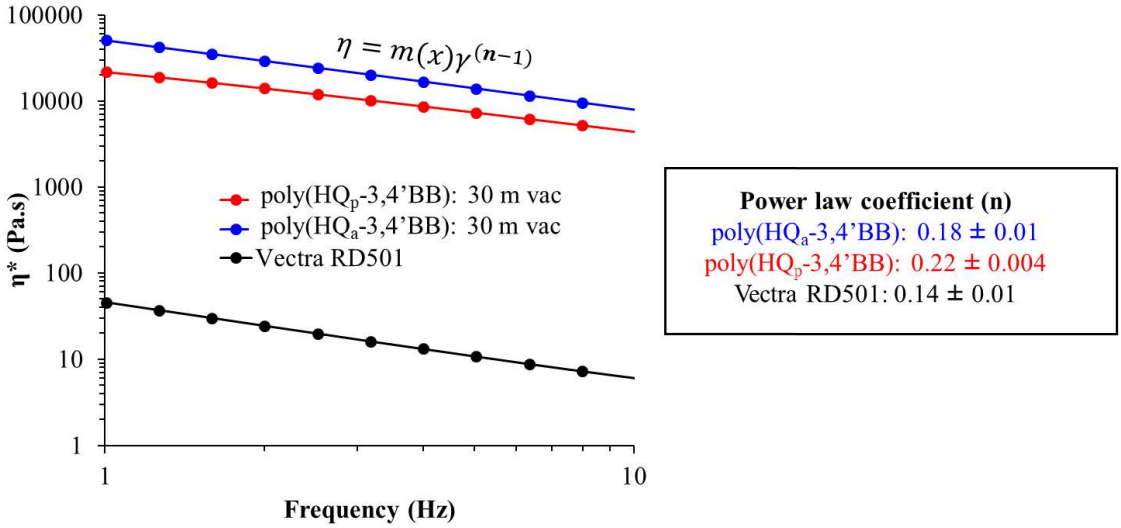

Figure 6.8. Viscosity profile of poly(HQ$_a$-3,4'BB) and poly(HQ$_p$-3,4'BB) at 340 °C within the power law region. Structural dependence of shear thinning characterized through analysis of power law coefficient.

from 0 to 1, where lower values result from steeper slopes (more significant shear thinning).

The inhibition of flow below the T_i due to crystallization required melt rheology measurements at 340 °C. The experiment utilized a strain-sweep to determine the linear viscoelastic region then a frequency sweep from 0.1 to 100 rad/s. Power law scaling determined the exponent of the logarithmic viscosity slope from 1 to 10 Hz in the power law region, as illustrated in **Figure 6.8**. Vectra® RD501, has a power law coefficient of 0.14 at the same temperature (340 °C) as poly(HQ-3,4'BB), which falls within the nematic mesophase for this polymer. In comparison, poly(HQ$_a$-3,4'BB) and poly(HQ$_p$-3,4'BB) resulted in slightly higher values of 0.18 and 0.22, respectively, although these values are within the isotropic phase of these polymers. Although similar to Vectra®, this slight difference in shear thinning could be attributed to different morphologies for each polymer at 340 °C. The significantly lower viscosity of Vectra RD501 may result from its expected lower molecular weight relative to poly(HQ-3,4'BB). The difference in shear

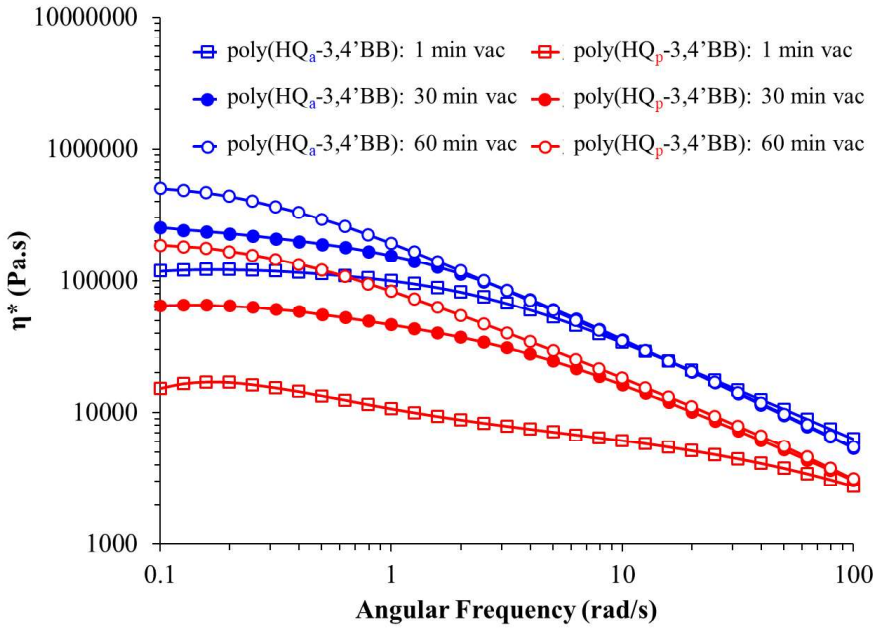

Figure 6.9. Frequency sweep at 340 °C with 1.25% strain of poly(HQ_a-3,4'BB) and poly(HQ_p-3,4'BB) polymers stopped at different % conversion during vacuum stage of polymerization.

thinning between poly(HQ_a-3,4'BB) and poly(HQ_p-3,4'BB) may result from the different end-groups or slight differences in polydispersity of the polymers. This characterization also revealed a significant difference between the zero-shear viscosities of poly(HQ_p-3,4'BB) and poly(HQ_a-3,4'BB). Due to the dependence of this value on molecular weight, a study was designed to probe the molecular weight growth of these two polymers.

6.4.5 Rheological study of molecular weight growth.

In order to probe the different molecular weight growth through the indirect measurement of zero-shear complex viscosity, six polymerizations of poly(HQ-3,4'BB) were performed (three utilizing HQ_a and three HQ_p). Consistent reaction scale, molar equivalents of HQ to 3,4'BB-COOH (1:1 mol eq.), and reaction times (with the exception of the vacuum stage) limited the errors occurring between the different reactions. As mentioned in the experimental section, stopping the three parallel reactions for HQ_a or

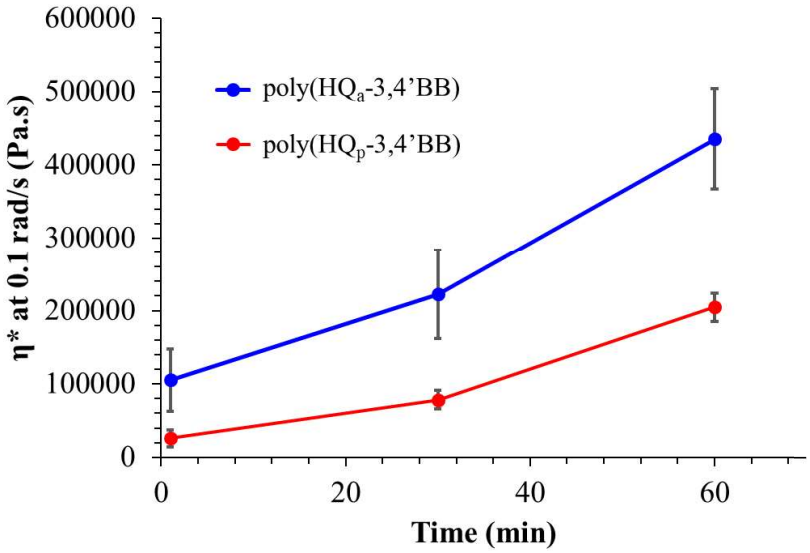

Figure 6.10. Comparison of the effects of length of time under vacuum during final polymerization on zero shear viscosity for poly(HQ_a-3,4'BB) and poly(HQ_p-3,4'BB) polymers.

HQ_p at different times in the vacuum stage (1 min, 30 min, and 60 min) enabled tracking of the molecular weight growth at different stages of the reaction. **Figure 6.9** displays the range of zero-shear viscosities achieved from the six polymer samples. The complex viscosity at 0.1 rad/s determined the zero-shear viscosity for each sample from triplicate runs, maintaining the same pre-shear treatment and instrument set-up to limit error. Plotting these two series in **Figure 6.10** as a function of vacuum time**,** enabled the observation that the zero-shear complex viscosity for the poly(HQ_a-3,4'BB) was consistently higher than poly(HQ_p-3,4'BB) with slightly higher slopes. This suggested that poly(HQ_a-3,4'BB) achieved higher molecular weight faster during the final stage of the reaction than poly(HQ_p-3,4'BB). The difference in condensate remains the only change between these two systems affecting molecular weight growth. The steric hinderance of ($C(CH_3)_3$) on the pivilate in comparison to acetate (CH_3) will result in slower conversion of the phenol to the mixed anhydride of the carboxylic acid slowing the molecular weight growth. Even so, depending on the color requirements for specific

applications the white product achieved at the end when utilizing the poly(HQ_p-3,4'BB) could outweigh the slower reaction time to obtain the same molecular weight as poly(HQ_a-3,4'BB).

6.5 Conclusions:

Melt acidolysis polymerization afforded the synthesis of poly(HQ-3,4'BB), utilizing two different derivatives of hydroquinone: HQ_a and HQ_p. The variation in chemical structure of these monomers afforded lower coloring through use of HQ_p, however these polymers also exhibited lower molecular weight. Structural analysis utilizing NMR spectroscopy confirmed that no significant difference in the polymer chemical structure occurred despite the condensate side-reactions causing a persistent color difference. Morphological characterization utilizing wide-angle x-ray scattering (WAXS) and polarized optical microscopy confirmed nematic morphology as well as limited crystallization under certain thermal and mechanical processing conditions. These results contradict previous understanding that kinked backbone structures inhibit the formation of a LC phase, presumably due to the longer biphenyl unit and its impact on the persistence length of the polymer. This LC polymer achieved comparable shear thinning results to the industrial standard, Vectra® RD501. This offers a competitive design for the synthesis of LC homopolymer without the necessity to complicate the structure through copolymerization in order to achieve processable temperature ranges. This material could be considered for a range of possible application in the areas of electronics and medical devices.

Acknowledgments:

The authors thank Dr. Ryan Mondschein and Dr. Eliot Edling for insightful discussions throughout the project. The morphological characterization is supported by National Science Foundation under Grant No. DMR-1809291.

Funding:

This work is sponsored by ExxonMobil Chemical Company

Notes:

The authors declare no competing financial interest

References:

(1) Donald, A. M.; Windle, A. H.; Hanna, S., *Liquid crystalline polymers*; 2nd ed.; Cambridge University Press: Cambridge, 2006.
(2) Windle, A. H., In *Liquid Crystalline and Mesomorphic Polymers*; Shibaev, V. P., Lam, L., Eds.; Springer New York: New York, NY, 1994, p 26.
(3) Dobb, M. G.; McIntyre, J. E., In *Liquid Crystal Polymers II/III*; Platé, N. A., Ed.; Springer Berlin Heidelberg: Berlin, Heidelberg, 1984, p 61.
(4) Chung, T., *Thermotropic liquid crystal polymers: thin-film polymerization, characterization, blends, and applications*; Technomic Pub. Co: Lancaster, Pa, 2001.
(5) Heifferon, K. V.; Long, T. E., In *Liquid Crystalline Polymers: Synthesis, Properties, and Applications*; Mittal, V., Ed.; Central West Publishing: Australia, 2018, p 205.
(6) Perkins, W. G.; Marcelli, A. M.; Frerking, H. W., The effect of blending temperature, composition, and shear rate on PET/Vectra A900 LCP blend viscosity and morphology, *Journal of Applied Polymer Science* **1991**, *43*, 329.
(7) Tai-Shung, C., The recent developments of thermotropic liquid crystalline polymers, *Polymer Engineering & Science* **1986**, *26*, 901.
(8) Flory, P. J., In *Recent Advances in Liquid Crystalline Polymers*; Chapoy, L. L., Ed.; Springer Netherlands: Dordrecht, 1985, p 99.
(9) Calundann, G. W., Polyester of 6-Hydroxy-2-napthoic Acid and Para-hydroxy Benzoic Acid Capable of Readily Undergoing Melt Processing. U.S. Patent 4,161,470, October, 20 1977.
(10) Jackson, W. J.; Morris, J. C., Liquid crystal copolyesters containing terephthalic acid and 2,6-naphthalenedicarboxylic acid. US4169933 A, Oct 2, 1979.
(11) Calundann, G. W.; Charbonneau, L. F.; Benicewicz, B. C., Melt Processing Polyester Capable of Forming an Anisotropic Melt Comprising a Relatively Low Concentration of 6-oxy-2-naphthoyl moiety, 4-benzoyl moiety, 1,4-dioxyphenylene moiety, isophthaloyl moiety, and terephthaloyl moiety. U.S. Patent 4,522,974, June 11, 1985.

(12) Jackson, W. J., Liquid Crystal Polymers. IV. Liquid Crystalline Aromatic Polyesters, *British Polymer Journal* **1980**, *12*, 154.
(13) Yerlikaya, Z.; Aksoy, S.; Bayramli, E., Structure and properties of fully aromatic thermotropic liquid-crystalline copolyesters containing m-hydroxybenzoic acid units, *Journal of Applied Polymer Science* **2003**, *90*, 3260.
(14) Economy, J.; Parkar, Z., In *100+ Years of Plastics. Leo Baekeland and Beyond*; American Chemical Society: 2011; Vol. 1080, p 93.
(15) Yerlikaya, Z.; Aksoy, S.; Bayramli, E., Synthesis and Properties of Thermotropic Liquid Crystalline Copolyesters Containing p-Hydroxyphenylacetic Acid and m-Hydroxybenzoic Acid Units, *Journal of Macromolecular Science, Part A* **2006**, *43*, 433.
(16) Erdemir, A. B.; Johnson, D. J.; Tomka, J. G., Thermotropic polyesters: Synthesis, structure and thermal transitions of poly(p-oxybenzoate-co-p-phenylene isophthalate), *Polymer* **1986**, *27*, 441.
(17) Tokita, M.; Watanabe, J., Several Interesting Fields Exploited through Understanding of Polymeric Effects on Liquid Crystals of Main-Chain Polyesters, *Polymer Journal* **2006**, *38*, 611.
(18) Watanabe, J.; Hayashi, M., Thermotropic liquid crystals of polyesters having a mesogenic p,p'-bibenzoate unit. 1. Smectic A mesophase properties of polyesters composed of p,p'-bibenzoic acid and alkylene glycols, *Macromolecules* **1988**, *21*, 278.
(19) Heifferon, K. V.; Mondschein, R. J.; Talley, S. J.; Moore, R. B.; Turner, S. R.; Long, T. E., Tailoring the glassy mesophase range of thermotropic polyesters through copolymerization of 4,4'-bibenzoate and kinked isomer, *Polymer* **2019**, *163*, 125.
(20) Lammert, M.; Wharmby, M. T.; Smolders, S.; Bueken, B.; Lieb, A.; Lomachenko, K. A.; Vos, D. D.; Stock, N., Cerium-based metal organic frameworks with UiO-66 architecture: synthesis, properties and redox catalytic activity, *Chemical Communications* **2015**, *51*, 12578.
(21) Orifici, A. F.; Vallés, E. M.; Garay, R. O.; Lenz, R. W., Preparation and characterization of thermotropic liquid crystal copolyesters containing m-hydroxybenzoic acid units, *Polymer* **1996**, *37*, 4357.
(22) Huang, J. N.; Leblanc, J. P.; Hall, H. K., Model studies on the kinetics and mechanism of polyarylate synthesis by acidolysis, *Journal of Polymer Science: Polymer Chemistry Edition* **1992**, *30*, 345.
(23) Jackson, W. J.; Kuhfuss, H. F., Liquid crystal polymers. I. Preparation and properties of p-hydroxybenzoic acid copolyesters, *Journal of Polymer Science: Polymer Chemistry Edition* **1976**, *14*, 2043.
(24) Bakir, M.; Meyer, J. L.; Economy, J.; Jasiuk, I., Heat-Induced Polycondensation Reaction with Self-Generated Blowing Agent Forming Aromatic Thermosetting Copolyester Foams, *Macromolecules* **2016**, *49*, 6489.
(25) Nelson, A. M.; Fahs, G. B.; Moore, R. B.; Long, T. E., High-Performance Segmented Liquid Crystalline Copolyesters, *Macromolecular Chemistry and Physics* **2015**, *216*, 1754.

(26) Arnold, F. E.; Van Deusen, R. L., Preparation and Properties of High Molecular Weight, Soluble Oxobenz[de]imidazobenzimidazoisoquinoline Ladder Polymer, *Macromolecules* **1969**, *2*, 497.
(27) Yeh, J.-M.; Liou, S.-J.; Lai, C.-Y.; Wu, P.-C.; Tsai, T.-Y., Enhancement of Corrosion Protection Effect in Polyaniline via the Formation of Polyaniline−Clay Nanocomposite Materials, *Chemistry Materials* **2001**, *13*, 1131.
(28) Dobkowski, Z., Determination of critical molecular weight for entangled macromolecules using the tensile strength data, *Rheologica Acta* **1995**, *34*, 578.
(29) Leblanc, J.-P.; Huang, J.; Padias, A. B.; Hall, H. K., Thermolysis of polyarylate model compounds, *Journal Polymer Science, Part A: Polymer Chemistry* **1992**, *30*, 2321.
(30) Mandal, P. K.; Siddhanta, S. K.; Chakraborty, D., Engineering properties of compatibilized polypropylene/liquid crystalline polymer blends, *Journal of Applied Polymer Science* **2012**, *124*, 5279.
(31) Kundu, M. K.; Pal, P.; Hatui, G.; Das, C. K.; Kalra, S. S., Investigation on crystallinity, performance and processability of naturally occurring halloysite nanotubes compatibilized sPS/LCP thermoplastic nanocomposites, *Journal of Polymer Research* **2015**, *22*, 29.
(32) Kim, W. N.; Denn, M. M., Properties of blends of a thermotropic liquid crystalline polymer with a flexible polymer (Vectra/PET), *Journal of Rheology* **1992**, *36*, 1477.
(33) Blackwell, J.; Biswas, A., In *Developments in Oriented Polymers—2*; Ward, I. M., Ed.; Springer Netherlands: Dordrecht, 1987, p 153.
(34) Odian, G. G., *Principles of polymerization*; Wiley: New York, 1991.
(35) Wang, Y.; Lu, G.; Wang, W.; Cao, M.; Luo, Z.; Shao, N.; Wang, B., Molecular design and synthesis of thermotropic liquid crystalline poly(amide imide)s with high thermal stability and solubility, *e-Polymers* **2017**, *17*, 199.
(36) Tian, Y.; Akiyama, E.; Nagase, Y., Liquid crystalline cyclic tetramethyltetrasiloxanes containing coumarin moieties, *Journal of Materials Chemistry* **2003**, *13*, 1253.
(37) Wilsens, C. H. R. M.; Noordover, B. A. J.; Rastogi, S., Aromatic thermotropic polyesters based on 2,5-furandicarboxylic acid and vanillic acid, *Polymer* **2014**, *55*, 2432.
(38) Hu, Y. S.; Schiraldi, D. A.; Hiltner, A.; Baer, E., Structural Model for Oxygen Permeability of a Liquid Crystalline Polymer, *Macromolecules* **2003**, *36*, 3606.
(39) Hu, Y. S.; Liu, R. Y. F.; Schiraldi, D. A.; Hiltner, A.; Baer, E., Solid-State Structure of Copolyesters Containing a Mesogenic Monomer, *Macromolecules* **2004**, *37*, 2128.
(40) Hu, Y. S.; Liu, R. Y. F.; Schiraldi, D. A.; Hiltner, A.; Baer, E., Oxygen Barrier Properties of Copolyesters Containing a Mesogenic Monomer, *Macromolecules* **2004**, *37*, 2136.
(41) Flory, P. J., Phase Equilibria in Solutions of Rod-Like Particles, *Proceedings of the Royal Society of London. Series A, Mathematical and Physical Sciences* **1956**, *234*, 73.
(42) Vectra: liquid crystal polymer (LCP), *Ticona: Technical Data Sheet* **2001**.

Supporting Information:

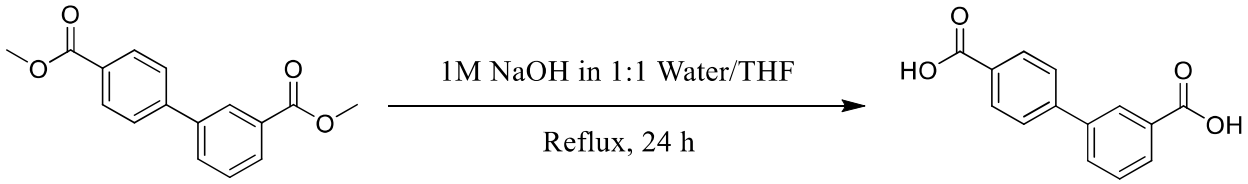

Scheme S6.1. Hydrolysis of dimethyl 3,4'- bibenzoate (3,4'BB) to synthesize diacid monomer, biphenyl 3,4'-dicarboxylic acid (3,4'BB-COOH), for acidolysis polymerization.

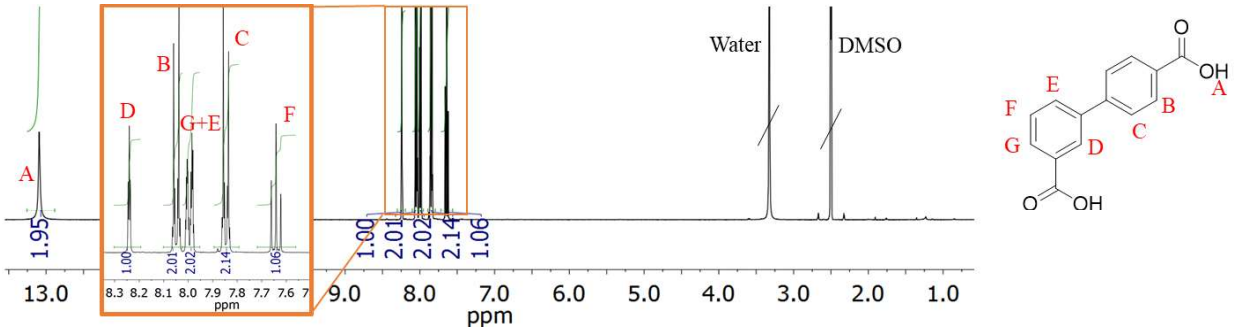

Figure S6.1. Successful hydrolysis of biphenyl 3,4'-dicarboxylic acid confirmed by ^{1}H NMR spectroscopy (DMSO-d_6, 400 MHz).

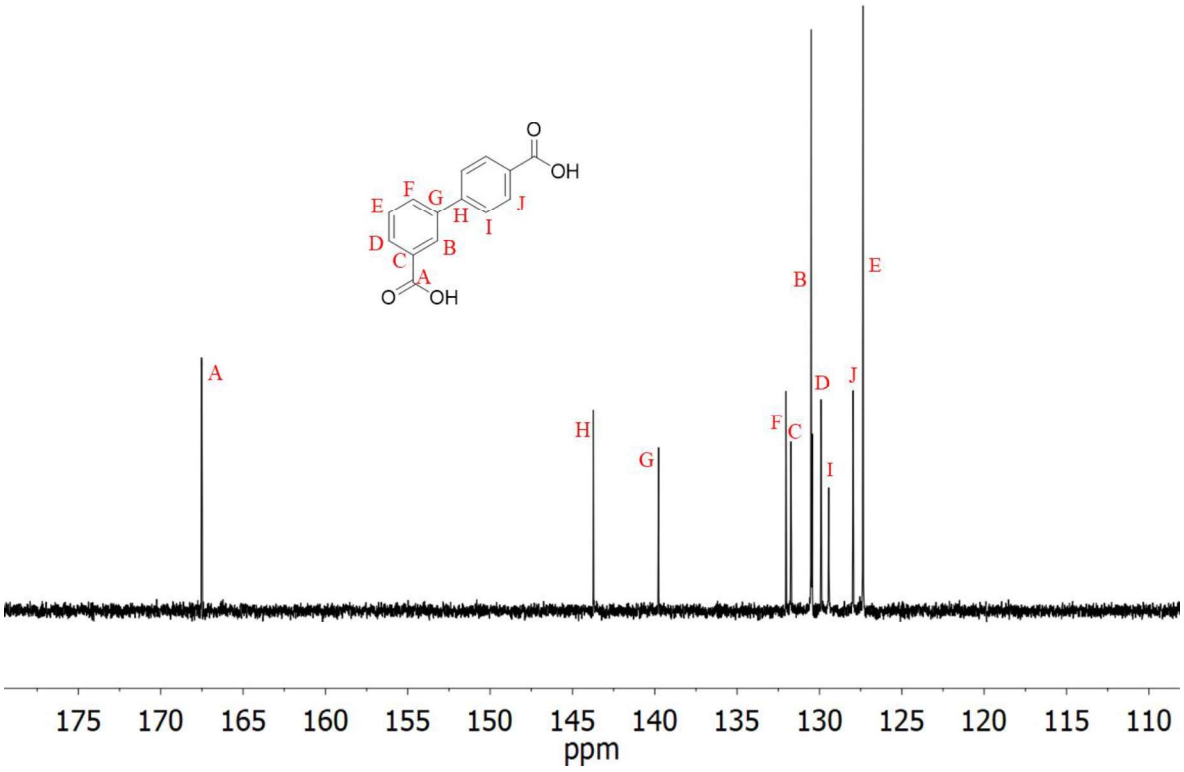

Figure S6.2. Successful hydrolysis of biphenyl 3,4'-dicarboxylic acid confirmed by ^{13}C NMR spectroscopy (DMSO-d_6, 400 MHz).

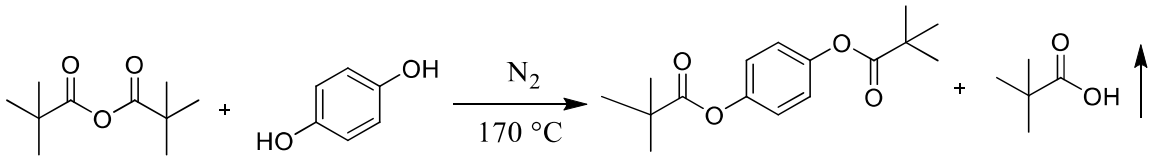

Scheme S6.2. Pivilation of hydroquinone with pivalic anhydride yields hydroquinone dipivilate for acidolysis polymerization.

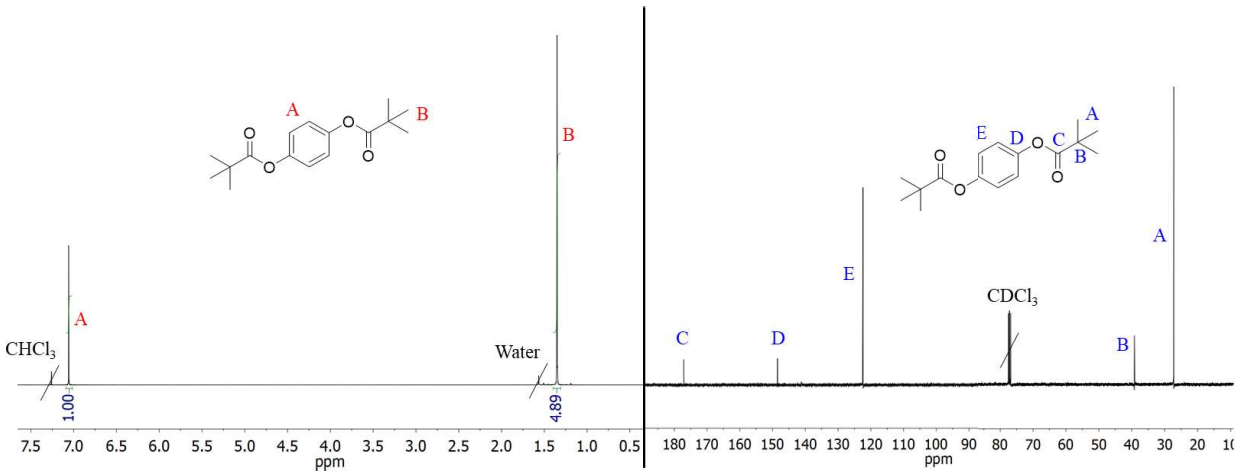

Figure S6.3. Successful pivalation of hydroquinone confirmed through ^{1}H and ^{13}C NMR spectroscopy. Left: Peak assignment and ^{1}H NMR ($CDCl_3$, 400 MHz). Right: Peak assignment and ^{13}C NMR ($CDCl_3$, 400 MHz).

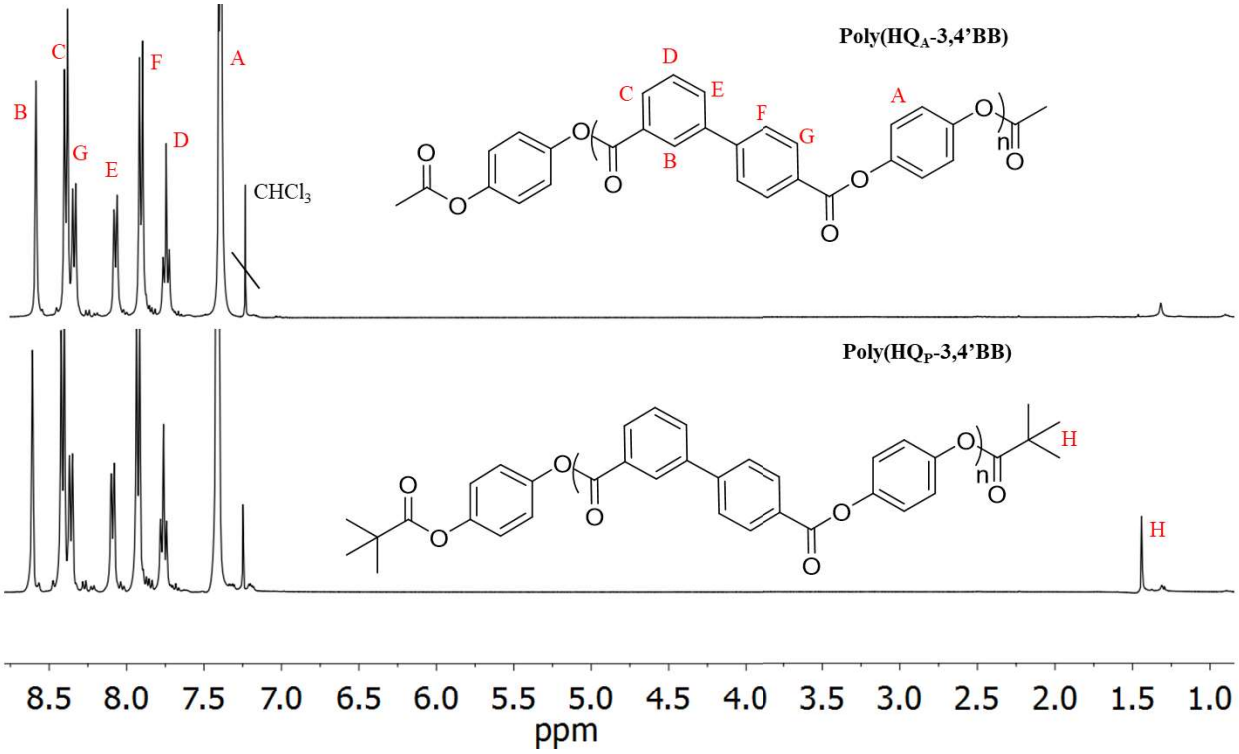

Figure S6.4. ^{1}H NMR ($CDCl_3$:TFA-*d*, 400 MHz) spectroscopy of poly(HQ_a-3,4'BB) (top) and poly(HQ_p-3,4'BB) (bottom).

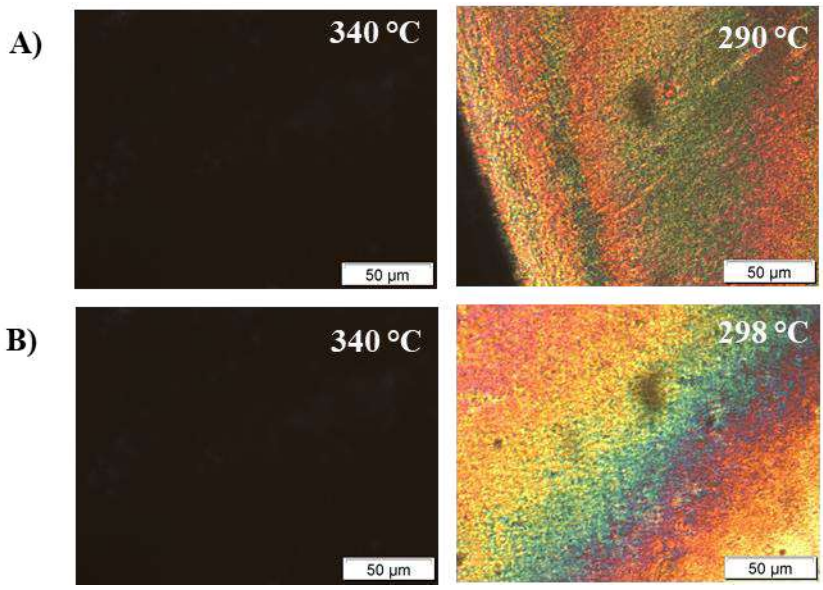

Figure S6.5. Polarized optical microscopy of poly(HQ-3,4'BB) with higher molecular weight due to receiving 30 m of vacuum during the polymerization reveals possible mosaic nematic texture birefringence. Both sets of images were taken during a slow cool at 10 °C/min from the isotropic phase. A) poly(HQ_p-3,4'BB) B) poly(HQ_a-3,4'BB).

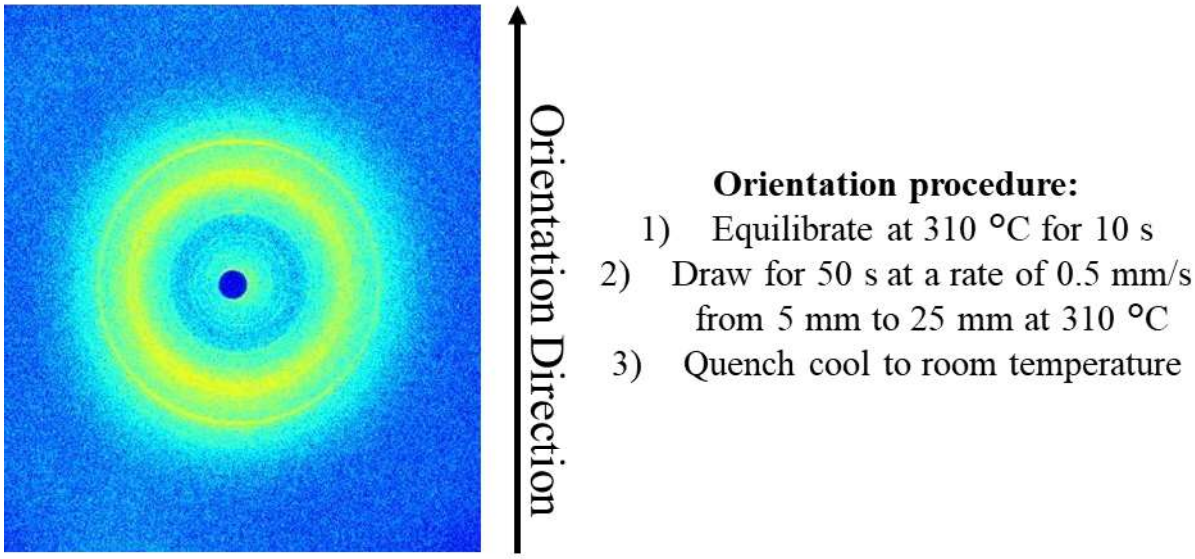

Figure S6.6. 2D WAXS profile of poly(HQ_p-3,4'BB) after attempts to orient the polymer below the T_i resulting in crystallization.

Chapter 7: Structure-property relationships of poly(phenylene bibenzoate) polymers through systematic variation of backbone linearity

(Manuscript in preparation for publication)

Katherine V. Heifferon, Samantha J. Talley, Glenn A. Spiering, Robert B. Moore, S. Richard Turner, and Timothy E. Long

Macromolecules Innovation Institute, Department of Chemistry, Virginia Tech, Blacksburg, VA 24061

Keywords: polyester, liquid crystalline, melt polymerization, bibenzoate, regioisomers

7.1 Abstract:

This report details poly(phenylene bibenzoates) with a range of tunable morphologies upon the systematic exchange of *para* monomers with their *meta* counterparts. Melt acidolysis polymerization of three diacid monomers (biphenyl 4,4'-dicarboxylic acid (4,4'BB), biphenyl 3,4' dicarboxylic acid (3,4'BB), or biphenyl 3,3' dicarboxylic acid (3,3'BB) with two dipivilate monomers (hydroquinone dipivilate (HQ) or resorcinol dipivilate (RS)) afforded six polymers with varied configurations from linear to kinked backbones. Analysis of the thermal stability revealed one-step weight loss profiles for all polymers with $T_{d,5\%}$ > 460 °C except for poly(RS-4,4'BB). Thermal and morphological characterization utilizing differential scanning calorimetry (DSC), polarized optical microscopy (POM), and X-ray diffraction revealed significant morphological differences between the polymers. The entirely linear poly(hydroquinone 4,4'-bibenzoate), yielded a semi-crystalline morphology without an observable melting temperature (T_m) prior to degradation. Incorporation of a single *meta* monomer e.g. poly(resorcinol 4,4'-bibenzoate) and poly(hydroquinone 3,4'-bibenzoate), generated liquid crystalline (LC) morphologies with a nematic mesophase. Depending on the

thermal history, crystalline domains formed with T_m's at 330 °C and 320 °C, respectively. Addition of more than one *meta* isomer in the repeating unit resulted in amorphous high T_g polymers. In contrast, poly(hydroquinone 3,3'-bibenzoate) exhibited a semi-crystalline morphology upon annealing.

7.2 Introduction:

Polyarylates, which are classified as engineering plastics, comprise polymers with fully aromatic backbones offer resistance to UV light, high glass transition temperatures, and inherent flame retardance.[1-3] Polymer structures in this field contain repeating units often based on aromatic dicarboxylic acids and diols, such as terephthalic (TA), isophthalic acid (IA), hydroquinone (HQ), and bisphenol A (BPA).[4] Publications on polyarylates first appeared in 1957 and demonstrated a wide range of valuable properties using polycarbonate structures before transitioning to polyesters.[3,5] Depending on monomer selection, these polymers exhibit morphologies ranging from fully amorphous to semi- and liquid crystalline. The choice of BPA for poly(bisphenol- A terephthalate) resulted in an amorphous polymer with high heat resistance.[6,7] In contrast, a linear aromatic monomer, such as *p*-hydroxybenzoic acid (*p*-HBA), generated a homopolymer (poly(*p*-hydroxybenzoic acid)) with a highly crystalline morphology and was no melt processable due to an extremely high T_m (~610 °C).[8,9] Poly(*p*-HBA), also known as Ekonol®, required processing through forging techniques in a similar fashion to a ductile metal.[10-12] In order to improve processability, the kinked configuration, poly(*m*-HBA), resulted in a low % crystallinity (10.5%) and reduced T_m (210 °C) due to disruption of packing. Random copolymerization of *p*-HBA with other linear monomers also provided improvements in the polymer processability, which facilitated a lower T_m and the formation of a LC phase.[13-15]

Polyarylates with thermotropic (LC) properties exhibit beneficial characteristics, such as high shear thinning and alignment during fiber production.[9] In order to induce a LC morphology, the polymer structure must achieve a balance between rectilinearity (straightness) and the disruption of chain packing. Most importantly, calamitic polymers must exhibit an aspect ratio (persistence length/diameter ratio) of > 6 in order to maintain a stable LC phase.[15,16] When designing LC polymers, the polymer structure must limit crystallizability and reduce the melting temperature in order to enable the transition from the semi-crystalline to the LC morphology prior to thermal degradation of the polymer. Random copolymerization with linear comonomers (6-hydroxy-2-napthoic acid or terephthalic acid) represents a common method of achieving industrially useful LC polymers.[17-19] The introduction of bulky aromatic substituents on the backbone also inhibits crystallization and disrupts translational symmetry to provide homopolymers with processable mesophase temperature ranges.[20-22] In previous literature, the incorporation of kinks through the choice of *ortho* or *meta* substituted monomers resulted in complete disruption of LC properties, which counteracted the beneficial reductions in the T_m.[8,23,24] In Chapter 6, Long et al. discovered unique LC properties for poly(hydroquinone 3,4'-bibenzoate) structure. This polymer demonstrated the first example of a kinked non-substituted homopolyester that successfully resulted in a processable LC polymer. In order to expand upon this earlier work, access to the *meta* and *para* regioisomers for the repeating unit of poly(phenylene bibenzoate) allowed a detailed analysis of physical properties achieved through systematic changes the number and location of *meta* linkages.

Here in, the synthesis of six isomeric polymers based on the same repeating unit structure, poly(phenylene bibenzoate) is discussed. Polymers with entirely linear backbones, (poly(*p*-phenylene-*p,p'*-bibenzoate) and poly(hydroquinone 4,4' bibenzoate)) to entirely kinked backbones (poly(*m*-phenylene-*m,m'*-bibenzoate) and poly(resorcinol 3,3' bibenzoate)) were prepared. This enabled a range of polymer properties including semi-crystalline, LC, and high T_g amorphous polyesters through variations in the polymer configuration. This study revealed that the presence of more than one *meta* isomer disrupted the formation of a LC phase, resulting in semi-crystalline and amorphous polymers.

7.3 Experimental:

7.3.1 Materials.

Dimethyl 3,4'-biphenyldicarboxylate (dimethyl 3,4' bibenzoate: 3,4'BB), dimethyl 3,3'-biphenyldicarboxylate (dimethyl 3,3' bibenzoate: 3,3'BB), and biphenyl 4,4'-dicarboxylic acid (4,4'BBCOOH), provided by ExxonMobil, were used as received. Pivalic anhydride (trimethylacetic anhydride: PVA) (Acros Organics, 99%), tetrahydrofuran (THF) (Fisher Chemical), sodium hydroxide (NaOH) (Fisher Chemical) (Acros Organics, 99%), trifluoroacetic acid-*d* (*d*-TFA) (Sigma-Aldrich, 99.5% atom D), chloroform-*d* ($CDCl_3$) (Cambridge Isotope Laboratories, 99.8% atom D), and dimethyl sulfoxide-d_6 (DMSO-d_6) (Cambridge Isotope Laboratories, 99.9% atom D) were used as received. Resorcinol (RS) (Sigma-Aldrich, ≥ 99%) and hydroquinone (HQ) (Sigma-Aldrich, ≥ 99%) were recrystallized from ethanol (Decon Labs, 200 proof).

7.3.2 Analytical Methods.

A Varian Unity 400 at 400 MHz (23 °C) provided both ^1H and ^{13}C nuclear magnetic resonance (NMR) spectroscopy of the monomers and polymers utilizing $CDCl_3$, DMSO-

d_6, and *d*-TFA as solvents depending on material solubility. A thermal ramp at a rate of 10 °C/min from 25 to 600 °C, under constant N_2 flow, on a TA Instruments Q50 thermogravimetric analyzer (TGA) afforded the weight loss profiles of the polymers. TA Instruments Q1000 differential scanning calorimeter (DSC) facilitated analysis of the polymer's thermal transitions after calibration with Indium (T_m = 156.60 °C) and zinc (T_m = 419.47 °C) standards. Unless otherwise specified, standard analysis utilized a heat/cool/heat cycle with rates of 10 °C/min, 100 °C/min, and 10 °C/min respectively under a 50 mL/min nitrogen flow. Data analysis was performed on the second heat cycles using the inflection point of the glass transition temperature (T_g) and the maximum of the melting/isotropic temperatures (T_i). During the annealing study of poly(p-phenylene 3,3'-bibenzoate), the polymer was heated at a rate of 10 °C/min to 250 °C where the temperature was held for 2 h. A second heat cycle occurred upon cooling the polymer to room temperature affording the DSC curve used in the analysis. Compression molding at a temperature of 340 °C provided the free-standing polymer films. This technique used a sandwich of aluminum plates, Kapton™ sheets coated with a Rexco Partall® Power Glossy Liquid mold release agent, and 150 μm thick stainless-steel shims. Quenching the plates and molten material in an ice bath following the molding cooled the sample rapidly to room temperature. A TA Instruments Q800 DMA in tension mode with an oscillatory amplitude of 0.1% strain, frequency of 1 Hz, a static force of 0.01 N, and a heating rate of 3 °C/min provided the thermomechanical properties of poly(RS-3,4'BB) and poly(RS-3,3'BB). Poly(HQ-3,4'BB) and poly(HQ-3,3'BB) utilized a heating rate of 3 °C/min until reaching 250 or 275 °C respectively at which the sample was rapidly cooled to room temperature. A second heat cycle was then performed at the same heating rate which was

utilized in the analysis. The maximum of the tan delta from DMA afforded the T_g of the polymers.

X-ray diffraction (XRD) patterns were obtained on a Rigaku MiniFlex II Desktop X-ray powder diffractometer. The radiation source was Cu Kα radiation, with a wavelength of 1.54 Å. The angular scanning range was 2θ = 5−40°, with 0.01° steps. A Nikon LV100 Eclipse optical microscope with a Nikon DXM1200 digital camera and Linkham TMS 94 hot stage afforded polarized optical microscopy (POM) images of the polymer series. Melting the samples in the isotropic state, pressing between glass slides, and cooling at a rate of 10 °C/min enabled the observation of birefringent textures. In the study of poly(hydroquinone-4,4' bibenzoate), a second quench-cooling analysis was performed by melting the sample at 400 °C then removing the glass slides from the heat stage and rapidly cooling on the benchtop. Sample nomenclature comprises poly(X-Y,Y'BB) where X refers to the isomer of the phenyl group utilized in the synthesis, either hydroquinone (HQ) or resorcinol (RS). Y,Y' refer to the configuration of the biphenyl component, either biphenyl 4,4'-dicarboxylic acid (4,4'BB), biphenyl 3,4'-dicarboxylic acid (3,3'BB), or biphenyl 3,3'-dicarboxylic acid (3,3'BB).

7.3.3 Synthesis of biphenyl dicarboxylic acids.

Conversion of both dimethyl 3,4'-bibenzoate (3,4'BB) and dimethyl 3,3'-bibenzoate (3,3'BB) to biphenyl 3,4'-dicarboxylic acid (3,4'BB-COOH) and biphenyl 3,3'-dicarboxylic acid respectively occurred through the following synthetic procedure. A solution of 400 mL 1 M sodium hydroxide using 1:1 THF:DI water with either 3,4'BB or 3,3'BB (39.94 g, 0.148 mol) refluxed for 24 h.[25] Filtration of the final solution afforded the removal of unreacted starting material as well as other impurities. Concentration via rotary evaporator and subsequent precipitation from the remaining solution through

addition of concentrated HCl afforded a white product. Filtration and washes with DI water neutralized the product and drying overnight *in vacuo* at 120 °C resulted in a fine white powder (34.69 g, 97% yield).

Biphenyl 3,4'-dicarboxylic acid:

^{1}H NMR (400 MHz, DMSO-d$_6$): δ 13.12 (s, 2H), 8.24 (s, 1H), 8.05(d, 2H), 7.99 (d, 2H), 7.84 (d, 2H), and 7.64 (t, 1H) ppm.

^{13}C NMR (400 MHz, DMSO-d$_6$): δ 167.51, 143.73, 139.78, 132.03, 131.73, 130.51, 129.90, 129.44, 127.96, and 127.36 ppm.

Melting Point (DSC): 103 °C

Biphenyl 3,3'-dicarboxylic acid:

^{1}H NMR (400 MHz, DMSO-d$_6$): δ 13.16 (s, 2H), 8.20 (t, 2H), 7.98 (d, 4H), and 7.64 (t, 2H) ppm.

^{13}C NMR (400 MHz, DMSO-d$_6$): δ 167.12, 139.55, 131.66, 131.19, 129.53, 128.69, and 127.33 ppm.

Melting Point (DSC): 104 °C

7.3.4 Synthesis of phenyl dipivilates.

Synthesis of hydroquinone dipivilate (phenyl-*p*-dipivilate, HQ_p) and resorcinol dipivilate (phenyl-*m*-dipivilate, RS_p) occurred utilizing the same method. Hydroquinone (5.1g, 0.046 mol) or resorcinol and pivalic anhydride (20 mL, 0.135 mol) were added into a dry 100-mL round-bottomed flask. The reaction vessel was equipped with an overhead mechanical stirrer, mechanical stir-rod, glass stir-rod adaptor, distillation tube with round-bottomed collection flask, and t-neck adaptor connected to the reaction flask. Evacuating the reaction vessel with a vacuum pump and back-filling with N_2 three times provided an inert atmosphere. A constant N_2 flow and reaction temperature of 170 °C

afforded the removal of the pivalic acid condensate and subsequent collection in the distillation flask. Thin-layer chromatography identified full conversion after 1 h, and increasing the reaction temperature to 200 °C for 1 h removed excess pivalic anhydride. Cooling the set-up to room temperature facilitated crystallization of the product from the solution. Filtration, washing with cold 200 proof ethanol, and drying *in vacuo* at 100 °C secured a pure white crystalline solid.

Hydroquinone dipivilate (HQ_p):

^{1}H NMR (400 MHz, $CDCl_3$): δ 7.04 (s, 4H) and 1.33 (s, 18H) ppm.

^{13}C NMR (400 MHz, $CDCl_3$): δ 176.91, 148.29, 122.20, 39.04, and 27.09 ppm

Melting Point (DSC): 104 °C

Resorcinol dipivilate (RS_p):

^{1}H NMR (400 MHz, $CDCl_3$): δ 7.36 (t, 1H), 6.94 (dd, 2H), 6.86 (t, 1H), and 1.35 (s, 18 H) ppm.

^{13}C NMR (400 MHz, $CDCl_3$): δ 176.66, 151.52, 129.51, 118.67, 115.34, 39.07,

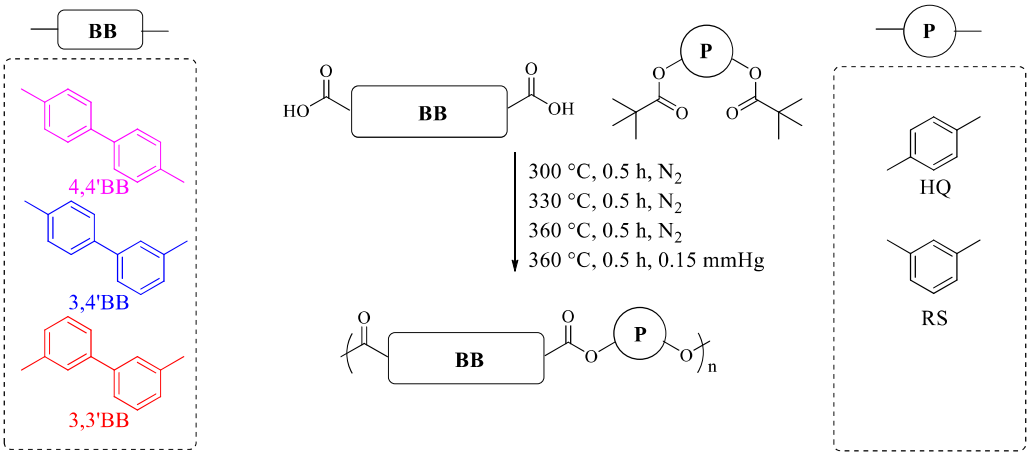

Scheme 7.1. Synthesis of six poly(phenylene bibenzoate) isomers utilizing three diacids (biphenyl 4,4'-dicarboxylate, 3,4'BB, and 3,3'BB) monomers as well as two pivilated isomers of diphenols (hydroquinone and resorcinol).

and 27.07 ppm

Melting Point (DSC): 79 °C

7.3.5 Synthesis of poly(phenylene bibenzoate) isomers.

Acidolysis polymerization afforded the six novel fully aromatic polymers, illustrated in **Scheme 7.1**, utilizing a previously employed method.[19,26,27] 4,4'BB-COOH, 3,4'BB-COOH (23.34 g, 0.0964), or 3,3'BB-COOH and either HQ_p or RS_p (26.819 g, 0.09635 mol) were measured into an oven dried 100-mL round-bottomed flask. Determination of starting material equivalents occurred using a modified Carothers equation with an estimated final M_n of 20 kg/mol and a 30 g final scale. The reaction set-up utilized a distillation tube with 100-mL round-bottomed collection flask, mechanical stir-rod, glass stir-rod adaptor, overhead mechanical stirrer, and t-neck adaptor. Evacuating the reaction flask and back-filling with N_2 three times ensured an inert atmosphere. Heating the reaction at 300 °C for 0.5 h, 330 °C for 0.5 h, and finally 360 °C for 0.5 h under N_2 flow facilitated molecular weight growth. A reduced pressure (0.15 mmHg) and temperature of 360 °C resulted in a highly viscous final polymer after 0.5 h. The final polymer was removed from the 100-mL round-bottomed flask, after the reaction cooled, by breaking away the glass flask and clipping the resulting material from the metal stir-rod. The polymer was then used without further purification.

7.4 Results and Discussion:

7.4.1 Synthesis and structural determination:

Acidolysis polymerization of different isomers of the biphenyl diacid (4,4'BB, 3,4'BB, or 3,3'BB) with one of two isomers of the pivilated diphenol (HQ or RS) resulted in the synthesis of six polymers, as illustrated in **Scheme 7.1.** While early patents focused on the *in-situ* polymerization route to form fully aromatic polymers through a one-pot reaction between the diacid, diphenol, and acetic anhydride, the use of

preacetylated monomers significantly improved upon this method by guaranteeing the presence of the acetate group on every monomer at the start of the polymerization.[28,29].[13,19,26] This enabled more control over the polymerization conditions, allowing consistency with the reaction times and temperatures across all polymers in this isomeric series. The monomer, hydroquinone dipivilate, represents a variation of these preacetylated monomers which imparted control over the final polymer color. This monomer lacks the α-proton present within hydroquinone diacetate that facilitates the color formation in the polymer through abstraction at high temperatures resulting in a small amount of ketene formation.[30] Leblanc et al. studied these side-reactions in model compounds, as well as the color prevention using pivilated molecules. In Chapter 6, we showed an example of this color prevention step in the polymerization of poly(HQ-3,4'BB).[30]

The pivilated derivatives of HQ and RS utilized a solvent-free synthetic pathway to recreate *in-situ* polymerization conditions, previously demonstrated in Chapter 6.A 3 eq. excess of the pivalic anhydride acted as both reactant and solvent, reacting with the two isomeric diphenols to form the pivilated product along with the by-product pivalic acid at a 170 °C. Increasing the temperature to 200 °C removed some of the excess pivalic anhydride, facilitating the recrystallization of the products out of the solution upon cooling. ^{1}H and ^{13}C NMR spectroscopy confirmed the structure and purity of the monomers after rinsing with cold ethanol and drying overnight.

Acidolysis polymerization conditions required the conversion of the provided diester monomers to the diacid functionality using a basic hydrolysis reaction. Lammert

et al. previously utilized this procedure to synthesize biphenyl 4,4'-dicarboxylic acid and it demonstrated success for the 3,4'BB and 3,3'BB isomeric forms as well.[25]

Acidolysis polymerization of the different biphenyl diacids (4,4'BB-COOH, 3,4'BB-COOH, and 3,3'BB-COOH) with the phenyl dipivilates (HQ_p and RS_p) generated six polymers ranging from a completely linear or *para* backbone to a completely kinked or *meta* structure. A molar ratio of 1:1.016 diacid:dipivilate should facilitate a final molecular weight after full conversion of 20,000 g/mol. Heating the polymerization from 300-360 °C for 1.5 h in 0.5 h increments enabled the maintenance of a transparent homogenous melt for most combinations throughout the reaction while limiting the oligomer distillation. During the final step of the reaction, vacuum application resulted in

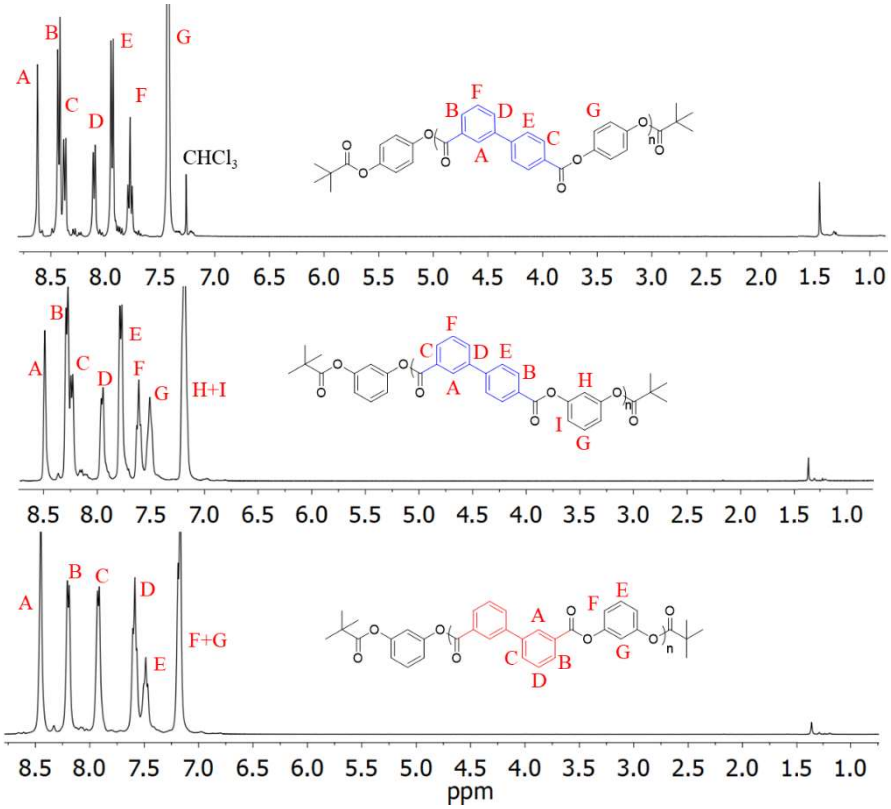

Figure 7.1. ^{1}H-NMR spectroscopy of the soluble poly(phenylene bibenzoate) isomers. Top: poly(HQ-3,4'BB) (TFA-*d*:$CDCl_3$ 400 MHz); Middle: poly(RS-3,4'BB) (TFA-*d*, 400 MHz); Bottom: poly(RS-3,3'BB) (TFA-*d*, 400 MHz).

the rapid removal of large quantities of the condensate, as well as a significant viscosity increase. The combination of these events resulted in foaming of the polymer and the melt becoming wrapped around the stir-rod.

While fluidity in the melt of poly(HQ-4,4'BB) initially was achieved at 300 °C, the reaction quickly became pasty and then solidified prior to the application of vacuum at 360 °C. Solidification during the polymerization, likely occurred from crystallization of the highly regular and rigid backbone, limiting the generation of a high molecular weight polymer resulting in brittle and powdery opaque products. Uniquely, poly(RS-4,4'BB) formed an opaque fluid melt which became viscous during the final vacuum stage. Often LC polymer, such as Vectra®, form opaque melts during polymerization due to a nematic morphology.[18] Three of the polymers (poly(HQ-3,4'BB), poly(RS-3,4'BB), and poly(RS-3,3'BB)) exhibited solubility in either TFA-*d* or a 1:1 mixture of $CDCl_3$:TFA-*d* enabling ^1H NMR spectroscopy. This analysis confirmed the backbone structure of the different isomers, illustrated in **Figure 7.1.** Unfortunately, insolubility of the polymers in traditional SEC solvents, such as $CHCl_3$, THF, or DMF, prohibited molecular weight analysis through this method.

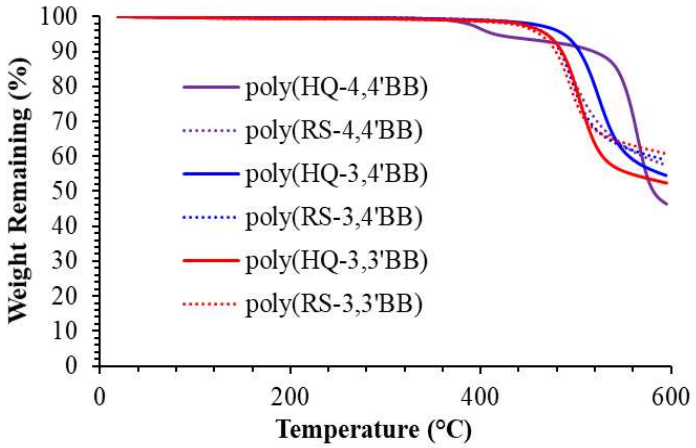

Figure 7.2. Thermogravimetric analysis of poly(phenylene bibenzoate) isomers.

7.4.2 Thermal Analysis:

Thermogravimetric analysis of the polymer series revealed the weight loss profile as a function of temperature under N_2. All polymers, except poly(HQ-4,4'BB), exhibit a one-step weight loss profile common for main-chain LC polyesters (**Figure 7.2**).[31] Poly(HQ-4,4'BB) generated a two-step profile with the first weight loss step occurring at 415 °C equating to a 7% weight loss while the second step occurred at 519 °C. The distillation or sublimation of the low molecular weight oligomers assumed to be present

Polymer	$T_{d,5\%}$ (°C)	Char yield at 600 °C (%)	T_g (°C)[b]	ΔC_p (W/g)[b]	T_m (°C)	ΔH_m (J/g)	T_i (°C)[b]	ΔH_i (J/g)[b]	T_g (°C)[a]
Poly(HQ-4,4'BB)	415/ 519	47	-	-	-	-	-	-	N/A
Poly(RS-4,4'BB)	469	58	205	0.06	330[b]	14.3[b]	363	8.3	N/A
Poly(HQ-3,4'BB)	487	55	189	0.05	315[e]	N/A	321	17.4	207[d]
Poly(RS-3,4'BB)	469	59	173	0.07	-	-	-	-	186
Poly(HQ-3,3'BB)	469	52	171	0.06	329[c]	2.4[c]	-	-	196[d]
Poly(RS-3,3'BB)	462	61	150	0.06	-	-	-	-	164

[a]Determined from DMA
[b]Determined from DSC second heat after a quench cool
[c]T_m determined from DSC after annealing at 250 °C for 2 h
[d]Determined from DMA second heat
[e]Determined from DSC second heat after a 10 °C/min cool

Table 7.1. Thermal characterization obtained from differential scanning calorimetry, dynamic mechanical characterization, and thermogravimetric analysis of the poly(phenylene bibenzoate) isomeric series.

in this brittle polymer likely provoked this early weight loss step in the TGA profile. All other polymers in the series possessed $T_{d,5\%}$ greater than 450 °C, analyzed in **Table 7.1**, corroborating with previous literature on fully aromatic polyesters.[27,32]

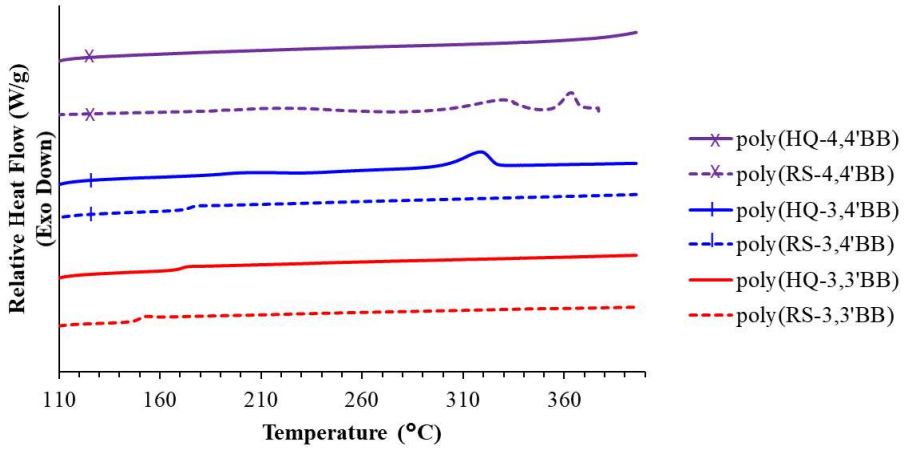

Figure 7.3. Second heating cycle of the poly(phenylene bibenzoate) isomers revealing the changing T_i, T_m, and T_g as a function of *meta* units.

Figure 7.3 depicts the DSC curves from the second heating trace following a quench cool in the DSC from 380 °C. The polymer bearing fully *para* monomers, poly(HQ-4,4'BB), revealed a DSC trace with no obvious thermal transitions. This follows expectations from other linear aromatic homopolymers, such as poly(*p*-HBA) and poly(*p*-phenylene terephthalate), which possess T_m's above the degradation temperature of the polymers.[8,32]

Poly(RS-4,4'BB) and poly(HQ-3,4'BB) contain very similar configurations, each with one *meta* unit within the backbone either in the phenylene or biphenyl moiety. Poly(HQ-3,4'BB) previously demonstrated the ability to form a LC glass with a nematic morphology upon quench cooling in Chapter 6. The single endothermic transition within this polymers DSC trace, identified as the isotropic temperature (T_i), corresponds to the transition temperature from nematic to isotropic morphologies. In contrast, slow cooling

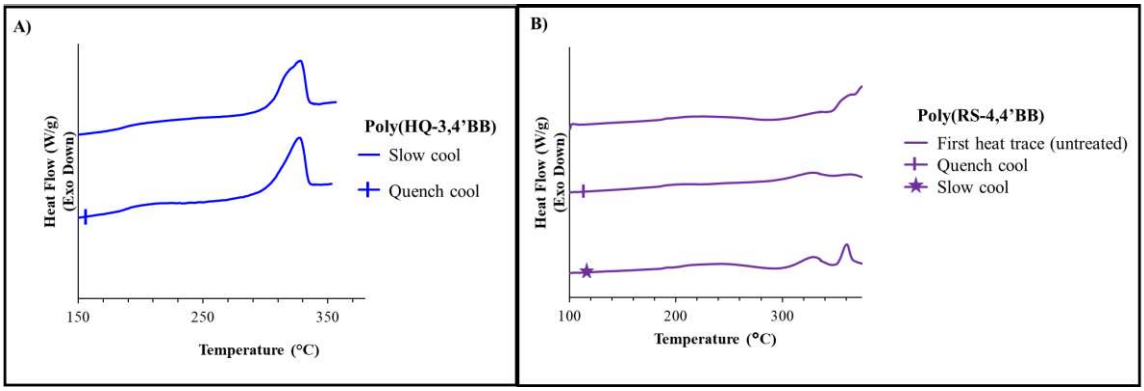

Figure 7.4. DSC heating traces of A) poly(HQ-3,4'BB) and B) poly(RS-4,4'BB) after a quench cool or slow cool from 360 or 380 °C, respectively.

(10 °C/min) from 360 °C induces crystal growth revealed in the emergence of a small T_m at 315 °C overlapping with the T_i in the following heating trace (**Figure 7.4A**).

Efforts were made to quench poly(RS-4,4'BB) as rapidly as possible by heating the DSC sample to 400 °C, equilibrating for 5 min, then placing the sample on a cold metal surface to cool rapidly. **Figure 7.4B** reveals the heat trace following this quenching procedure. Unlike poly(HQ-3,4'BB), poly(RS-4,4'BB) generates two endothermic transitions at 327 °C and 365 °C after quench-cooling. These thermal transitions represent the T_m and T_i of poly(RS-4,4'BB) with ΔH_m of 5.0 J/g and ΔH_i of 2.1 J/g. No significant changes occurred in the location of the thermal transition following the slow cool but both $\Delta H_{i/m}$ increased, as illustrated in **Figure 7.4B**. The first heating trace evaluates the thermal properties of the polymer sample taken directly from the reaction flask, generating primarily one endothermic transition at 358 °C. This insinuates that under certain conditions the formation of a LC glass occurs, similar to poly(HQ-3,4'BB).

The final three polymers in the series contain structures with either two or three *meta* moieties in the backbone. Poly(RS-3,4'BB), poly(HQ-3,3'BB), and poly(RS-3,3'BB) all yield DSC traces with no endothermic transitions but obvious T_g*'s* upon

quench cooling implying that these polymers are amorphous. Poly(HQ-3,3'BB) and poly(RS-3,4'BB), both featuring two *meta* units in the backbone, display very similar T_g's of 171 and 173 °C, respectively. Overall a decrease in the T_g's becomes apparent as the number of *meta* units in the backbone increases with poly(RS-3,3'BB) generating the lowest T_g at 150 °C. Two previous studies by Karayannidis et al. and Li et al., exhibited similar T_g trends when comparing poly(ethylene terephthalate) and poly(ethylene isophthalate). During this work, the T_g decreased from 82 °C to 65 °C respectively.[33,34] These groups cite the increased flexibility in the chain conformation as a function of *meta* units for the resulting drop in the glass transition temperature.[34]

As with poly(RS-4,4'BB) and poly(HQ-3,4'BB), the morphology of poly(HQ-3,3'BB) appears to change depending on the thermal treatment performed on the sample. **Figure 7.5** illustrates the change in this polymer DSC curve that occurs upon annealing at

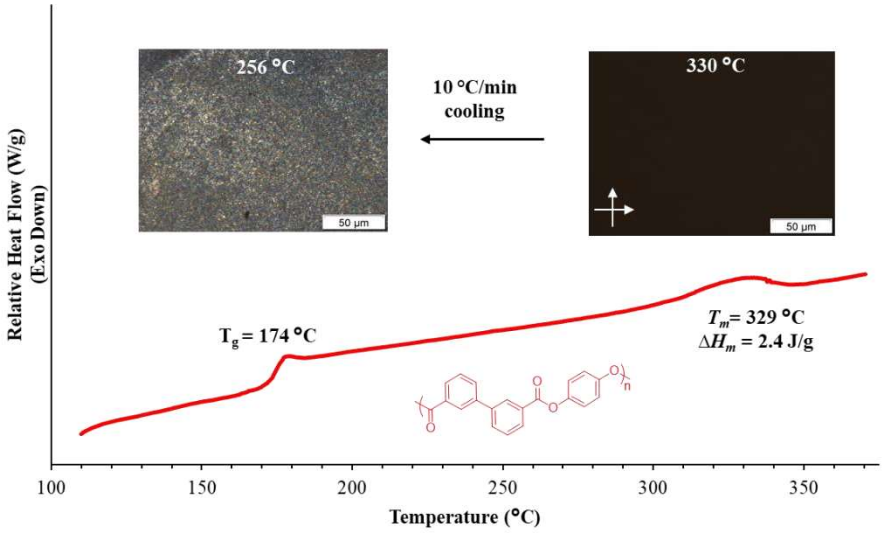

Figure 7.5. First heating trace of poly(HQ-3,3'BB) after annealing the polymer at 250 °C for 2 h. Corresponding polarized optical microscopy upon cooling from the isotropic state at 10 °C/min reveals a birefringent texture.

250 °C for 2 h. A small endothermic transition emerges at 329 °C which corresponds with the T_m of this polymer.

7.4.3 Morphological Analysis:

Polarized optical microscopy helped facilitate the morphological characterization of the six polymers. Thin samples suitable for microscopic analysis were prepared by pressing the samples between glass slides at a temperature that induced an isotropic melt. The samples were cooled from the isotropic state (temperature varied for each polymer) at 10 °C/min to a temperature below the $T_{i/m}$ or below the T_g for the amorphous polymers. No birefringent texture formed upon cooling poly(RS-3,4'BB) or poly(RS-3,3'BB) from 380-150 °C or 340 -135 °C respectively (**Figure 7.6C** and **Figure 7.6D)** concluding that these polymers maintain an amorphous morphology.

Poly(HQ-3,4'BB) revealed birefringence upon cooling to 290 °C with a fine-scale optical texture restricting identification of the morphology. Chapter 6 previously utilized a lower molecular weight sample to reveal a schlieren texture for this polymer. This texture in combination with WAXS analysis enabled the identification of a nematic

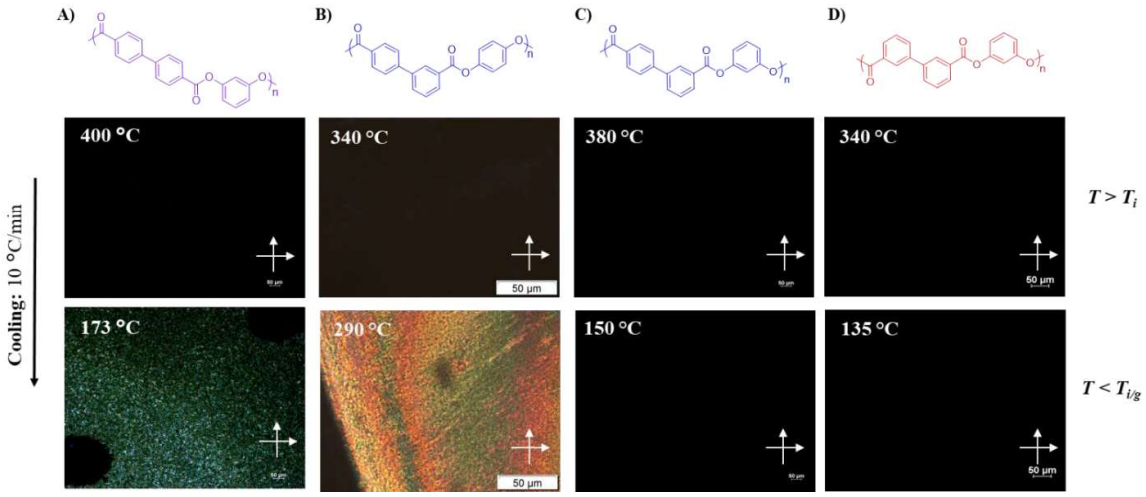

Figure 7.6. Polarized optical microscopy of the poly(phenylene bibenozate) isomers during a 10 °C/min cool from the isotropic state. A) poly(RS-4,4'BB) B) poly(HQ-3,4'BB) C) poly(RS-3,4'BB) D) poly(RS-3,3'BB)

morphology after both a quench cool and slow cool from the isotropic state.

More in depth analyses of poly(RS-4,4'BB) were performed following different thermal treatments to improve understanding of the thermal transitions observed in the DSC traces after the first heat. **Figure 7.7** illustrates POM images of poly(RS-4,4'BB) during heat cycles from below the T_g following two different cooling rates (quench or slow cool). Following a 10 °C/min slow cool a fine-scale texture emerged (**Figure 7.6A or 7.7A)**. In some instances, high molecular weight polymer with nematic mesophases produce grainy fine-scale textures associated with the presence of a large number of disclinations in the nematic phase resulting in small domain sizes. Presence of this texture may also indicate crystal growth but limitations of the microscope magnification inhibited further characterization of the texture.[35] No significant change occurred upon heating until the polymer transitioned into an isotropic state and lost the birefringence. Quenching the polymer from 400 °C to room temperature, by placing the hot slides on a

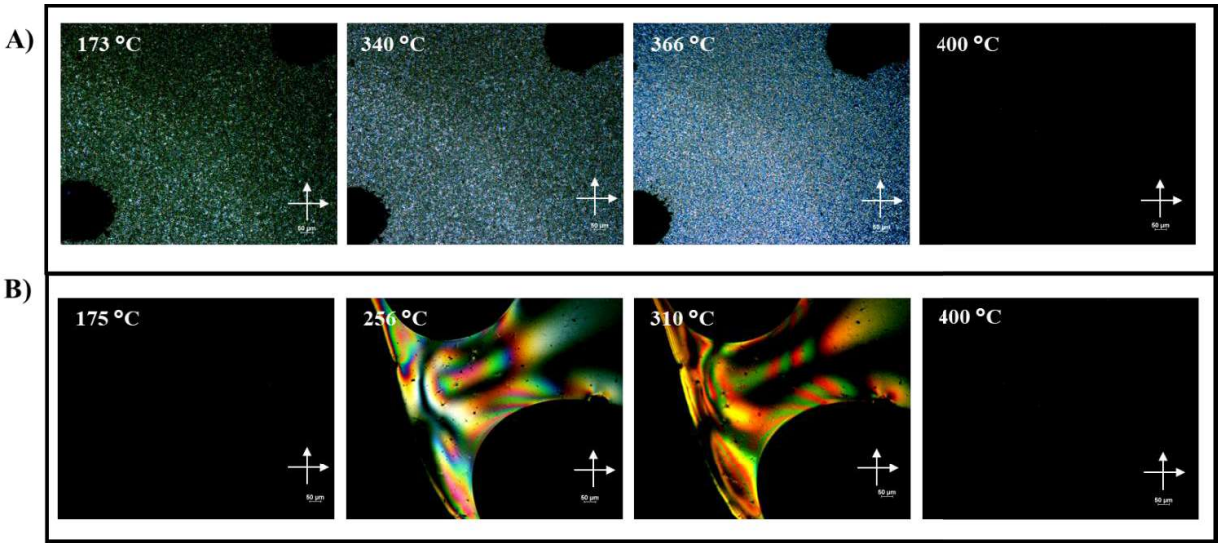

Figure 7.7. Polarized optical microscopy of poly(RS-4,4'BB) during 10 °C/min heat traces following different cooling rates from 400 °C. A) 10 °C/min cooling rate B) quench cool (~100 °C/min)

cold countertop, enabled much faster cooling temperatures then achieved using DSC. This quench resulted in a clear polymer sample that displayed no birefringence at 175 °C due to the fast cool kinetically trapping the polymer into the amorphous state. Heating above the T_g resulted in an opaque sample and generated a schlieren optical texture, at 256 °C a common optical texture for a nematic morphology. This texture remained until transitioning into an isotropic state at above 380 °C.

Poly(HQ-3,3'BB) grew into a fine-scale grey and white birefringence upon cooling at 10 °C/min from isotropic (**Figure 7.6**). This texture corresponds with the appearance of an endothermic transition in the DSC trace upon annealing at 250 °C for 2 h. This texture, similar to the texture observed from poly(RS-4,4'BB), is difficult to identify without further conformation using X-ray scattering methods.

XRD analysis further confirmed the morphology of the series of polymers. The four polymers that afforded free-standing films through compression molding were quench-cooled for the analysis in **Figure 7.8**. In contrast, measurement of poly(HQ-

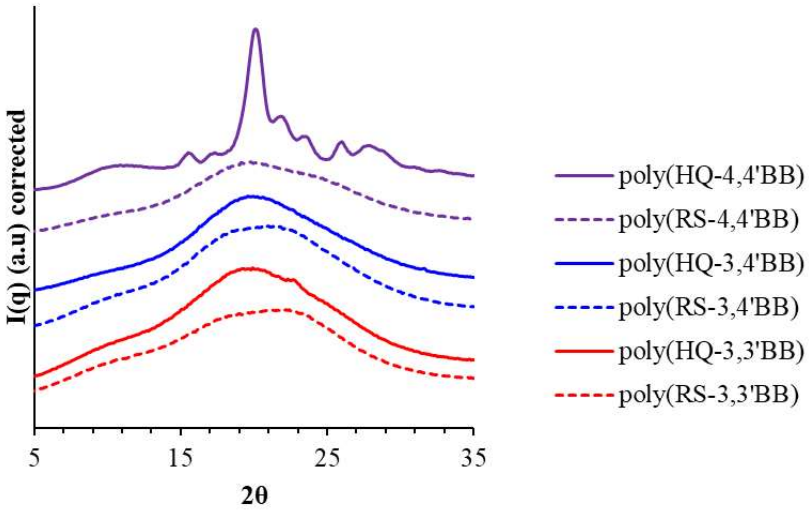

Figure 7.8. XRD scattering profile of the poly(phenylene bibenzoate)s.

4,4'BB) and poly(RS-4,4'BB) occurred on polymers taken directly from the reaction flask without further treatment. Poly(HQ-4,4'BB) afforded sharp angular reflections at 15.5, 17.3, 20.1, 21.8, 23.5, 26, and 27.9° 2θ indicating that this polymer exhibits a semi-crystalline morphology.

Conversely, poly(HQ-3,4'BB) revealed a single diffuse peak, centered about 20° 2θ. In previous studies of quench-cooled poly(HQ-3,4'BB), the elimination of sharp reflections in combination with the presence of birefringence in the POM upon quench cooling revealed a nematic LC morphology at room temperature (LC glass). Other LC morphologies, such as smectic, form lateral packing structures which result in low 2θ angular reflections, not present in this curve. Annealing poly(HQ-3,4'BB) at 280 °C created sharp reflections at 5.2, 6.1, 13.1, 14.2, 18.6, 19.6, 24.6, and 31.7° 2θ corresponding with the growth of crystalline domains, as examined in Chapter 6. These studies concluded that poly(HQ-3,4'BB) formed a LC glass upon quench cooling but

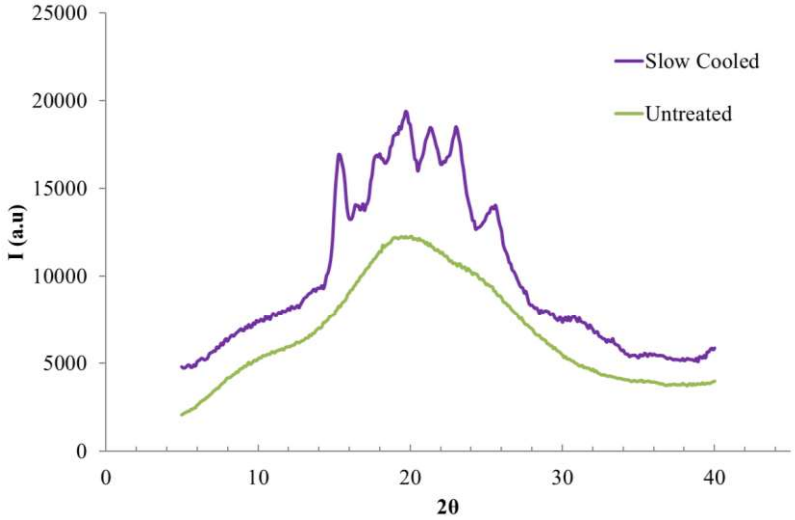

Figure 7.9. XRD scattering profile of the poly(RS-4,4'BB) after slow cool (10 °C/min) or untreated from polymerization.

annealing resulted a semi-crystalline morphology at room temperature which would transition into a LC phase between the T_m and T_i (315-321°C).

When analyzing the XRD of the untreated sample of poly(RS-4,4'BB), a single diffuse peak centered about 20° 2θ appeared. While the POM procedure could rapidly cool this sample achieving an amorphous morphology, that drastic of a temperature decrease is unlikely to have occurred upon cooling the reaction flask to room temperature by removing it from the 360 °C metal bath. As a result, the omittance of sharp angular reflections in untreated sample (**Figure 7.9)** more likely indicates of the formation of a nematic LC glass rather than an amorphous polymer. The opaque nature of this sample further corroborates this conclusion. XRD analysis of the slow-cooled sample in **Figure 7.9** occurred on a 10-mg sample after slow cooling from 380 °C in the DSC. This analysis revealed sharp reflections at 15.3, 18, 19.7, 21.3, 23, and 25.6° 2θ indicative of a crystalline packing structure.

Quench-cooled films from the polymers with more than one *meta* unit all produced one single diffuse peak centered about 20° 2θ with the exception of poly(HQ-3,3'BB) which also revealed one low intensity angular reflection at 22.7° 2θ. For the polymers that did not exhibit birefringence during the POM study (poly(RS-3,4'BB) and poly(RS-3,3'BB)), this single diffuse peak acted as further confirmation of their amorphous morphology. In order to expand the analysis of poly(HQ-3,3'BB), the quench-cooled film was annealed for 12 h at 250 °C then retest in the XRD. Sharp angular reflections emerged in the annealed sample at 15.4, 18.5, 20.5, 22.5, and 29.4° 2θ where the reflection originally in the quenched sample overlaps with the most intense reflection at 22.5° 2θ (**Figure 7.10**). This correlates with the observed birefringence that

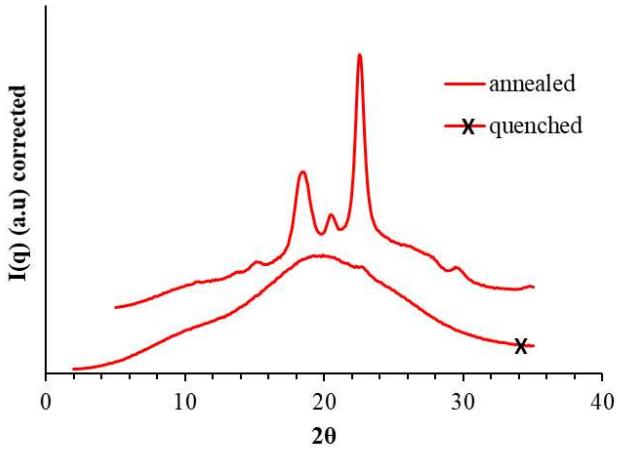

Figure 7.10. XRD scattering profile of the poly(HQ-3,3'BB) compression molded films after quench cooling from the isotropic state and subsequent annealing for 12 h at 250 °C.

emerged in the POM and confirms that this polymer exhibits a semi-crystalline morphology.

Considering all the morphological studies and thermal characterization in their totality, a trend emerged based on the number of *meta* units within the backbone of the basic poly(phenylene bibenzoate) structure. No *meta* units (completely *para* structure) resulted in a polymer too symmetric and rigid to allow melt processing due to the high crystallinity and high T_m. The addition of a single *meta*-unit, regardless of location in the repeat unit, resulted in a LC polymer with a nematic mesophase. The kinked configuration lowered the polymers crystallizability allowing the polymer to be kinetically trapped into a LC glass under certain processing conditions.

As observed in other studies with kinked backbones, the incorporation of more than one *meta* group resulted in a disruption of rectilinearity of the polymer inhibiting the formation of a stable LC mesophase. Previous literature attributed this loss of LC stability to a reduction in the persistence length within the polymer due to the kink in the backbone. This reduction limited the polymer's ability to achieve the necessary aspect

ratio to achieve a LC phase.[18] The polymers with more than one *meta* unit exhibited amorphous morphologies with the exception of poly(HQ-3,3'BB). Poly(HQ-3,3'BB) garnered a semi-crystalline morphology possibly due to its more linear and symmetric structure, relative to the other polymers.

7.4.4 Thermomechanical analysis:

Dynamic mechanical analysis enabled characterization of the thermomechanical properties for this set of polymers. A combination of low molecular weight and inability to flow at temperature below the degradation of the polymer limited the film formation of poly(HQ-4,4'BB). While poly(RS-4,4'BB) exhibited an endothermic transition at about 350 °C in the DSC, studies during compression molding revealed the inability to flow below 360 °C while temperature above 360 °C resulted in significant discoloration possibly resulting from degradation under air. As a result, only the polymers using 3,4'BB and 3,3'BB formed films that allowed examination using DMA. The quench-

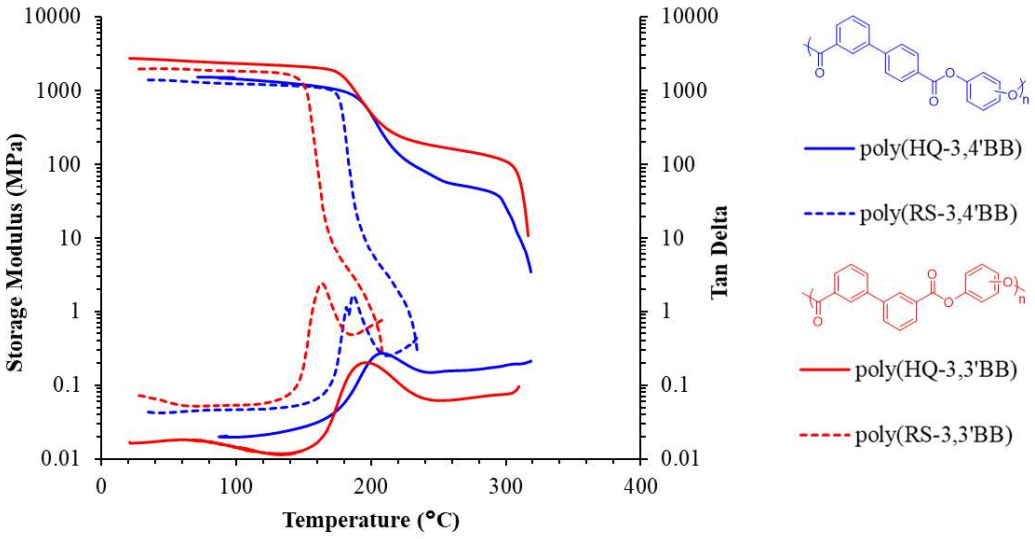

Figure 7.11. Dynamic mechanical analysis of the film-forming polymers within the poly(phenylene bibenzoate) series. Poly(RS-3,4'BB) and poly(RS-3,3'BB) measured from first heat of quench cooled films. Poly(HQ-3,4'BB) and poly(HQ-3,3'BB) represents the second heat after a quench cool in the DMA from 250 and 275 °C, respectively.

cooled films of poly(RS-3,3'BB) and poly(RS-3,4'BB), which exhibited amorphous characteristics in DSC and XRD, afforded DMA curves after the first heat cycle (**Figure 7.11)**. These polymers exhibited flow shortly after transitioning through the α-relaxation exhibiting T_g's, determined at the maximum of the tan-delta, of 164 °C and 186 °C, respectively.

During the first heat of poly(HQ-3,4'BB) and poly(HQ-3,3'BB), both materials exhibited an increase in the plateau modulus following the α-relaxation. This increase resulted in a peak in the modulus at about 250 °C and 275 °C, respectively, before the modulus decreased and flow occurred. In the past, this peak has been associated with recrystallization or increase in ordering of a quench-cooled film upon chain mobility above the T_g.[36] Annealing the film in the DMA to remove these peaks, involved heating them to the maximum of the modulus spike then rapidly cooling them back to room temperature. Heating the film again afforded the curves observed in **Figure 7.11**. Poly(HQ-3,4'BB) and poly(HQ-3,3'BB) both exhibited flow after an extended plateau region in comparison to the amorphous polymers. This results from the ordered crystalline morphologies that arise in these polymers upon annealing, as identified in the WAXS/XRD characterization. The different modulus of the plateaus for these two polymers may represent different amounts of crystallinity persisting in these polymers after the thermal treatment.

7.5 Conclusions:

Synthesis of the isomeric series of polymers utilizing the different configurations of the same basic backbone structure, poly(phenylene bibenzoate), occurred through acidolysis melt polymerization. Three different diacid monomers (4,4'BB, 3,4'BB, and 3,3'BB) and two dipivilate monomers (HQ_p and RS_p) afforded six different structures

ranging from completely *para* to entirely *meta* monomeric units. Thermal and morphological characterization revealed that the number of *meta* units in the backbone drastically impacts the polymer morphology. An entirely symmetric, linear, and rigid polymer (poly(HQ-4,4'BB)) resulted in an intractable material due to the crystallinity resulting in a high T_m. The addition of a single *meta* unit (poly(RS-4,4'BB) and poly(HQ-3,4'BB)) resulted in a LC polymer with a nematic mesophase, independent of the kink location (phenylene or bibenzoate moiety). Crystallization occurred within these two polymers depending on thermal history. Any further addition of *meta* units into the backbone structure resulted in disruption of the LC stability affording primarily amorphous polymer morphologies. Poly(HQ-3,3'BB) afforded an amorphous morphology upon quenching but annealing revealed crystal growth. These amorphous polymers generated high T_g's comparable to those of some polysulfones and polycarbonates. This series offers a pathway to a wide range of interesting polymer morphologies and properties enabling tunability based on the application desired. They could be applied in the areas of LC polymers, such as electronic and medical devices, or possibly the application space of polyarylates.

Acknowledgments:

The authors thank Dr. Ryan Mondschein, Dr. Maruti Hegde, and Dr. Eliot Edling for helpful discussions. The morphological characterization is supported by National Science Foundation under Grant No. DMR-1809291.

Funding:

This work is sponsored by ExxonMobil Chemical Company

Notes:

The authors declare no competing financial interest

References:

(1) Diepens, M.; Gijsman, P., Photostabilizing of bisphenol A polycarbonate by using UV-absorbers and self protective block copolymers based on resorcinol polyarylate blocks, *Polymer Degradation and Stability* **2009**, *94*, 1808.

(2) Bristow, J. F.; Kalika, D. S., Dielectric Relaxation Studies of Bisphenol A Polyarylates, *Macromolecules* **1994**, *27*, 1808.

(3) Svetlana, V. V.; Valery, A. V.; Petr, M. V., Polyarylates. Synthesis and properties, *Russian Chemical Reviews* **1994**, *63*, 833.

(4) Waghmare, P. B.; Pathak, P.; Deshmukh, S. A.; Idage, S. B.; Idage, B. B., Synthesis and characterization of copolyarylates using tin octoate as a catalyst, *Journal of Applied Polymer Science* **2006**, *101*, 70.

(5) Levine, M.; Temin, S. C., Properties of polyesters of bisphenols and dicarboxylic acids, *Journal of Polymer Science* **1958**, *28*, 179.

(6) Haward, R. N.; Hay, J. N.; Parsons, I. W.; Adam, G.; Owadh, A. A. K.; Boxnyak, C. P.; Aref-Azaf, A.; Cross, A., The effect of chain structure on the annealing and deformation behaviour of polymers, *Colloid and Polymer Science* **1980**, *258*, 643.

(7) Bosnyak, C. P.; Parsons, I. W.; Hay, J. N.; Haward, R. N., Relations between structure and properties in bisphenol A polyester carbonates, *Polymer* **1980**, *21*, 1448.

(8) Yerlikaya, Z.; Aksoy, S.; Bayramli, E., Synthesis and Properties of Thermotropic Liquid Crystalline Copolyesters Containing p-Hydroxyphenylacetic Acid and m-Hydroxybenzoic Acid Units, *Journal of Macromolecular Science, Part A* **2006**, *43*, 433.

(9) Jackson, W. J., Liquid Crystal Polymers. XI. Liquid Crystal Aromatic Polyesters: Early History and Future Trends, *Molecular Crystals and Liquid Crystals Incorporating Nonlinear Optics* **1989**, *169*, 23.

(10) Economy, J.; Parkar, Z., In *100+ Years of Plastics. Leo Baekeland and Beyond*; American Chemical Society: 2011; Vol. 1080, p 93.

(11) Economy, J., Aromatic Polyesters of p-Hydroxybenzoic Acid, *Molecular Crystals and Liquid Crystals Incorporating Nonlinear Optics* **1989**, *169*, 1.

(12) Economy, J.; Storm, R. S.; Matkovich, V. I.; Cottis, S. G.; Nowak, B. E., Synthesis and structure of the p-hydroxybenzoic acid polymer, *Journal of Polymer Science: Polymer Chemistry Edition* **1976**, *14*, 2207.

(13) Calundann, G. W., Polyester of 6-Hydroxy-2-naphthoic Acid and Para-hydroxy Benzoic Acid Capable of Readily Undergoing Melt Processing. U.S. Patent 4,161,470, October, 20 1977.

(14) Yoon, H. N.; Charbonneau, L. F.; Calundann, G. W., Synthesis, processing and properties of thermotropic liquid-crystal polymers, *Advanced materials (Weinheim)*, *4*, 206.

(15) Jackson, W. J.; Kuhfuss, H. F., Liquid crystal polymers. I. Preparation and properties of p-hydroxybenzoic acid copolyesters, *Journal of Polymer Science, Part A: Polymer Chemistry* **1996**, *34*, 3031.

(16) Flory, P. J., Phase Equilibria in Solutions of Rod-Like Particles, *Proceedings of the Royal Society of London. Series A, Mathematical and Physical Sciences* **1956**, *234*, 73.
(17) Flory, P. J., In *Recent Advances in Liquid Crystalline Polymers*; Chapoy, L. L., Ed.; Springer Netherlands: Dordrecht, 1985, p 99.
(18) Windle, A. H., In *Liquid Crystalline and Mesomorphic Polymers*; Shibaev, V. P., Lam, L., Eds.; Springer New York: New York, NY, 1994, p 26.
(19) Chung, T., *Thermotropic liquid crystal polymers: thin-film polymerization, characterization, blends, and applications*; Technomic Pub. Co: Lancaster, Pa, 2001.
(20) Calundann, G. W.; Charbonneau, L. F.; Benicewicz, B. C., Melt Processing Polyester Capable of Forming an Anisotropic Melt Comprising a Relatively Low Concentration of 6-oxy-2-naphthoyl moiety, 4-benzoyl moiety, 1,4-dioxyphenylene moiety, isophthaloyl moiety, and terephthaloyl moiety. U.S. Patent 4,522,974, June 11, 1985.
(21) Bhowmik, P. K.; Han, H., Fully aromatic liquid-crystalline polyesters of phenyl-substituted 4,4'-biphenols and 1,1'-binaphthyl-4,4'-diol with either 2-bromoterephthalic acid or 2-phenylterephthalic acid, *Macromolecules* **1993**, *26*, 5287.
(22) Bhowmik, P. K.; Han, H., Fully aromatic thermotropic liquid crystalline polyesters of 3-phenyl-4,4′-biphenol with 4,4′-benzophenone dicarboxylic acid, *Journal of Polymer Science, Part A: Polymer Chemistry* **1995**, *33*, 415.
(23) Bhowmik, P. K.; Han, H.; Garay, R. O., Fully aromatic thermotropic liquid crystalline homopolyesters of 3,4′-benzophenone dicarboxylic acid, *Journal of Polymer Science, Part A: Polymer Chemistry* **1994**, *32*, 333.
(24) Hu, Y. S.; Liu, R. Y. F.; Schiraldi, D. A.; Hiltner, A.; Baer, E., Solid-State Structure of Copolyesters Containing a Mesogenic Monomer, *Macromolecules* **2004**, *37*, 2128.
(25) Erdemir, A. B.; Johnson, D. J.; Tomka, J. G., Thermotropic polyesters: Synthesis, structure and thermal transitions of poly(p-oxybenzoate-co-p-phenylene isophthalate), *Polymer* **1986**, *27*, 441.
(26) Lammert, M.; Wharmby, M. T.; Smolders, S.; Bueken, B.; Lieb, A.; Lomachenko, K. A.; Vos, D. D.; Stock, N., Cerium-based metal organic frameworks with UiO-66 architecture: synthesis, properties and redox catalytic activity, *Chemical Communications* **2015**, *51*, 12578.
(27) Jackson, W. J.; Morris, J. C., Liquid crystal copolyesters containing terephthalic acid and 2,6-naphthalenedicarboxylic acid. US4169933 A, Oct 2, 1979.
(28) Orifici, A. F.; Vallés, E. M.; Garay, R. O.; Lenz, R. W., Preparation and characterization of thermotropic liquid crystal copolyesters containing m-hydroxybenzoic acid units, *Polymer* **1996**, *37*, 4357.
(29) Han, X. H.; Padias, A. B.; Hall, H. K., Syntheses of polyarylates by alcoholysis and esterolysis, *Journal of Polymer Science, Part A: Polymer Chemistry* **1999**, *37*, 2891.
(30) Han, X. H.; Padias, A. B.; Hall, H. K.; Sung, H. N., Synthesis of thermotropic LCPs using p-methoxycarbonyloxy aromatic acids, *Journal of Polymer Science, Part A: Polymer Chemistry* **1999**, *37*, 1703.

(31) Leblanc, J.-P.; Huang, J.; Padias, A. B.; Hall, H. K., Thermolysis of polyarylate model compounds, *Journal of Polymer Science, Part A: Polymer Chemistry* **1992**, *30*, 2321.
(32) Heifferon, K. V.; Mondschein, R. J.; Talley, S. J.; Moore, R. B.; Turner, S. R.; Long, T. E., Tailoring the glassy mesophase range of thermotropic polyesters through copolymerization of 4,4'-bibenzoate and kinked isomer, *Polymer* **2019**, *163*, 125.
(33) Yerlikaya, Z.; Aksoy, S.; Bayramli, E., Structure and properties of fully aromatic thermotropic liquid-crystalline copolyesters containing m-hydroxybenzoic acid units, *Journal of Applied Polymer Science* **2003**, *90*, 3260.
(34) Karayannidis, G. P.; Sideridou, I. D.; Zamboulis, D. N.; Bikiaris, D. N.; Sakalis, A. J., Thermal behavior and tensile properties of poly(ethylene terephthalate-co-ethylene isophthalate), *Journal of Applied Polymer Science* **2000**, *78*, 200.
(35) Li, B.; Yu, J.; Lee, S.; Ree, M., Poly(ethylene terephthalate co ethylene isophthalate)—relationship between physical properties and chemical structures, *European Polymer Journal* **1999**, *35*, 1607.
(36) Demus, D., *Handbook of liquid crystals*; Weinheim ; New York : Wiley-VCH, c1998., 1998.
(37) Dennis, J. M.; Fahs, G. B.; Moore, R. B.; Turner, S. R.; Long, T. E., Synthesis and Characterization of Polysulfone-Containing Poly(butylene terephthalate) Segmented Block Copolymers, *Macromolecules* **2014**, *47*, 8171.

Supporting Information

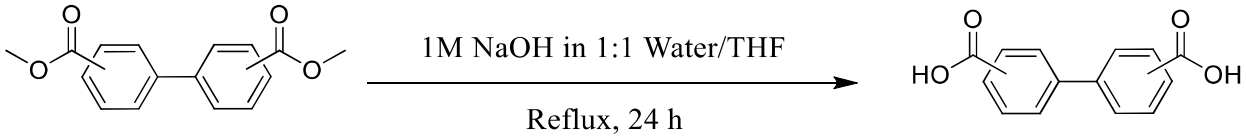

Scheme S7.1. Hydrolysis of dimethyl 3,4'- bibenzoate (3,4'BB) and dimethyl 3,3'- bibenzoate (3,3'BB) to synthesize the corresponding diacid monomer for acidolysis polymerization.

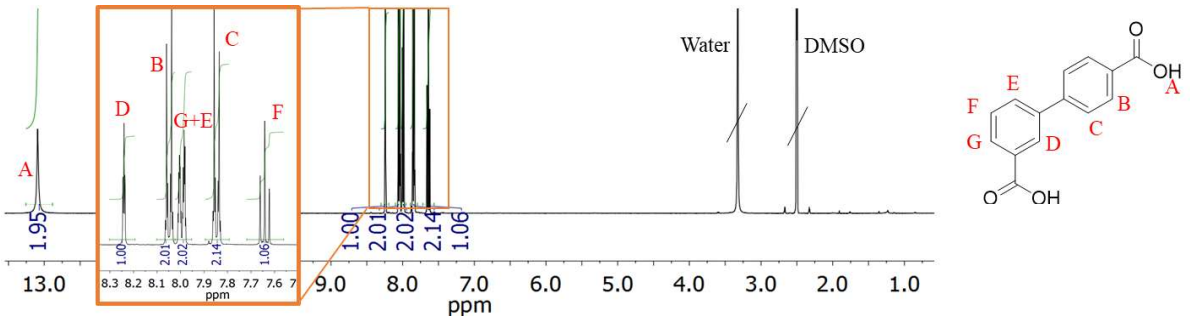

Figure S7.1. ^{1}H NMR spectroscopy (DMSO-d_6, 400 MHz) of biphenyl 3,4'-dicarboxylic acid after successful hydrolysis.

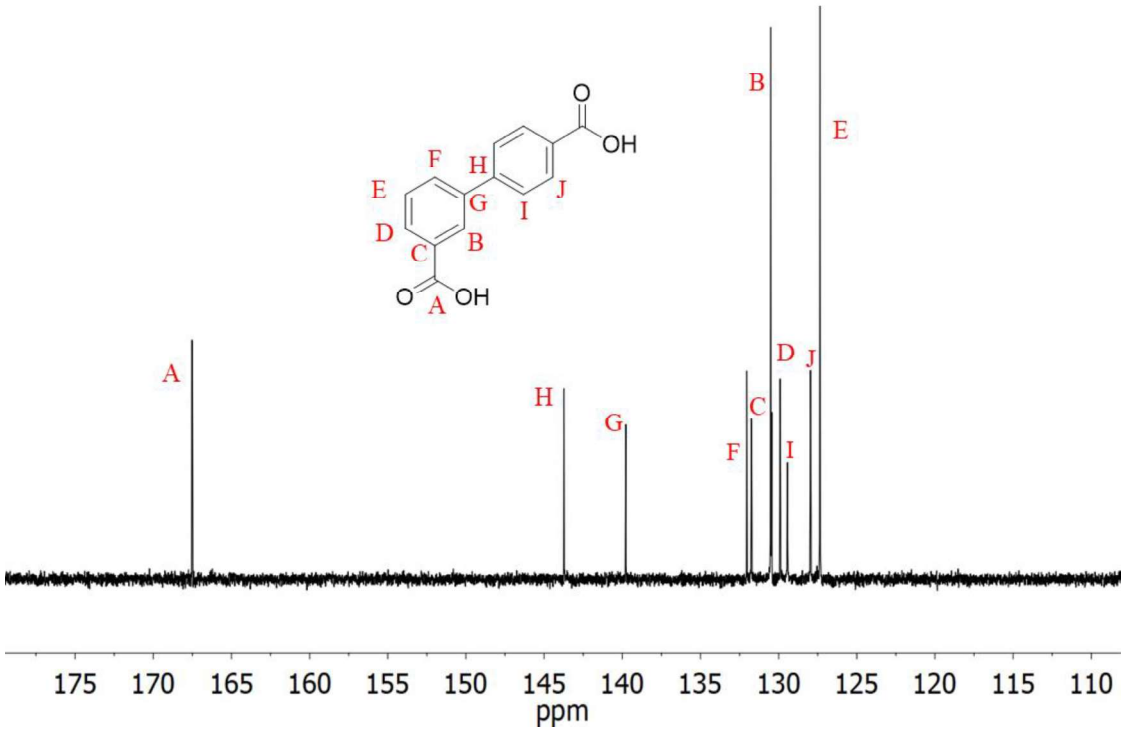

Figure S7.2. ^{13}C NMR spectroscopy (DMSO-d_6, 400 MHz) of biphenyl 3,4'-dicarboxylic acid after successful hydrolysis.

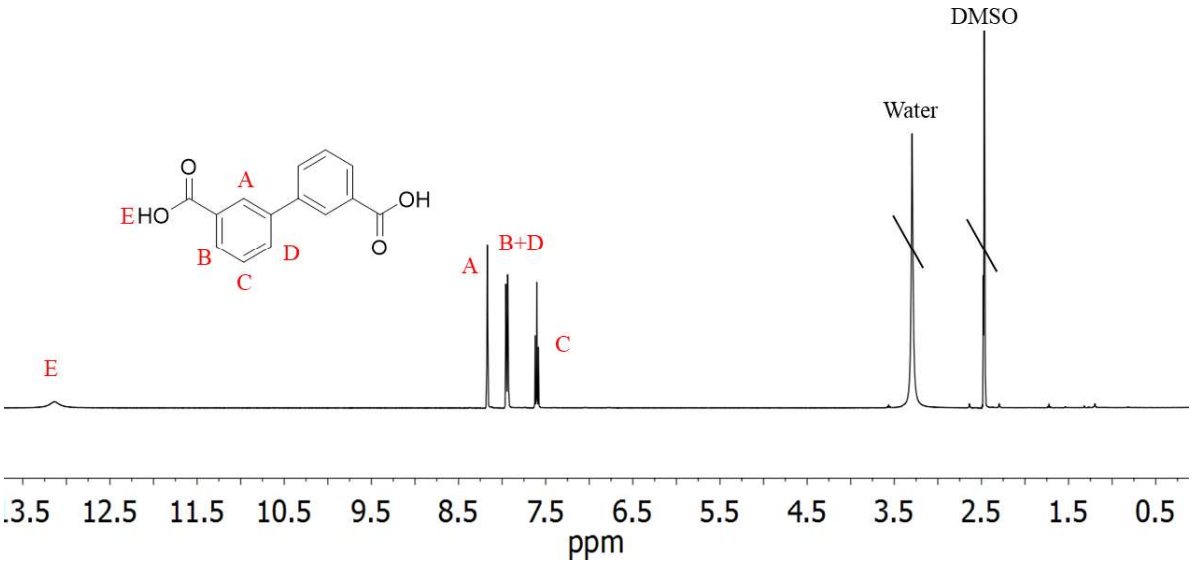

Figure S7.3. ^{1}H NMR spectroscopy (DMSO-d_6, 400 MHz) of biphenyl 3,3'-dicarboxylic acid after successful hydrolysis.

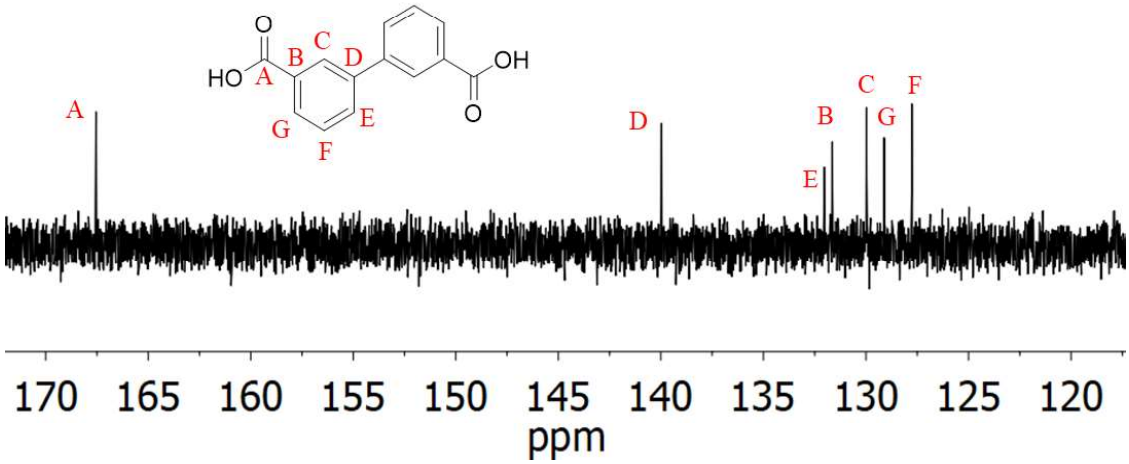

Figure S7.4. ^{13}C NMR spectroscopy (DMSO-d_6, 400 MHz) of biphenyl 3,3'-dicarboxylic acid after successful hydrolysis.

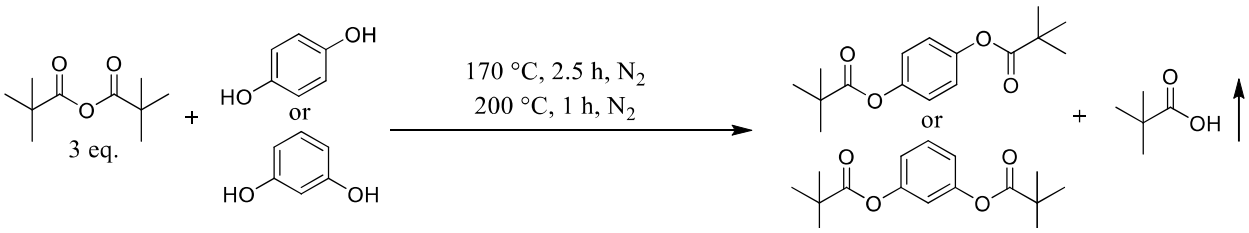

Scheme S7.2. Pivilation of hydroquinone or resorcinol with pivalic anhydride yields hydroquinone dipivilate or resorcinol dipivilate respectively for acidolysis polymerization.

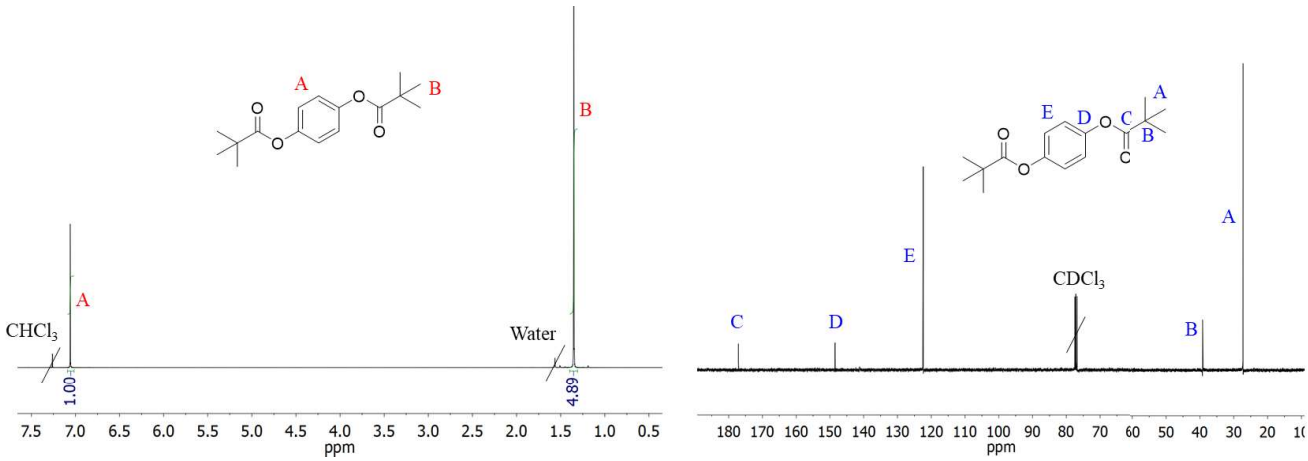

Figure S7.5. ^{1}H and ^{13}C NMR spectroscopy confirms successful pivilation of hydroquinone. Left: Peak assignment and ^{1}H NMR ($CDCl_3$, 400 MHz). Right: Peak assignment and ^{13}C NMR ($CDCl_3$, 400 MHz).

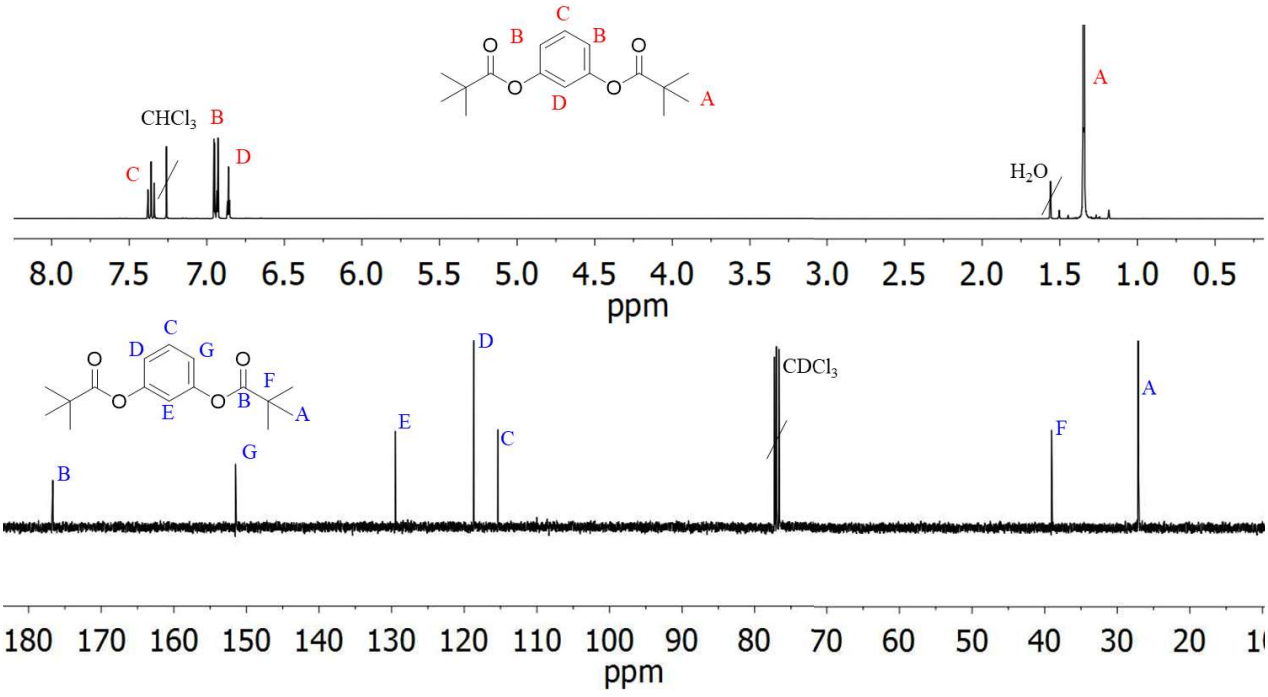

Figure S7.6. ^{1}H and ^{13}C NMR spectroscopy confirms successful pivilation of hydroquinone. Top: Peak assignment and ^{1}H NMR ($CDCl_3$, 400 MHz). Bottom: Peak assignment and ^{13}C NMR ($CDCl_3$, 400 MHz).

Chapter 8: Designing novel semi-aromatic polyesters utilizing dimethyl 3,3'-bibenzoate

(Manuscript in preparation for publication)

Katherine V. Heifferon, Cody W. Weyhrich, Ryan J. Mondschein, and Timothy E. Long

Macromolecules Innovation Institute, Department of Chemistry, Virginia Tech, Blacksburg, VA 24061

Keywords: polyester, melt polymerization, bibenzoate, regioisomers

8.1 Abstract:

Melt polycondensation of dimethyl 3,3'-bibenzoate (3,3'BB) with various linear and cycloaliphatic diols enabled the synthesis of a series of semi-aromatic polyesters. Size exclusion chromatography (SEC) analysis confirmed high molecular weight (M_n > 20 kg/mol). Compression molding resulting in ductile films further established molecular weights desirable for mechanical performance. ^{1}H NMR spectroscopy confirmed each polymer structure and retainment of the *cis/trans* ratios for the cyclohexyldimethylene (CHDM) based polyesters before and after polymerization. Thermogravimetric analysis (TGA) revealed high onset of weight loss temperatures for the novel semi-aromatic polymers ($T_{d,5\%}$ > 380 °C). Differential scanning calorimetry (DSC) and dynamic mechanical analysis (DMA) determined the polymer's glass transition temperatures (T_g) and melting temperatures (T_m). Further evaluation of these thermal transitions against previously synthesized 4,4'BB, 3,4'BB, and isophthalate (IA) based polymers elucidated the structure-property relationships of these systems.

8.2 Introduction:

The tunable thermal properties, good mechanical properties, inexpensive production, and low starting materials costs of semi-aromatic polyesters facilitates their wide use as commodity and specialty materials. After its initial disclosure in 1946,

poly(ethylene terephthalate) (PET) evolved into one of the most produced polyesters in the industry.[1,2] Current production of PET comprises 70% of all global polyester, polyamide, and acrylic fiber production.[3] The food packaging industry heavily relies on PET as barrier materials in the form of biaxial oriented bottles which exhibit recyclability afforded from the hydrolysable nature of the ester moeities.[4,5]

Employing dimethyl 4,4'-bibenzoate (dimethyl 4,4'-biphenyldicarboxylate, 4,4'BB) enables the synthesis of semi-aromatic homopolyesters exhibiting liquid crystalline properties due to the symmetric biphenyl structure.[6,7] Spacing the mesogenic monomer out through the incorporation of flexible aliphatic diols affords a range of liquid crystalline polymer exhibiting smectic morphologies.[6,7] Copolymerization of 4,4'BB with terephthalate generated polymer with higher T_g's, increased mechanical properties, and improved barrier properties relative to PET through the ability to form a highly oriented film.[8-11] Dimethyl 3,4'-bibenzoate (3,4'BB), the kinked regioisomer of 4,4'BB, recently came of interest after a number of studies emerged copolymerizing 4,4'BB and 3,4'BB with various diols. These studies demonstrated improvements to gas permeability and Young's modulus in the amorphous state upon increased incorporation of 3,4'BB.[12-16] This monomer imparted a higher amorphous polymer density as well as an increased entanglement density.[13] Studying the impact of 3,4'BB on 4,4'BB based LCP revealed destabilization of the LC phase at high concentrations of 3,4'BB.[17]

The rise of these studies progressed from the development of a commercially viable pathway to the bibenzoate regioisomers through a green one-pot reaction.[18] This route not only developed a cost reduced method to achieve 4,4'BB and 3,4'BB, but enabled the synthesis of a number of unstudied isomers, such as dimethyl 3,3'-bibenzoate

(3,3'BB). The field of metal organic frameworks remains the primary focus for the limited literature using 3,3'BB.[19-28] In the polymer literature, a single patent using 3,3'BB in the synthesis of novel polyesterimides remains the only source of information.[29] This lack of knowledge identifies a wide area of scientific growth for the structure-property relationships of these regioisomers as polyester units.[29]

In this manuscript, we describe the synthesis of five novel homopolyesters utilizing 3,3'BB and various linear and cycloaliphatic diols. These polymers exhibited a mixture of semi-crystalline and amorphous morphologies with T_g's ranging from 39 to 107 °C. All polymers exhibited $T_{d,5\%}$ of > 380 °C with one-step weight loss profiles. Thermal properties of 4,4'BB, 3,4'BB, and IA based analogues of these homopolymers enabled determination of the structure-property relationships and aided in determining the role of polymer configuration on final material properties. The incorporation of *meta* units resulted in increased chain flexibility facilitating a systematic decrease in the thermomechanical properties. In contrast, the biphenyl structure increased the rigidity of the polymer chains resulting in higher T_g's overall in comparison to IA analogues.

8.3 Experimental:

8.3.1 Materials.

Ethylene glycol (EG) (Sigma-Aldrich, ≥ 99%), 1,6-hexanediol (Sigma-Aldrich, 97%), trifluoroacetic acid-*d* (*d*-TFA) (Sigma-Aldrich, 99.5% atom D), 1,4-*trans*-cyclohexanedimethanol (*t*-CHDM), 1,4-cyclohexanedimethanol (*c/t*-CHDM) **(**Sigma-Aldrich, 99%**),** dimethyl sulfoxide-d_6 (*DMSO-*d_6) (Cambridge Isotope Laboratories, 99.9% atom D), 1,4-butanediol (BD) (Sigma-Aldrich, ≥ 99%), chloroform-*d* ($CDCl_3$) (Cambridge Isotope Laboratories, 99.8% atom D) were used as received. Dimethyl 3,3'-biphenyldicarboxylate (3,3'BB) was provided by Exxon Mobil and used after purification

in hot acetone. All solvents were used as received after purchase from Spectrum. A 0.01g/mL solution of titanium tetra(isopropoxide) (Sigma-Aldrich, 99%) in 1-butanol (Sigma-Aldrich, anhydrous 99.8%) was prepared using a reference procedure.[30]

8.3.2 Analytical Methods.

A Varian Unity 400 at 400 MHz (23 °C) provided both the ^{1}H and ^{13}C nuclear magnetic resonance (NMR) spectroscopy of the monomers and polymers. A Waters e2695 Separations Module Size Exclusion Chromatographer (SEC) with two Shodex KF-806M Columns and one Shodex K-G Guard Column connected to both a Waters 2414 refractive index detector and a Wyatt TREOS II light scattering detector afforded molecular weight information of the polymers. The chloroform soluble polymers were dissolved at a concentration of 1 mg/mL and sampled into the SEC at a flow rate of 1 mL/min at a temperature of 35 °C. Solubility of the polymers in chloroform was confirmed prior to SEC analysis using a Malvern Zetasizer Nano ZS dynamic light scattering instrument. A TA Instruments Q50 thermogravimetric analyzer (TGA) afforded the weight loss profiles for the polymers from 25 to 600 °C, under constant N_2 flow at a heating rate of 10 °C/min. A TA Instruments Q1000 differential scanning calorimeter (DSC) revealed the thermal transitions for the novel polymer under N_2 flow. A heat/cool/heat cycle used rates of 10/100/10 °C/min, respectively, in order to remove thermal history from the material prior to analysis. Analysis of the second heat trace determined the glass transition temperature (T_g) using the inflection point of the step-change. Annealing at 100 °C above each polymer's specific T_g for 1 h then cooling and reheating at a rate of 10 °C/min determined the presence of a melting temperature (T_m)

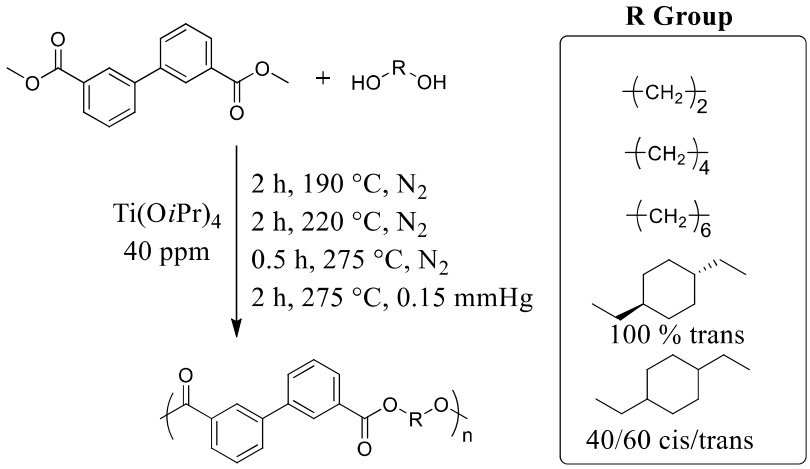

Scheme 8.1. Synthesis of five dimethyl 3,3' bibenzoate (3,3'BB) based homopolymers utilizing different aliphatic spacers (ethylene glycol, butanediol, hexanediol, 100 % *trans*-cyclohexanedimethanol, and *cis/trans*-cyclohexanedimethanol).

which was analyzed using the signal maximum. Calibration of the instrument with indium (T_m = 156.60 °C) and zinc (T_m = 419.47 °C) standards occurred prior to analysis. Compression molding using a heat release cycle at 275 °C afforded free-standing films of the polymer series. A sandwich of aluminum plates, Rexco Partall® Power Glossy Liquid mold release agent coated Kapton™ sheets, and 150 μm thick stainless-steel shims yielded transparent films after quenching in an ice-bath. Dynamic mechanical analysis (DMA) utilized a static force 0.01 N, amplitude of 0.1% strain, frequency of 1 Hz, and a heating rate of 3 °C/min. The instrument used was a TA Instruments Q800 DMA in tension mode. T_g analysis occurred using the maximum of the tan delta. The polymers discussed will be identified as poly(X-3,3'BB) where X refers to the short hand for the chosen diol used in the repeating unit, such as EG for ethylene glycol and BD for butanediol.

8.3.3 Synthesis of poly(X-3,3'BB) series:

Synthesis of the polyester series utilized melt transesterification and polycondensation methods previously demonstrated in our group, shown in **Scheme**

8.1.[12,13,17] Dimethyl 3,3' bibenzoate (8.71 g, 0.032) and the chosen linear aliphatic diol (EG, BD (5.81 g, 0.064 mol), or HD) or 3,3'BB (7.71 g, 0.029 mol) and the chosen cycloaliphatic diol (*t*-CHDM (4.94 g, 0.034 mol) or *c/t*-CHDM) were weighed into a 100-mL round-bottomed flask. The titanium isopropoxide catalyst at a 40-ppm concentration was added to the reaction. The reactor set-up comprised the reaction flask connected to a t-neck adaptor, a metal-stir rod with stir rod adaptor, a mechanical overhead stirrer, and distillation tube with collection flask (100-mL round-bottomed flask). Evacuation with vacuum and back-filling with N_2 provided an inert atmosphere within the reaction set-up. Heating the starting materials at 190 °C for 2 h, 220 °C for 2 h, and 275 °C for 0.5 h facilitated oligomer growth while maintaining a clear homogenous melt. Finally, application of reduced pressure (0.15 mmHg) at 275 °C for 2 h generated a significant viscosity increase in the polymer which was used upon cooling without further purification.

8.4 Results and Discussion:

Melt transesterification and polycondensation enabled the synthesis of the 3,3'BB based polymers utilizing well defined polymerization procedures, depicted in **Scheme 8.1**.[12-14,17,31-33] In previous studies, the titanium isopropoxide catalyst chosen for this polymerization demonstrated catalytic activity towards transesterification.[34] The structure of the diol impacted the amount of excess diol utilized in the polymerization, due to its effect on boiling points and volatility. The linear aliphatic diols (EG, BD, and HD) utilized 2 eq. excess in relation to the diester based on success during the synthesis of poly(BD-4,4'BB) and poly(HD-4,4'BB).[17,35] In contrast both the 100% *trans* and *cis/trans* mixed CHDM used an excess of 1.2 due to the lower volatility of these cyclic monomers.[13,17] The addition of excess diol aids in the initial transesterification of the

Table 8.1. Molecular weight analysis through SEC for the 3,3'BB based polymers in chloroform utilizing a light scattering detector. Chloroform insoluble polymers noted with N/A.

Aliphatic Diol	M_n (kg/mol)	M_w (kg/mol)	Đ M_w/M_n
EG	72.7	137	1.89
BD	36.4	68.4	1.88
HD	N/A	N/A	N/A
100% trans-CHDM	N/A	N/A	N/A
60 % trans-CHDM	24.5	44.1	1.81

diester monomer.[36,37] Heating the reaction from 190-275 °C under N_2 enabled the transesterification of the diester forming methanol as the condensate, which is collected in the condensation flask facilitated tracking of the reaction. The final application of vacuum at 275 °C removed the excess diol inducing polycondensation using Le Chatelier's principle to drive the polymerization to high conversion.[5,38] All polymers achieved a transparent melt throughout the polymerization and experienced a significant viscosity increase upon application of vacuum enabling the material to wrap around the metal stir rod. Poly(EG-3,3'BB), poly(BD-3,3'BB), and poly(*c/t*-CHDM-3,3'BB) remained transparent upon cooling while poly(HD-3,3'BB) and poly(*t*-CHDM-3,3'BB) formed opaque products.

Three of the polymers (EG, BD, *c/t*-CHDM) proved soluble in chloroform enabling SEC analysis with light-scattering and determination of absolute M_w, while M_n was measured from polydispersity indices (Đ), as illustrated in **Table 8.1**. The polymers achieved high molecular weight peaks with M_n ranging from 24.5 to 72.7 kg/mol and PDI's close to 2, as expected for step-growth polymers.[38] While the insolubility of poly(HD-3,3'BB) and poly(*t*-CHDM-3,3'BB) inhibit SEC analysis, these polymers

formed ductile, creaseable films upon compression molding which many studies attribute to the achievement of molecular weight growth above the critical molecular weight.[35,39-41]

^{1}H NMR spectroscopy confirmed the structure of the monomers and polymers (**Figure S8.1-S8.9**). Separation of the proton shifts for CHDM facilitated the determination of the *cis/trans* ratio at 38:62 *cis:trans* for both the monomer and poly(*c/t*-CHDM-3,3'BB). Poly(*t*-CHDM-3,3'BB) exhibited none of the characteristic *cis* proton shifts before or after polymerization. Poly(EG-3,3'BB) demonstrated a small amount of diethylene glycol formation (0.44 mol%), a common occurrence when undergoing a high temperature polymerization with ethylene glycol.[30]

TGA measurements revealed a one-step weight loss profile for all of the 3,3'BB based polymers, as illustrated in **Figure 8.1**. While all polymers exhibited $T_{d,5\%}$ > 380 °C, poly(EG-3,3'BB) revealed the highest value of 417 °C and poly(HD-3,3'BB) provided the lowest at 380 °C. The char yields at 600 °C ranged from 0% for poly(HD-3,3'BB) and to 33% for poly(EG-3,3'BB). The structure of poly(EG-3,3'BB) contains the lowest concentration of aliphatic carbons which presumably contributes to the substantially

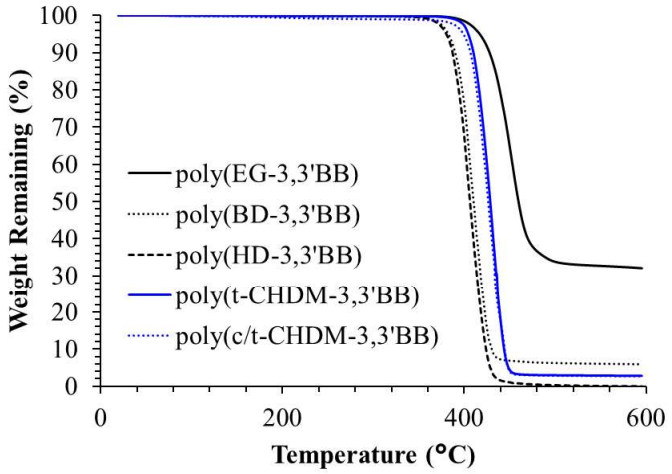

Figure 8.1. Thermogravimetric analysis of the series of 3,3'BB based polymers incorporating a range of linear and cyclic aliphatic diols.

higher char formation and higher $T_{d,5\%}$.

Differential scanning calorimetry revealed the thermal transitions for the polymers with different linear and cycloaliphatic spacers. Preliminary analysis took place on the second heat trace following a quench cool from 275 °C, in an effort to remove thermal history. All polymers produced DSC traces with no endothermic peaks and a broad range of T_g's from 39-107 °C, exemplified in **Table 8.2**. The linear aliphatic series revealed a trend in the T_g with a systematic decrease from 94 °C for poly(EG-3,3'BB) to 39 °C for poly(HD-3,3'BB) as the number of carbons in the aliphatic diol increased. While the molecular weight likely effected the values, the underlying cause of this trend involves the increase in chain flexibility through the incorporation of more methylene units.[38] Comparisons of poly(ethylene terephthalate) (PET) and poly(butylene terephthalate) (PBT) observed a similar drop in the T_g upon addition of a longer spacers.[42-44] CHDM based polymers overall produce higher T_g's relative to the linear diols. Bulky rigid monomers, such as CHDM, previously demonstrated the ability to increase the chain rigidity of polymers resulting in higher T_g's.[13,33,37,45,46]

Table 8.2. Thermal characterization of the series of 3,3'BB based polymers utilizing thermogravimetric analysis, differential scanning calorimetry, and dynamic mechanical analysis.

Aliphatic Diol	T_g (°C)[a]	ΔC_p (W/g)	T_m (°C)	ΔH_m (J/g)	$T_{d,5\%}$	Char Yield (%) at 600 °C	T_g[d] (°C)
EG	94	0.08	N/A[b]	N/A[b]	417	33	93
BD	55	0.08	N/A[b]	N/A[b]	383	6	61
HD	39	0.08	148[b]	46.2[b]	380	0	44
100% trans-CHDM	107	0.15	231[b]	38.9[b]	404	3	110
60% trans-CHDM	99	0.1	N/A[b]	N/A[b]	399	3	100

[a] DSC measurement determined after quench cool
[b] DSC measured after annealing for 1 h at 100 °C above the T_g
[d] Calculated from DMA using quenched films

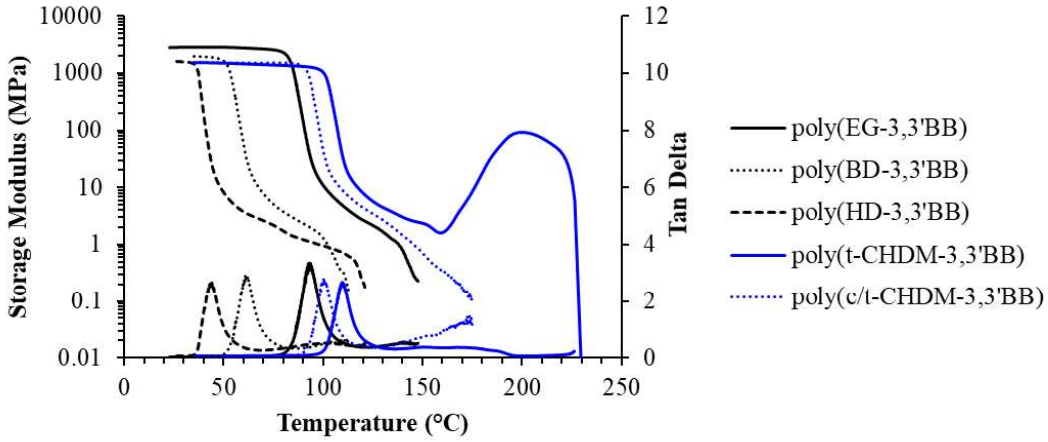

Figure 8.2. Dynamic mechanical analysis of compression molded films produced from the 3,3'BB based polymer series using either linear or cyclic aliphatic diols.

During the first heating trace of poly(HD-3,3'BB) and poly(*t*-CHDM-3,3'BB), one small endothermic transition appeared in each which corroborated with the opaque white appearance of the polymers prior to analysis. These two indicators revealed the polymers semi-crystalline morphology and the necessity to perform annealing studies to understand which polymers form crystalline domains. In an effort to maintain consistency across the different polymers, annealing occurred at 100 °C above each respective T_g. The annealing analysis revealed that only poly(HD-3,3'BB) and poly(*t*-CHDM-3,3'BB) formed semi-crystalline morphologies with T_m*'s* at 148 °C and 231 °C, respectively.

Compression molding the polymer at 275 °C afforded transparent ductile films of all the polymers following a quench cool in an ice bath. DMA facilitated characterization of the thermomechanical properties of the 3,3'BB based polymers, as illustrated in **Figure 8.2**. The T_g's measured from the maximum of the tan delta followed closely with the values determined from DSC. The amorphous polymers (EG, BD, and *c/t*-CHDM) exhibited a short plateau, following the α-relaxation, with flow occurring near 50 °C after the T_g. In contrast, poly(*t*-CHDM-3,3'BB) and poly(HD-3,3'BB) revealed extended

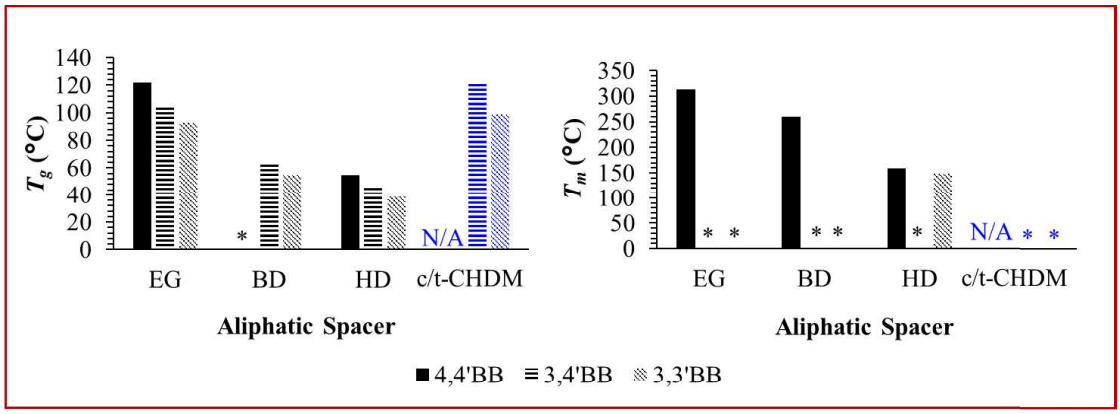

Figure 8.3. Comparison of the thermal transitions determined from DSC for the 3,3'BB polymer series to their polymeric isomers obtained through exchanging the diester monomer for 4,4'BB or 3,4'BB. * notates that the transition could not be observed in the DSC analysis while N/A indicates the values were not available in references.

plateaus with about 100 °C between the T_g and the flow temperature. The polymer flow occurred at a temperature similar to the T_m observed in DSC after annealing. Poly(*t*-CHDM-3,3'BB) experience a unique DMA curve with an increase in the plateau modulus occurring 50 °C after the T_g. This plateau modulus peak fell within the temperature range at which annealing occurred which afforded a semi-crystalline morphology. As a result, this curve presumably represents the crystallization of poly(*t*-CHDM-3,3'BB). Long et al. demonstrated similar DMA curves for polysulfone containing PBT segmented block copolymers, attributing the maximum to crystallization.[32] While poly(HD-3,3'BB) did not experience a drastic plateau modulus spike, the slight inflection observed at 64 °C presumably also indicate crystallization. The visual transition of the samples from clear to opaque following DMA further verified this conclusion.

Comparison of the thermal transitions determined for these polyesters to previously studied materials based on the regioisomers of 3,3'BB (4,4'BB and 3,4'BB) demonstrated a trend for the *meta* units, as illustrated in **Figure 8.3**. A variety of

literature sources and lab made samples (poly(HD-3,4'BB) garnered the thermal transitions for the 4,4'BB and 3,4'BB based polymers when available.[13,17,47] The 4,4'BB based polymers, with the exception of poly(EG-4,4'BB), exhibited smectic liquid crystalline mesophases revealing a second endothermic transition, T_i, observed at temperatures above the T_m. The incorporation of kinks into the aromatic monomers (3,4'BB and 3,3'BB) destabilized the LC mesophase inhibiting its formation, following observations made in previous literature.[17,48]

Analysis of the T_m indicated that the irregular kinked structure also impacted the crystallizability of the polymers. The transition from the linear 4,4'BB regioisomer to either 3,3'BB or 3,4'BB, inhibited the formation of a T_m with the exception of poly(HD-3,3'BB) and poly(*t*-CHDM-3,3'BB). Annealing poly(HD-3,3'BB) enabled the observation of a T_m at a slightly lower temperature to linear poly(HD-4,4'BB). DSC studies of poly(HD-3,4'BB) only occurred after quench cooling therefore under different thermal treatment a semi-crystalline morphology presumably emerges. The hexyl unit combats the hindered formation of semi-crystallinity by decreasing kink relative to EG and BD.

The T_g's of the different regioisomers demonstrated a systematic decrease where 4,4'BB > 3,4'BB > 3,3'BB for all polymer analogues. Previously melt-rheology and thermal studies identified that 4,4'BB increased the rigidity of the polymer affording a stiffer chain which required more energy to undergo segmental motion of the backbone.[12,13] In contrast, *meta* moieties impart more flexible chains resulting in lower T_g's.

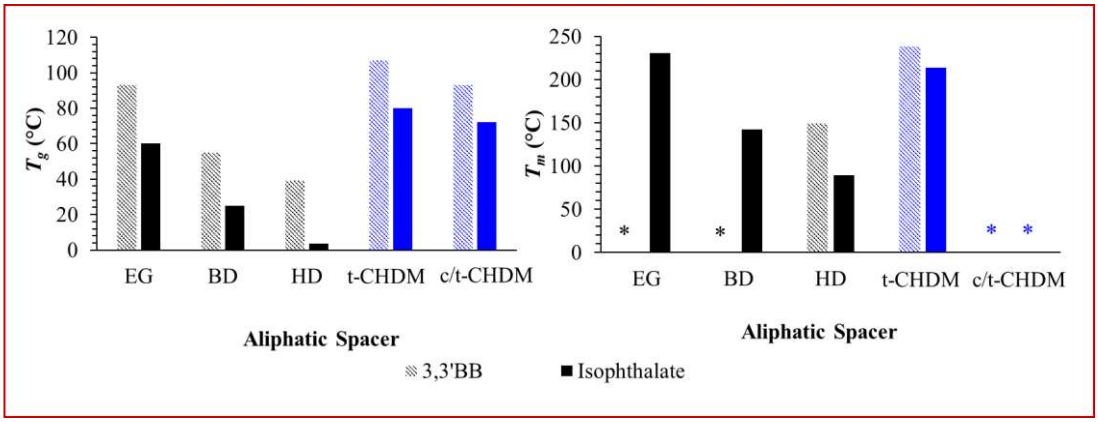

Figure 8.4. Comparison of the thermal transitions determined from DSC for the 3,3'BB polymer series to the equivalent polymer after exchanging the diester monomer for isophthalate. * identifies that the transition could not be observed in the DSC analysis.

Literature values for IA based polymer analogues of the 3,3'BB series revealed further structure-property relationships for the prepared polymers, shown in **Figure 8.4**, though the DSC methods fluctuated between studies.[14,49,50] The structure of 3,3'BB closely resembles that of IA with two linked benzene rings instead of a single phenyl group in the *meta* configuration. The biphenyl structure afforded a higher chain rigidity in comparison to IA resulting in systematically higher T_g's for 3,3'BB based polymers. The secondary kink within the biphenyl monomer also reduces the crystallizability of the polymers inhibiting the observation of a T_m for poly(EG-3,3'BB) and poly(BD-3,3'BB). In contrast, both poly(EG-IA) and poly(BD-IA) exhibited semi-crystalline morphologies with T_m's at 231 °C and 142 °C. The exchange from two to one ring for HD and *t*-CHDM, polymers which exhibited semi-crystalline morphologies using either 3,3'BB or IA, facilitated a decrease in the T_m. PBT and poly(BD-4,4'BB) exhibited similar trends revealing T_m's of 222 °C and 250 °C, respectively.[6,32]

8.5 Conclusions:

The melt transesterification and polycondensation of 3,3'BB with a variety of linear and cycloaliphatic diols afforded a series of novel semi-aromatic polyesters. ^{1}H

NMR spectroscopy enabled the structural analysis of the materials before and after polymerization confirming no isomerization occurred with CHDM. SEC analysis of the soluble materials revealed that these polymers achieved high molecular weights with PDI's close to 2. The formation of ductile films through compression molding further confirmed this for the entire series. DSC and DMA generated the thermal and thermomechanical analysis of the polymers. Trends emerged consistent with previous literature demonstrating lower T_g*'s* for more flexible diols with longer linear aliphatic chains. Poly(*c/t*-CHDM-3,3'BB) exhibited the highest T_g of 107 °C coming close to the thermal properties desired in high performance polyesters. Comparing the 3,3'BB based polymers its regioisomers revealed a T_g trend in which 4,4'BB > 3,4'BB > 3,3'BB for all analogues. Finally, the biphenyl structure of 3,3'BB resulted in systematically higher T_g's than IA based polymers while the biphenyl *meta* structure also imparted a lower crystallizability.

Acknowledgments:

The authors thank Dr. Ryan Mondschein, Emily Wilts, and Clay Arrington for insightful discussions.

Funding:

This work was sponsored by ExxonMobil Chemical Company.

Notes:

The authors declare no competing financial interest.

References:

(1) Whinfield, J. R., Chemistry of 'Terylene', *Nature* **1946**, *158*, 930.
(2) Whinfield, J. R.; Dickson, J. T., British Patent 578,079, June 16, 1946.
(3) Geyer, R.; Jambeck, J. R.; Law, K. L., Production, use, and fate of all plastics ever made, *Science Advances* **2017**, *3*.

(4) Ji, L. N., Study on Preparation Process and Properties of Polyethylene Terephthalate (PET), *Applied Mechanics and Materials* **2013**, *312*, 406.
(5) Scheirs, J.; Long, T. E., *Modern polyesters: chemistry and technology of polyesters and copolyesters*; John Wiley: Hoboken, NJ;Chichester, England;, 2003.
(6) Tokita, M.; Watanabe, J., Several Interesting Fields Exploited through Understanding of Polymeric Effects on Liquid Crystals of Main-Chain Polyesters, *Polymer Journal* **2006**, *38*, 611.
(7) Krigbaum, W. R.; Asrar, J.; Toriumi, H.; Ciferri, A.; Preston, J., Aromatic polyesters forming thermotropic smectic mesophases, *Journal of Polymer Science: Polymer Letters Edition* **1982**, *20*, 109.
(8) Liu, R. Y. F.; Hu, Y. S.; Hibbs, M. R.; Collard, D. M.; Schiraldi, D. A.; Hiltner, A.; Baer, E., Comparison of statistical and blocky copolymers of ethylene terephthalate and ethylene 4,4′-bibenzoate based on thermal behavior and oxygen transport properties, *Journal of Polymer Science, Part B: Polymer Physics* **2003**, *41*, 289.
(9) Schiraldi, D.; Lee, J.; A. C. Gould, S.; L. Occelli, M., *Mechanical Properties and Atomic Force Microscopic Cross Section Analysis of Injection Molded Poly(ethylene terephthalate/ethylene 4,4-bibenzoate)*, 2001; Vol. 7.
(10) Liu, R. Y. F.; Schiraldi, D. A.; Hiltner, A.; Baer, E., Oxygen-barrier properties of cold-drawn polyesters, *Journal of Polymer Science, Part B: Polymer Physics* **2002**, *40*, 862.
(11) Liu, H.; Mondschein, R. J.; Chen, T.; Long, T. E.; Turner, S. R., Terephthalate-co-bibenzoate polyesters. WO 2017/112031 A1, June 29, 2017.
(12) Mondschein, R. J.; Dennis, J. M.; Liu, H.; Ramakrishnan, R. K.; Nazarenko, S.; Turner, S. R.; Long, T. E., Synthesis and Characterization of Amorphous Bibenzoate (Co)polyesters: Permeability and Rheological Performance, *Macromolecules* **2017**, *50*, 7603.
(13) Mondschein, R. J.; Dennis, J. M.; Liu, H.; Ramakrishnan, R. K.; Sirrine, J. M.; Weiseman, T.; Colby, R. H.; Nazarenko, S.; Turner, S. R.; Long, T. E., Influence of Bibenzoate Regioisomers on Cyclohexanedimethanol-Based (Co)polyester Structure–Property Relationships, *Macromolecules* **2019**.
(14) Edling, H. E.; Liu, H.; Sun, H.; Mondschein, R. J.; Schiraldi, D. A.; Long, T. E.; Turner, S. R., Copolyesters based on bibenzoic acids, *Polymer* **2018**, *135*, 120.
(15) Eliot Edling, H.; Mondschein, R. J.; Davis, M. K.; Long, T. E.; Richard Turner, S., Amorphous copolyesters based on bibenzoic acids and neopentyl glycol, *Journal of Polymer Science, Part A: Polymer Chemistry* **2019**, *57*, 579.
(16) Polyakova, A.; Liu, R. Y. F.; Schiraldi, D. A.; Hiltner, A.; Baer, E., Oxygen-barrier properties of copolymers based on ethylene terephthalate, *Journal of Polymer Science, Part B: Polymer Physics* **2001**, *39*, 1889.
(17) Heifferon, K. V.; Mondschein, R. J.; Talley, S. J.; Moore, R. B.; Turner, S. R.; Long, T. E., Tailoring the glassy mesophase range of thermotropic polyesters through copolymerization of 4,4'-bibenzoate and kinked isomer, *Polymer* **2019**, *163*, 125.
(18) Clary, R. S.; Lee, C. D.; IV, W. G. M.; Vaughn, D. A.; Ragheb, R. T.; III, J. W. E.; Brown, D. M.; Schiraldi, D. A., A Green, One-Pot Route to the

Biphenyldicarboxylic Acids: Useful Intermediates in Polymer Synthesis, *International Journal of Organic Chemistry* **2013**, *Vol.03No.02*, 5.
(19) Blagg, B. S. J.; Kusuma, B. R., Dynamic inhibitors of heat shock protein 90.
(20) Fan, T.-T.; Li, J.-J.; Qu, X.-L.; Han, H.-L.; Li, X., Metal(II)-organic frameworks with 3,3'-diphenyldicarboxylate and 1,3-bis(4-pyridyl)propane: preparation, crystal structures and luminescence, *CrystEngComm* **2015**, *17*, 9443.
(21) Kusuma, B. R.; Peterson, L. B.; Zhao, H.; Vielhauer, G.; Holzbeierlein, J.; Blagg, B. S. J., Targeting the Heat Shock Protein 90 Dimer with Dimeric Inhibitors, *Journal of Medicinal Chemistry* **2011**, *54*, 6234.
(22) Liu, B.; Shi, J.; Yue, K.-F.; Li, D.-S.; Wang, Y.-Y., Distinct Temperature-Dependent CO2 Sorption of Two Isomeric Metal-Organic Frameworks, *Crystal Growth and Design* **2014**, *14*, 2003.
(23) Park, J. S.; Yoon, Y. J.; Park, C. M.; Na, Y. S.; Cho, M. J.; Lee, H. B.; Han, M. R.; Park, Y. J.; Kim, J. D., Preparation of pyridinylhydrazide derivatives as antifungal agents. WO2015034271A1, **2015**.
(24) Qian, J.; Jiang, F.; Su, K.; Li, Q.; Yuan, D.; Hong, M., Self-Assembly of Polyhedral Indium-Organic Nanocages, *Inorganic Chemstry* **2014**, *53*, 12228.
(25) Qian, J.; Jiang, F.; Su, K.; Li, Q.; Zhou, K.; Wu, M.; Yuan, D.; Hong, M., Sorption comparison of two indium-organic framework isomers with syn-anti configurations, *CrystEngComm* **2014**, *16*, 7434.
(26) Wang, G., Crystal structure of catena-[pyridine-μ-biphenyl-3,3'-dicarboxylato-κ4O,O':O",O'"-zinc(II)], C61H37NO16Zn4, *Z. Kristallogr. - New Cryst. Struct.* **2013**, *228*, 425.
(27) Wang, H. B.; Wu, Y. P.; Xu, G. W.; Wang, J. F.; Guo, S. S., Three new Co(II)/Ni(II) cordination polymers based on 3,3-biphenyl dicarboxylic acid and N-donor Co-ligands: Synthesis, crystal structures and magnetic properties, *Russian Journal of Coordination Chemistry* **2015**, *41*, 664.
(28) Zhang, Q.; Li, W.; Li, X., Heterocyclic compounds containing bis(2-sulfonyl-1,3,4-oxadiazol-5-yl) and their preparation, agricultural compositions and use in the treatment of plant diseases. CN103864711A, **2014.**
(29) Gu, A.; Guan, Q.; Liang, G.; Yuan, L., Aromatic polyesterimide with good processability and mechanical properties and preparation method thereof. CN106810695A, **2017**.
(30) Kang, H.; Lin, Q.; Armentrout, R. S.; Long, T. E., Synthesis and Characterization of Telechelic Poly(ethylene terephthalate) Sodiosulfonate Ionomers, *Macromolecules* **2002**, *35*, 8738.
(31) Eliot Edling, H.; Mondschein, R. J.; Davis, M. K.; Long, T. E.; Richard Turner, S., Amorphous copolyesters based on bibenzoic acids and neopentyl glycol, *J. Polym. Sci., Part A: Polym. Chem.*, *0*.
(32) Dennis, J. M.; Fahs, G. B.; Moore, R. B.; Turner, S. R.; Long, T. E., Synthesis and Characterization of Polysulfone-Containing Poly(butylene terephthalate) Segmented Block Copolymers, *Macromolecules* **2014**, *47*, 8171.
(33) Dennis, J. M.; Enokida, J. S.; Long, T. E., Synthesis and Characterization of Decahydronaphthalene-Containing Polyesters, *Macromolecules* **2015**, *48*, 8733.
(34) Rogers, M. E.; Long, T. E., *Synthetic Methods in Step-Growth Polymers*.

(35) Nelson, A. M.; Fahs, G. B.; Moore, R. B.; Long, T. E., High-Performance Segmented Liquid Crystalline Copolyesters, *Macromolecular Chemistry and Physics* **2015**, n/a.
(36) Zhang, M.; Moore, R. B.; Long, T. E., Melt transesterification and characterization of segmented block copolyesters containing 2,2,4,4-tetramethyl-1,3-cyclobutanediol, *Journal of Polymer Science, Part A: Polymer Chemistry* **2012**, *50*, 3710.
(37) Kelsey, D. R.; Scardino, B. M.; Grebowicz, J. S.; Chuah, H. H., High Impact, Amorphous Terephthalate Copolyesters of Rigid 2,2,4,4-Tetramethyl-1,3-cyclobutanediol with Flexible Diols, *Macromolecules* **2000**, *33*, 5810.
(38) Odian, G. G., *Principles of polymerization*; Wiley: New York, 1991.
(39) Arnold, F. E.; Van Deusen, R. L., Preparation and Properties of High Molecular Weight, Soluble Oxobenz[de]imidazobenzimidazoisoquinoline Ladder Polymer, *Macromolecules* **1969**, *2*, 497.
(40) Yeh, J.-M.; Liou, S.-J.; Lai, C.-Y.; Wu, P.-C.; Tsai, T.-Y., Enhancement of Corrosion Protection Effect in Polyaniline via the Formation of Polyaniline−Clay Nanocomposite Materials, *Chemistry Materials* **2001**, *13*, 1131.
(41) Dobkowski, Z., Determination of critical molecular weight for entangled macromolecules using the tensile strength data, *Rheologica Acta* **1995**, *34*, 578.
(42) Bikiaris, D. N.; Karayannidis, G. P., Thermomechanical analysis of chain-extended PET and PBT, *Journal of Applied Polymer Science* **1996**, *60*, 55.
(43) Cheng, S. Z. D.; Pan, R.; Wunderlich, B., Thermal analysis of poly(butylene terephthalate) for heat capacity, rigid-amorphous content, and transition behavior, *Die Makromolekulare Chemie* **1988**, *189*, 2443.
(44) Avramova, N., Amorphous poly(ethylene terephthalate)/poly(butylene terephthalate) blends: miscibility and properties, *Polymer* **1995**, *36*, 801.
(45) Dennis, J. M.; Fazekas, N. A.; Mondschein, R. J.; Ramakrishnan, R.; Nazarenko, S.; Long, T. E., Influence of cyclobutane segments in cycloaliphatic decahydronaphthalene-containing copolyesters, *High Performance Polymers* **2017**, *29*, 750.
(46) Iyer, K. A., Chain mobility, secondary relaxation, and oxygen transport in terephthalate copolyesters with rigid and flexible cyclic diols, *Polymer* **2017**, *129*, 117.
(47) Wendling, J.; Gusev, A. A.; Suter, U. W.; Braam, A.; Leemans, L.; Meier, R. J.; Aerts, J.; Heuvel, J. v. d.; Hottenhuis, M., Crystal Morphology and Thermodynamics of Poly(ethylene-4,4‘-biphenyl dicarboxylate) and Related Copolymers with Ethylene-2,6-naphthalene Dicarboxylate, *Macromolecules* **1999**, *32*, 7866.
(48) Chung, T., *Thermotropic liquid crystal polymers: thin-film polymerization, characterization, blends, and applications*; Technomic Pub. Co: Lancaster, Pa, 2001.
(49) Weidner, S. M.; Kricheldorf, H. R.; Scheliga, F., Cyclization and dispersity of poly(alkylene isophthalate)s, *J. Polym. Sci., Part A: Polym. Chem.* **2016**, *54*, 197.
(50) June, S. M.; Bissel, P.; Long, T. E., Segmented block copolyesters using click chemistry, *Journal of Polymer Science, Part A: Polymer Chemistry* **2012**, *50*, 3797.

Supporting Information:

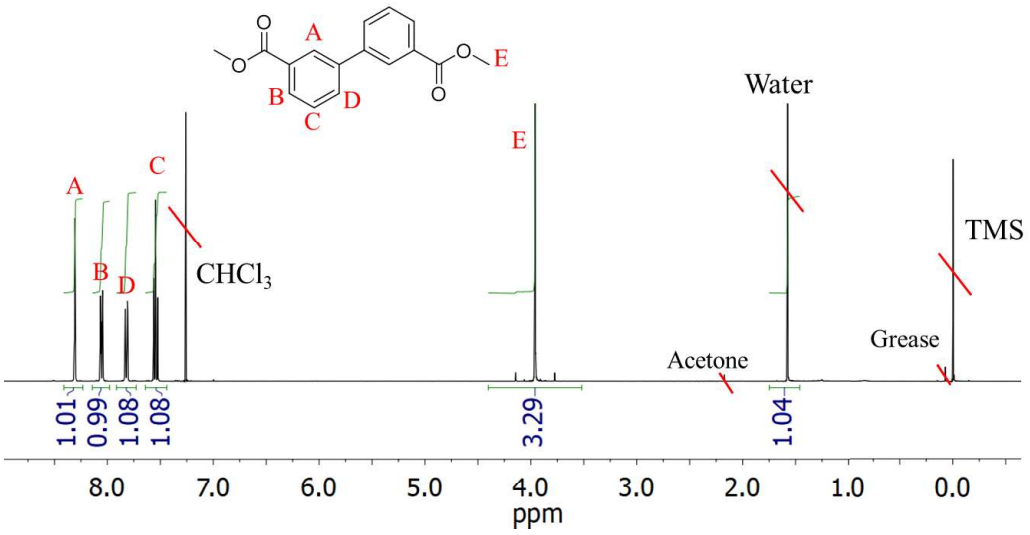

Figure S8.1. ^{1}H NMR spectroscopy ($CDCl_3$, 400 MHz) of dimethyl 3,3'-bibenzoate after successful purification.

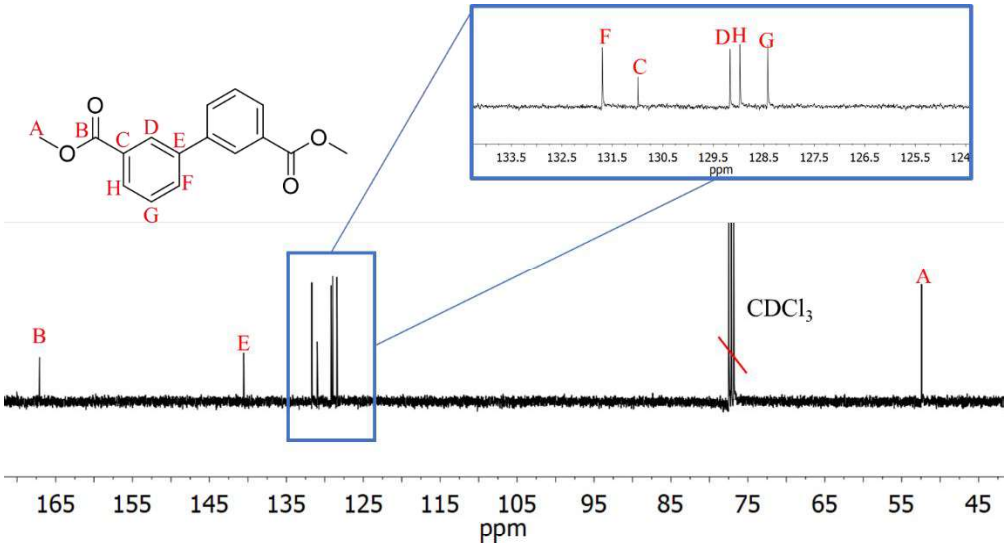

Figure S8.2. ^{13}C NMR spectroscopy ($CDCl_3$, 400 MHz) of dimethyl 3,3'-bibenzoate (3,3'BB) after successful purification.

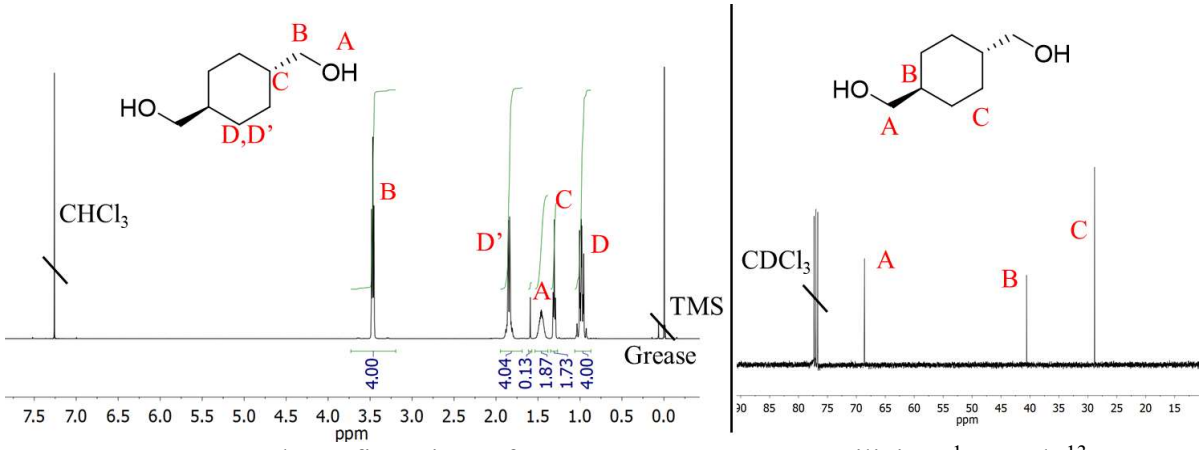

Figure S8.3. Structural confirmation of 100 % *trans*-CHDM utilizing ^{1}H and ^{13}C NMR spectroscopy. Left: Peak assignment and ^{1}H NMR ($CDCl_3$, 400 MHz). Right: Peak assignment and ^{13}C NMR ($CDCl_3$, 400 MHz).

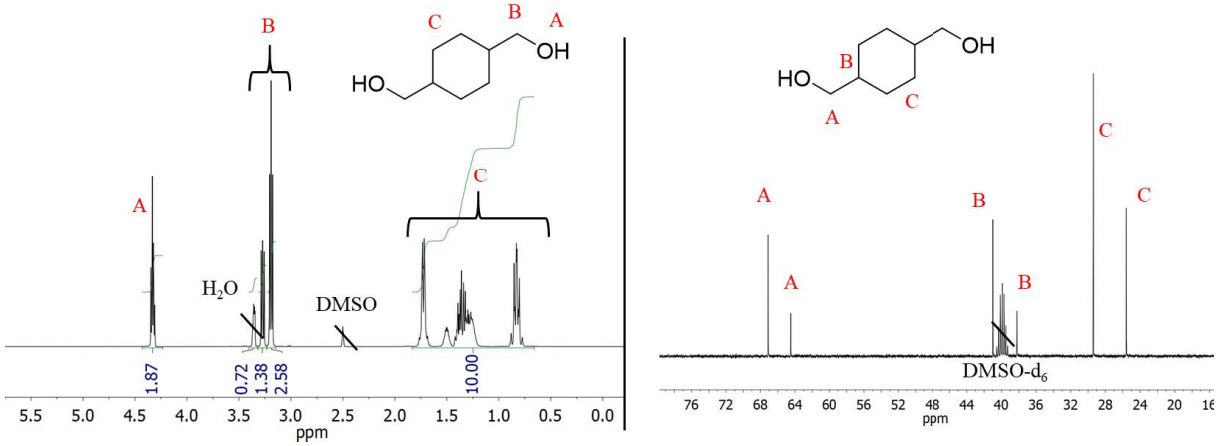

Figure S8.4. Structural confirmation of CHDM with a *cis/trans* mixtures utilizing ^{1}H and ^{13}C NMR spectroscopy. Left: Peak assignment and ^{1}H NMR (DMSO-d_6, 400 MHz). Right: Peak assignment and ^{13}C NMR (DMSO-d_6, 400 MHz).

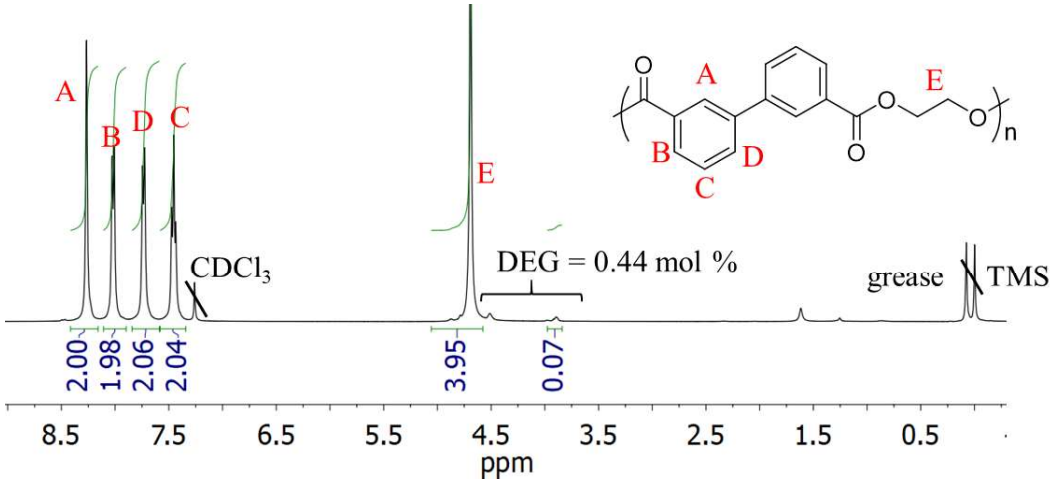

Figure S8.5. ^{1}H NMR spectroscopy ($CDCl_3$, 400 MHz) of poly(ethylene 3,3' bibenzoate).

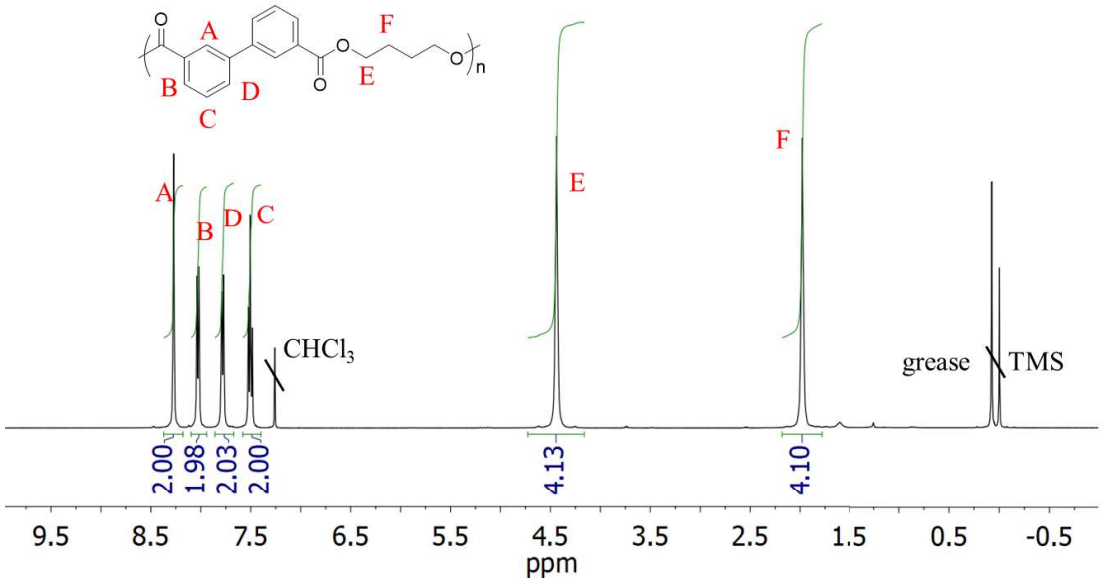

Figure S8.6. ^{1}H NMR spectroscopy ($CDCl_3$, 400 MHz) of poly(butylene 3,3' bibenzoate).

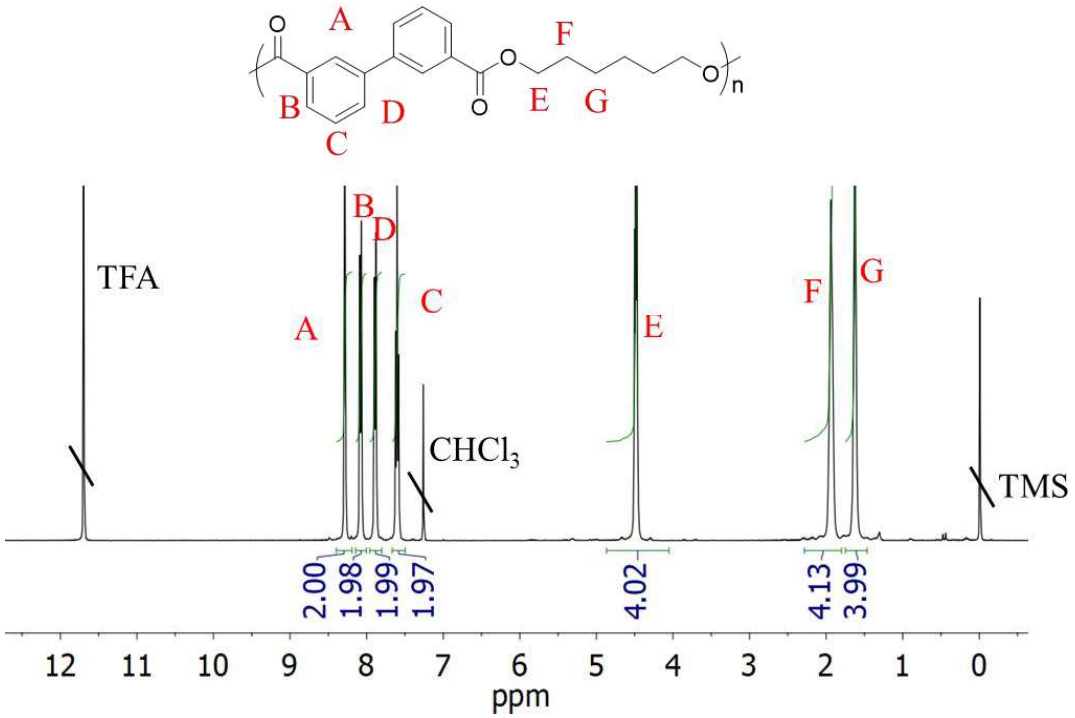

Figure S8.7. ^{1}H NMR spectroscopy (TFA-*d:*$CDCl_3$, 400 MHz) of poly(hexamethylene 3,3' bibenzoate).

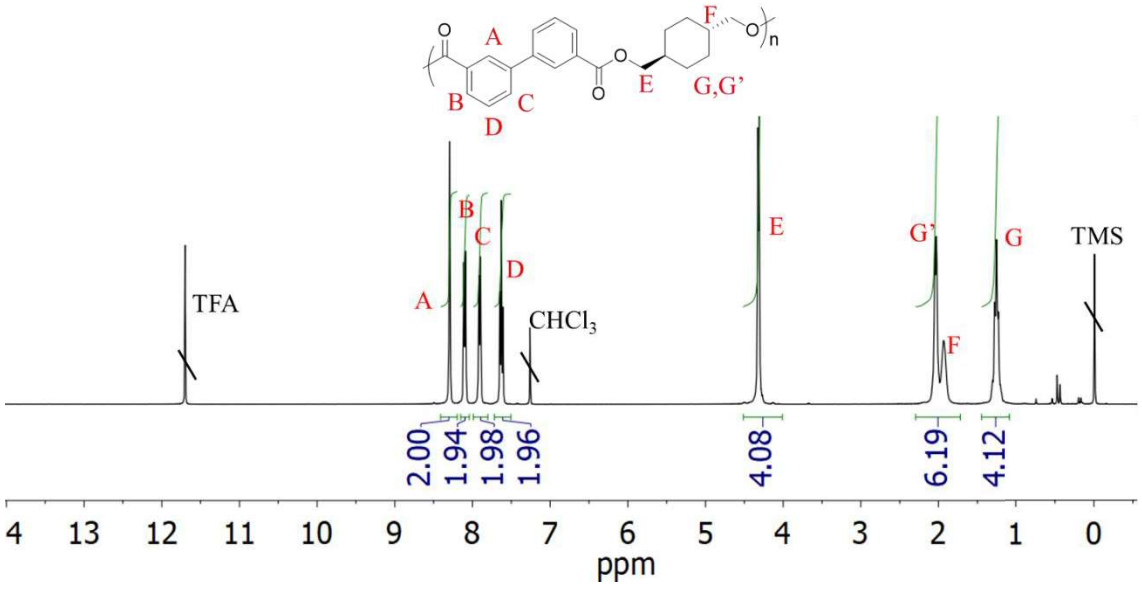

Figure S8.8. ^{1}H NMR spectroscopy (TFA-*d:*$CDCl_3$, 400 MHz) of poly(*t*-CHDM-3,3'BB).

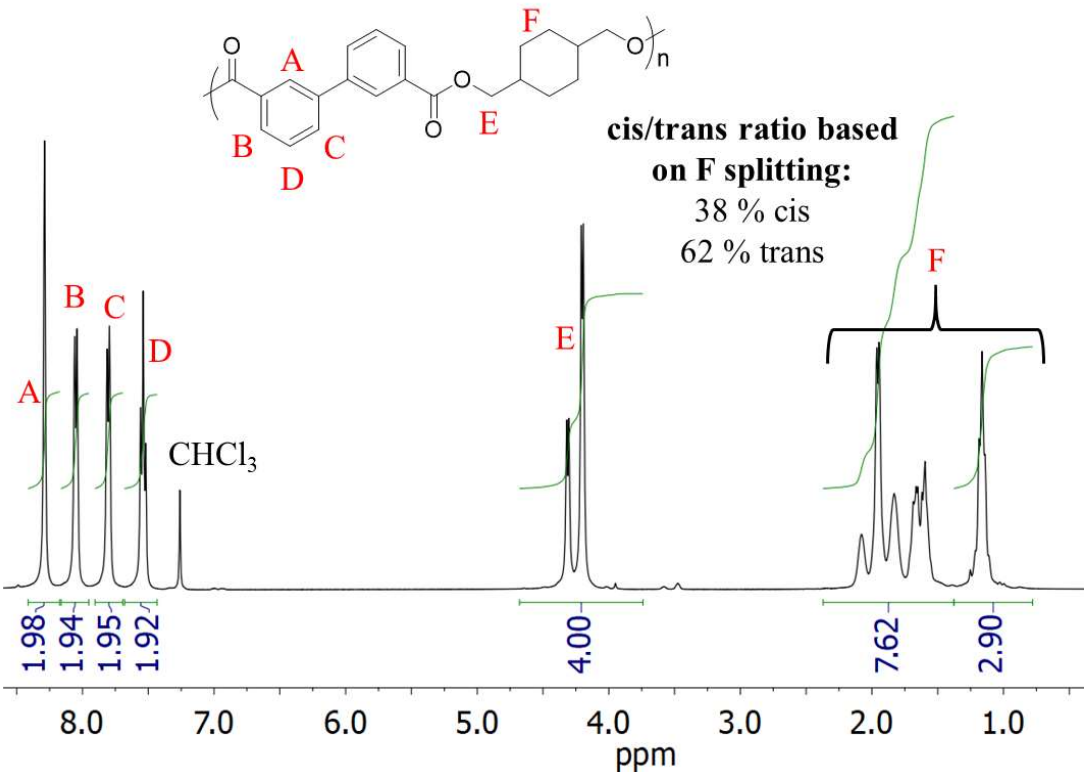

Figure S8.9. ^{1}H NMR spectroscopy ($CDCl_3$, 400 MHz) of poly(*c/t*-CHDM-3,3'BB).

Chapter 9: Molecular design of polyarylene ether sulfones for stereolithographic based 3D printing via telechelic functionalization

Katherine V. Heifferon[1], Clay B. Arrington[1], Cody W. Wehyrich[1], Justin M. Sirrine[1], Viswanath Meenakshisundaram[2], Nicholas A. Chartrain[2], Christopher B. Williams[2], and Timothy E. Long[1]

[1]*Department of Chemistry and Macromolecules Innovation Institute (MII), Virginia Tech, Blacksburg, VA 24061, United States*
[2]*Department of Mechanical Engineering and Macromolecules Innovation Institute (MII), Virginia Tech, Blacksburg, Virginia 24061, United States*

Keywords: 3D printing, polysulfones, vat photopolymerization

9.1 Abstract:

Vat photopolymerization (VPP) represents an advance manufacturing technique that provides complex 3D structures unachievable through traditional processing techniques. Telechelic functionalization of polysulfones provided a route to processing through VPP. Two molecular weight series (6, 10 and 20 kg/mol) of polysulfones, either phenol-terminated or hydroxyethyl-terminated, provided a handle for the attachment of a photocurable acrylate moieties. Differential scanning calorimetry (DSC) and thermogravimetric analysis (TGA) revealed the thermal properties of the polymers while advanced permeation chromatography (APC) characterized the molecular weight prior to functionalization with acrylate groups. Photorheology and photoDSC determined the photocuring kinetics of the two series concluding that the ethyl spacer does not provide significant benefit to the acrylate homopolymerization. A 30 wt% solution of the acrylate-terminated PSU with a M_n of 6 kg/mol, 1 wt% photoinitiator, and 0.05% avobenzone afforded a well-defined lattice structure using VPP.

9.2 Introduction:

Research into additive manufacturing (AM), also commonly referred to as 3D printing, boomed in the early 2000's following the expiration of a number of patents from the 1980's; enabling the formation of a large range of commercially available machines.[1] These manufacturing technique generates complex geometries unattainable through traditional manufacturing methods.[2,3] Expansion of the research in AM stimulated the design of many types of 3D printing systems varying in printing parameters and material choice. A few of these systems include material extrusion, powder bed fusion, vat photopolymerization, material jetting, binder jetting, sheet lamination, and directed energy deposition.[4]

Charles Hull of 3D system Corp. first developed vat photopolymerization (VPP) in 1984. VPP utilizes photo-curable materials which transition from a liquid resin to a solid gel structure upon selective exposure to UV-light.[4,5] Patterned UV-light creates a selective design on the surface of the resin, enabling controlled curing and an intricate, high-resolution 3D part through a layer-by-layer process.[3] A combination of machine design and material selection contributed to VPP achieving the highest part resolution relative to other AM technique. As a result, applications requiring miniaturized parts, such as intricate cell scaffolds, feature VPP.[3,4,6,7] The wide range of material types capable of processing through VPP emphasizes the diversity of this technique. Dependent on resin choice, VPP achieves a range of final material properties from high performance thermoplastics (Kapton®) to flexible elastomers.[3,8-13]

Resin requirements revolve around the necessity to covalently crosslink upon exposure to UV-light. Photoinitiators, included at low concentrations in the polymer resin, form reactive intermediates (radicals, anions, or cations) upon UV irradiation

enabling the chain-growth polymerization of reactive moieties, such as acrylate groups. Many previous studies feature 2,2-dimethoxy-2-phenyl-acetophenone (DMPA) and diphenyl(2,4,6-trimethylbenzoyl) phosphine oxide (TPO) as photoinitiators in VPP due to their UV absorption occurring between 300 – 400 nm, equivalent to the machine's optical capabilities.[14-16] Alternatively, the photopolymer instead may contain naturally UV-initiating functional group eliminating the need for a photoinitiator.[17]

Low molecular weight or monomeric photo-curable precursors based on acrylate functional groups typically constitute the commercially available resins.[18-20] These result in high crosslink densities and low molecular weight between crosslinks (M_c) inevitably resulting in high modulus parts that often exhibit brittle failure at low strain.[20,21] A number of studies proved that higher M_c improves the elastic restoring force and enables chain uncoiling and recoiling upon macroscopic deformation, affording materials with higher toughness.[3,8,9,22] In order to achieve high M_c, the detrimental increase in viscosity that occurs through use of high molecular weight polymers must be overcome, as it impact the recoating process during VPP.[3,19,23] Efforts to lower viscosity into a printable range focus on the use of diluents, either reactive or non-reactive. Reactive diluents participate in the crosslinking mechanism becoming part of the network ultimately resulting in altered final part properties. Unreactive diluents, such as solvents, do not participate in the reaction enabling their removal at the end of the printing process.[24-26] A few studies demonstrated benefits in improving final part resolution and layer consolidation through formation of an organogel as the greenbody part followed by solvent removal.[11,12]

Polysulfones (PSU) represent a type of high-performance thermoplastic desirable for its clarity, high thermal stability, and chemical resistance. Applications such as fiber membrane resins for water purification, kidney dialysis, and desalination separation preferably utilize Udel® PSU.[27] Udel® PSU utilizes the monomers bisphenol A (BPA) and dichlorodiphenyl sulfone (DCDPS) to generate a high T_g polymer (190 °C) through nucleophilic aromatic substitution. Telechelic functionalization of PSU's with acrylates impart photo-curability while maintaining high M_c. A variety of studies focused on the telechelic functionalization of PSU through endcapping with a monofunctional *m*-aminophenol during the polymerization. Post-polymerization functionalization of the amine afforded acrylamides, ethynyl phthalic anhydrides, and maleic anhydrides. These functional group provided thermal and photo-curability enabling reduced swelling and water uptake in the final membranes.[28,29]

This manuscript demonstrates the first instance of 3D printing a polysulfone through VPP. Phenol-terminated polysulfones were synthesized using solution polymerization of BPA and DCDPS using a selective excess of BPA to afford a range of M_n (6, 10 or 20 kg/mol). Post-polymerization functionalization of the phenol with ethylene carbonate afforded a hydroxyethyl-terminated PSU to characterize the impact of the ethyl spacer on the photo-curing kinetics. Further derivatization of both alcohol-terminated PSU's with acryloyl chloride afforded acrylate moieties. Photocalorimetry and photorheology of the acrylate-terminated PSU in solutions with N-methylpyrrolidone (NMP) enabled characterization of the photopolymerization. VPP afforded a lattice scaffold structure with defined resolution using the 6000 g/mol acrylate-terminated PSU.

9.3 Experimental:

9.3.1 Materials.

N,N-dimethylacetamide (DMAc) (anhydrous 99.8%), Celite® filter agent, aluminum oxide activated basic Brockmann I, ethylene carbonate (98%), potassium carbonate (K_2CO_3), diphenyl(2,4,6-trimethylbenzoyl) phosphine oxide (TPO) (97%), acryloyl chloride (≥97%), and 2,2-dimethoxy-2-phenyl-acetophenone (DMPA) (99%) were purchased from Sigma-Aldrich and used as received. Sodium hydroxide, N-methylpyrrolidinone (NMP), hydrochloric acid, chloroform ($CHCl_3$) (HPLC Grade), toluene, and sodium chloride were used as received from Fisher Chemical. Sodium bicarbonate, N,N-dimethylformamide (DMF) (Spectrophotometric Grade A.C.S.), magnesium sulfate (Mg_2SO_3) (anhydrous, contains ~400 ppm phenothiazine as stabilizer) were used as received from Spectrum. Chloroform-*d* ($CDCl_3$) (99.8% atom D) and oxybenzone (avobenzone) were purchased from Cambridge Isotope Laboratories and Making Cosmetics, respectively, and used as received. Bis(4-chlorophenyl) sulfone (DCDPS) (98%) and bisphenol A (BPA) (≥ 99 %) were purchased from Sigma Aldrich and recrystallized in toluene prior to use. Triethylamine (TEA) (Sigma-Aldrich, ≥99%) was stirred over calcium hydride (Sigma-Aldrich, 95%) overnight then distilled at 90 °C prior to use.

9.3.2 Analytical Methods.

^1H and ^{13}C nuclear magnetic resonance (NMR) spectroscopy of the polymers occurred in $CDCl_3$ on a Varian Unity 400 at 400 MHz (23 °C). Waters Acquity Advanced Permeation Chromatography (APC) elucidated the molecular weight profiles of the PSUs compared to polystyrene standards at 35 °C. A sample concentration of 1 mg/mL in chloroform with a flow rate of 1 mL/min enabled separation on Acquity APC XT Columns. Dynamic light scattering (DLS) using a Malvern Zetasizer Nano ZS confirmed solubility of the polymers in chloroform prior to APC analysis.

Thermogravimetric (TGA) analysis was performed on a TA Instruments Q50 under constant N_2 flow using a temperature ramp from 25 to 600 °C at a rate of 10 °C/min. The value for $T_{d,5\%}$ was quantified as the temperature at which 95% weight remained. A TA Instruments Q1000 differential scanning calorimeter (DSC) revealed the thermal transitions of the polymers using a heat/cool/heat cycle with rates of 10/100/10 °C/min, respectively, under a 50 mL/min N_2 flow rate. Data analysis was performed on the second heat trace by measuring the T_g at the inflection point. Calibration with indium (T_m = 156.60 °C) and zinc (T_m = 419.47 °C) standards occurred prior to analysis. UV-Vis characterization occurred using a Cary 5000 UV-Vis-NIR from 600-200 nm in single beam mode.

Rheological measurements, such as solution viscosity and photorheology, were performed on a TA Instruments DHR-2 at 25 °C. Solution viscosity measurements utilized a peltier plate lower geometry with 40-mm parallel plate upper geometry set at a gap of 1000 μm. A shear sweep from 1 to 100 rad/s provided the viscosity measurement of the PSU in NMP. The solution viscosity at 200 1/s (8 rad/s) was normalized against the solvent viscosity to provide the specific viscosity (η_{sp}) for each concentration measured. Photorheology utilized a Smart Swap™ UV geometry with an Omnicure S2000 high-pressure mercury light source containing a 320-500 nm filter. A 20-mm quartz parallel plate on the lower geometry and 20 mm aluminum parallel plate upper geometry were set to an initial gap of 500 μm though slight gap adjustments occurred during testing to maintain an axial force of 0 N. UV-light output was measured prior to analysis using a Silverline radiometer with 20-mm sensor attachment. Data was gathered using a sampling frequency of 2 s^{-1}, 1 Hz, 0.1% strain, and 250 mW/cm^2 light intensity

with UV-irradiation occurring 30 s into the 240 s test. Analysis was performed in triplicate for all PSU samples to verify reproducibility. The modulus crossover function in the TA Instruments TRIOS software evaluated the storage modulus (G') and loss modulus (G") crossover time point for each test while plateau storage moduli (G_N^0) were averaged from the last 50 s of the G' curve.

Gel fraction measurements occurred using the photo-cured disks achieved after the photorheology measurements. The films (in triplicate) were dried for 18 h under reduced pressure at 220 °C, weighed, then extracted in a chloroform bath for 4 days which was exchanged with fresh solvent daily. The samples were again dried under reduced pressure for 18 h at 200 °C and reweighed to measure the loss in sample weight.

Photocalorimetry (photoDSC) occurred on a TA Instruments Q2000 using an Omnicure S2000 photo-attachment with fiber optic cable. Samples were loaded into T-Zero aluminum pans and characterized against an empty reference pan. The samples equilibrated at 25 °C for 1 min then UV-irradiatied (10 mW/cm^2) for 6 min after which the light was turned off and equilibrated again to note the background heat. Integrations of the exothermic peaks determined the heat of polymerization for the acrylate moieties after a background heat correction. The standard value for ΔH_{rxn} acrylate homopolymerization (86 kJ/mol) enabled the calculation of the percent conversion of the acrylates.[31] This analysis occurred after normalizing each sample based on weight and the assumption that every PSU contained two terminal acrylate groups.[30,31] Statistical analysis of these measurements utilized JMP software with an ANOVA test. Tukey's HSD determined the difference between data sets at 95% confidence.[30]

Additive manufacturing occurred using vat photopolymerization on a MPμSL machine. The instrument imaging set up consisted of a Hamamatsu LightningCure LC-L1V3 UV LED light source, conditioning optics from Edmund Optics, a mirror, a dynamic mask controlled by a computer, and imaging optics to reduce image dimensions and focus the prepatterned light. The Flexlight X1 DLP Development system from Keynote Photonics with a DLP 0.95 1080p DMD from Texas Instruments and a developer board acted as the dynamic mask. The DMD utilized an array of 1920 x 1080 aluminum micromirrors each measuring 10.8 μm in length and 0.95-in diagonally resulting in projection area of 5.4 μm x 5.4 μm per micromirror on the resin surface. The optics enabled a maximum part size in the XY plane of 6 x 8 mm. The polymer resin was held in a glass beaker on a custom stage mounted on a Zaber NA11B60 linear actuator to control movement. The custom build platform was manufactured from ULTEM® using filament extrusion. In order to print, the build platform lowered into the resin by 100 μm. Slicing the STL file of the lattice structure into 100 μm segments then converting them into mono-chrome Bitmap images enabled their projection on the resin surface in the appropriate order (bottom to top). The images were projected onto the resin surface using a 365 nm light source with an intensity of 15 mW/cm^2. Lowering the build platform further into the resin enabled recoating then subsequent exposure continued the part fabrication. The fabricated 3D parts were removed from the platform, rinsed with excess NMP, and finally wiped dry with Kim Wipes™ before transferring it to a glass slide to measure dimensions.

Sample nomenclature comprises #K-PSU_x where the #K refers to the targeted molecular weight of each polymer (6, 10 or 20 kg/mol). X identifies the type of post-

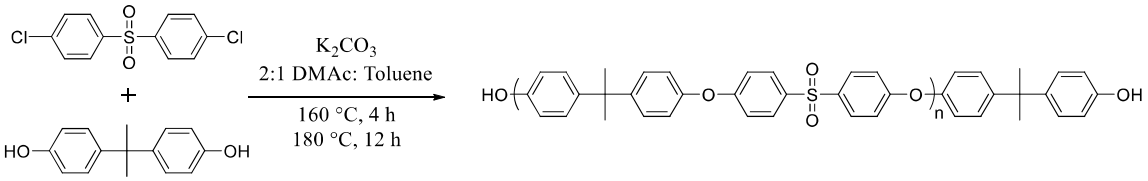

Scheme 9.1. Synthesis of phenol-terminated polysulfones with controlled molecular weight.

polymerization functionalization the polymer has undergone. For the different polymers throughout the manuscript, X = P for phenol-terminated PSU, X = H for hydroxyethyl-terminated PSU, X= PA for acrylate-terminated PSU, and X= HA for acrylate ethyl-terminated PSU. For example, 6K-PSU_{HA} refers to a 6000 g/mol targeted PSU backbone that was functionalized to form the hydroxyethyl-terminated PSU then derivatized to form the acrylate end-group with ethyl spacer.

9.3.3 Synthesis of phenol-terminated PSU.

The following established procedure describes the synthesis of phenol-terminated polysulfones, as illustrated in **Scheme 9.1**, and summarizes the synthesis of the 6000 g/mol oligomer.[32,33] Bisphenol A (11.11 g, 0.049 mol), 4,4'-dichlorophenyl sulfone (12.98 g, 0.045 mol), potassium carbonate (8.07 g, 0.058 mol), anhydrous N,N-dimethylacetamide (160 mL), and toluene (80 mL) were weighed into a three-neck, round-bottomed flask. The reaction flask was fitted with a Dean-Stark trap and condenser, glass mechanical stir rod, Teflon™ paddle, and stir-rod adaptor. The heterogenous solution was purged with N_2 for 10 min prior to heating the reaction to 160 °C. Monitoring the water removal through a toluene reflux tracked the reaction progress over the first 4 h. The reaction temperature was subsequently increased to 180 °C and the toluene removed over a 12 h period. The resulting heterogenous colored solution was

filtered through a 1" Celite plug to remove the formed salts. Titration with 1 M HCl resulted transitioned the solution to a clear pale-yellow color. Precipitation dropwise into 4 L of distilled water followed by filtration and drying *in vacuo* at 210 °C for 24 h afforded phenol-terminated PSU with targeted M_n = 6000 g/mol. Adjusting the BPA excess enabled the polymerization of both the 10 and 20 kg/mol PSU.

9.3.4 Synthesis of hydroxyethyl-terminated PSU.

Earlier literature demonstrated the post-polymerization functionalization of phenol-terminated PSU to form a hydroxyethyl-terminated, as illustrated in **Scheme 9.2**.[32,34] The following example demonstrates this procedure on the 5900 g/mol PSU though the same procedure was utilized for all molecular weight PSU. Ethylene carbonate (0.746 g, 0.0085 mol), potassium carbonate (0.70 g, 0.0051 mol), DMF (100 mL), and the 6K-PSU_P (10 g, 0.0017 mol) were weighed into a single-neck, round-bottomed flask with magnetic stir bar resulting in a heterogenous solution. The reaction mixture was purged for a minimum of 10 m with N_2 then heated to 120 °C and reacted for 24 h. Filtering the final solution through a 1" Celite plug removed undesired salts

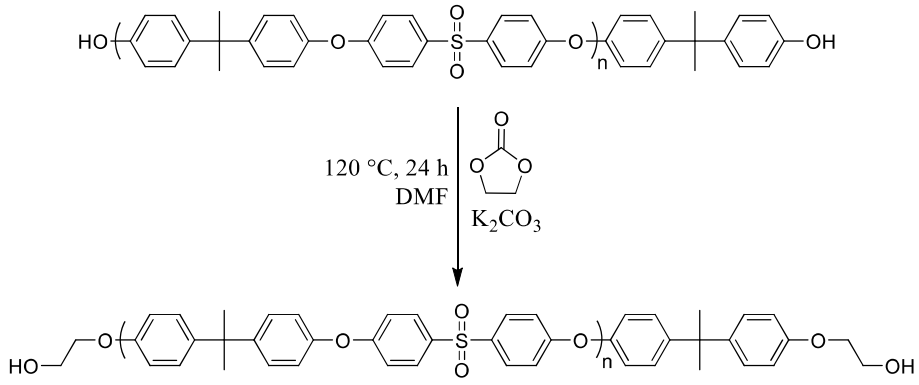

Scheme 9.2. Synthesis of hydroxyethyl-functionalized polysulfones from the phenol-terminated PSU precursor.

followed by neutralization with 1 M HCl and drying *in vacuo* at 210 °C for 24 h. ^{1}H NMR spectroscopy confirmed quantitative conversion of to the hydroxyethyl group.

9.3.5 Synthesis of acrylate-terminated PSU.

Scheme 9.3 outlines the general synthesis for the acrylate-terminated PSU oligomers from either the phenol- or hydroxyethyl-terminated PSUs. M_n, as measured from end group analysis of the ^{1}H NMR spectroscopy, was utilized to quantify the amount of each starting material required. The same procedure, based on previous literature precedence, was utilized for all functionalization's with different PSU though the 6K-PSU$_P$ is summarized.[28,29,35,36] 5300 g/mol PSU$_P$ (35 g, 0.0066 mol) was measured into a 100-mL single-neck round-bottomed flask. The addition of anhydrous $CHCl_3$ (200 mL) occurred after purging the reaction flask for 10 m with N_2. Once homogenous, the

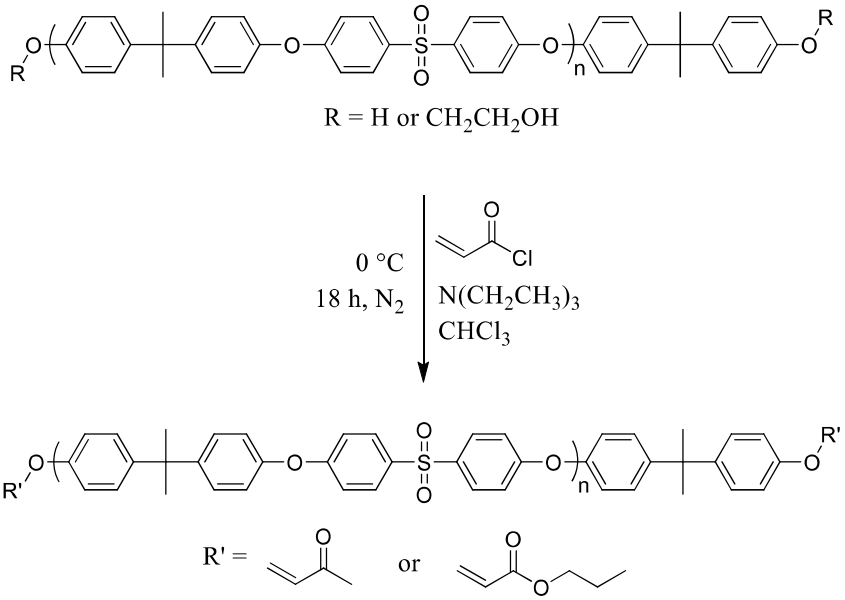

Scheme 9.3. Synthesis of acrylate-functionalized polysulfones from the phenol (PSU$_{PA}$) or hydroxyethyl (PSU$_{HA}$) terminated PSU precursors.

reaction was cooled to 0 °C and a balloon of N_2 replaced the constant flow. Addition of triethylamine (5.35 g, 0.053 mol) occurred slowly allowing time for the reactant to dissolve prior to the dropwise addition of the acryloyl chloride (2.99 g, 0.033 mol). The solution color turned to orange as the reaction warmed to room temperature overnight. Washes with 3 aliquots of 2 M aqueous HCl then stirring the solution over basic alumina for 1 h removed the excess TEA. After filtration, the solution was washed twice with 1 M NaOH, saturate bicarbonate solution, and brine. Stirring over $MgSO_4$ removed the remaining water followed by filtration and concentration via a rotary evaporator. The solid product was triturated in MeOH for 24 h to remove the chloroform then filtered and dried *in vacuo* at 40 °C for 18 h resulting in a slightly yellow product.

9.3.6 Preparation of samples for photorheology, photocalorimetry, and vat photopolymerization.

Various concentration of PSU in NMP were utilized in photorheology and photoDSC studies. The solvent and PSU, totaling 2.00 g, were weighed into a 6-dram scintillation vial, and heated to a maximum of 80 °C to afford a homogenous solution. Separately the appropriate concentration of TPO (based on weight of PSU) was weighed into a 2-dram scintillation vial then dissolved in a few drops of NMP facilitated by mixing with a vortexer until a clear solution was achieved. The TPO solution was then transferred into the PSU vial and mixed with a vortexer to achieve a homogenous solution. All samples were utilized within two days and stored cold, covered with aluminum foil. Preparation of the samples for VPP occurred utilizing the same procedure with the exception of exchanging TPO with DMPA as the photoinitiator in the resin.

9.4 Results and Discussions:

9.4.1 Synthesis and characterization of PSU_P and PSU_H.

Table 9.1. Molecular weight analysis of the phenol-terminated polysulfones utilizing ^{1}H NMR spectroscopy and advanced permeation chromatography.

Polymer	Goal M_n (g/mol)	^{1}H NMR: M_n (g/mol)	APC: M_n (g/mol)	Đ (M_w/M_n)
Phenol-terminated PSU				
20K-PSU$_P$	20,000	14,800	14,600	2.22
10K-PSU$_P$	10,000	9000	9300	2.29
6K-PSU$_P$	6000	6700	5700	2.41

Synthesis of phenol-terminate PSU with controlled molecular weight occurred utilizing a nucleophilic aromatic substitution of BPA and DCDPS in a step-growth polymerization.[32-34] A stoichiometric offset with an excess of BPA facilitate phenol-terminal groups while calculations using modified Carothers equation targeted the final polymer M_n of 20, 10, or 6 kg/mol. ^{1}H NMR spectroscopy enabled end group analysis to determine the actual M_n of the 6K-PSU$_P$, 10K-PSU$_p$, and 20K-PSU$_p$(**Figure S9.1-S9.3**). Two doublets at 6.75 and 7.08 ppm represent the four protons on the benzene ring directly adjacent to the terminal phenol. Comparisons of these proton integrations relative to the aromatic protons in the repeat unit enabled calculation of the M_n, as illustrated in **Table 9.1.** The calculate M_n revealed similar values to the targeted chain lengths, with the exception of 20K-PSU$_P$. APC analysis further characterized the polymer molecular weight and polydispersity index (Đ). The values obtained based on polystyrene standard through the APC provided relative M_n similar to the ^{1}H NMR spectroscopy analysis. The continued deviation of the 20K-PSU$_P$ from its targeted M_n could presumably be associated with error measuring the monomers during polymerization preparation. The APC curves, using columns that enable analysis of low molecular weight species, exhibited separation of low molecular weight species exhibiting Đ = 1. This main peak at

5.5 min in **Figure S9.4** is presumably associated with cyclic oligomers species commonly observed in this polymerization technique.[27,37-39] These oligomers were excluded from the integrations used in the M_n and Đ analysis.

Post-polymerization functionalization of the PSU_P with ethylene carbonate utilizing a well-studied procedure generated a primary alcohol with a two carbon spacer (hydroxyethyl-terminated PSU) at the terminal sites, as illustrated in **Scheme 9.2**.[32] Tracking the shift in the phenyl group protons with ^1H NMR spectroscopy confirmed the quantitative conversion of the end group for each of the molecular weight species. The two doublets at 6.75 and 7.08 ppm in the spectra of the PSU_P shifted to 6.84 and 7.15 ppm, respectively, after conversion to PSU_H (**Figure S9.5)**. The addition of two triplets at 4.06 and 3.95 ppm, associated with the protons in the carbon spacer, further confirmed the quantitative functionalization of the end groups.

Thermal characterization of the PSU_P and PSU_H molecular weight series occurred using TGA and DSC with the thermal transitions collected in **Table 9.2**. TGA analysis provided the weight loss profiles exhibiting a one-step curve for the entire PSU_H series

Table 9.2. Thermal characterization of phenol- and hydroxyethyl-terminated polysulfones using TGA and DSC analysis

Polymer	T_g (°C)[a]	ΔC_p (W/g)[a]	$T_{d,5\%}$ (°C)[b]	Char Yield at 600 °C[b]
Phenol-terminated PSU				
6K-PSU_P	172	0.054	417	38
10K-PSU_P	182	0.046	438	39
20K-PSU_P	187	0.035	496	39
Hydroxy ethyl-terminated PSU				
6K-PSU_H	161	0.052	482	31
10K-PSU_H	179	0.046	494	34
20K-PSU_H	185	0.049	501	35

[a] Determined from 2nd heat in DSC
[b] Determined from TGA

and 20K-PSU$_P$ with $T_{d,5\%}$ > 480 °C. The 6K-PSU$_P$ and 10K-PSU$_P$ exhibited two-step weight loss profiles in **Figure 9.1A,** presumably associated with the higher amount of low molecular weight oligomers present in these materials. These polymers exhibited reduced $T_{d,5\%}$ of 417 and 438 °C, respectively. The second precipitation performed during the work-up of PSU$_H$ may have resulted in further fractionation removing the low molecular weight species that caused the two-step weight loss.

DSC analysis revealed amorphous polymers with T_g's ranging from 161 to 185 °C. The analysis revealed systematic increase in the T_g was observed as a function of molecular weight increase as expected.[40] Between the two series, the 10 kg/mol and 20 kg/mol samples of PSU$_H$ and PSU$_P$ exhibited nearly identical T_g's. In contrast, the 6K-PSU$_P$ revealed a significantly higher T_g (172 °C) relative to 6K-PSU$_H$ (161 °C). This presumably results from a higher flexibility of the hydroxyethyl end group relative to the phenol end group.

UV-Vis spectroscopy determined the absorbance of the 6K-PSU$_P$ to confirm no overlap occurred between the polymer and photoinitiators and light sources chosen for

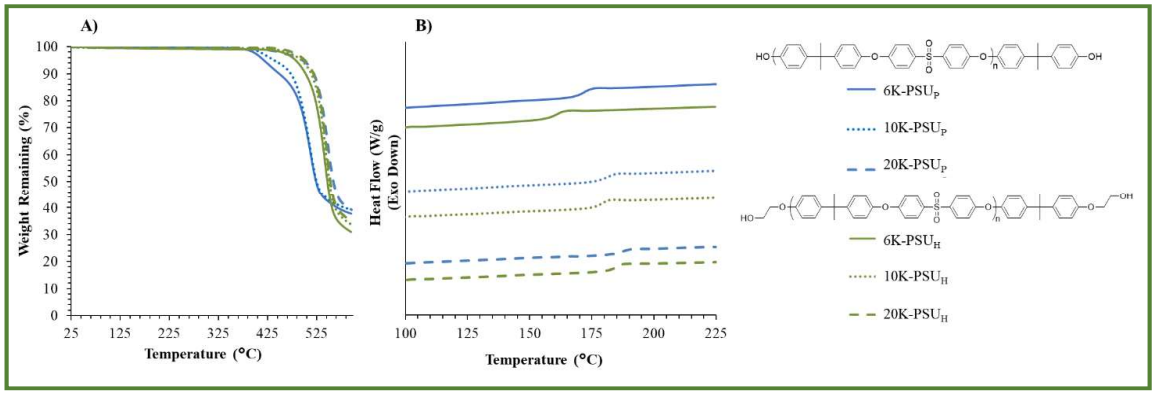

Figure 9.1. Thermal analysis of phenol- and hydroxyethyl-functionalized polysulfones using A) thermogravimetric analysis and B) differential scanning calorimetry.

the 3D printing. Dissolved in NMP, the PSU exhibited a peak absorbance at 269 nm with a range from 304 nm to beyond the instrument limit of 254 nm (**Figure S9.8**). This value falls outside the range of absorbance for both photoinitiators, TPO and DMPA, as well as the light source utilized for both photorheology and photoDSC studies.[15,41]

9.4.2 Acrylate terminated PSU (PSU_{HA} and PSU_{PA}).

Scheme 9.3 illustrates the derivatization of the alcohol/phenol terminated $PSU_{P\ or\ H}$ to form acrylate-functionalized PSU (PSU_{HA} or PSU_{PA}). Previous literature demonstrate the acrylate functionalization of PSUs utilizing both Schotten-Bauman conditions, as well as acryloyl chloride and TEA.[28,29,35,36] Our study exhibited the most success using 5 eq. of acryloyl chloride and 8 eq. of TEA. These conditions demonstrated quantitative conversion of both the phenol (PSU_P) and the primary alcohol of PSU_H. ^{1}H NMR spectroscopy confirmed the functionalization through the emergence of two doublets and a doublet of a doublet at 6.59, 6.00 and 6.31 ppm, respectively, associated with the three protons on the acrylate group (**Figure S9.6 and S9.7**). These chemical shifts differ from acryloyl chloride or acrylic acid. The functionalization also resulted in a change to the aromatic protons of the end groups for PSU_{PA}. In **Figure S9.6**, the phenol proton at 6.75 and 7.08 ppm shifted to overlap with the repeat unit protons associated with BPA. In contrast, **Figure S9.7** of PSU_{HA} exhibits no change in the aromatic protons at 6.84 and 7.15 ppm due to the separation of the acrylate group from the backbone. Instead, the triplets associated with the protons on the ethyl spacer at 4.06 and 3.95 ppm shifted to 4.50 and 4.19 ppm, respectively.

9.4.3 Photocuring properties of PSU_{HA} and PSU_{PA}.

Solutions of the 6K-PSU_{PA} and 6K-PSU_{HA} were prepared in NMP with 1 wt% TPO at concentrations ranging from 10 to 40 wt% PSU. The low molecular weight PSU

provided the highest concentration of end groups for the comparison of photo-curing kinetics between acrylates with and without the ethyl spacer. PhotoDSC measured the heat of reaction (ΔH_{rxn}) for the acrylate photopolymerization after UV-irradiation (10 mW/cm^2). This enabled the estimation of % conversion of the acrylate groups for each solution by comparing the measured ΔH_{rxn} against the standard ΔH_{rxn} for acrylate homopolymerization (86 kJ/mol). This calculation assumed that each PSU chain possessed an acrylate at both ends and (**Figure 9.2**). The 6K-PSU$_{PA}$ exhibited an increase in the % conversion across the solution concentration range from near 55 % to about 90 % conversion. Higher % conversion occurred in concentration falling above the critical entanglement concentration (c_e) for 6K-PSU$_P$, identified as 22 wt% in **Figure S9.9** using solution rheology. The choice of using 30 wt% PSU in further analysis balanced the high

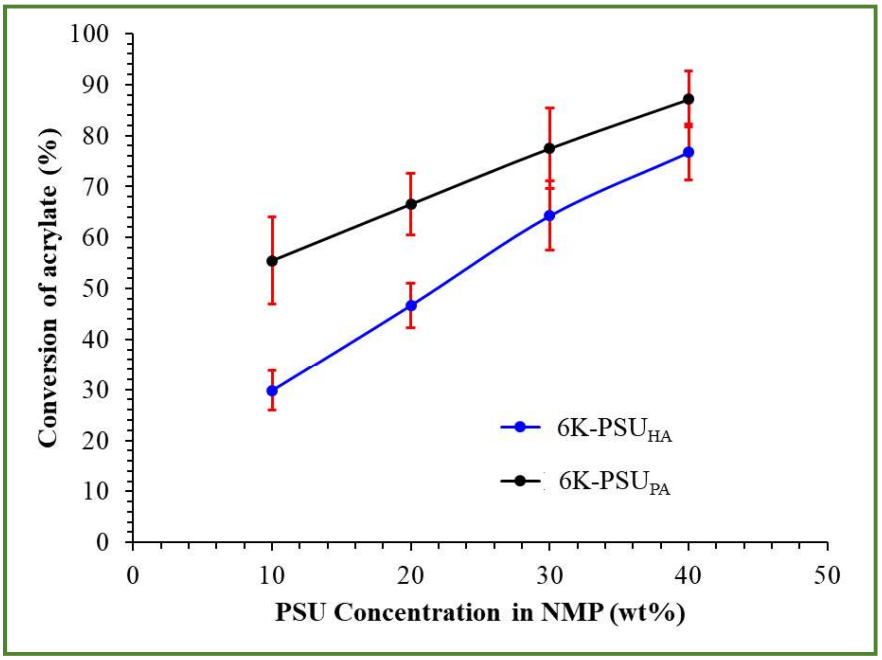

Figure 9.2. Conversion of acrylates based on photoDSC measurements comparing acrylate ethyl-terminated PSU (PSU$_{HA}$) and acrylate-terminated PSU (PSU$_{PA}$) both with M_n = 6000 g/mol. Samples utilized 1 wt% TPO based on the PSU and 30 wt% PSU in NMP measured using a light intensity of 10 mW/cm^2.

% conversion of this concentration and the need for low solution viscosities.

Analysis of 6K-PSU_{HA} revealed lower % conversions than 6K-PSU_{PA} ranging from 30 to 75 % at low concentrations. Concentrations of 30 and 40 wt% exhibited no statistical differences in % conversion between 6K-PSU_{PA} and 6K-PSU_{HA}. These studies revealed no significant improvements to utilizing the acrylate with the ethyl spacer though further analysis will need to determine whether crosslinked structures exhibit different environmental stability. As a result, the added complexity of the three-step synthesis over the two-step synthesis of PSU_{PA} outweighed the high conversion achieved at 40 wt%. For further analysis and application in VPP, a focus was instead placed on PSU_{PA}.

PhotoDSC further characterized the molecular weight series of PSU_{PA} using a concentration of 30 wt% in NMP with a range of TPO concentrations relative to the PSU. The standard photoDSC curve in **Figure 9.3A** exhibited a peak after 1 min upon

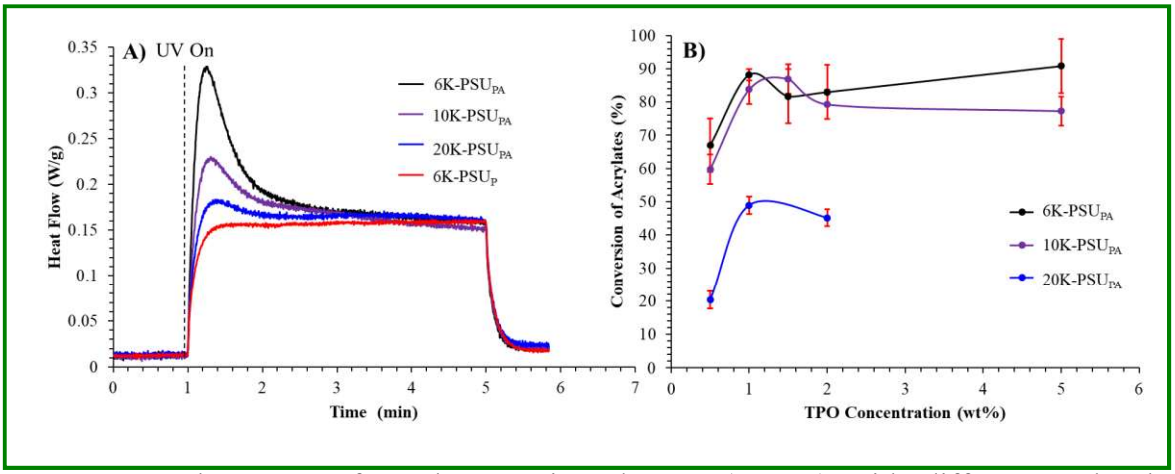

Figure 9.3. PhotoDSC of acrylate-terminated PSU (PSU_{PA}) with different molecular weights (M_n = 6, 10, and 20 kg/mol) and a non-functionalized phenol-terminated PSU (PSU_P). Samples utilized 30 wt% PSU_{PA} in NMP with a light intensity of 10 mW/cm^2. A) Standard photoDSC trace of the three molecular weights using 1 wt% TPO and the non-acrylated PSU_P. B) Analysis of conversion of acrylates in comparison to concentration of TPO.

exposure to UV-light and subsequent initiation of the acrylate polymerization. 6K-PSU_{PA} exhibited the highest intensity peak due to the largest concentration of end groups. The peak height systematically decreased with increasing molecular weight, as expected. 20K-PSU_{PA} afforded a very low intensity exotherm resulting in less accurate integrations. The non-functionalized phenol-terminated PSU revealed the background heat associated with the UV lamp. **Figure 9.3B** provided the % conversion of the three PSU_{PA} as a function of TPO concentration. Below 1 wt% TPO, the acrylate conversion significantly dropped for all polymers. The 6K and 10K-PSU_{PA} plateaued near 80-90 % conversion for solutions with ≥ 1 wt% TPO. Over all the TPO concentrations, 20K-PSU_{PA} exhibited low % conversion of less than 50 %. This presumably results from a combination of high solution viscosity and low end group concentration limiting the reaction between acrylates.

Photorheology further characterized the photocuring kinetics of different molecular weight PSU_{PA} with a range of TPO concentrations. Photorheology afforded both the crossover time and plateau modulus for the acrylate terminated polymers (**Figure 9.4A and 9.4B)**. Upon UV-irradiation (250 mW/cm^2), a rapid increase in G' and crossover of the G' and G" occurred followed by a plateau of the G' (G_N^0). The crossover time represents an important parameter for understanding the 3D printability of a photopolymer resin. This values often acts as an indicator for gelation time and represent the transition from a liquid to a solid state.[3,8,9,42] Utilizing < 1 wt% TPO resulted in long G'/G" crossover times, from 5 to 35 s depending on the molecular weight (**Figure 9.4A**). Photoinitiator concentrations ≥ 1 wt% TPO afforded rapid crossover times of ≤ 5 s demonstrating efficient gelation for VPP. Overall, the higher molecular weight PSU_{PA}

exhibited faster G'/G" crossover times relative to 6K-PSU$_{PA}$. The high molecular weight polymers exhibited higher G' and higher viscosities prior to photocuring which presumably shortened this time point.

Plateau moduli (G_N^0) represents the stiffness of the final organogel following the photocuring. **Equation 9.1** demonstrates an inverse relationship between G_N^0 and M_c. In this equation, ρ relates to polymer density while R refers to the universal gas constant, and T represents the temperature.[3,22]

$$G_N^0 = \frac{\rho RT}{M_c} \tag{9.1}$$

Photorheology provide the analysis of G_N^0 in **Figure 9.4B** for 6K-PSU$_{PA}$ and 10K-PSU$_{PA}$. Unfortunately, slipping from between the plate of 20K-PSU$_{PA}$ following UV-irradiation resulted in inaccurate G_N^0 values. 10K-PSU$_{PA}$ provided consistently lower G_N^0 relative to 6K-PSU$_{PA}$ across all TPO concentrations. This relates to the higher molecular weight between crosslinks due to the polymer structure.

The photocured rheology disks provided samples for gel fraction studies. The 6K-

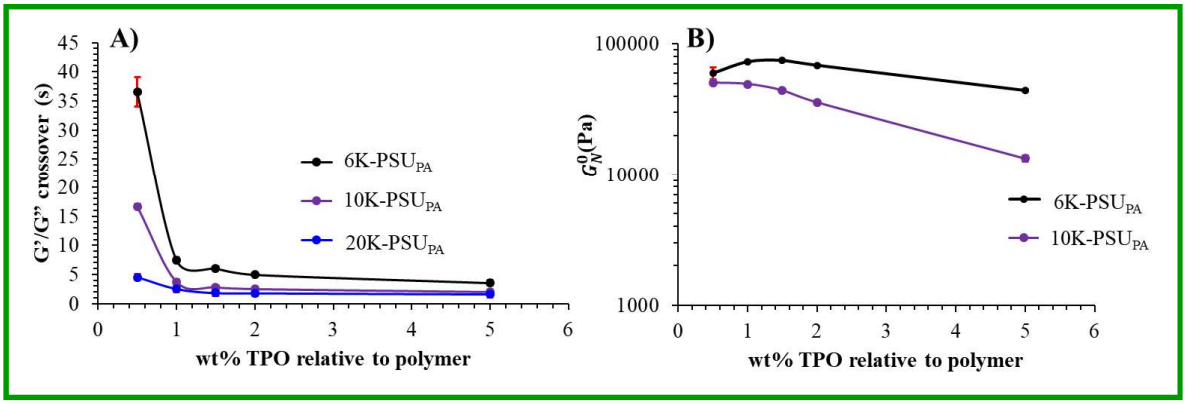

Figure 9.4. Photorheology of acrylate-terminated PSU (PSU$_{PA}$) with different molecular weights (6, 10, and 20 kg/mol). Samples utilized 30 wt% PSU$_{PA}$ in NMP with a light intensity of 250 mW/cm^2. Panel (A) and (B) depict the crossover time for storage (G') and loss modulus (G") and the G' plateau modulus (G_N^0) respectively in comparison to concentration of photoinitiator (TPO).

PSU_{PA}, 10K-PSU_{PA}, and 20K-PSU_{PA} revealed gel fractions of 73.9 ± 7.5, 62.7 ± 2.7, and 42.8 ± 5.1 %, respectively. The low gel fraction elucidates the difficulty of the acrylate photopolymerization for samples with low end group concentration. McGrath et al. also revealed low gel fractions (58 %) for photocrosslinked acrylamide terminated PSU.[29] The combination of lower gel fractions, softer organogels, and lower % conversion for the 10K and 20K-PSU_{PA} assisted in the choice to utilize 6K-PSU_{PA} for further VPP testing.

9.4.4 Vat photopolymerization of 6K-PSU_{PA}.

6K-PSU_{PA} was chosen for VPP due to the combination of the simpler synthesis, fast G'/G" crossover time, high G_N^0, high % conversion, and the highest gel fraction. The base resin formulation for VPP comprised a 30 wt% solution of 6K-PSU_{PA} in NMP with 1 wt% photoinitiator (DMPA). The instrument chosen to print this solution previously demonstrated rapid printing times and fine part features using other photocurable resins.[6,13] The lattice structure, illustrated in **Figure 9.5A,** possessed a 4.5-mm height, width, and length with 1-mm squares throughout the structure. **Figure 9.5B** and **9.5C** displayed images of two final parts using the base resin formulation with either 0 wt% or

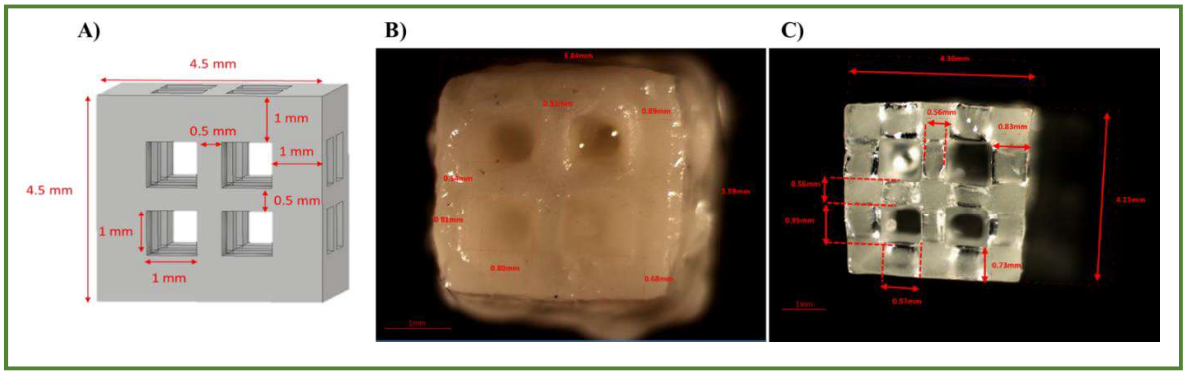

Figure 9.5. Vat photopolymerization of lattice structure using 30 wt% of 6K-PSU_{PA} in NMP with 1 wt% photoinitiator (DMPA). Print parameter used a 365 nm light source with 15 mW/cm^2 intensity and an 8s/layer exposure time. A) CAD model of lattice structure B) Print using resin with 0 wt% photo-blocker (avobenzene) C) Print using resin with 0.05 wt% photo-blocker.

0.05 wt% avobenzone, respectively. Avobenzone acts as a photo-blocker (absorbs from 320-400 nm) preventing over cure which causes structural imperfections, as observed in **Figure 9.5B**.[43] This print exhibited poor consistency with the CAD model and filled in lattice squares. In contrast, the addition of 0.05 wt% avobenzone to the resin resulted in a well-defined 3D part with measurements consistent with the CAD model and a rapid print time (8s/layer). Future analysis will be performed to understand the mechanical and thermal properties of the final cured parts. While the 6000 g/mol PSU exhibited the most successful printing, the 20 and 10 kg/mol PSU are likely to exhibit higher final toughness.

9.5 Conclusions:

Telechelic functionalization of polysulfones enabled their processing through advanced manufacturing methods, vat photopolymerization. Solution polymerization of BPA and DCDPS afforded a molecular weight series of phenol-terminated PSU with the basic Udel® backbone structure. Post-polymerization functionalization with ethylene carbonate created a series of hydroxyethyl-terminated PSU. These two sets of PSUs underwent further derivatization to form acrylate-terminated PSU (PSU_{HA} and PSU_{PA}). Photorheology and photoDSC analysis determined that 6K-PSU_{PA} possessed fast photo-curing, high % conversion, and high G_N^0 when utilized a 30 wt% solution in NMP and > 1 wt% photoinitiator facilitating its application to VPP. Due to the complicated three-step synthesis of PSU_{HA} outweighed its possible use in VPP. VPP using a low concentration of photo-blocker afforded a well-defined 3D part based on a lattice structure. This represents the first successful attempt to 3D print this high-performance polymer using VPP.

Acknowledgments:

The authors thank Emily Wilts and Dr. Jana Herzberger for insightful discussions.

Funding:

This work was sponsored by Solvay.

Notes:

The authors declare no competing financial interest.

References:

(1) Bechtold, S., 3D Printing, Intellectual Property and Innovation Policy, *Iic-International Review of Intellectual Property and Competition Law* **2016**, *47*, 517.

(2) Huang, Y.; Leu, M. C.; Mazumder, J.; Donmez, A., Additive Manufacturing: Current State, Future Potential, Gaps and Needs, and Recommendations, *Journal of Manufacturing Science and Engineering-Transactions of the Asme* **2015**, *137*.

(3) Sirrine, J. M.; Meenakshisundaram, V.; Moon, N. G.; Scott, P. J.; Mondschein, R. J.; Weiseman, T. F.; Williams, C. B.; Long, T. E., Functional siloxanes with photo-activated, simultaneous chain extension and crosslinking for lithography-based 3D printing, *Polymer* **2018**.

(4) Gao, W.; Zhang, Y.; Ramanujan, D.; Ramani, K.; Chen, Y.; Williams, C. B.; Wang, C. C. L.; Shin, Y. C.; Zhang, S.; Zavattieri, P. D., The status, challenges, and future of additive manufacturing in engineering, *Computer-Aided Design* **2015**, *69*, 65.

(5) Cooper, K., *Rapid prototyping technology: selection and application*; CRC press, 2001.

(6) Chartrain, N. A.; Vratsanos, M.; Han, D. T.; Sirrine, J. M.; Pekkanen, A.; Long, T. E.; Whittington, A. R.; Williams, C. B., Microstereolithography of tissue scaffolds using a biodegradable photocurable polyester, *Solid Freeform Fabrication Sympossium* **2016**.

(7) Sirrine, J. M.; Pekkanen, A. M.; Nelson, A. M.; Chartrain, N. A.; Williams, C. B.; Long, T. E., 3D-Printable Biodegradable Polyester Tissue Scaffolds for Cell Adhesion, *Australian Journal of Chemistry* **2015**, *68*, 1409.

(8) Scott, P.; Meenakshisundaram, V.; Chartrain, N.; Sirrine, J.; Williams, C. B.; Long, T. E., Additive Manufacturing of Hydrocarbon Elastomers via Simultaneous Chain Extension and Crosslinking of Hydrogenated Polybutadiene, *ACS Applied Polymer Materials* **2019**.

(9) Sirrine, J. M.; Zlatanic, A.; Meenakshisundaram, V.; Messman, J. M.; Williams, C. B.; Dvornic, P. R.; Long, T. E., 3D Printing Amorphous Polysiloxane Terpolymers via Vat Photopolymerization, *Macromolecular Chemistry and Physics* **2019**, *220*, 1800425.

(10) Aduba, D. C.; Margaretta, E. D.; Marnot, A. E. C.; Heifferon, K. V.; Surbey, W. R.; Chartrain, N. A.; Whittington, A. R.; Long, T. E.; Williams, C. B., Vat photopolymerization 3D printing of acid-cleavable PEG-methacrylate networks for biomaterial applications, *Materials Today Communications* **2019**.

(11) Hegde, M.; Meenakshisundaram, V.; Chartrain, N.; Sekhar, S.; Tafti, D.; Williams, C. B.; Long, T. E., 3D Printing All-Aromatic Polyimides using Mask-Projection Stereolithography: Processing the Nonprocessable, *Advanced Materials* **2017**, *29*, 1701240.
(12) Herzberger, J.; Meenakshisundaram, V.; Williams, C. B.; Long, T. E., 3D Printing All-Aromatic Polyimides Using Stereolithographic 3D Printing of Polyamic Acid Salts, *ACS Macro Letters* **2018**, 493.
(13) Schultz, A. R.; Lambert, P. M.; Chartrain, N. A.; Ruohoniemi, D. M.; Zhang, Z.; Jangu, C.; Zhang, M.; Williams, C. B.; Long, T. E., 3D Printing Phosphonium Ionic Liquid Networks with Mask Projection Microstereolithography, *ACS Macro Letters* **2014**, *3*, 1205.
(14) Fouassier, J.-P., *Photoinitiators for polymer synthesis: scope, reactivity, and efficiency*; John Wiley & Sons, 2012.
(15) Mucci, V.; Vallo, C., Efficiency of 2,2-dimethoxy-2-phenylacetophenone for the photopolymerization of methacrylate monomers in thick sections, *Journal of Applied Polymer Science* **2012**, *123*, 418.
(16) Karasu, F.; Croutxé-Barghorn, C.; Allonas, X.; Van Der Ven, L. G. J., Free radical photopolymerization initiated by UV and LED: Towards UV stabilized, tack free coatings, *Journal of Polymer Science, Part A: Polymer Chemistry* **2014**, *52*, 3597.
(17) Sanai, Y.; Kagami, S.; Kubota, K., Cross-linking photopolymerization of monoacrylate initiated by benzophenone, *Journal of Polymer Science, Part A: Polymer Chemistry* **2018**, *56*, 1545.
(18) Wallin, T. J.; Pikul, J. H.; Bodkhe, S.; Peele, B. N.; Mac Murray, B. C.; Therriault, D.; McEnerney, B. W.; Dillon, R. P.; Giannelis, E. P.; Shepherd, R. F., Click chemistry stereolithography for soft robots that self-heal, *Journal of Materials Chemistry B* **2017**, *5*, 6249.
(19) Melchels, F. P. W.; Feijen, J.; Grijpma, D. W., A review on stereolithography and its applications in biomedical engineering, *Biomaterials* **2010**, *31*, 6121.
(20) Wohlers, T. T., *Wohlers Report...: 3D Printing and Additive Manufacturing, State of the Industry, Annual Worldwide Progress Report*; Wohlers Associates Incorporated, 2014.
(21) Eckel, Z. C.; Zhou, C. Y.; Martin, J. H.; Jacobsen, A. J.; Carter, W. B.; Schaedler, T. A., 3D PRINTING Additive manufacturing of polymer-derived ceramics, *Science* **2016**, *351*, 58.
(22) Rubinstein, M.; Colby, R. H., *Polymer physics*; Oxford university press New York, 2003; Vol. 23.
(23) Odian, G. G., *Principles of polymerization*; Wiley: New York, 1991.
(24) Yue, J.; Zhao, P.; Gerasimov, J. Y.; van de Lagemaat, M.; Grotenhuis, A.; Rustema-Abbing, M.; van der Mei, H. C.; Busscher, H. J.; Herrmann, A.; Ren, Y. J., 3D-Printable Antimicrobial Composite Resins, *Adv. Funct. Mater.* **2015**, *25*, 6756.
(25) Schuller-Ravoo, S.; Zant, E.; Feijen, J.; Grijpma, D. W., Preparation of a Designed Poly(trimethylene carbonate) Microvascular Network by Stereolithography, *Advanced Healthcare Materials* **2014**, *3*, 2004.

(26) Melchels, F. P. W.; Feijen, J.; Grijpma, D. W., A poly(D,L-lactide) resin for the preparation of tissue engineering scaffolds by stereolithography, *Biomaterials* **2009**, *30*, 3801.
(27) Savariar, S.; Underwood, G. S.; Dickinson, E. M.; Schielke, P. J.; Hay, A. S., Polysulfone with lower levels of cyclic dimer: use of MALDI-TOF in the study of cyclic oligomers, *Desalination* **2002**, *144*, 15.
(28) Nebipasagil, A.; Sundell, B. J.; Lane, O. R.; Mecham, S. J.; Riffle, J. S.; McGrath, J. E., Synthesis and photocrosslinking of disulfonated poly(arylene ether sulfone) copolymers for potential reverse osmosis membrane materials, *Polymer* **2016**, *93*, 14.
(29) Sundell, B. J.; Lee, K.-s.; Nebipasagil, A.; Shaver, A.; Cook, J. R.; Jang, E.-S.; Freeman, B. D.; McGrath, J. E., Cross-Linking Disulfonated Poly(arylene ether sulfone) Telechelic Oligomers. 1. Synthesis, Characterization, and Membrane Preparation, *Industrial & Engineering Chemistry Research* **2014**, *53*, 2583.
(30) Wilts, E. M.; Pekkanen, A. M.; White, B. T.; Meenakshisundaram, V.; Aduba, D. C.; Williams, C. B.; Long, T. E., Vat photopolymerization of charged monomers: 3D printing with supramolecular interactions, *Polymer Chemistry* **2019**.
(31) Andrzejewska, E.; Andrzejewski, M., Polymerization kinetics of photocurable acrylic resins, *Journal of Polymer Science, Part A: Polymer Chemistry* **1998**, *36*, 665.
(32) Dennis, J. M.; Fahs, G. B.; Moore, R. B.; Turner, S. R.; Long, T. E., Synthesis and Characterization of Polysulfone-Containing Poly(butylene terephthalate) Segmented Block Copolymers, *Macromolecules* **2014**, *47*, 8171.
(33) Viswanathan, R.; Johnson, B. C.; McGrath, J. E., Synthesis, kinetic observations and characteristics of polyarylene ether sulphones prepared via a potassium carbonate DMAC process, *Polymer* **1984**, *25*, 1827.
(34) Celebi, O.; Lee, C. H.; Lin, Y.; McGrath, J. E.; Riffle, J. S., Synthesis and characterization of polyoxazoline–polysulfone triblock copolymers, *Polymer* **2011**, *52*, 4718.
(35) Khan, A. L.; Cano-Odena, A.; Gutiérrez, B.; Minguillón, C.; Vankelecom, I. F. J., Hydrogen separation and purification using polysulfone acrylate–zeolite mixed matrix membranes, *Journal of Membrane Science* **2010**, *350*, 340.
(36) Dizman, C.; Ates, S.; Torun, L.; Yagci, Y., Synthesis, characterization and photoinduced curing of polysulfones with (meth)acrylate functionalities, *Beilstein journal of organic chemistry* **2010**, *6*, 56.
(37) Montaudo, G.; Samperi, F.; Montaudo, M. S., Characterization of synthetic polymers by MALDI-MS, *Progress in Polymer Science* **2006**, *31*, 277.
(38) Jacobson, H.; Stockmayer, W. H., Intramolecular Reaction in Polycondensations. I. The Theory of Linear Systems, *The Journal of Chemical Physics* **1950**, *18*, 1600.
(39) Jacobson, H.; Beckmann, C. O.; Stockmayer, W. H., Intramolecular Reaction in Polycondensations. II. Ring-Chain Equilibrium in Polydecamethylene Adipate, *The Journal of Chemical Physics* **1950**, *18*, 1607.
(40) Jr., T. G. F.; Flory, P. J., Second-Order Transition Temperatures and Related Properties of Polystyrene. I. Influence of Molecular Weight, *Journal of Applied Polymer Physics* **1950**, *21*, 581.

(41) Retailleau, M.; Ibrahim, A.; Allonas, X., Dual-cure photochemical/thermal polymerization of acrylates: a photoassisted process at low light intensity, *Polymer Chemistry* **2014**, *5*, 6503.
(42) Winter, H. H., Can the gel point of a cross-linking polymer be detected by the G′ – G″ crossover?, *Polymer Engineering & Science* **1987**, *27*, 1698.
(43) Afonso, S.; Horita, K.; Sousa e Silva, J. P.; Almeida, I. F.; Amaral, M. H.; Lobão, P. A.; Costa, P. C.; Miranda, M. S.; Esteves da Silva, J. C. G.; Sousa Lobo, J. M., Photodegradation of avobenzone: Stabilization effect of antioxidants, *Journal of Photochemistry and Photobiology B: Biology* **2014**, *140*, 36.

Supporting Information:

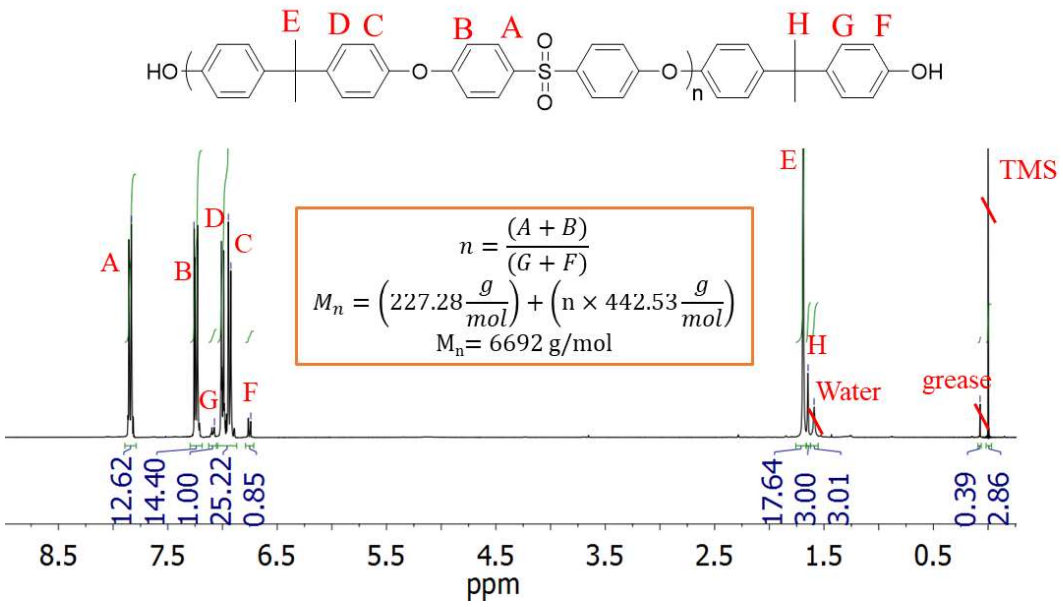

Figure S9.1. ^{1}H NMR spectroscopy of phenol-terminated PSU with targeted M_n of 6000 g/mol.

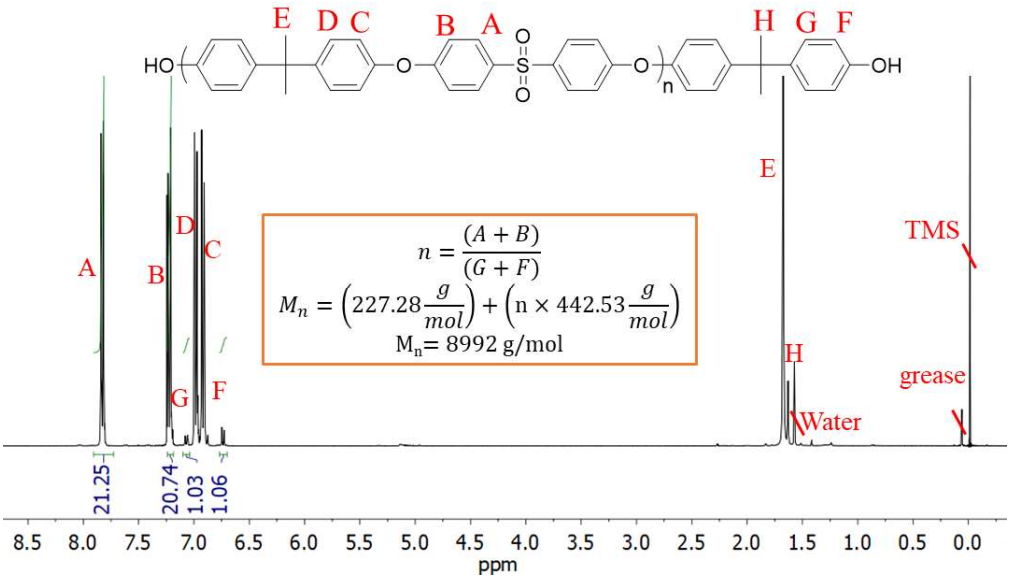

Figure S9.2. [1]H NMR spectroscopy of phenol-terminated PSU with targeted M_n of 10,000 g/mol.

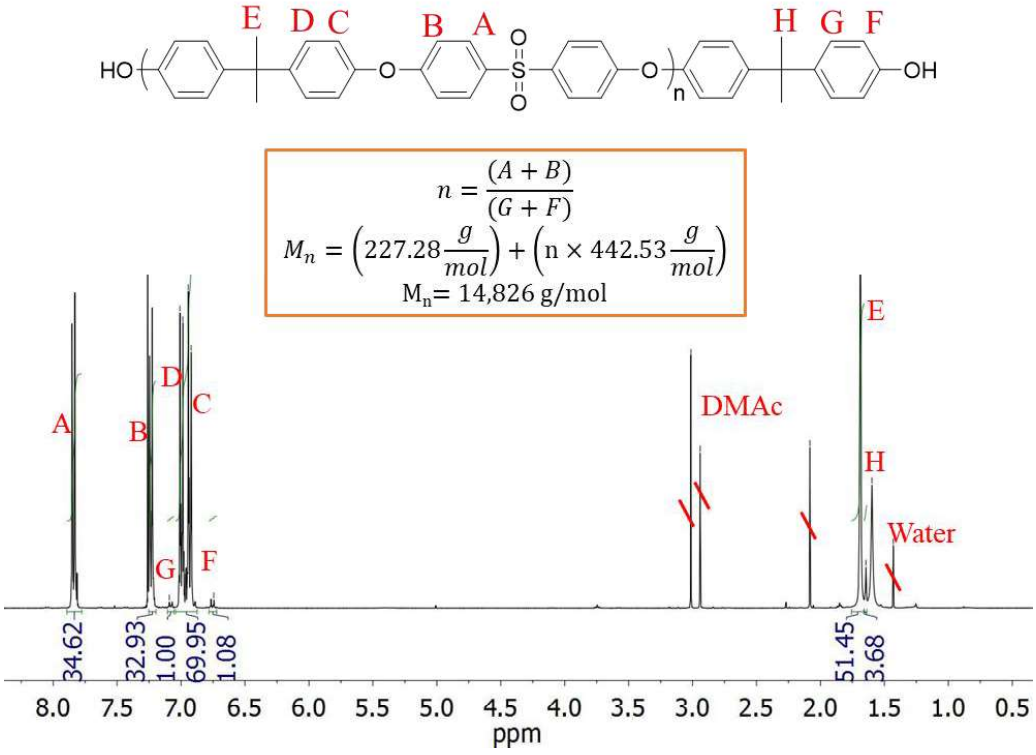

Figure S9.3. [1]H NMR spectroscopy of phenol-terminated PSU with targeted M_n of 20,000 g/mol.

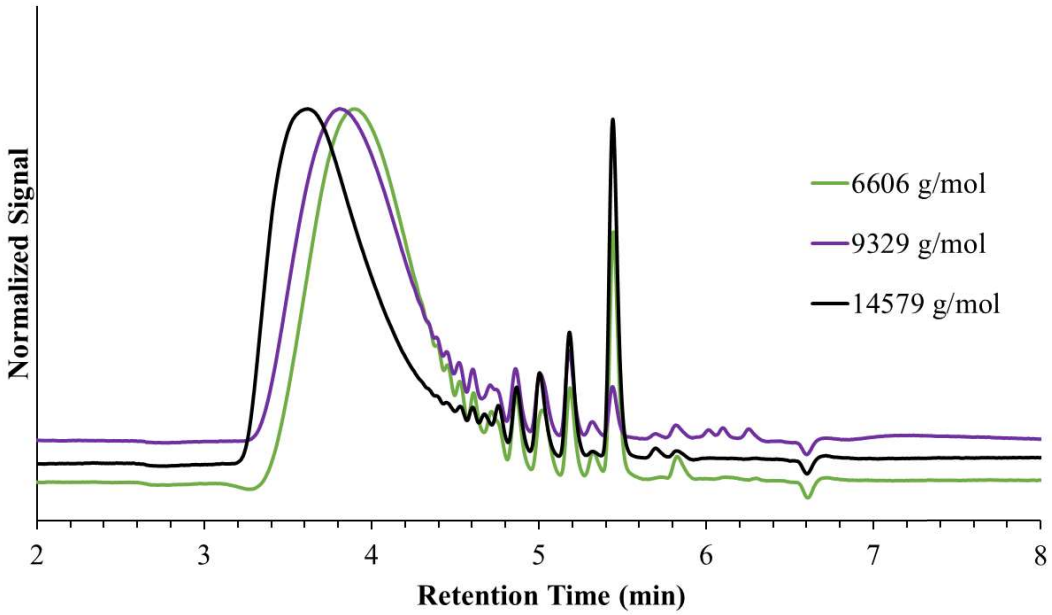

Figure S9.4. Advanced permeation chromatography of phenol-terminated PSU with targeted M_n of 20, 10, and 6 kg/mol in chloroform. Analysis based on polystyrene standards.

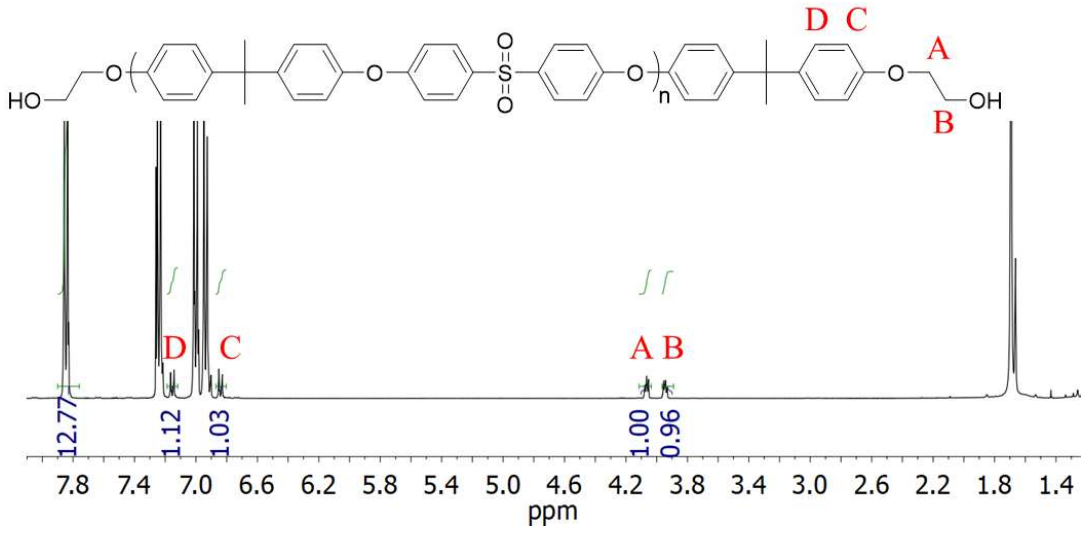

Figure S9.5. ^{1}H NMR spectroscopy of successful hydroxyethyl-functionalization of the 6000 g/mol phenol-terminated PSU.

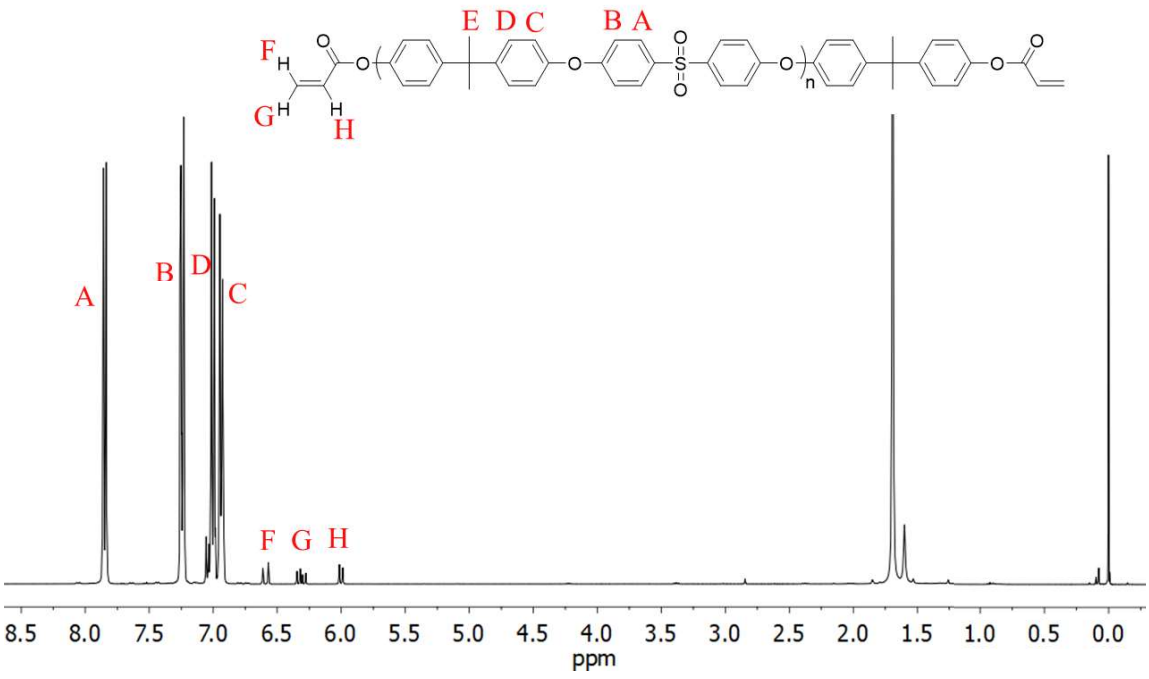

Figure S9.6. [1]H NMR spectroscopy of successful acrylate functionalization of the 6000 g/mol phenol-terminated PSU.

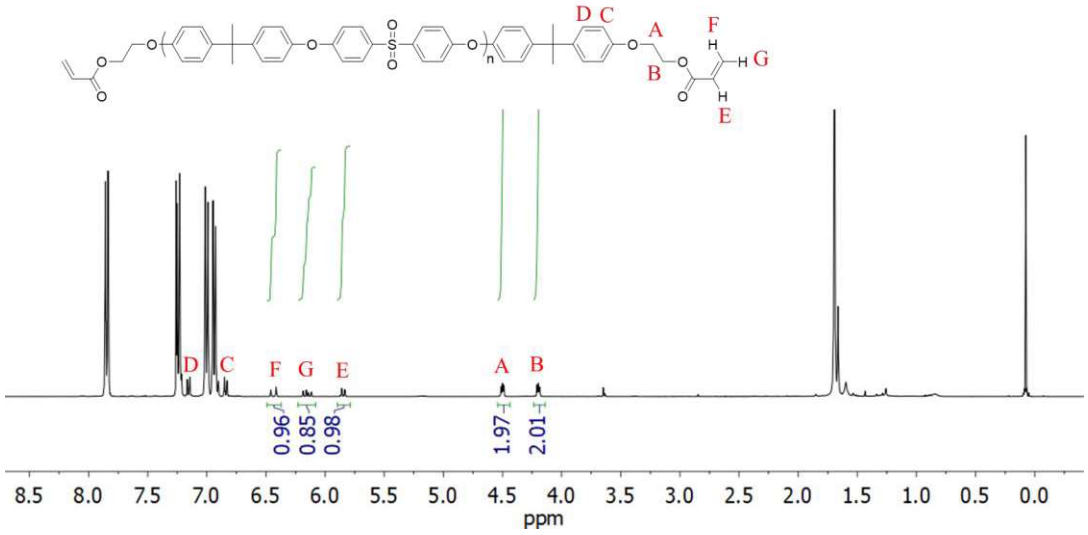

Figure S9.7. [1]H NMR spectroscopy of successful acrylate functionalization of the 6000 g/mol hydroxyethyl-terminated PSU.

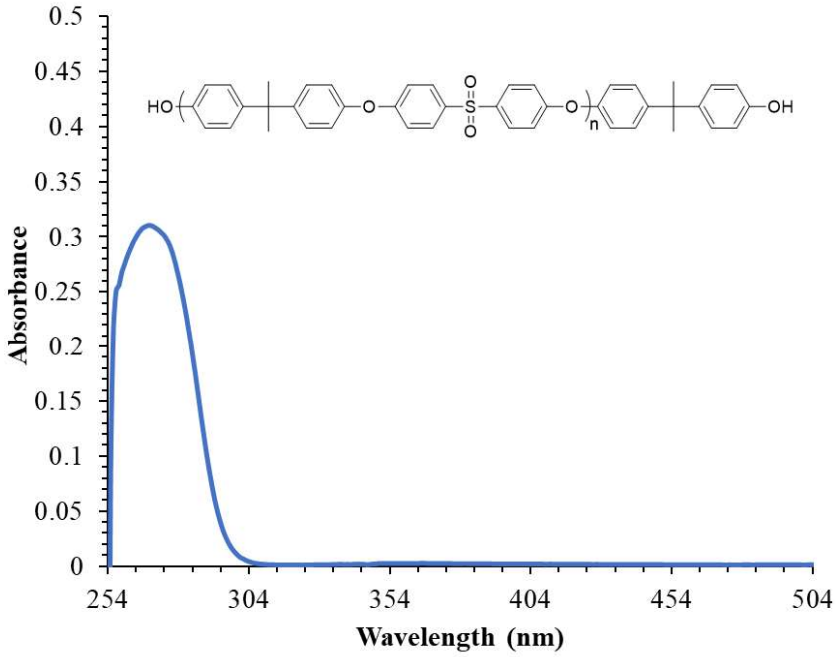

Figure S9.8. UV-Vis spectroscopy of phenol-terminated PSU exhibiting a peak absorbance at 269 nm.

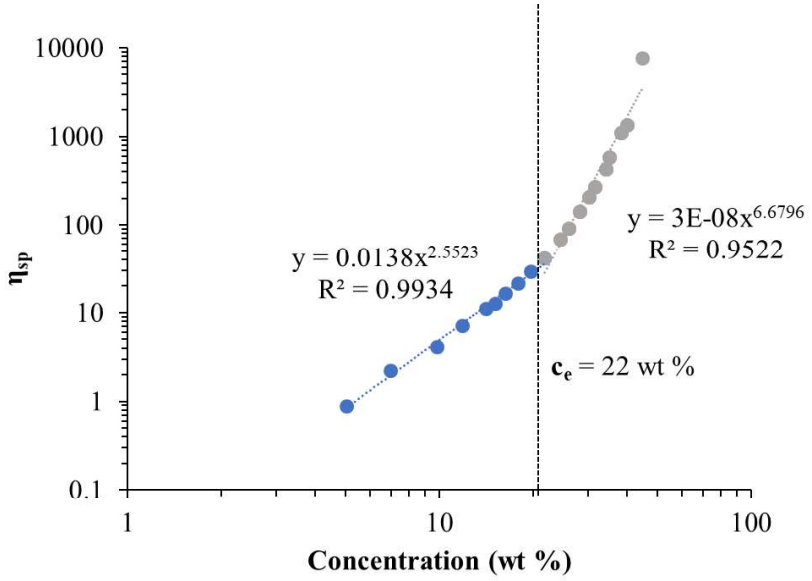

Figure S9.9. Solution rheology of phenol-terminated PSU with M_n= 5500 g/mol comparing the specific viscosity (η_{sp}) to the concentration of the PSU in NMP.

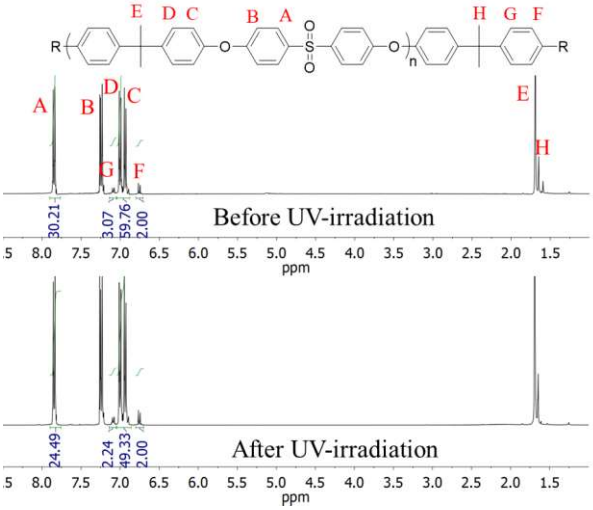

PSU End group (R)	Before UV	After UV
	6900 g/mol	5600 g/mol (↓ 20 %)
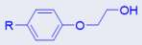	5600 g/mol	4200 g/mol (↓ 25 %)

Figure S9.10. Characterization of the Photo-Claisen rearrangement based photodegradation using ^{1}H NMR spectroscopy. 20 mg/mL solutions of phenol- or hydroxyethyl-terminated PSU in CDCl3 analyzed before and after UV-irradiation for 10 min at intensity of 100 mW/cm^{2}.

Chapter 10: Overall Conclusions

Step-growth polymerization enabled the synthesis and characterization of a number of novel polyesters and polysulfones. Systematic variations to backbone and end group structures enabled tunability to the polymer properties and provided a variety of morphologies and novel processing conditions.

Two series of (co)polyesters with tunable LC properties were polymerized using melt transesterification through the systematic exchange of the 4,4'-bibenzoate moieties with its *meta* regioisomer in the semi-aromatic LCP's, poly(butylene 4,4'-bibenzoate) and poly(diethylene glycol 4,4'-bibenzoate). The (co)polyester series, poly(diethylene glycol 3,4'-bibenzoate-*co*-4,4' bibenzoate) exhibited a smectic CA morphology for all compositions exhibiting a LC mesophase. The limited crystallinity of this series primarily resulted from the flexible ether linkage and became unobservable as incorporation of 3,4'BB increased in the polymer structure. The LC morphology withstood higher incorporation of 3,4'BB content prior to disruption enabling a range of LC glasses. The more rigid butylene spacer resulted in a larger window of compositions in this copolymer crystallizing. Even so, the 3,4'BB structure exhibited a more selective effect on crystallizability relative to the LC phase which withstood higher concentrations of the kink in the backbone. The LC glasses achieved through selective inhibition of crystalline domains exhibit much broader mesogenic windows than the semi-crystalline/LC polymers. This provided an increased temperature window in which processing could occur for these materials and revealed a method toward the formation of LC glass not previously explored.

The unique selectivity afforded to the longer kink structure of 3,4'BB relative to other structures, such as isophthalate, indicated it as a good candidate in the polymerization of fully-aromatic LCP. Fully-aromatic LCPs often focus on reduction of the T_m and degree of crystallinity. Melt acidolysis polymerization with different derivatives of hydroquinone facilitated the synthesis of poly(*p*-phenylene 3,4'-bibenzoate). The hydroquinone derivative provided control over the final polymer color through changes to the condensate. The kinked structure in the backbone reduced the crystallizability of the polymer without inhibiting the formation of a LC phase. This directly contrasted with results from similar structures, such as poly(hydroquinone isophthalate) which did not exhibit a LC phase. WAXS and POM confirmed the presence of a nematic mesophase within poly(*p*-phenylene 3,4'-bibenzoate). Rheological analysis demonstrated competitive shear thinning results to the industrial standard, Vectra® RD501. These novel polyesters reveal a new method towards achieving fully aromatic LCPs eliminating the necessity for complicated random copolyester structures. Ultimately, this discovery could lower the cost of production due to reduced number of comonomers and provide a more controllable morphology.

In order to better understand the limitation of this structural effect on the LC phase, a series of isomeric polymers utilizing different configurations of the structure, poly(phenylene bibenzoate) were synthesized using melt acidolysis polymerization. Six different structures ranging from entirely *para* to completely *meta* were provided through the selective choice of three different diacid monomers (4,4'BB, 3,4'BB, and 3,3'BB) and two dipivilate monomers (HQ_p and RS_p). The linear symmetric structure, poly(HQ-4,4'BB) afforded a highly crystalline intractable material with an immeasurable T_m. Both

poly(HQ-3,4'BB) and poly(RS-4,4'BB), with a single *meta* unit, resulted in a LC polymer exhibiting a nematic mesophase. This further confirms the effectiveness of this strategy towards achieving fully aromatic LCP without random copolymerization. Additional *meta* units resulted in either semi-crystalline or amorphous morphologies. While these polymers do not exhibit a LC phase, the high T_g's and high thermal stability of the amorphous compositions could lead to their use in the application space of polysulfones, polycarbonates, or polyarylates.

The melt transesterification of the diester form of 3,3'BB with different linear and cycloaliphatic diols enabled the synthesis of novel semi-aromatic polyesters without a LC morphology. DSC and DMA demonstrated a trend in the thermal and thermomechanical properties in which increased chain flexibility through diol choice resulted in lower T_g's. As a result, the bulky and rigid CHDM diol exhibited the highest T_g of 107 °C while hexanediol possessed the lowest value of 39 °C. Comparison of the 3,3'BB polymers with their regioisomer analogues demonstrated a trend in thermal properties in which 4,4'BB > 3,4'BB > 3,3'BB for T_g's possibly due to increased chain flexibility. Overall, the biphenyl structure provided higher thermal transitions to the isophthalate polymer analogues, as well as lower crystallizability. This series of polymers expanded the library of materials achieved using the BB isomers, providing a more thorough understanding of the impact of regioisomers on polymer properties.

The addition of monofunctional monomers to the polymerization of the LC polyester, poly(hexamethylene 4,4'-bibenzoate), afforded novel telechelic LCP. Sodium 3-sulfomethylbenzoate's incorporation during the polymerization, enabled the synthesis of LCPs with ionic end groups providing non-covalent interactions between the chains in

the form of ionic aggregates. The ionic aggregates slowed chain mobility resulting in decreases to both the T_m and T_i of the LCP at 10 mol % end group concentration in contrast to the non-ionic analogues. Restriction of the ionic groups to the chain ends maintained the formation of the LC though smaller domain sizes were observed. Rheological measurements assessed the zero-shear viscosity of polymers revealing higher viscosities from the ionic end capped polymers in comparison to the non-ionic analogue.

Finally, post-polymerization functionalization of polysulfone oligomers afforded two molecular weight series of acrylate terminated polymers. The acrylate functionality provided a photo-curable moiety with which to crosslink the polymer into a thermoset. Acrylation of the phenol-terminated PSU or the hydroxyethyl-terminated PSU provided a comparison for photocuring kinetics. Photorheology and photoDSC analysis revealed no significant improvement to the photocuring process through the use of the more synthetically complex structure with the ethyl spacer. The 6000 g/mol oligomer acrylated from the phenol terminated PSU in a 30 wt % solution of NMP was determined as the optimal composition for processing using the additive manufacturing method, vat photopolymerization. 3D printing the solution with VPP after the addition of low concentrations of photo-blocker afforded a well-defined lattice structure. This research further expanded the library of resins for VPP enabling the design of 3D printed parts using high performance materials.

In summary, a fundamental and systematic analysis of the role that backbone and end group structure plays on polymer properties and processing techniques enabled the synthesis of a wide-range of novel polymers. This encourages the expansion of not only

material libraries but application into fields not previously considered resulting inevitably in a broader impact on technological development.

Chapter 11: Suggested Future Work

11.1 Telechelic liquid crystalline ionomers featuring divalent cations

The exchange of monovalent cations in sulfonated polymers for divalent cations, such as Ca^{2+} or Zn^{2+}, exhibited success in the achieving ionomer capable of compatibilization in blends with poly(ethyl acrylate-*co*-4-vinyl pyridine).[1,2] Relative to the monovalent cation, multivalent systems exhibit greater coulombic interactions due to the ability to form an ionic bond between two monovalent anions resulting in a stronger physical crosslink.[3,4] These ionic aggregation affords a thermo-reversible crosslink within the polymer architecture which exhibits added benefits toward compressive strength and transverse mechanical properties. While monofunctional ionic end groups in Chapter 5 demonstrated minor impacts to the LCP's morphology and thermal properties, divalent cations may exhibit enhanced chain-extension. This would enable a low molecular weight oligomer to provide high molecular weight polymer properties with the added benefit of significantly lower viscosity and processing conditions due to the thermo-reversible network. Ionic exchange of the SSMB monomer prior to polymerization, as illustrated in

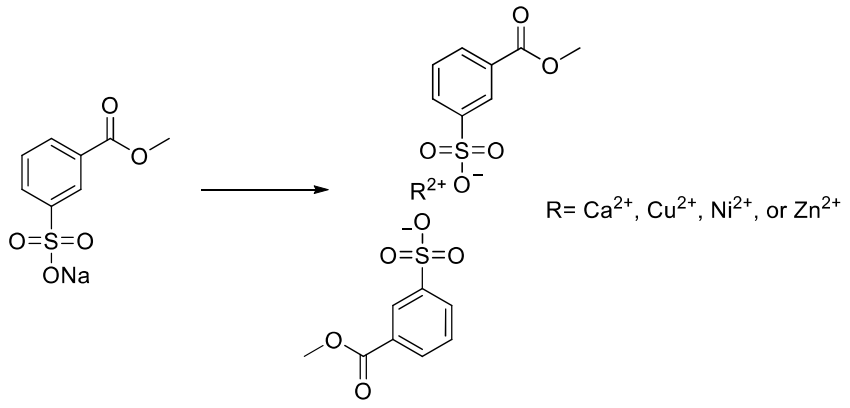

Scheme 11.1. Ionic exchange of sodium 3-sulfomethylbenzoate with a divalent cation.

Scheme 1, would be required due to the insolubility of poly(HD-4,4'BB) following polymerization. In contrast, choosing an alternative polymer backbone structure, such as poly(DEG-4,4'BB), which exhibits solubility in chloroform would enable post-polymerization ionic exchange. Synthesis of these two polyesters would utilize melt-transesterification of with a monofunctional end group following the procedure laid out in the synthesis of the ionic endcapped poly(HD-4,4'BB) in Chapter 5. A systematic study of the influence of mol % ionic end group with divalent cation on morphology and mechanical properties would provide basis for chain extension understanding.

11.2 3D printing semi-aromatic LC polyesters through material extrusion

Additive manufacturing through material extrusion represents a large area of the 3D printing literature, as well a large consumer presence expanding from the numerous inexpensive consumer printers on the market using this technique.[5] A typical schematic

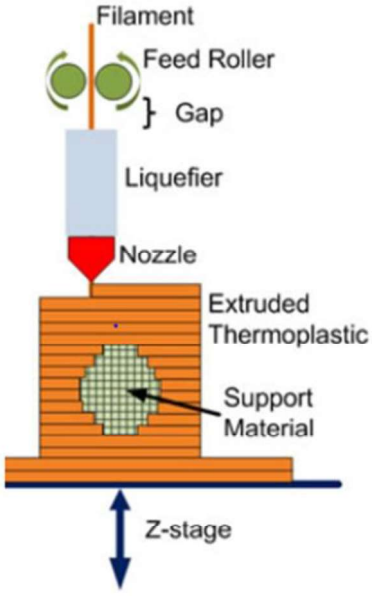

Figure 11.1. Basic schematic of a material extrusion 3D printer.

of this 3D printing methodology is illustrated in **Figure 11.1**. The processing of fully-aromatic polyesters, such as Vectra®, through this technique primarily focuses on the use of LCPs as a blend material for enhancement of final filament mechanical properties.[6] The high processing temperatures of these fully-aromatic polymer often limit the ability to 3D print the pure material and ultimately benefit from the significant shear thinning exhibited by LCPs. One recent example demonstrated the 3D printing of Vectra® alone revealing the significant benefit of LC alignment during the process of fused deposition modeling.[7] Other literature shows the importance of a shear thinning regime in polymers to this printing process emphasizing the added benefit of utilizing LCP with low working temperature ranges.[8,9]

The flexible spacers in semi-aromatic LCP traditionally result in lower mesogenic windows than their fully aromatic counterparts. The biphenyl monomer, 4,4'BB, makes up the aromatic component in a large number of LC polyesters and control over the LC morphology occurs through choice of the diol. **Figure 11.2** illustrates the structures of

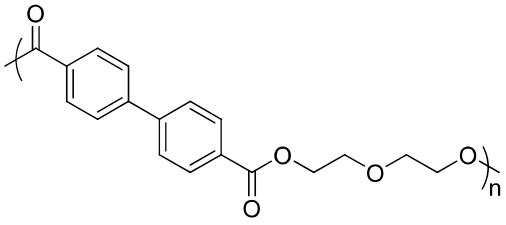

Smectic CA

T_m = N/A
T_i = 204 °C

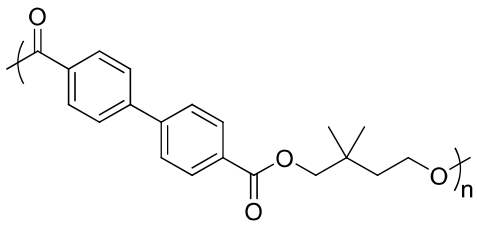

Nematic

T_m = 124 °C
T_i = 162 °C

Figure 11.2. Semi-aromatic liquid crystalline polyesters based on 4,4' bibenzoate with different aliphatic diols exhibiting different LC morphologies and lowed temperature mesogenic windows.

two known semi-aromatic LCP which exhibit smectic or nematic morphologies with different mesogenic windows.[10,11] The lower temperature windows of these two polymers would improve material extrusion of the pure materials. While both LC morphologies exhibit shear thinning, nematic morphologies exhibit more significant shear thinning due to the presence of only orientational ordering and elimination of layers resulting in a more fluid morphology. One morphology may prove more beneficial than another so in depth analysis of two types of polymers is recommended. Poly(DEG-4,4'BB) would be an optimal choice for the smectic polymer as it uniquely exhibits a LC glass morphology due to the flexible diethylene glycol resulting in a polymer with low crystallizability. This morphology could act an added benefit to the 3D printing technique as this may exhibit less shrinkage than a semi-crystalline polymer which ultimately impact the part quality and regularity.

Once an understanding is developed toward the structure-property relationships of LC polymers in material extrusion 3D printing, novel polymers with added functionality can be explored within this field. One possible structure would utilize stilbene-based semi-aromatic LCP which could facilitate post-printing crosslinking with UV-light to further strengthen the interfacial adhesion between layers of the print. The stilbene structure varies from the bibenzoate system through the addition of a double bond between the two phenyl groups. Studies revealed that the double bond undergoes cyclic dimerization upon exposure to UV-light enabling the presence of an additional crosslinking group in the polymer architecture.[12,13]

Dimethyl stilbene has been utilized to synthesize LC polyesters through the same synthetic pathway as bibenzoate based polymers.[12] These semi-aromatic polyesters

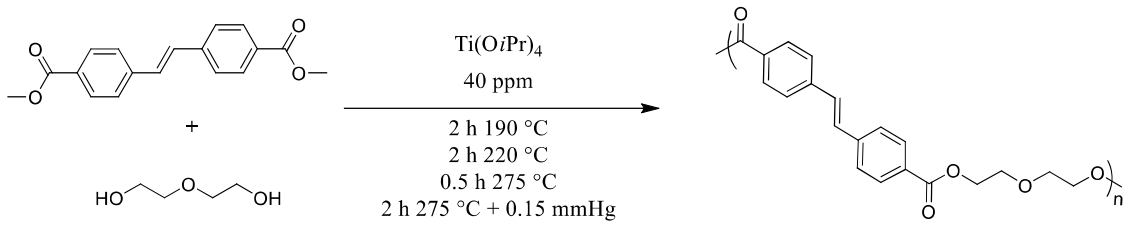

Scheme 11.2. Proposed synthetic method through melt-transesterification to poly(diethylene glycol-stilbene).

typically exhibit nematic, rather than smectic, mesophases which could be beneficial to the 3D printing process. **Scheme 11.2** illustrates a possible synthetic pathway toward the novel poly(diethylene glycol-4,4'-stilbene dicarboxylate). While never before studied, this polymer may exhibit similar LC glass morphologies relative to its biphenyl counterpart and would require thorough characterization. Other aliphatic diols could also be analyzed, such as butanediol and hexanediol, which have previously demonstrated LC properties. Solid-state crosslinking of the stilbene following extrusion could improve interlayer adhesion following the print ultimately resulting in stronger final parts and eliminating the need for thermal annealing. Systematic analysis of 3D printed tensile bars upon selective exposure to UV-light would characterize the influence of cyclic dimerization on the final mechanical properties.

11.3 Synthesis of semi-aromatic LC polyester using organocatalysts

Organocatalysts recently gained footing in the area of step-growth polymers by demonstrating the successful synthesis of a wide range of polymer families from polyurethanes to polycarbonates to polyesters.[14] These catalysts represent a bio-friendly alternative to traditional heavy metal catalyst, such as antimony, tin, and titanium catalysts. This supports application of these materials into the biomedical field where the presence of the metal catalysts represents a limiting factor in many materials due to

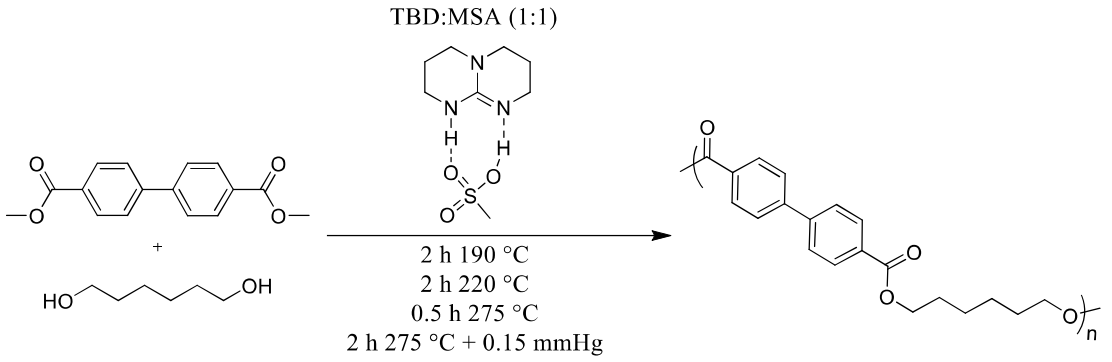

Scheme 11.3. Proposed melt-transesterification of poly(hexamethylene 4,4'-bibenzoate) utilizing an organocatalyst salt.

toxicity. Traditionally, low boiling points and low thermal stability exhibited by organocatalysts limited their use in high temperature melt polymerizations. Recent literature demonstrated the formation of coordinated salts through acid-base reactions of the organocatalysts which result in significantly higher thermal stabilities.[15,16] These have demonstrated success in the polymerization and depolymerization of poly(ethylene terephthalate) utilizing 5 mol % of a 1:1 mixture of triazabicyclodecene (TBD) and methanesulfonic acid (MSA).

Unlike fully-aromatic LCP, semi-aromatic LC polyester are commonly synthesized using melt-transesterification methods and often require metal catalyst, such as titanium isopropoxide. **Scheme 11.3** demonstrates a possible novel synthetic method to achieving a semi-aromatic LCP using the organocatalysts salts. This would follow the same temperature ramps as previously demonstrated in Chapter 4 and 5 while eliminating the need for harsh metal catalysts providing a more biofriendly alternative to achieving high molecular weight polymers. A systematic study of different catalyst ratios and different backbone structures would elucidate the catalytic activity and versatility of this polymerization method.

11.4 Synthesis of fully-aromatic liquid crystalline polyesters utilizing triphenyl molecules

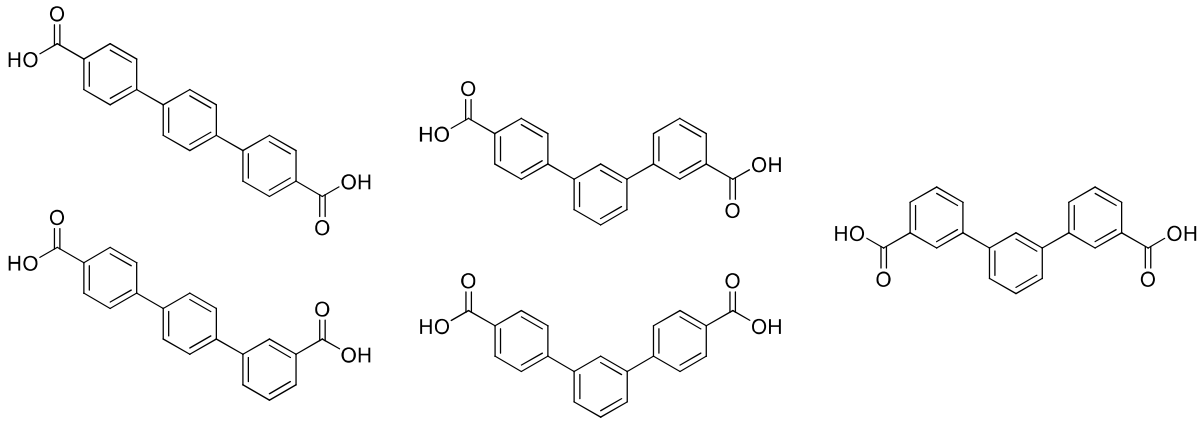

Figure 11.3. Possible triphenyl diacid structures for use in acidolysis polymerization.

In Chapters 6 and 7 the biphenyl isomers demonstrated the importance of balancing kink in a poly(phenylene bibenzoate) structure when developing a liquid crystalline polyester. Within these system, short kinked structures, such as isophthalate, resulted in semi-crystalline materials without a LC phase associated with the reduced persistence length which impacts the aspect ratio of the polymer. The biphenyl structure hypothetically provides a longer persistence length achieving the necessary aspect ratio to form a LC phase. Taking this into consideration, it remains conceivable that a triphenyl

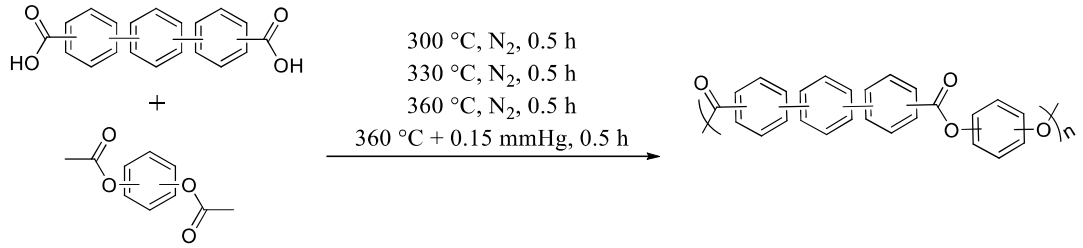

Scheme 11.4. Proposed synthesis of a triphenyl based fully-aromatic polyester utilizing melt-acidolysis polymerization.

structure could further provide tunability to the LC phase in a polymer. **Figure 11.3** demonstrates a few examples of possible triphenyl diacid architectures that could be suitable for acidolysis polymerization. Previous work by Edling et al. demonstrated the successful polymerization/copolymerization of polyesters based on the linear triphenyl diacid.[18] A Suzuki coupling procedure would be the logical first step in synthesizing these structure due to its success in the synthesis of the biphenyl configurations.[19] This synthesis would need to deviate from the original study through the addition of a dibromophenyl molecule in order to generate the triphenyl architecture.

The polymer synthesis would take place utilizing melt acidolysis polymerization, as illustrated in **Scheme 11.4**. This follows procedure studied in Chapter 7 for the poly(phenylene bibenzoate) polymerization. The choice of the acetylated hydroquinone followed the desire to achieve high molecular weight within the reaction times which is a limiting factor when considering the pivilate condensate. Based on the study in chapter 7, the structure with at least one *meta* unit should produce LC polymers with nematic morphologies. A systematic study of the diacids with hydroquinone and resorcinol would provide understanding of whether this longer structure could withstand a second *meta* moiety while maintain a stable LC phase. These structures are reminiscent of banana-shape LC small molecules therefore interesting LC structures may be observed for these materials.

11.5 Next steps in the 3D printing of acrylate terminated PSU

While the synthesis of acrylate terminate PSU was thoroughly demonstrated in Chapter 9, expanding upon the understanding of the 3D printed parts will be necessary to fully realize the high performance structures achieved. Thermal and mechanical testing

following extraction of crosslinked films will provided information into how the aliphatic crosslinking group impacts the PSU high performance properties. TGA of these films will demonstrated the impact the aliphatic polyacrylate structure between each PSU on the overall polymer thermal stability while DSC analysis will determine how the crosslink density effects the T_g. Tensile analysis of the extracted films will enable comparison of mechanical properties achieved in the crosslinked film relative to a high molecular weight PSU. Tensile specimens should be provided from both 3D printing and a lab made crosslinked film in order to reveal any anisotropy that may occur through the printing method. A drying procedure will need to be determined in order to obtain isotropic shrinkage of the films upon removal of the solvent from the organogel green bodies. This shrinkage should be characterized and determine whether resolution is improved upon removal of the solvent.

The exchange of the solvent, NMP, with a reactive diluent could help improve not only % conversion of the higher molecular weight PSU but also eliminate the need for a carcinogenic diluent. McGrath et al. demonstrated the incorporation of pentaerythritol tetraacrylate (PETA) into the crosslinking of acrylamide terminated PSU, effectively increasing the gel fraction of UV-crosslinked films.[20] Other efforts to remove the solvent could include the use of heat to melt the polymer and reduce viscosity into a processable range. In order for this to be successful, the acrylate crosslinking group would need to be exchanged with more thermally stable moieties. Both cinnamates and chalcone derivatives exhibit the necessary thermal stability and undergo crosslinking through a cyclic dimerization. Exchange of the acrylate group with a monofunctional cinnamate or

chalcone derivative could afford crosslinking while enabling reduction of viscosity in a special high temperature VPP chamber.

References

(1) Ng, C. W. A.; MacKnight, W. J., Ionomeric Blends of Poly(ethyl acrylate-co-4-vinylpyridine) with Zinc-Neutralized Sulfonated Poly(ethylene terephthalate). 3. Effects of Functionalization Level, *Macromolecules* **1996**, *29*, 2412.

(2) Ng, C.-W. A.; Lindway, M. J.; MacKnight, W. J., Ionomeric Blends of Poly(ethyl acrylate-co-4-vinylpyridine) with Zinc-Neutralized Sulfonated Poly(ethylene terephthalate). 1. Effect of Specific Interactions upon the Amorphous Phase, *Macromolecules* **1994**, *27*, 3027.

(3) Ju, L.; Pretelt, J.; Chen, T.; Dennis, J. M.; Heifferon, K. V.; Baird, D. G.; Long, T. E.; Moore, R. B., Synthesis and characterization of phosphonated Poly(ethylene terephthalate) ionomers, *Polymer* **2018**, *151*, 154.

(4) Shi, Y.; Yu, Q.; Meng, W.; Zhang, Z., Maximum product of effective channel gains: an innovative user selection algorithm for downlink multi-user multiple input and multiple output, *Wireless Communications and Mobile Computing* **2014**, *14*, 1732.

(5) Gao, W.; Zhang, Y.; Ramanujan, D.; Ramani, K.; Chen, Y.; Williams, C. B.; Wang, C. C. L.; Shin, Y. C.; Zhang, S.; Zavattieri, P. D., The status, challenges, and future of additive manufacturing in engineering, *Computer-Aided Design* **2015**, *69*, 65.

(6) Gray, R. W.; Baird, D. G.; Helge Bøhn, J., Effects of processing conditions on short TLCP fiber reinforced FDM parts, *Rapid Prototyping Journal* **1998**, *4*, 14.

(7) Gantenbein, S.; Masania, K.; Woigk, W.; Sesseg, J. P. W.; Tervoort, T. A.; Studart, A. R., Three-dimensional printing of hierarchical liquid-crystal-polymer structures, *Nature* **2018**, *561*, 226.

(8) Anderegg, D. A.; Bryant, H. A.; Ruffin, D. C.; Skrip, S. M.; Fallon, J. J.; Gilmer, E. L.; Bortner, M. J., In-situ monitoring of polymer flow temperature and pressure in extrusion based additive manufacturing, *Additive Manufacturing* **2019**, *26*, 76.

(9) Gilmer, E. L.; Miller, D.; Chatham, C. A.; Zawaski, C.; Fallon, J. J.; Pekkanen, A.; Long, T. E.; Williams, C. B.; Bortner, M. J., Model analysis of feedstock behavior in fused filament fabrication: Enabling rapid materials screening, *Polymer* **2018**, *152*, 51.

(10) Watanabe, J.; Hayashi, M.; Morita, A.; Tokita, M., Thermotropic Liquid Crystals of Main-Chain Polyesters Having a Mesogenic 4,4'-Biphenyldicarboxylate Unit. 6. Chiral Mesophases of Polyesters with a (S)-2-Methylbutylene Spacer, *Macromolecules* **1995**, *28*, 8073.

(11) Heifferon, K. V.; Mondschein, R. J.; Talley, S. J.; Moore, R. B.; Turner, S. R.; Long, T. E., Tailoring the glassy mesophase range of thermotropic polyesters through copolymerization of 4,4’-bibenzoate and kinked isomer, *Polymer* **2019**, *163*, 125.

(12) Hu, Y. S.; Schiraldi, D. A.; Hiltner, A.; Baer, E., Structural Model for Oxygen Permeability of a Liquid Crystalline Polymer, *Macromolecules* **2003**, *36*, 3606.
(13) Jackson, W. J.; Morris, J. C., Liquid crystal polymers. IX. Copolyesters of trans-4,4′-stilbenedicarboxylic acid, 1,4-butanediol, and aromatic dicarboxylic acids, *J. Polym. Sci., Part A: Polym. Chem.* **1988**, *26*, 835.
(14) Montgomery, S. J.; Kannan, G.; Galperin, E.; Kim, S. D., Thermally Stable UV Crosslinkable Copolyesters: Synthesis, Crosslinking, and Characterization of Poly(1,4-cyclohexylenedimethylene−1,4-cyclohexane dicarboxylate-co-4,4′-stilbene dicarboxylate), *Macromolecules* **2010**, *43*, 5238.
(15) Bossion, A.; Heifferon, K. V.; Meabe, L.; Zivic, N.; Taton, D.; Hedrick, J. L.; Long, T. E.; Sardon, H., Opportunities for organocatalysis in polymer synthesis via step-growth methods, *Prog. Polym. Sci.* **2018**.
(16) Basterretxea, A.; Gabirondo, E.; Jehanno, C.; Zhu, H.; Flores, I.; Müller, A. J.; Etxeberria, A.; Mecerreyes, D.; Coulembier, O.; Sardon, H., Polyether Synthesis by Bulk Self-Condensation of Diols Catalyzed by Non-Eutectic Acid–Base Organocatalysts, *ACS Sustainable Chemistry & Engineering* **2019**, *7*, 4103.
(17) Jehanno, C.; Pérez-Madrigal, M. M.; Demarteau, J.; Sardon, H.; Dove, A. P., Organocatalysis for depolymerisation, *Polymer Chemistry* **2019**, *10*, 172.
(18) Edling, H. E., Dissertation; Synthesis and Structure-Property Relationships of Polyesters Containing Rigid Aromatic Structures,Virginia Polytechnic Institute and State University, 2018.
(19) Clary, R. S.; Lee, C. D.; IV, W. G. M.; Vaughn, D. A.; Ragheb, R. T.; III, J. W. E.; Brown, D. M.; Schiraldi, D. A., A Green, One-Pot Route to the Biphenyldicarboxylic Acids: Useful Intermediates in Polymer Synthesis, *International Journal of Organic Chemistry* **2013**, *Vol.03No.02*, 5.
(20) Sundell, B. J.; Lee, K.-s.; Nebipasagil, A.; Shaver, A.; Cook, J. R.; Jang, E.-S.; Freeman, B. D.; McGrath, J. E., Cross-Linking Disulfonated Poly(arylene ether sulfone) Telechelic Oligomers. 1. Synthesis, Characterization, and Membrane Preparation, *Industrial & Engineering Chemistry Research* **2014**, *53*, 2583.